An Investigation of Poly(imidazolium)s for Alkaline Energy Storage and Conversion Devices

by

Kate Fraser

Master of Chemistry, Lancaster University, 2019

Thesis Submitted in Partial Fulfillment of the
Requirements for the Degree of
Doctor of Philosophy

in the
Department of Chemistry
Faculty of Science

SIMON FRASER UNIVERSITY
Fall 2023

Declaration of Committee

Name:	**Kate Fraser**
Degree:	**Doctor or Philosophy**
Title:	**An Investigation of Poly(imidazolium)s for Alkaline Energy Storage and Conversion Devices**
Committee:	**Chair:** **Neil Branda** Professor, Chemistry
	Steven Holdcroft Supervisor Professor, Chemistry
	Tim Storr Committee Member Professor, Chemistry
	Loren Kaake Committee Member Associate Professor, Chemistry
	Vance Williams Examiner Professor, Chemistry
	Kevin Noonan External Examiner Associate Professor, Chemistry Carnegie Mellon University

Abstract

Most of the global energy demand is met using environmentally damaging and finite fossil fuel sources. Electrochemical energy conversion devices generating and using hydrogen fuel offer a solution which relies exclusively on renewable energy sources. However, implementation of such technologies has been stalled by high device cost. Alkaline energy conversion devices enable the use of cheaper and more environmentally friendly, non-perfluorinated ion conducting polymers. The development of these devices has been impeded by the low durability of organic materials in high pH conditions and the low mobility of hydroxide, limiting material conductivity. Poly(imidazolium)s have emerged as a highly durable, highly conductive materials and are the leading candidates for hydroxide conducting polymers.

The focus of this thesis is the implementation of novel poly(imidazolium) synthetic routes for a greater understanding of the structure-property correlations. In Chapters 3, 4 and 5, the poly(imidazolium)s are prepared using an AB-type step growth polymerisation mechanism enabling precise control of functionalization and end group chemistry. In Chapter 3, a one-pot three-component reaction was developed for the synthesis of tetrasubstituted poly(imidazole)s. The reaction was modified in chapter 4 for the synthesis of a poly(imidazolium) with targeted macromolecular properties for implementation as an ionomer, into the catalyst layer. The poly(imidazolium) allowed for the investigation of ionomer-catalyst interactions and their impact on the hydrogen evolution and hydrogen oxidation reactions.

The alkaline stability of poly(imidazolium)s was explored in chapters 5 and 6. Using the AB-type polymerisation method, the poly(imidazolium) end groups are defined in chapter 5 and the impact of reactive carbonyl end groups on main chain polymer alkaline stability is investigated. In Chapter 6, a series of imidazolium model compounds with varying N-functionalities were explored and the different methodologies available for alkaline stability investigation were discussed. This data was compared to the alkaline stability of analogous poly(imidazolium) materials.

Through this work, a simple and modular synthetic route was established for poly(imidazolium)s, allowing for future systematic variation of polymer structure to be

investigated. The structural variation and subsequent macromolecular properties can be correlated for the development of tuneable materials for specific applications.

Keywords: Poly(imidazolium)s; alkaline energy conversion devices; Debus Radziszewski; ion conducting polymers; ionenes; alkaline stability

To my family, for never failing to support me.

Acknowledgements

This work would not have been possible without the support and supervision of Prof. Steven Holdcroft, I am grateful for the opportunity to work in the Holdcroft Group and for your steadfast belief in my abilities.

I would like to thank my committee members, Prof Loren Kaake, and Prof. Timonthy Storr for their guidance and constructive criticism throughout my time in graduate school. My thanks also go to all the other faculty members of the SFU Chemistry Department who helped me through my PhD journey.

There are many members, both past and present, from the Holdcroft Lab who I would like to extend my thanks to and the following is in no particular order.

To Dr. Thomas Skalski, Dr. Simon Cassegrain, Dr. Peter Mardle, and Dr. Amelia Hohenadel Hinshaw, thank you for your guidance during the beginning of my PhD time. You all taught me the true meaning of a good scientific work ethic, along with sharing your expertise, and collectively helping me through the rough COVID-times.

To the electrochemistry team at the University of Strasbourg, France: thank you for teaching an organic chemist the world of electrochemistry. Your shared expertise and assistance helped me immensely.

Dr. Anastasiia Konovalova, thank you for not only the assistance and encouragement you provided me with inside the lab, but also your immense kindness that has truly helped me in some of my hardest times. Matthew Siebert, your positive attitude, and our agreement to ask each other no-judgement scientific questions has provided many laughs throughout your time at SFU. Dr. Torben Saatkamp, your unwavering belief in my scientific abilities, despite my own insecurities, has been a driving force throughout the challenging final months of my PhD. Your interest and excitement in science has been an inspiration to me, I look forward to witnessing the development of your research career.

To the Martelinos, thank you for providing me a home-away-from-home, your love and support throughout these pass 4 years has helped me more than you can imagine. A special mention must go to Pierre Noujeim, without your friendship, constant

encouragement, and unwavering support I would not be where I am today. Thank you for the long chats, even if it was during 12 Km runs.

To my family in the UK, thank you for encouraging me to pursue my dreams, even when it involved moving to the other side of the World. The steadfast support I have received from you, at all hours of the day, has driven my time at SFU and through the many years that lead up to this. And thank you to my mother, Janet Fraser, for always answering my calls, even if they are at 3 am GMT.

And finally, to Diego Martelino: I did not know that moving to Vancouver and starting a PhD would also lead me to finding my life partner. The support you have provided me throughout this process is indescribable, and I know without this I would not be where I am today. I look forward to the many happy years we have ahead of us.

Table of Contents

List of Tables

List of Figures

List of Acronyms

4-MBA	4-Methyl Benzaldehyde
ACN	Acetonitrile
AEM	Anion Exchange Membrane
AEMFC	Anion Exchange Membrane Fuel Cell
AEMWE	Anion Exchange Membrane Water Electrolyzer
AIBN	Azobisisobutyronitrile
ATR-FTIR	Attenuated Total Reflectance Fourier Transform Infrared Spectroscopy
BTMA	Benzyl Trimethyl Ammonium
Bu	Butyl
Bz	Benzyl
DCM	Dichloromethane
DFT	Density Functional Theory
DMF	Dimethyl Formamide
DMP-PHPI-M	Poly(2-(2,6-dimethylphenyl)-1-methyl-3-hexyl-5-diphenyl-1H-imidazolium)
DMP-PMPI	Poly(2-(2,6-dimethylphenyl)-1,3-dialkyl-5-diphenyl-1H-imidazolium)
DMP-PPI-AD	Poly(2-(2,6-dimethylphenyl)-5-phenyl-1H-imidazolium)-Aldehyde-Diketone
DMSO	Dimethyl sulfoxide
DR	Debus Radziszewski
DVS	Dynamic Vapor Sorption
EA	Elemental Analysis
ECSA	Electrochemical Active Surface Area
EIS	Electrochemical Impedance Spectroscopy
FC	Fuel Cell
HER	Hydrogen Evolution Reaction
HMT-PDMBI	Poly[2,2′-(2,2″,4,4″,6,6″-hexamethyl-p-terphenyl-3,3″-diyl)-1,1′,3,3′-tetramethyl-(5,5′-bibenzimidazolium)
HMT-PMBI	Poly[2,2′-(2,2″,4,4″,6,6″-hexamethyl-p-terphenyl-3,3″-diyl)-1,1′,3,3′-tetramethyl-(5,5′-bibenzimidazolium)

HOMO	Highest Occupied Molecular Orbital
HOR	Hydrogen Oxidation reaction
ICP	Ion Conducting Polymer
IEC	Ion Exchange Capacity
LUMO	Lowest Unoccupied Molecular Orbital
Me	Methyl
MesIm	Mesityl Imidazolium
Mes-PBI	Mesityl Poly(benzimidazolium)
MS	Mass Spectrometry
NMR	Nuclear Magnetic Resonance
OER	Oxygen Evolution Reaction
OPAB	4-(2-oxo-2-phenylacetyl) benzaldehyde
ORR	Oxygen Reduction Reaction
PBI	Poly(benzimidazolium)
PDPI	Poly(2-(2,6-dimethylphenyl)-phenyl-imidazole)
PEB	4-(phenylethynyl)benzaldehyde
PEM	Proton Exchange Membrane
PEMFC	Proton Exchange Membrane Fuel Cell
PEMWE	Proton Exchange Membrane Water Electrolyzer
Ph	Phenyl
PSIM	Poly(Styrene Imidazolium)
QA	Quaternary Ammonium
RDE	Rotating Disk Electrode
RH	Relative Humidity
RHE	Relative Hydrogen Electrode
SEC	Size Exclusion Chromatography
TEA	Triethylamine
TFA	Trifluoroacetic acid
TGA	Thermogravimetric Analysis
THF	Tetrahydrofuran
TMA	Trimethyl Ammonium

TMP-PMPI	Poly(2,2′-(2,3,5,6-tetramethyl)-1,4-phenylene)bis-(1,3-dialkyl-4,5-diphenyl-1H-imidazolium)
TST	Transition State Theory
WE	Water Electrolyzer

Chapter 1.

Introduction

1.1. The Energy Problem

In the past 50 years global energy demand has more than doubled and will continue to rise.[1] By 2045, global energy consumption is predicted to increase up to 75%, in comparison to 2015.[2] However, over 80% of our energy consumption in 2021 was derived from finite fossil fuels such as coal, oil, and natural gas.[1] These fuels when combusted, release greenhouse gases into the atmosphere, contributing to global warming.

Despite the increasing energy demand, the use of renewable energy sources has only increased 1.2 % in the past 50 years (1971 = 12.9 % to 2019 = 14.1 %).[1] A significant roadblock in the integration of renewable energy systems into the energy supply is the lack of reliability.[3] Many renewable energy sources, such as wind, solar, and tidal, vary considerably on a daily and seasonal basis. Often these energy sources will not reach the required energy demand, other times the energy supplied surpasses demand and is wasted. An energy system based on renewable sources must have the ability to store energy and balance out variations.[4]

Hydrogen has emerged as a sustainable fuel to integrate into the renewable energy economy.[5,6] Hydrogen has the highest known energy content of any fuel by mass, is non-toxic and only releases a water by-product when combusted making it a potential energy storage medium for the future economy.[6]

Hydrogen stores energy indefinitely as covalent bonds. Using a fuel cell, hydrogen is combined with oxygen, releasing energy and water as a by-product. However, although hydrogen is the most abundant element in the universe, hydrogen gas is not naturally available. If hydrogen is to be used as a clean energy storage medium, the production must be renewable. Using a water electrolyser, the excess energy from wind, solar and tidal sources, water can be split into hydrogen, with only oxygen as the by-product.[3,7] Coupling water electrolysis with fuel cells creates a hydrogen economy that is sustainable and environmentally friendly.[3,7]

1.2. Zero Gap Electrolysers and Fuel Cells

Water electrolysis (WE) uses energy to split water into hydrogen and oxygen. When the energy is derived from the surplus from solar and wind, WE is a sustainable method for high purity hydrogen production. The basic water electrolysis reaction is described in Equation 1:

$$H_2O + Energy \rightarrow H_2 + {}^{1}/_{2}\, O_2 \qquad (1)$$

The hydrogen and oxygen evolve at the cathode and anode, respectively, which are separated by an electrolyte. The separator can be either a liquid electrolyte which transports the ions, coupled with a porous diaphragm to prevent product gas crossover or a or a solid electrolyte which acts as both the ion transporting material and the gas separator. Electrolysers using a solid polymer electrolyte are known as zero-gap electrolysers, referencing the reduced distance between the electrodes in comparison to a liquid electrolyte.[8,9] The thin device structures enable fast start ups, high energy efficiency and capability for discontinuous operation.[10,11]

The hydrogen fuel can be recombined with oxygen in a fuel cell (FC), generating only water as a by-product. The basic fuel cell reaction is described in Equation 2:

$$2H_2 + O_2 \rightarrow 2H_2O \qquad (2)$$

In this case, hydrogen and oxygen are reduced at the anode and cathode, respectively. Like the electrolyser the anode and cathode are separated by a solid polymer electrolyte, creating zero-gap devices.

The solid polyelectrolyte is an ion conducting polymer (ICP) and exists in two forms within WE and FCs. The first is as an ion conducting membrane between the electrodes and the other is as an ionomer dispersed within the electrodes to enhance ion transport between the catalyst and membrane.

The zero-gap WE and FCs can be separated into two classes:[12] those that use a proton exchange membrane in an acidic environment and those that use an anion exchange membrane in an alkaline environment.

Proton Exchange Membrane Water Electrolyzers and Fuel Cells

In an acidic environment the mobile ions in a Proton Exchange Membrane Water Electrolyser (PEMWE) and Proton Exchange Membrane Fuel Cell (PEMFC) are protons and the reactions that occur at the electrodes of the devices are given in Table 1:

Table 1.1: The chemical reactions that occur in PEMWEs and PEMFCs.

	PEMWE	**PEMFC**
ANODE	$2H_2O \rightarrow O_2 + 4H^+ + 4e^-$	$H_2 \rightarrow 2H^+ + 2e^-$
CATHODE	$2H^+ + 2e^- \rightarrow H_2$	$4e^- + 4H^+ + O_2 \rightarrow 2H_2O$

However, the acid environment inside these devices requires the use of costly and environmentally damaging materials.[13] All metal parts must be corrosive-resistant in acidic conditions which results in the continued use of expensive platinum group metal catalysts.[13,14] The ion conducting polymers in acidic PEMFCs and PEMWEs must be fluorinated to prevent degradation, further increasing the stack cost.[15,16] In an acidic environment, hydroxyl radicals are formed and degrade the organic polyelectrolytes.[17–19] Fluorinating the material is an effective way of mitigating radical degradation, however these perfluorinated ICPs have been found to be both health and environmentally hazardous. Whilst there has been research into the development of hydrocarbon ICPs for acidic devices to move away from the perfluorinated materials,[16,20] shifting to a high pH environment has the potential to alleviate the cost associated with PEMWE and PEMFCs.[21,22]

Anion Exchange Membrane Water Electrolyzers and Fuel Cells

In an alkaline environment the mobile ion is the hydroxide anion and the reactions that occur at the electrodes are given in Table 2:

Table 1.2: The reactions that occur in AEMWEs and AEMFCs.

	AEMWE	**AEMFC**
ANODE	$2H_2O + 2e^- \rightarrow H_2 + 2OH^-$	$2OH^- + H_2 \rightarrow 2H_2O + 2e^-$

CATHODE	$4OH^- \rightarrow O_2 + 4e^- + 2H_2O$	$O_2 + 2H_2O + 4e^- \rightarrow 2OH^-$

Using a high pH environment increases the number of materials available for use in AEMWE and AEMFC.[21,23] In particular, there are viable options for non-platinum group metals as the catalysts.[24] The variety of metal materials available applies not only to catalysts but also to the entire AEMWE/FC stacks, further reducing the cost of the devices.[23]

In an alkaline environment, the hydroxide anion is the mobile ion species and is generally considered as the main cause of ion conducting polymer degradation for AEMFCs and AEMWEs.[25,26] Although recent publications have shown the formation of radical species may also have an impact on the stability of the hydroxide conducting polymers,[27,28] there has been a focus on the development of hydrocarbon based hydroxide ion conducting materials. However, there are two main problems with hydrocarbon ICPs in alkaline devices: (i) low hydroxide conductivities, particularly when compared to H^+ conductivity in PEMWE/FCs[29] and (ii) low stabilities of ion conducting polymers with hydroxide counterions, especially at low hydrations.[26,30] However, these issues are not considered insurmountable by the field and a great deal of attention has been focused on ICP material design to progress AEMFC and AEMWE development.

1.3. Material Design Considerations

For effective ion conducting polymer material design, the relationship between chemical structure and observed macromolecular properties must be understood. The synthetic route, backbone structure, cationic group, and functionalization all have important and intertwining implications on the properties of the final material. Beginning from the polymerisation method, this section explores potential design choices available for informed development of high performance ICPs for alkaline energy conversion devices.

1.3.1. Polymer Synthesis

Synthetic polymers can be classified into two categories based on the synthetic route.[31] Chain and step polymerisations differ through the reactive species and the relationship between molecular weight and monomer conversion (Figure 1.1).

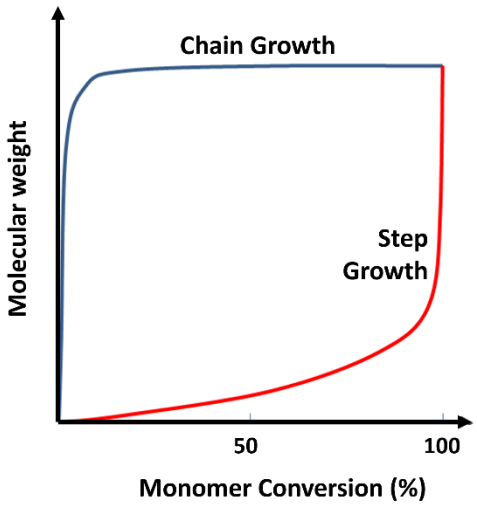

Figure 1-1: The molecular weight change for chain growth (blue line) and step growth (red line) polymerisations with respect to monomer conversion.

Chain Growth Polymerization

Chain polymerisations occur through the addition of an initiator compound that reacts with a monomer species to create a reactive centre on the monomer. The reactive centre propagates the polymerisation by the sequential addition of monomer molecules.[32] A key characteristic of the chain polymerisations is that polymer growth only occurs when the monomer reacts with an initiated reactive centre. In this case, the molecular weight of the increases rapidly with low monomer conversion as many reactive centres are initiated simultaneously enabling chain growth propagation. Then, as the concentration of reactive centres decreases, the molecular weight plateaus and the polymerisation terminates when the reactive centre is quenched.

Chain growth polymers are categorised by the initiator species used, with the most common initiator being a radical species. Most monomers will undergo radical initiation, but the rate of reaction determines the viability of the polymerisation. The rate of monomer initiation depends on the inductive and resonance characteristics of the substituents present. For example, despite the C=O bonds of aldehydes and ketones being one of the most used linkages for radical initiation, the polarizability of the carbonyl groups limits stable radical formation. Therefore, vinyl groups are the commonly used group for radical chain growth polymerisations. Resonance stabilisation of the propagating radical occurs

with almost all substituents by delocalizing the radical over two or more atoms, limiting possibility of the reactive site being quenched and therefore improving the polymer molecular weight.

Step Growth polymerizations

Step polymerisations occur through the reaction of difunctional monomers,[33–35] where the monomers react in a stepwise manor to create dimers, trimers and tetramers *etc*., Due to the stepwise nature of the reaction, the molecular weight of the polymer increases slowly with low conversion of monomers (Figure 1.2). At high monomer conversion, reactions result in long chains connecting and rapidly increasing the molecular weight. An important distinction between step polymerisations and chain polymerisations is, in step polymerisations, the reactions occur between any sized polymer chain, whereas in chain polymerisations the reactions only occur between the monomer and the propagated reactive centre on the polymer main chain.

Step growth polymerisations can be separated into two categories based on the type of monomer used. AA-BB step growth reactions require two different monomer molecules, whereas the AB-type step growth polymerisation only require one monomer unit. The intricacies, along with the pros and cons of each method are discussed in the next sections.

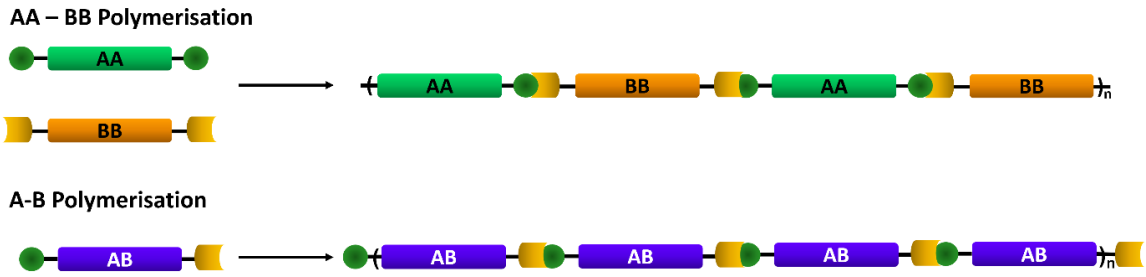

Figure 1-2: The different synthetic routes for step growth polymerisations. ***AA – BB requires two monomers (monomer AA in green and monomer BB in orange). Monomer AA has two identical end group functionalities (green circles), that react with monomer BB's end group functionalities (orange curves). AB requires only one monomer (AB in purple) with two different end groups (green circles and orange curves).***

- **AA+BB step growth**

In the AA-BB method, two different bifunctional monomers are used, where each monomer only possess a single type of functional group (Figure 1.2) and react together to form the polymer. However, to attain high molecular weights, there must be near to exact stoichiometric quantities of the two monomers. Having an imbalance of either functionality will result in polymer chains that only have end groups of the higher stoichiometry functionality, effectively terminating the polymerisation. Quantitatively, the number average degree of polymerisation ($\bar{X}_n$) can be related to the concentration of each functional group (N_A and N_B), extent of reaction (p), and the stoichiometric ratio of functional groups (r) by equation (3):

$$\bar{X}_n = \frac{N_A \left(\frac{1+1}{r}\right)/2}{[N_A(1-p) + N_B(1-rp)]/2} = \frac{1+r}{1+r-2rp} \tag{3}$$

When there is an exact stoichiometric amount of N_A and N_B ($N_A = N_B$), $r = 1$. In this case, the degree of polymerisation is only related to the extent of reaction (p):

$$\bar{X}_n = \frac{1}{1-p} \tag{4}$$

Equations (3) and (4) quantify the importance of a stoichiometric balance of functionalities for high molecular weight AA-BB type step polymerizations. However, there are practical limitations to perfect stoichiometric balance. Often very small quantities of water, impurities, or even balance error, will result in $r \neq 1$.

- **AB Step growth**

In the case of AB step growth polymerisations, only one monomer is required with two different functionalities (Figure 1.3). One functionality of the AB monomer will react with the corresponding functionality on a different molecule to undergo polymerisation. The main benefit of AB step growth polymerisations is the internally defined stoichiometry of functional groups. In this case, the degree of polymerisation only depends on equation (4) as the monomer design defines $N_A = N_B$, regardless of impurities. Theoretically, the polymerisation dependence only on equation (4) makes high molecular weight AB-type step growth polymers more attainable.

Using a single difunctional monomer also gives an accurate knowledge of both end group functionalities, enabling reactions to occur specifically at the end groups of the polymer (Figure 1.3). Using this knowledge copolymers can be created by reacting two AB-type polymers with known and complementary end groups, leading to the formation of highly defined and controlled copolymers. The end groups can also be end-capped using a complementary small molecule which can be useful for the control of further reactions.

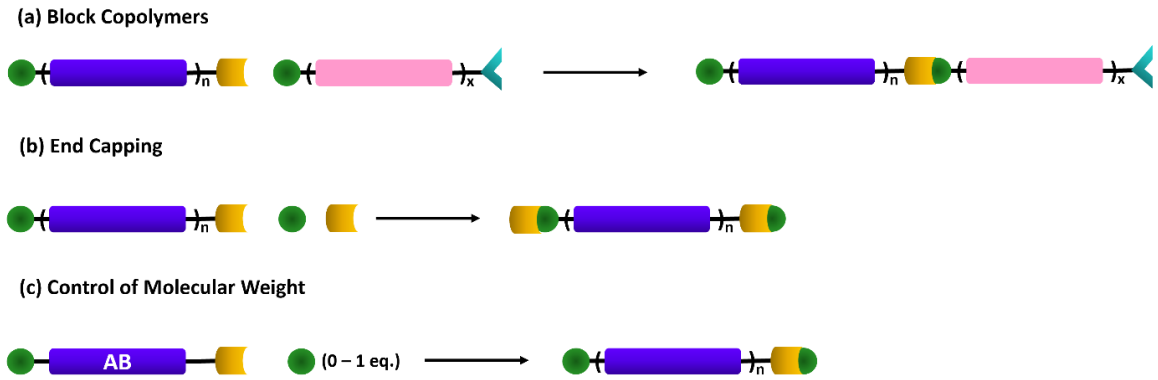

Figure 1-3:The different reactions available for polymers with known end groups. ***(a) AB-type polymers (purple and pink) have known end groups (green circles, orange curves, and blue triangles. The compatible end groups (green circles and orange curves) of the two different polymers can react together to form a copolymer. (b) the end groups (green circles and orange curves) can be reacted with compatible functionalities to end-cap the polymer to prevent any further reactions from taking place. (c) the AB monomer can be reacted with varying amounts of a compatible end capping reagent to control the termination of the polymerisation reaction and leading to a control of molecular weight.***

1.3.2. Ion Conducting Polymers

Most electrochemical conversion and storage devices rely on the integration of ion conducting polymers into the systems.[20] ICPs, often named polymer electrolytes for their role in device ion transport, can exist with either a positive or negative fixed charge. Polyanions are negatively charged with positive counterions and polycations are positively charged with negative counterions. The ICPs can exist as either ionenes,[36] where the charged group is integrated into the backbone, or as pendant chain polymers,[37] where the charged group is attached to an uncharged backbone through a linker unit (Figure 1.4).

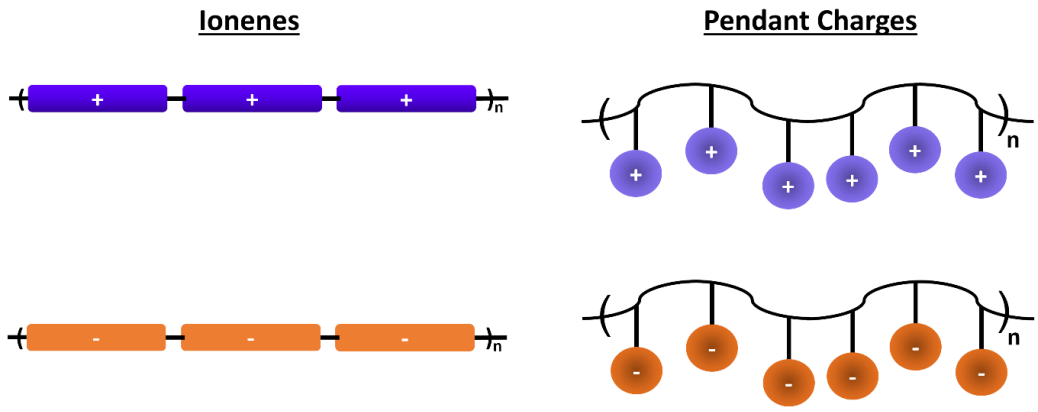

Figure 1-4: The structural difference between ionenes and pendant charged polymers.

Polycations

Polycations have immobilised positive charges integrated into the polymer structure and can transport anions to be used as an electrolyte Some of the most commonly used cationic groups are quaternary ammonium, [30,38,39] quaternary phosphonium,[40,41] guanidinium, [42] benzimidazolium[43–45] and imidazolium.[43,46–48] These cationic groups can be embedded in in the backbone of the polymer to create an ionene[36] or as pendent chains attached to an uncharged backbone.[37] When the cation is a pendant group there is a variety of backbones available such as: poly(arylene ether)-based, poly(olefin)-based, and polyphenylene-based backbones.[25]

Within this thesis, polycations will be discussed for integration into alkaline-based devices such as AEMFCs and AEMWEs. Within these devices, the cationic ion conducting polymers must exhibit high hydroxide conductivity, thermal and alkaline stability. The low mobility of the hydroxide ion, relative to protons, has encouraged the development of cationic ICPs with a high number of cationic groups. However, the strong nucleophilic character of the hydroxide limits the available structures for polycation synthesis, as few organic materials can withstand such high pH. The relationship between ICP chemical structure and the observed macromolecular properties (alkaline stability, conductivity, water uptake *etc.*) is nuanced and, in many cases, complementary. For a full

understanding of the design considerations associated with the development of cationic ICPs for AEMWE/FC applications, the desirable macromolecular properties must be discussed in detail. The next section reviews various design considerations for a high performance cationic ICP material and the methodologies used for structure-property correlations.

1.3.3. Polycation Design Considerations

The development of high-performance ion conducting polymers relies on several key characteristics: (i) convenient synthetic scalability, (ii) high ion conductivity, (iii) high chemical and thermal stability, (iv) robust mechanical properties. However, designing a polyelectrolyte that satisfies all the required criteria is challenging as many of the characteristics are connected and have trade-off effects.

Hydroxide ions exhibit extremely high conductivities, attributable to the high mobility in aqueous solutions.[49] However, in comparison to proton conducting polyelectrolytes, the first hydroxide conducting materials exhibited much lower ionic conductivities,[50] attributable to the diffusion coefficient of OH^- being almost half of the H^+ diffusion coefficient.[51] The diffusion coefficient of an ionic species is proportional to the mobility,[52] and is a key variable in the definition of ionic conductivity (σ) which can be expressed using Equation 5:

$$\sigma = Fc\mu \tag{5}$$

where F is Faraday's constant, c is the molar concentration of charge carriers and μ is the mobility of charge carriers. Despite the lower mobility of hydroxide ions, in comparison to protons, the design of materials can be targeted to achieve a high concentration of charge carriers and high ion mobility to improve the overall conductivity of hydroxide conducting polyelectrolytes.

The theoretical molar concentration of charge carriers can be defined by the ion exchange capacity (IEC) of a polyelectrolyte. The IEC describes the number of charged functional groups per unit mass of polymer (mmol/g) and can be calculated using Equation 6:[53]

$$IEC_{theoretical}(mmol/g) = \frac{n|Z|\varphi_{+/-}}{M_{+/-}\varphi_{+/-} + M_0\varphi_0} \times 1000 \quad (6)$$

where n is the number of charges per repeat unit, $|Z|$ is the absolute charge on the repeat unit, $\varphi_{+/-}$ is the mole fraction of positive or negative units in the polymer, dependent on whether polycations or polyanions are being studied, φ_0 is the mole fraction of neutral units, $M_{+/-}$ is the molecular weight of the positive or negative units and M_o is the mole fraction of neutral units. Each charged unit on the polyelectrolyte will have a corresponding mobile charge carrier, otherwise called the counterion, therefore increasing the IEC will increase the molar concentration of charge carriers. Incomplete dissociation of the counterions from the polymer backbone will limit the concentration of charge carriers that are mobile within the polyelectrolyte, regardless of the IEC, and negatively impact the ion conductivity.[54] Synthetically, counterion dissociation can be improved by delocalizing the immobilized charges across the polymer backbone using conjugated systems[55] or by increasing the spatial segregation of stationary and mobile ions through polyelectrolyte microphase separation with block copolymers.[56]

The ion mobility through the polyelectrolyte is more challenging to control and is influenced by polymer segmental motion, counterion dissociation and the distribution of hydrated polymer domains.[54,57] The segmental motion of polyelectrolytes promotes ion movement through the formation and destruction of a coordination sphere around the mobile ion. The variation of coordination sphere enables the creation of free volume within the polyelectrolyte, allowing for ion diffusion under the influence of an electric field.[58] The Vogel-Fulcher-Tammann equation (Equation 7) is commonly used to elucidate the impact of segmental motion,[54] related to the activation energy for conduction (E_a) on overall conductivity, at a given temperature (T):

$$\sigma = Aexp\left(-\frac{E_a}{R(T - T_0)}\right) \quad (7)$$

where the preexponential factor (A) represents in intrinsic conductivity at very high temperature. T_0 is the Vogel temperature, typically taken as 50 °C below the glass transition temperature (T_g) in polyelectrolytes,[59] and R is the gas constant. Below T_0 there is assumed to be no free volume. Equation 7 suggests that the thermal motion above T_0 contributes to the relaxation and transport processes that govern ionic conductivity. The relationship between increased segmental motion and improved ionic conductivity, following the Vogal-Fulcher-Tammann relationship, has been demonstrated by reducing T_g of various polyelectrolytes to improve ionic conductivity.[60,61]

The activation energy of hydroxide transportation through the polyelectrolyte is also governed by the diffusion mechanism through water-filled nanodomains.[62] In materials with large sections of free volume, the hydroxide transport is controlled by a vehicular mechanism where the ions diffuse through the water-filled space.[57,63] However, in materials with limited free volume and the charge transport is governed by the hydroxide mobility through a subnanometer wide water channel network, Grotthuss hopping has a lower activation energy and is therefore the main transport mechanism.[64,65] Whilst it is challenging to synthetically control the distribution of free volume and water channels, studies have investigated the relationship between hydroxide conducting polyelectrolytes, morphology, water uptake and ionic conductivity, where the use of flexible side chains facilitates the formation of a microphase-separated morphology.[66–69]

The IEC can also be used to modulate water uptake in ICPs. As the number of charged polymer units increases to increase the IEC, the overall polarity of the ICP is also increased, and therefore so is the water solubility. Thus, increasing the IEC of the ion conducting polymer, increases the water uptake of the sample. The relationship between IEC and water uptake is given by the water content (λ), or hydration number, of the material in equation (8):[70]

$$\lambda = \frac{WU\ (\%) \times 10}{IEC_{exp} M_{H_2O}} \tag{8}$$

where M_{H_2O} is the molar mass of water in g/mol. However, An ICP with a high water uptake and hydration number will likely exhibit excessive dimensional swelling.[71] Dimensional swelling is the percentage expansion of a fully hydrated ICP, in comparison to a the dry ICP. High ICP swelling can result in poor mechanical integrity due to the negative impact

of excess water on chain entanglements.[72] If the water uptake is too high the ICP will dissolve in water, resulting in a material that is incompatible with electrochemical devices. Water uptake, hydration number, and dimensional swelling of the ICPs are effected by the IEC, but are also affected by the type and concentration of charge carriers,[51] along with crosslinking[73] and ICP reinforcement.[74]

Despite the importance of high ICP ionic conductivity, the chemical stability of hydroxide conducting polyelectrolytes has been at the forefront of material development. The highly nucleophilic hydroxide ion is known to readily degrade organic polyelectrolytes and the development of alkaline-stable materials will be discussed in Section 1.3.4 of this thesis. To characterise chemical stability of ICPs, the materials are immersed in highly basic solutions,[75,76] and NMR is used to observe any chemical changes,[76] and water uptake, IEC and conductivity measurements are used to observe loss of charged functionalities, and tensile strength testing to probe the impact on mechanical properties.

For these properties, a balance is required to obtain an ICP that has sufficient properties for the selected application (Figure 1.5). There is a focus on highly conductive and alkaline stabile ICPs, however, to develop a material that is suitable for alkaline electrochemical conversion devices, a balance of many macromolecular properties must be considered. This is of particular importance when developing highly conductive cationic ICPs where increasing the IEC can result in a material that is mechanically unstable due to high dimensional swelling or soluble in aqueous solutions that prevents integration into devices.

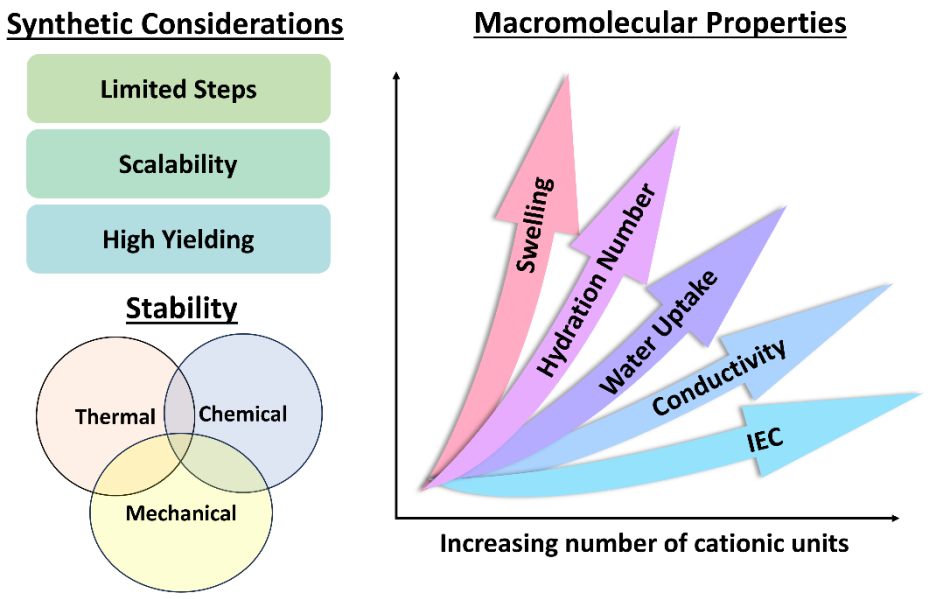

Figure 1-5: The various design considerations for cationic ICPs.

1.3.4. Cationic ICP Structures

Pendant Group ICPs

Cationic ICPs with a neutral backbone and cationic side groups are generally considered as pendant group ICPS (Figure 1.4). In these cases, the characteristics of the backbone and cationic groups have been discussed in the literature separately, as neutral backbone and molecular cation, to elucidate each specific contribution to the polycationic materials. Then informed design choices could be made to synthesize the pendant group cationic ICPs with the best likelihood of high alkaline stability. In this section, the polymer backbone and cationic group will be discussed separately, along with the impact of integrating the two components.

- **Backbones**

In an acidic environment, polymer backbones containing aryl ether bonds such as poly(phenylene oxide) and poly(arylene ether sulfone) were shown to have high thermal and oxidative stability and were therefore the first backbones to be tested for AEM

applications. Other backbone chemistries integrated into AEMs are polysulfones,[77] polyphenylenes,[78] poly(aryl ether ketones),[79] poly(phenylene oxides),[80] and polystyrenes (Figure 1.6).[81] These backbones, when used in alkaline conditions without a cationic group, showed good stability with respect to hydroxide degradation.[82] Despite the rotational freedom around the heteroatom linkages (aryl C-O or C-S) improving polymer solubility,[83] it was found that the presence of any electron withdrawing group, such as the pendent cations, facilitates degradation of the ether and sulfone linkages on the polymer backbone.[84] The cationic group at the *ortho* positions of the C-O bonds pull electron density from the backbone, facilitating the ether bond cleavage.[85,86] This degradation mechanism was shown to become more severe when electron withdrawing groups, such as the sulfone linkages, were adjacent to the phenyl rings (Figure 1.6).[84] It was also suggested that the instability of the cationic groups may be triggered by the cleavage of ether bonds (Figure 1.6).[83] The effect of ether linkage degradation was mitigated by the addition of a spacer group between the cation and backbone,[87] but despite this the alkaline stability of heteroatom backbones inhibits further integration into AEMFC and AEMWEs.

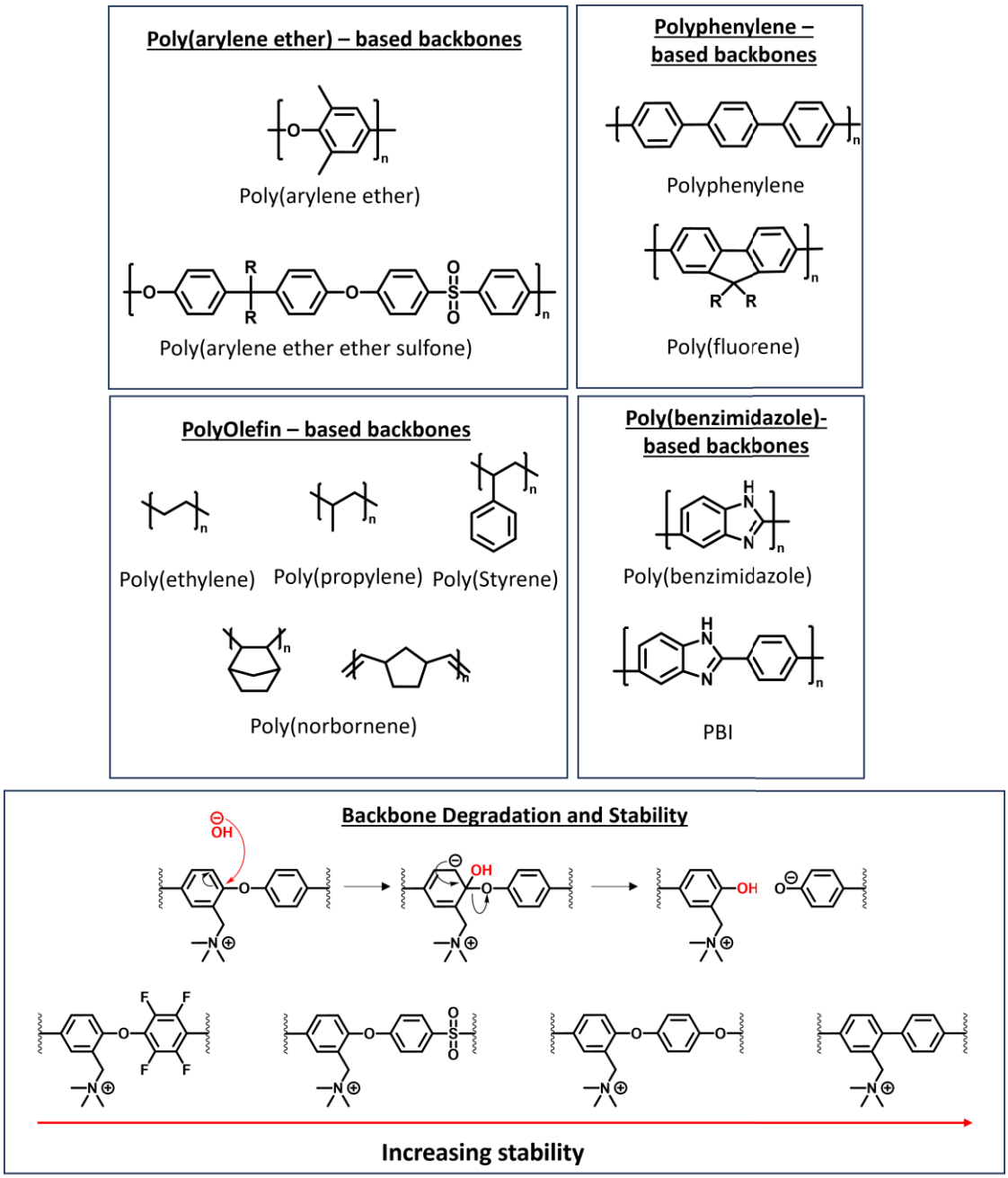

Figure 1-6: The different available polymer backbones. ***The degradation pathways of poly(arylene ether) backbone, along with the impact of electron withdrawing groups on said backbone are indicated.***

Heteroatom-free, all-carbon backbones, such as polyolefins and polyphenylenes have been shown to possess no facile hydroxide-mediated degradation pathways.[84,88] The all-aromatic polyphenylene backbones enables the resulting ICPs to possess the high

glass transition temperatures, high impact strength and high chemical, thermal and mechanical stabilities that are characteristic of polyaromatics.[89] However, integration of the cationic group requires post-polymerisation functionalization of the polyaromatic backbone. Using this method, the degree and location of the cationic functionalities are challenging to control, and side products can be difficult to identify.[82]

Polyolefin backbones, in particular, have been shown to exhibit extremely high alkaline stability, where Mohanty *et al*.,[84] observed minimal molecular weight change after alkaline treatment of a polystyrene-based backbone. This study also highlighted the challenges associated with post-polymerisation functionalization, where the authors struggled to achieve a polyolefin structure with a high degree of functionalization and without the presence of side reactions.[84] However, the radical step growth polymerisation mechanism used to synthesise polyolefins allows for the incorporation of cationic functionalities prior to polymerisation to alleviate the functionalization issues whilst utilizing the highly alkaline stable all-carbon backbone (Chapter 6).

- **Cations**

The electrophilic cationic groups are the most susceptible to hydroxide attack in pendant group ICPs, and therefore considerable effort has been taken to create highly stable cationic groups for polycationic electrolyte applications. There have been numerous alkaline stability reports of small molecular analogues of polycations.[21,38,39,41,76,90–94] Although the small molecule studies do not fully represent the cation stability when integrated into a polycation structure, it does offer valuable insights into the potential degradation mechanisms and possible alkaline stable cationic groups.

Quaternary ammonium (QA) cations are the most common pendant groups incorporated onto the uncharged polymer backbone, due to their synthetic ease and high conductivity.[39] However, model compound QA cations have been shown to be generally unstable at high pH, an effect that is exacerbated at the elevated temperatures required for alkaline devices.[38] Benzyltrimethylammoniums (BTMA) have been regularly employed as QA cations, with benzyl acting as the linker to the backbone.[95] However, the BTMAs degrade through Hoffmann elimination of the hydrogen at the β position, which has been proven to be detrimental to the stability of the linkers binding the backbone and QAs.[38,39] Removing the β-hydrogen has little impact on stability as the trimethylammonium cations

(TMA) have been shown to degrade via S_N2 nucleophilic substitution of the -CH_3 group, removing the methyl group to form methanol.[38,96]

Several cations have emerged in recent years to combat the instability of the QAs. These include cyclised QAs such as pyrrolidinium cations that have shown better electrochemical stability than traditional QAs.[38] Phosphonium cations with electron withdrawing groups without α-hydrogens or with sterically hindered α-hydrogens, have been shown to have high stability in 15 M KOH.[97] Guanidinium cations with electron donating groups have reasonable stability in alkaline conditions and have been used as ionomers in AEMFCs.[98,99] Pyridinium cations and metal-ligand complexes have started to become of interest with improved stability in high pH conditions.[100] Benzimidazolium and imidazolium model compounds have been well-studied for alkaline stability,[43,44,91,101–104] with steric encumberment around the electrophilic C2-position being the key to limiting hydroxide attack. However, the complicated chemistry associated with incorporating these groups onto a polymer backbone has limited investigations into these cations as pendant groups.

Despite the studies into novel cationic groups for high stability, incorporating these cations into a polymer has proven to be somewhat challenging.[37] Cations are often added through a post-functionalization step on the already synthesised polymer backbone, the degree and location of such additions are challenging to control and can be limited by the solubility of the polymer backbone. In some cases, the functionalization occurs through a multistep process during which side reactions may occur and can be challenging to detect.[84] Most importantly, there is often a focus on facile bond formation of the linker unit between the polymer and cation, which can be subsequently easy to degrade in harsh environments, such as the commonly used benzyl linker.[83] Therefore, there has been an increased interest in the development of ionenes with the cation integrated as the polymer backbone.[36] Synthesising the functionality as part of the polymerisation defines the location of the cations and alleviates the requirement for any linker units that could impact the stability of the ICP.

Ionenes

Classically defined as polymers which contain ionic amines in the backbone, ionenes are of great interest in the development of ICP materials for alkaline devices.[36] Ionenes have diverse synthetic routes that has enabled the development of materials that

are highly stable in the alkaline conditions and can be incorporated into AEMWEs and AEMFCs.[36]

- **Poly(benzimidazolium)s**

Recently cationic poly(benzimidazolium)s have been developed as a class of high-performance ionenes.[36,101,104,105] The synthesis of poly(benzimidazolium)s occurs through a two-step N-functionalization of commercially available poly(benzimidazole)s (PBIs) (Figure 1.7).[105] A typical procedure requires the deprotonation of the benzimidazole N***H*** with base, followed by the addition of an alkyl or aryl halide. The second N-functionalization proceeds through a slower reaction that usually requires heating, with excess of the alkyl/aryl halides. The final product is a polycationic poly(benzimidazolium) with a halide counterion that can be used as a polyelectrolyte.

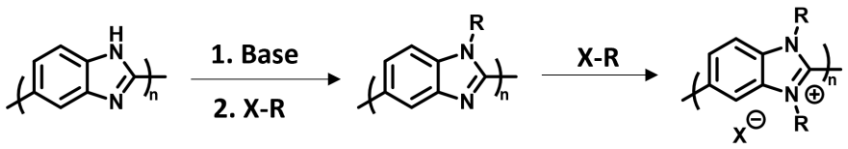

Figure 1-7: Synthetic route for N-functionalisation of poly(benzimidazole)s. ***The deprotonation step is followed by functionalisation with an aryl or alkyl halide. The quaternization is completed by a second N-functionalisation, again with an alkyl or aryl halide. The same N-functionalisation route is used for poly(imidazole)s.***

Synthesis of the poly(benzimidazolium)s provided a wealth of opportunity for this molecule class to be used as a ionene ICP in AEMFCs and AEMWEs.[106] However, the poly(benzimidazolium)s exhibited low alkaline stability.[107] The positive charge on the benzimidazolium group increases the electrophilicity of the C2 position which is readily attacked by hydroxide and degrades via a ring opening mechanism (Figure 1.8). Attempts to stabilise the C2 position were conducted by adding electron-donating substituents to the C2-aromatic ring and adding bulky groups to the N-atoms.[108] Although these methods did supress degradation, it was on the scale of days in 1 M KOH, not nearly stable enough to incorporate into alkaline devices. The most effective method for suppression of the hydroxide mediated degradation at the C2 position is to add steric crowding on the C2-phenyl group (Mes-PBI, Figure 1.9(a)).[104] The addition of 2,6-dimethyl units onto the C2-phenyl group forces the mesityl group to sit at 90 ^{o}C to the benzimidazolium ring, sterically encumbering hydroxide attack at this position. The C2-protected poly(benzimidazolium)

was observed to have no degradation in 2 M KOH solutions at 60 °C over a period of 10 days.[104]

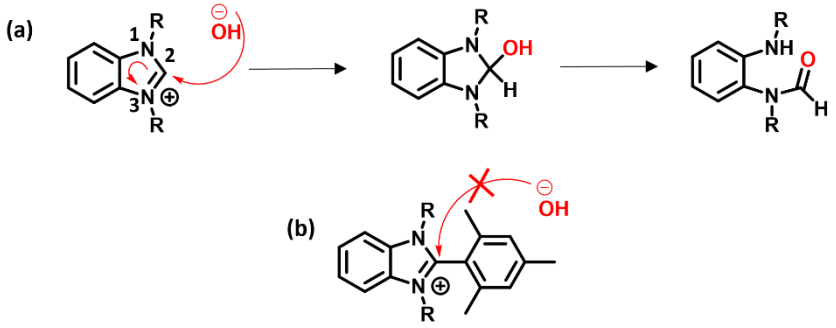

Figure 1-8: The main hydroxide-mediated degradation mechanism for benzimidazoliums. ***(a) The nucleophilic hydroxide attacks the C2-position resulting in the formation of an uncharged alcohol and subsequent ring opening. (b) the incorporation of a mesityl group in replacement of the C2-phenly group physically blocks hydroxide attack at the C2 position.***

However, Mes-PBI (Figure 1.9(a)) had a very high IEC of 4.5 mmol/g, resulting in a water-soluble polymer that hindered its applications in electrochemical cells with aqueous environments.[104] In subsequent work, the alkylation step was controlled to reduce the number of cationic benzimidazolium units on the polymer chain and a hydrophobic aromatic group was added to yield HMT-PDMBI (Figure 1.9(b)).[101] This polymer was highly stable in alkaline environments, water insoluble but methanol soluble for improved processability. The additional aromatic group also increased the distance between the adjacent benzimidazolium cation, a method that had previously been shown to improve the thermal and chemical stability of poly(benzimidazolium)s.[109] The next iteration saw a poly(benzimidazolium) with three distinct blocks (HMT-PMBI, Figure 1.9(c)): (i) with 50 % methylation, for an uncharged Mes-PBI block (ii) a 75 % methylated block where half of the repeat units were charged poly(benzimidazolium)s and the other half were uncharged Mes-PBIs and (iii) with 100 % methylation and every repeat unit is a charged poly(benzimidazolium).[110] HMT-PMBI was highly stable in alkaline conditions, showing no degradation in 1 M NaOH at 80 °C, over 7 days and the mechanical properties were reported to be superior to that of industry standard Nafion 212. When incorporated as a membrane and ionomer in an AEMFC, HMT-PMBI demonstrated > 100 h of operation and achieved the first fully restored restart of an AEMFC.[110]

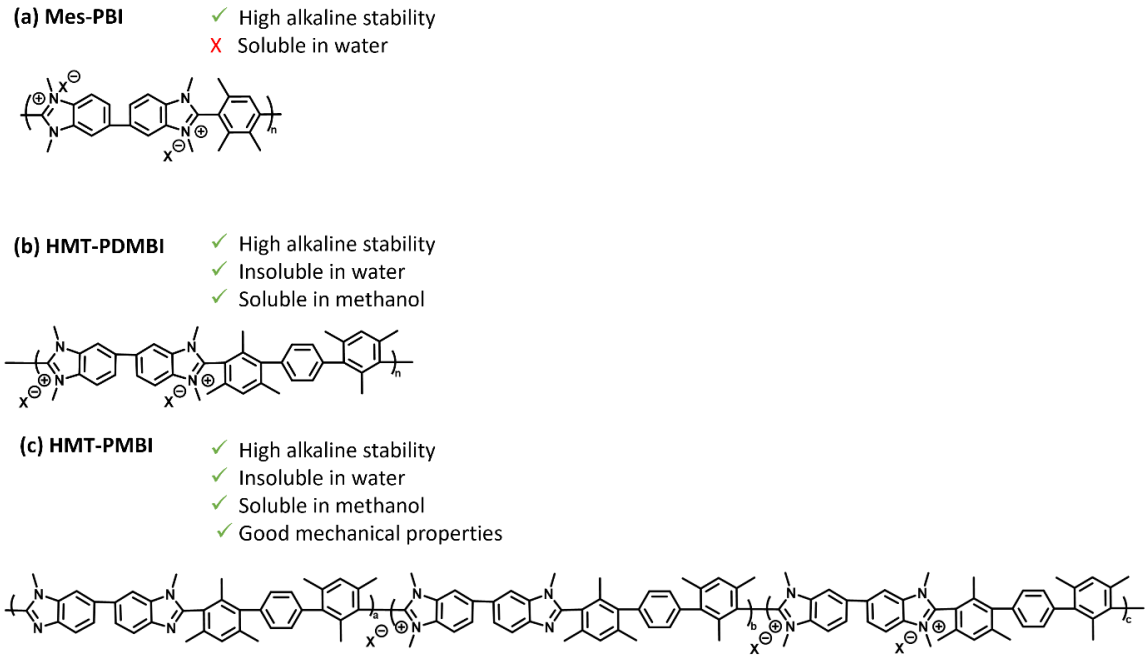

Figure 1-9:The poly(benzimidazolium)s discussed. ***(a) Mes-PBI was the first C2-protected poly(benzimidazolium), followed by (b) HMT-PDMBI with improved solubility for simple processability and then (c) HMT-PMBI that exhibited high alkaline and thermal stability, in addition to improved mechanical properties.***

- **Poly(imidazolium)s**

There have been a number of studies ranging from theoretical DFT, to experimental model compound investigations that suggest N-functionalised imidazolium cations are more stable against C2-hydroxide attack than benzimidazoliums.[43,103] The imidazolium model compounds were shown to have a lifetime 10 times as long as the benzimidazolium, in high pH conditions.[103] For this reason, the focus for ICPs in alkaline devices shifted from poly(benzimidazolium)s to poly(imidazolium)s.

The Debus-Radziszewski (DR) multicomponent reaction is an efficient route for imidazole, poly(imidazole), and poly(imidazolium) synthesis (Figure 1.10).[111] Reacting an α-dicarbonyl, an aldehyde, and ammonia or ammonium, in acidic conditions will form a heterocyclic imidazole. When the α-dicarbonyl is a 1,2-diketone, high temperatures are

required (120 °C) but will form a high yielding, highly pure trisubstituted imidazole.[112] Poly(tri-arylimidazole)s can be synthesized *via* the DR reaction,[111] using a *bis*-1,2-diketone and a dialdehyde in the presence of ammonium acetate and acetic acid, an AA-BB step growth polycondensation occurs. In this case, the polymer backbone consists of 2,4,5-trisubstituted imidazoles and occurs through the same DR mechanism as the small molecule synthesis (Figure 1.10). A C2-protected trisubstituted poly(imidazole) can be synthesised if methyl units exist at the meta positions on the dialdehyde monomer.[103] HMP-PMPI (Figure 1.11(c)) was the imidazolium analogue to HMT-PMBI (Figure 1.11(c)) but exhibited superior alkaline stability (>5000 h in 10 M KOH at 100 °C), but the high level of N-methylation resulted in a high IEC (2.61 mmol/g) and therefore solubility in water at 80 °C.[103]

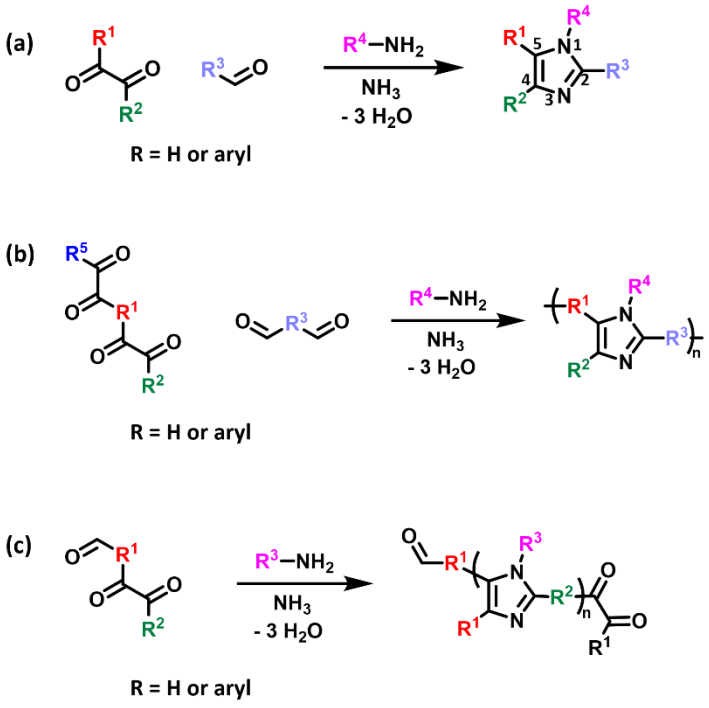

Figure 1-10: Imidazole synthesis using the DR reaction. ***(a) a general synthesis for small molecule imidazoles, (b) a general synthesis for poly(imidazole)s from AA-BB type step growth polymerisations and (c) a general synthesis for poly(imidazole)s synthesised from AB type step growth polymerisations.***

Trisubstituted poly(imidazole)s can be synthesised through AB step growth polycondensation, utilising the DR reaction (Figure 1.10(c)).[53] Similarly, to the PBI work by Vogel and Marvel,[113] an AB type monomer can be synthesised but with aldehyde and

diketone functionalities. The C2 protection can be incorporated by addition of methyl groups at the meta positions at the aldehyde functionality.[114] This poly(imidazole) can be subsequently alkylated twice to form the poly(imidazolium), DMP-PMPI (Figure 1.11(c)). The low solubility of the poly(imidazole) hindered the alkylation steps and resulted a low number of charged imidazolium repeat units and DMP-PMPI therefore had a low experimental IEC and conductivity.

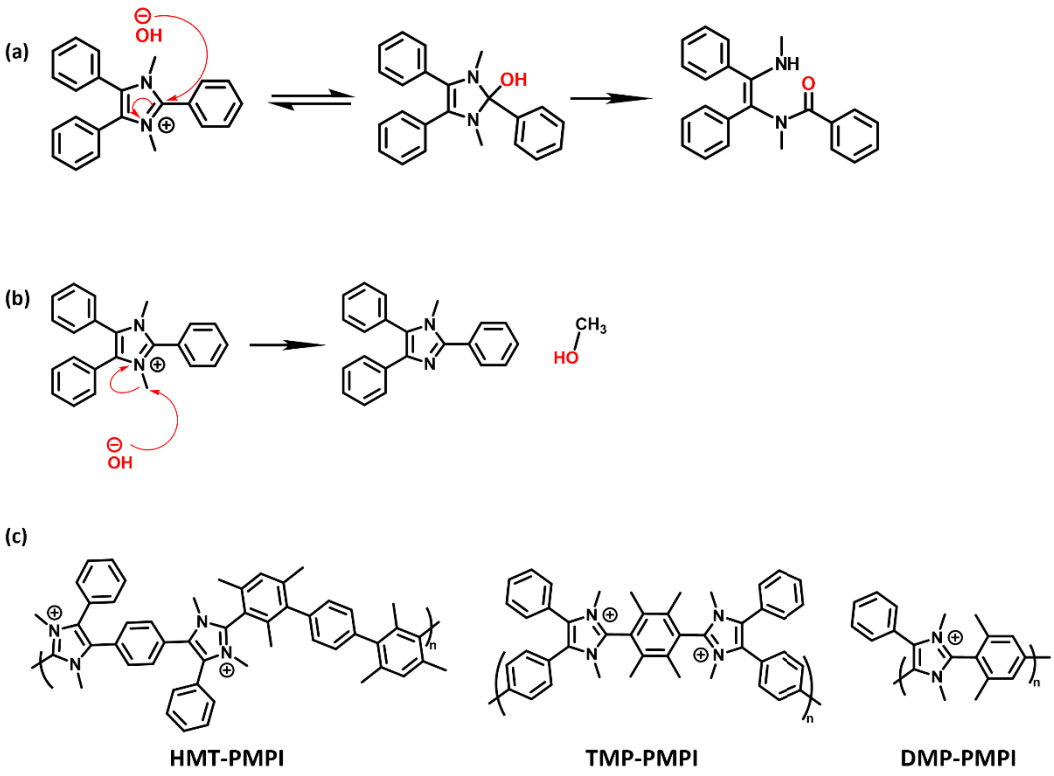

Figure 1-11: The two main imidazolium hydroxide-mediated degradation pathways. ***(a) the C2 hydroxide attack that leads to imidazolium ring opening and (b) the defunctionalisation mechanism that is observed when the C2 steric encumberment prevents hydroxide attack and subsequent ring opening. (c) the different poly(imidazolium) chemistries discussed in this section.***

Trisubstituted imidazoles can also be used as the monomer units.[111] A trisubstituted arylimidazole-containing dicarboxylic acid monomer was synthesised from diethyl-4,4'-benzildicarboxylate, benzaldehyde and ammonium acetate, in acetic acid, followed by a hydrolysis of the ester units to form the carboxylic acids and were polymerised with different aromatic amines. [115] C2-protected poly(imidazolium)scan be

synthesised from *bis*-imidazole monomers with a single N-functionalisation.[102] In this case, the C2-protected trisubstituted imidazoles are formed from 2,3,5,6-tetramethyldialdehyde and 4-chlorobenzil, in the presence of ammonium acetate. The dichloro-imidazole precursor was N-alkylated to create the monomer. The single N-alkylation enhanced the solubility of the monomer to reach higher molecular weight poly(imidazole)s through a nickel catalysed Yamamoto Coupling polymerisation step and the second N-alkylation yielded poly(imidazolium) TMP-PMPI (Figure 1.11(c)). However, despite the suppression of the C2 degradation pathway through steric encumberment, dealkylation of the N-functionalities started to occur (Figure 1.11(a),(b)). Investigation of the dealkylation found that adding long alkyl chains as the N-functionalities improved the half-life of imidazolium model compounds in 3 M NaOD to over 10,000 h. Incorporating long butyl chains as the N-functionalities in TMP-PMPI created an ICP that degraded only 2.3 % in 10 M KOH at 80 ^{o}C over 10 days. TMP-PMPI was used as a membrane and ionomer in AEMFCs and AEMWEs, showing promising performance and chemical durability.[102]

1.4. Thesis Overview

The following chapters of this thesis describe the investigation of novel poly(imidazolium)-based cationic ICPs for potential integration into electrochemical conversion devices such as AEMFCs and AEMWEs. To achieve poly(imidazolium) application in electrochemical devices, the synthetic route must be robust and reproducible. In this work, new step growth and chain growth polymerization techniques were investigated as potential routes for poly(imidazolium) development, where the characteristics of the resulting ionene and pendant group polymer materials were thoroughly studied.

This thesis builds upon the fundamentals established in the Holdcroft laboratory, specifically the use of C2-protected imidazolium cations as alkaline stable cationic groups for hydroxide conducting ICPs. The versatility of the Debus Radziszewski reaction is investigated as an efficient synthetic route for imidazole synthesis, along with the design strategies employed to improve upon the pre-existing poly(imidazolium) materials.

Chapter 2 outlines the methods and techniques used to synthesize and characterize the poly(imidazolium)s used throughout this thesis. This chapter will provide background information regarding the experimental procedures utilized routinely throughout this thesis.

Chapter 3 describes the development of a new synthetic strategy to synthesize tetrasubstituted poly(imidazolium)s in an AB-type Debus Radziszewski step growth polymerization. Three novel poly(imidazolium)s were synthesized to demonstrate the versatility of said polymerization method and statistical copolymers were developed to illustrate the control this synthetic route allows on the chemical structure of the polymer.

Chapter 4 builds upon the highly controllable and simple synthetic route described in Chapter 3 by creating analogous poly(imidazolium)s with the additional C2-protection required for high alkaline stability. The poly(imidazolium) material discussed in this chapter will be designed for incorporation into the catalyst layer as an ionomer. The impact of this ionomer on the Hydrogen Evolution Reaction (HER) and Hydrogen Oxidation Reaction (HOR) will be realized by studying the impact of ionomer content on the reaction kinetics and electrochemical active surface area (ECSA) of the catalyst.

Chapter 5 discusses the impact of end group chemistry on the use of poly(imidazolium)s in electrochemical devices. Using the same synthetic route as Chapter 4, the end groups of the poly(imidazolium) are defined and investigated for the impact on alkaline stability. The reactivity of the end groups were used to create a poly(imidazolium) with end groups identical in chemical structure to the polymer main chain repeat units.

Chapter 6 will discuss the various methods established and used to determine poly(imidazolium) alkaline stability. The capabilities of theoretical and experimental cation model compound stability investigations will be determined and considered. A comparison between small model compounds and polymer stability were conducted for a thorough investigation into the characterization of a novel poly(imidazolium) with imidazolium pendant groups.

Chapter 7 summarizes the work discussed in this thesis and explore possible directions for future work. Building upon the knowledge gained from this thesis, three different routes for structural modification of poly(imidazolium)s will be suggested. Two synthetic routes offer simple modifications to the monomer synthesized in chapter 4, that would alter the poly(imidazolium) structure for potential control of macromolecular properties. The final method will use the end group definition described in chapter 5 for development of copolymers.

Chapter 2. Techniques and Methods

This chapter describes the general methodologies for techniques that have been used in multiple chapters of this thesis. Where experimental set up is specific to the thesis chapter, the details are reported in the experimental section of said chapter. The discussion surrounding the use of the Debus Radziszewski reaction for imidazole and poly(imidazole) synthesis occurs in Chapter 3 and to prevent redundancy, has been omitted from this chapter.

2.1. Synthesis

2.1.1. Formylation Reaction

This family of reactions refers to a chemical process in which a compound is functionalised with a formyl group. This reaction can occur between various different reagents, catalysts and formylation reagents.[116] Specifically in this work, the focus is on the selective formylation of aryl halides using *i*-PrMgCl as the Grignard reagent and dimethylformamide (DMF) as the formylation agent. The reactivity of the aryl halides follows the trend: *Ar*-I > *Ar*-Br > *Ar*-Cl > *Ar*-F. This decrease in reactivity allows for selective reaction for control of formylation onto aryl di-halides, if ~ 1 eq. of i-PrMgCl is used. The reaction must be conducted under O_2-free conditions to limit the risk of pyrophoric i-PrMgCl and water-free to prevent quenching of the Grignard.

The reaction first proceeds through substitution of the $MgCl^+$ onto the aryl halide (Figure 2.1). The highly polarised C-Mg bond allows for the electron rich carbon acts as a nucleophile and attack the carbonyl carbon through a 1,2-addition to give an alkoxide. Quenching of the reaction occurs with either an acid or water to yield the final reaction product.

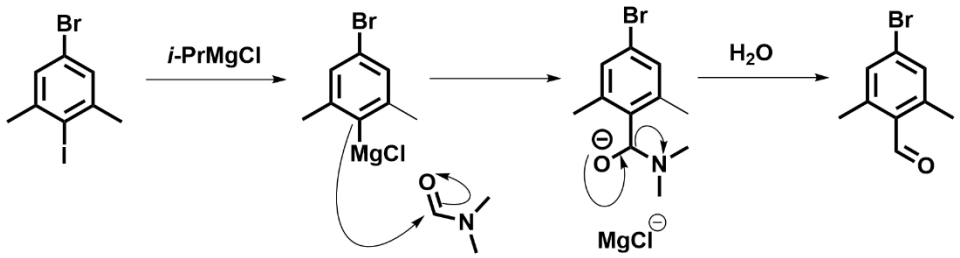

Figure 2-1: Reaction mechanism for the formylation of 5-bromo-2-iodo-1,3-dimethylbenzene

2.1.2. Pd-Catalysed Sonogashira Cross Coupling Reaction

The Pd-catalysed cross coupling reaction between sp^2-C halides and terminal alkynes were first reported by Heck, Cassier and Sonogashira, with the latter utilising a combination of Pd and Cu catalysts. With the presence of catalytic amounts of Pd, Cu^I and base, the cross coupling between terminal alkyne and aryl halide can occur to form an aryl acetylene. Generally, $Pd(PPh_3)_4$ is used as the Pd-source, but more recently there has been a shift towards the utilisation of air-stable $Pd(PPh_3)_2Cl_2$. CuI usually employed as the Cu^I salt.

The cross coupling takes place through two independent but complementary catalytic cycles (Figure 2.2). The Cu catalysed transmetellation of CuI occurs in the presence of the amine base (usually triethylamine and/or diethylamine). The amine appears to deprotonate the acetylene-Cu complex which releases the triethylammonium-iodide. Following the dissociation of the PPh_3 ligands, the Pd^0 catalyst undergoes oxidative addition to the sp^2-carbon halide. The now Pd^{II} complex undergoes transmetellation with the Cu-acetylene complex, creating another Pd^{II} complex and regenerating the Cu^I catalyst. The Pd^{II} undergoes isomerisation for reductive elimination of the substituted alkyne and regeneration of the Pd^0 species.

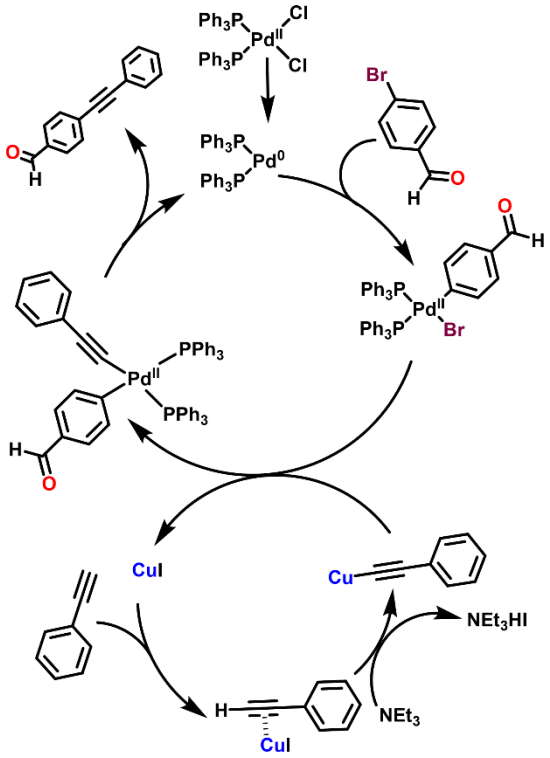

Figure 2-2: The two catalytic cycles occuring in the Sonogashira cross coupling of phenylacetylene and 4-bromobenzalehyde.

2.1.3. Oxidation of Substituted Alkynes to 1,2-Diketones

Various oxidation methods exist that allow for the formation of diketones from alkyne groups. However, in the syntheses described in Chapters 3, 4 and 5, the oxidation reaction must be specific to the alkyne group in the presence of an aldehyde group, ensuring there is no oxidation of the aldehyde. Therefore, in this work two oxidation methods were explored.

Iodine Promoted Oxidation with DMSO

Whilst the exact mechanism for the oxidation of substituted alkynes with iodine and DMSO is not confirmed, a suggested mechanism is given in Figure 2.3. It is proposed that the mechanism begins with the electron rich alkyne acting as a nucleophile, attacking the iodine, and forming an iodonium intermediate. The now electrophilic carbons can be attacked by the activated DMSO molecule. A tautomerization occurs to regenerate the iodine catalyst, eliminate sulphur-based byproducts, and form the substituted diketone

product. This oxidation reaction was proven to be selective to the alkyne functionalities and no oxidation of the aldehyde group was observed (Chapter 3).

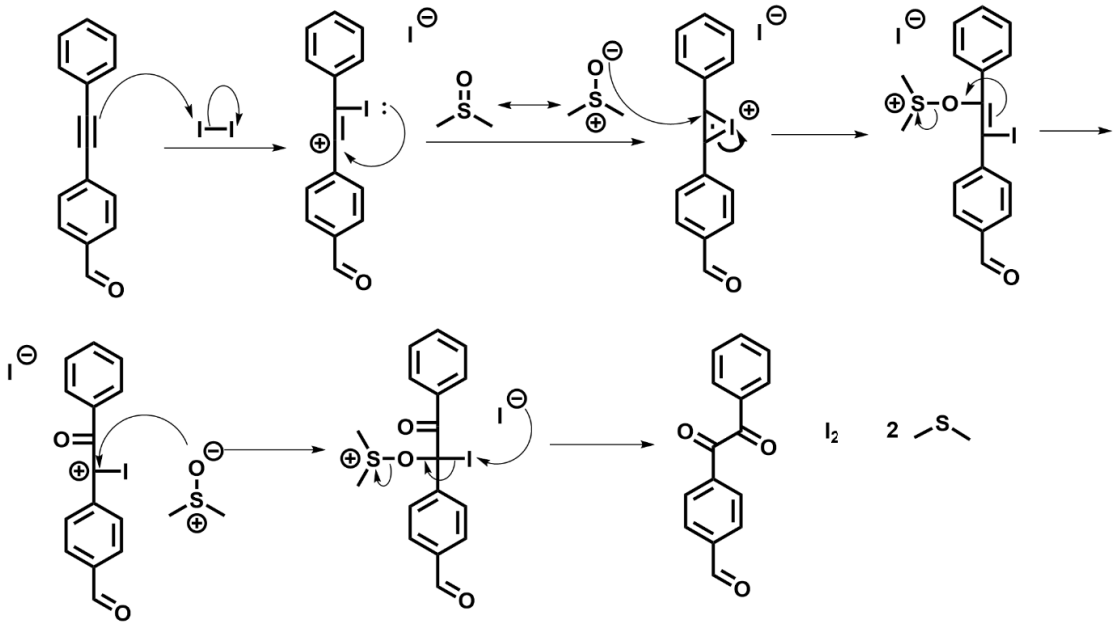

Figure 2-3:The proposed mechanism for the oxidation for 4-(phenylethynyl)benzaldehyde to 4-(2-oxo-2-phenylacetyl)benzaldehyde with iodine and DMSO.

However, using this approach its is challenging to obtain high reaction yields that are preferable for monomer syntheses and a large amount of sulphurous and iodide byproducts are obtained during the reaction, making purification difficult.

Pd-Catalyzed Oxidation using Pyridine-N-Oxide

The oxidation of 1,2-diaryl alkynes using Pd-catalysts was well summarised by Muzart *et al.*,[117] including work conducted on 4-(phenylethynyl)benzaldhyde (PEB, Chapter 3). Using a combination of PdI_2 and DMSO, the alkyne functionality was reported to have been successfully oxidised (93% yield) without any impact on the aldehyde functionality by Mousset and coworkers.[118] Pyridine N-oxide was reported as an effective oxidant in the oxidation of 1,2-diphenylacetylene catalysed by Pt/C. In work comparing the oxidative ability of DMSO and Pyridine N-oxide, the latter was found to be more efficient for the oxidation 1,2-diphenylacetylene giving an 87% yield with $Pd(OAc)_2$ as the catalyst,

in comparison to 17 % with DMSO as the oxidant. In this work (Chapters 4 and 5), a combination of PdI_2 and pyridine N-oxide was used for the synthesis of PEB.[114]

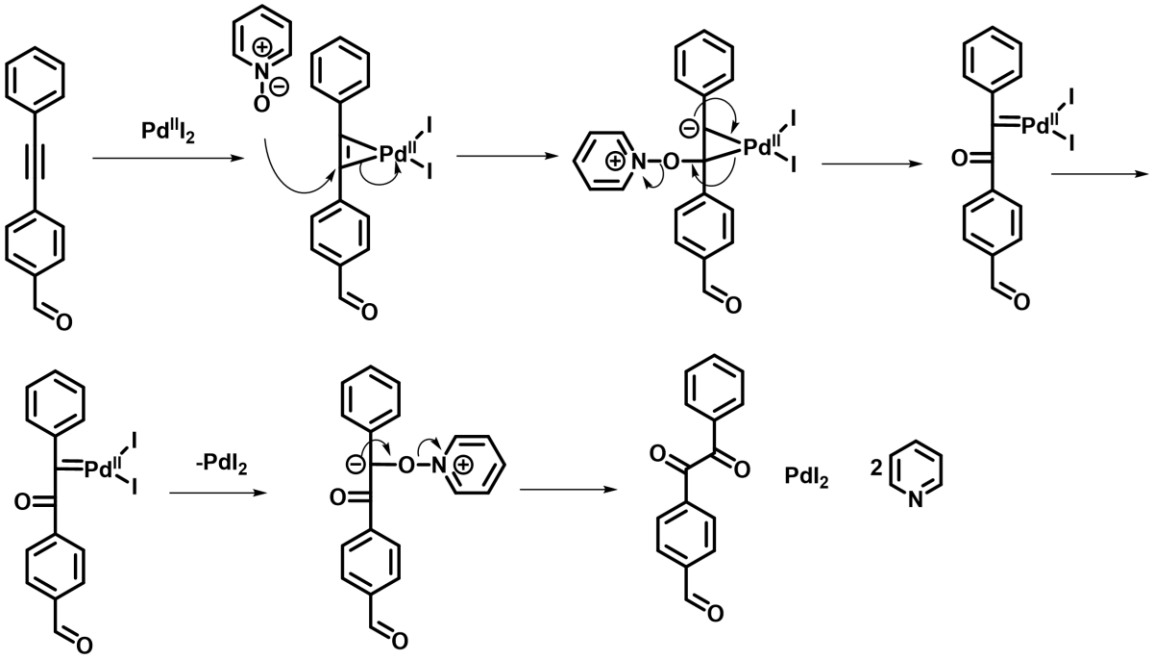

Figure 2-4: The proposed mechanism for the oxidation for 4-(phenylethynyl)benzaldehyde to 4-(2-oxo-2-phenylacetyl)benzaldehyde with PdI_2 and pyridine N-oxide.

2.1.4. N-functionalization of imidazoles

The N-functionalization of trisubstituted imidazoles occurs through a three-step reaction (Figure 2.5). The imidazole must first be deprotonated with a base to yield a negatively charged imidazolate, the nucleophilic N atom attacks the carbon of a C-X bond, where X is a halide, in a S_N2 reaction to form the single alkylated imidazole. The singly functionalised imidazole can then be quaternized to a cationic imidazolium, again through the nucleophilic substitution of an aryl or alkyl halide by the remaining N atom. Tetrasubstituted imidazoles must only undergo the final nucleophilic substitution step for quaternization.

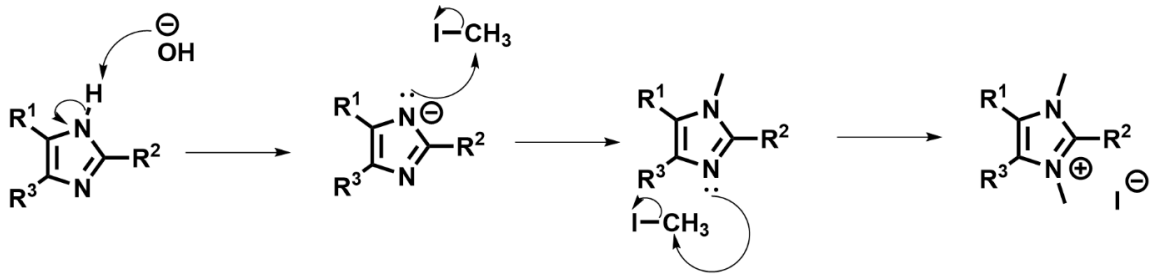

Figure 2-5: The nucleophilic substitution mechanism of imidazoles to form the cationic imidazolium.

2.2. Chemical Characterisation

2.2.1. Nuclear Magnetic Resonance Spectroscopy (NMR)

^{1}H NMR and ^{13}C NMR spectra were obtained on a Bruker AVANCE III 400 MHz, 500 MHz, or 600 MHz, running IconNMR under TopSpin 2.1, as indicated. ^{1}H spectra residual solvent peaks for DMSO-d_6, CD_3Cl, $(CD_3)_2CO$, CD_3OD, CD_2Cl_2 and THF-d_8 were set to 2.50, 7.26, 2.05, 3.31, and 5.32 ppm, respectively. ^{13}C spectra were set to DMSO-d_6 39.52 ppm.

2.2.2. Mass Spectrometry

All mass spectrometry experiments (MS) were performed with the assistance of Dr. Christophe Cantelli. Mass spectra were recorded on Time-of-Flight LC/MS mass spectrometer (Model 6210), using an electron spray ionisation source and a direct injection method of 50 % water- 50 %ACN (5mM NH_4OAc), in positive mode.

2.2.3. Infrared Spectroscopy

Fourier transform infrared (FT-IR) spectroscopy was conducted on a PerkinElmer Spectrum TwoTM spectrometer operating in attenuated total reflectance (ATR) mode, using the PerkinElmer UATR TwoTM module (PerkinElmer Corp., Waltham, MA, USA). IR absorbance was measured by 16 scans in the 450–4000 cm-1 range, at 4 cm-1

resolution. The ATR-FTIR spectrum of each sample was measured relative to the background absorbance of ambient air.

2.2.4. Elemental Analysis

Elemental analysis of insoluble polymers was conducted by Ms. Carol Wu or Mr. Yoghoub Alkhansa on an EA CHN 1110 instrument, under an O_2 environment, up to 960 ^oC. 2-sulfanilamine was used as the standard.

2.2.5. X-Ray Diffraction

X-ray data was collected on a Bruker Smart instrument equipped with an APEX II CCD area detector fixed at 5.0 cm from the crystal and a Cu Kα fine focus sealed tube (1.54178 Å) operated at 1.5 kW (50 kV, 30 mA), filtered with a graphite monochromator. Data was collected at ambient conditions. All diffraction data were processed with the Bruker Apex II software suite. The structures were solved with direct methods (SIR92) and subsequent refinements were performed using ShelXle.35

2.3. Characterisation of Polymer Properties

2.3.1. Thermogravimetric Analysis

Polymer thermal stabilities were assessed on a Shimadzu TGA-50 thermogravimetric analyser operating under constant N_2 flow. Samples averaging 10 mg mass were heated from ambient temperature (approximately 21 °C) to 600 °C at a rate of 2 °C · min^{-1}.

2.3.2. Ion Exchange

Ionic polymers were converted to chloride form over 3 days in reducing concentrations of NaCl solution to encourage polymer swelling and complete ion exchange. The NaCl solution was exchanged every half day starting at 3 M and ending at 0.5 M. The resulting polymer with chloride counterion was placed into dialysis tubes and suspended in MilliQ water to enable excess ions to leach into the water.

2.3.3. Ion Exchange Capacity Measurement

20 mg samples of polymer in chloride form were exchanged with 1 M KNO_3 (30 g) over 2 days. The concentration of Cl^- ions in the exchange solution was measured using a chloride selective electrode and converted into ion exchange capacity using equation 9:

$$IEC = \frac{\frac{M_{Cl^-}\, m_{solution}}{Mr_{Cl^-}}}{m_{ICP(Cl^-)}} \quad (9)$$

where M_{Cl^-} is the concentration of chloride ions (ppm), $m_{solution}$ is the mass of exchange solution (g), Mr_{Cl^-} is the molar mass of chloride ions (g/mol) and $m_{ICP(Cl^-)}$ is the mass of ion conducting polymer in chloride form (g).

2.3.4. Water Uptake

The water uptake was measured using Dynamic Vapor Sorption (DVS), using a DVS Adventure humidity chamber and Ultrabalance (Surface Measurement Systems Ltd., UK). The humidity was controlled by a source of deionized water delivered under nitrogen gas flow at a volumetric flow rate of 200 standard cubic centimeters per minute (sccm). The mass change was recorded with varying relative humidity. All experiments began with a drying step of 4 hours at 40 °C or 70 °C and 0% RH, before the initial sample mass was taken. The RH was then increased stepwise.

2.3.5. Chloride Conductivity

Ex situ chloride conductivity was measured using alternating current (ac) impedance spectroscopy. With the polymer in chloride form, the chloride conductivity was measured in the through-plane direction using a two-point probe by electrochemical impedance spectroscopy. Cells were placed in an Espec model SH-241 humidity chamber to control temperature and relative humidity (RH) and connected to a Solartron 1260 frequency response analyzer. The membrane charge transfer resistance (R), determined from a best fit of a standard Randle's circuit to the measured Nyquist plot (Figure 2.6) R_{el} is the electrolyte resistance, R_{ct} is the charge transfer resistance and C_d is the electrode/electrolyte double layer capacitance. At high

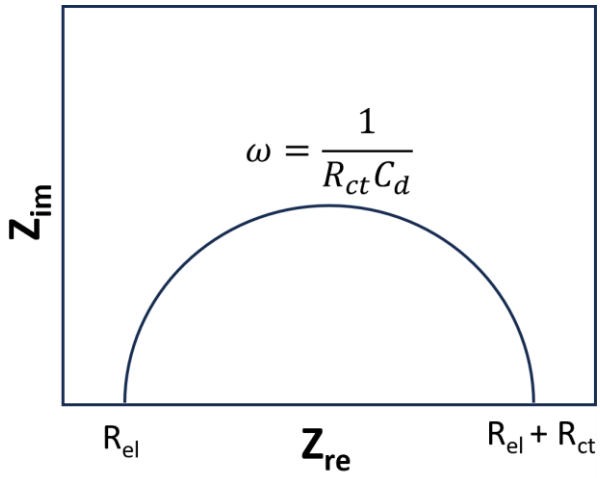

Figure 2.6: Representative Nyquist plot.

frequencies the imaginary impedance (Z_{im}, y-axis) approaches zero and the overall circuit resistance is equal to R_{el}. At low frequencies, the overall circuit resistance is the sum of R_{el} and R_{ct}. For the investigation of ion conducting polymer hydroxide conductivity, the R_{el} value was of primary interest. Using equation 10, the ion conductivity of the ICP could be calculated:

$$\sigma = \frac{l}{AR_{el}} \tag{10}$$

where l is the membrane thickness (mm) and A is the cross sectional area of the sample (cm^2).

2.3.6. Membrane Preparation

A 10 wt% solution of polymer was made with DMSO. The solution was stirred overnight at 80 °C and deposited directly onto a hot casting dish in the oven. The solution was dried overnight at 87 °C, leaving a film of polymer.

Chapter 3. A One-Pot AB-Type Polymerisation of Tetrasubstituted Poly(imidazole)s

3.1. Introduction

A multicomponent reaction is a one-pot reaction that involves three or more starting materials, where most of the atoms in the starting materials are incorporated into the final product.[119,120] There are a number of advantages for the use of multicomponent reactions over multistep reactions, including the high atom economy as the majority of the starting material atoms are incorporated into the product and the high reaction efficiency, reducing the cost of multiple reagents and volume of solvents required for workups.

Multicomponent reactions are used to avoid long multi-step synthetic pathways and therefore have been well studied for applications related to drug discovery[119] and more recently, highly functionalized polymer materials.[121,122] The Debus Radziszewski multicomponent reaction (Figure 3.1) is of particular interest within the alkaline energy storage and conversion field, where imidazoles are precursors to cationic imidazoliums that are showing high performance when incorporated into ionene ion conducting polymers.[36,111] Heterocyclic imidazoles can be synthesized in a one-pot DR reaction using an aldehyde, α-dicarbonyl and ammonia, where a condensation reaction occurs, expelling three water molecules per heterocycle (Figure 3.1). Highly pure products, with high reaction yields have been obtained for this type of multicomponent reaction, under various conditions (in AcOH, EtOH, thermal or microwave heating, and using different acid catalysts).[46,112,121,123–126] From imidazoles, the cationic imidazolium functionality can be synthesized in just one or two simple N-functionalization steps.[111]

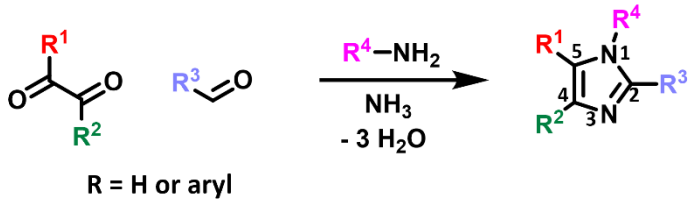

Figure 3-1: A general DR reaction.

Trisubstituted poly(imidazole)s synthesized using a step growth DR reaction have been reported in the literature.[46,114,127] Chauveau *et al*., first described the microwave-assisted synthesis of poly(triarylimidazole)s using a three component DR, AA-BB step growth polymerization.[127] The authors reacted a sulfonated *bis*-diketone with a dialdehyde containing various ether and aromatic linkages, in the presence of ammonium acetate and an acetic acid catalyst to create high molecular weight poly(triarylimidazole)s. Fan *et al*., adapted this synthesis by removing the labile sulfonate and ether linkages and adding steric protection around the C2 position to create a poly(imidazolium) that was suitable for incorporation into AEMWE and AEMFCs.[46] Two simple N-functionalization steps were then required to obtain the alkaline stable cationic poly(imidazolium).[46,114] Overton *et al.,* [114] also synthesized a poly(triarylimidazolium) using a DR reaction but utilized an AB-type step growth polymerization method. In this work, the AB monomer required only a two-step synthesis and the polymer end groups were pre-defined by the use of the single difunctional monomer. The authors used the accurate end group information to control the molecular weight of the polymer during the polymerization step. Again, two simple post-polymerization functionalization steps were used to synthesize the final cationic poly(imidazolium) compound.

Tetrasubstituted poly(imidazole)s have been obtained using the DR reaction in an AA-BB step growth polymerization, as described by Chauveau *et al*.[128] The authors used a four component DR reaction, differing from the previous study by the addition of an aryl-amine. Aniline and 4-butylaniline was used in addition to ammonium acetate in the polymerization step, to create a poly(imidazole) with a single N-functionality. Although the authors did not synthesize the charged poly(imidazolium), only one further synthetic step would have been required for quaternization, providing simplified route for poly(imidazolium) synthesis.

This chapter focuses on the development of a one-pot tetrasubstituted poly(imidazole) synthesis using AB-type step growth polymerization (Figure 3.2). The use of an AB-type monomer enables the chemical structure of the final polymer, including the end groups, to be well-defined. In addition, the one-pot synthesis of the tetrasubstituted poly(imidazole) reduces the number of steps required for formation of the final poly(imidazolium). The AB monomer was synthesized in two synthetic steps from commercial starting materials and the tetrasubstituted poly(imidazole) homopolymers were synthesized using various primary amines (Figure 3.2). The amines selected were

4-methylbenzylamine (4-MBA), butylamine and hexylamine to investigate the variability of the synthetic route creating PDPI-Bz, PDPI-Bu, and PDPI-H, respectively. Increasing the length of the alkyl chain, improved the solubility of the poly(tetra-arylimidazole) and PDPI-H was post-functionalized with a methyl unit to create a polycationic poly(imidazolium), PDPI-H-M. PDPI-Bz was used to investigate the use of the AB-type step growth DR reaction to synthesis poly(imidazole) copolymers. The methylbenzyl unit provided adequate ^{1}H NMR peaks to quantify the mole fraction of benzyl-substituted repeat units (φ_{Bz}) to demonstrate a copolymerization synthetic route where the variation chemical structure can be controlled and characterized. Until the present study, one-pot tetrasubstituted poly(imidazole)s are yet to be explored as candidates for ICPs, with the synthesized homopolymers and copolymers demonstrating the synthetic simplicity, versatility and tunability of DR AB step growth polymerizations.

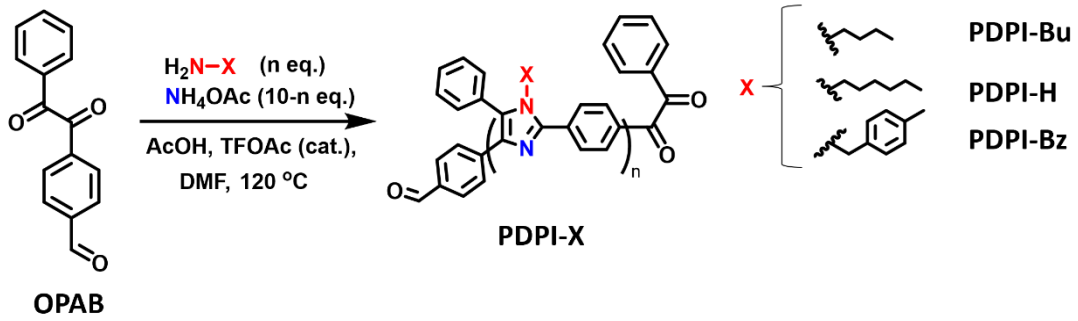

Figure 3-2: The tetrasubstituted poly(imidazole)s synthesized in this work through AB-type DR step growth polymerization.

3.2. Experimental

3.2.1. Monomer Synthesis

Synthesis of 4-(phenylethylnyl) benzaldehyde

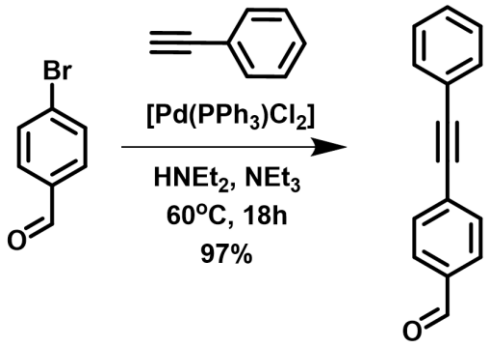

Figure 3-3: Sonogashira coupling of phenylacetylene with 4 – bromobenzaldehyde for synthesis of 4 – (phenylethylnyl) benzaldehyde (PEB).

4-bromobenzaldehyde was recrystallized from hot ethanol and dried in a desiccator overnight. Phenylacetylene was distilled under vacuum, dried over 4 Å molecular sieves and stored in the fridge. Triethylamine was dried over 4 Å sieves. CuI was stored under argon in the glove box. 4-bromobenzaldehyde (1eq.), $[Pd(PPh_3)_2Cl_2]$ (varying equivalence depending on scale of reaction), and triphenylphosphine (equal eq. to Pd-catalyst) was placed in a dry Schlenk flask under vacuum and then filled with argon. Triethylamine (TEA) (8 eq.) and phenylacetylene (1 eq.) was weighed into a pear-shaped flask and bubbled with argon for an hour. The phenylacetylene/TEA mixture was added to the Schlenk flask via cannular and subsequently freeze-pump-thawed to remove any remaining atmosphere and filled with argon. CuI (equal eq. to Pd-catalyst) was dissolved in degassed diethylamine and added to the reaction vessel via cannular. The reaction was run for 16-18h in a sealed vessel at 50 °C. The reaction mixture was filtered of the white precipitate and diethyl ether (400 mL) was added to the brown filtrate. The mixture was washed with excess NH_4Cl until the aqueous was clear and colourless. The organic layer was washed with 1M HCl until the aqueous layer was pH 1, then washed with $NaHCO_3$, water until neutral and then brine. The diethyl ether solution was dried over $MgSO_4$. The solution was filtered and then evaporated under reduced pressure to give a brown solid that was recrystallized from hot ethanol to give grey/brown crystals. (Yield > 99%). (500 MHz, DMSO) δ 10.05 (s, 1H), 8.00 – 7.94 (m, 2H), 7.82 – 7.76 (m, 2H), 7.66 – 7.58 (m, 2H), 7.52 – 7.43 (m, 3H).

Synthesis of 4-(2-oxo-2-phenylacetyl) benzaldehyde (OPAB)

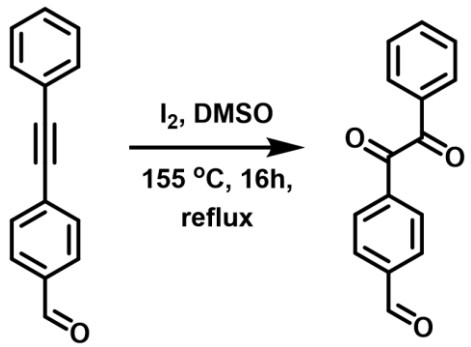

Figure 3-4: Oxidation of PEB.

A round bottom flask was charged with 4-(phenylethynyl) benzaldehyde (1 equiv.), DMSO (58 eq.) and Iodide (16 eq.). The solution was refluxed and stirred overnight (155°C, 16h). The reaction mixture was cooled to room temperature and DCM was added (20 mL). The mixture was extracted with $Na_2S_2O_3$ and then the aqueous layer was back extracted with DCM (3 x 20 mL). The organic layer was washed with 1M HCl until the aqueous layer was pH 1 (3 x 50 mL) and then washed with water until neutral (5 x 20 mL). The mixture was dried with brine (3 x 50 mL) and then over $MgSO_4$. The compound was purified through a basic alumina/silica plug followed by precipitation of the product from cold hexane and recrystallization from ethyl acetate/hexane mixture. Yielding yellow crystals (60%). (400 MHz, DMSO) δ 10.15 (s, 1H), 8.24 – 8.08 (m, 4H), 8.06 – 7.93 (m, 2H), 7.89 – 7.78 (m, 1H), 7.72 – 7.60 (m, 2H).

3.2.2. Polymer Synthesis

General Synthesis of PDPI-X

A 25 mL 2-neck pear-shaped flask was dried in the oven and where appropriate so was the dean stark trap. OPAB and NH_4OAc were dried under high vacuum for at least 5 hours before use. All solvents were dried over 4 Å sieves. The acid was measured by mass into the flask which was subsequently fitted with a condenser and placed into a water bath at 20 °C. The primary amine (4-MBA, butylamine or hexylamine) was added

dropwise to the stirring acid to enable the formation of a non-volatile ammonium salt. The protonation is exothermic, and the combination of condenser and water bath ensured all amine condensed into the acid. OPAB, NH_4OAc and solvent were subsequently added. The reaction was run at 140 °C for 7 days. Once completed the reaction was precipitated into cold ethyl acetate to remove any small organic molecules. The precipitate was off-white and the solution yellow. Once dried, the precipitate was dissolved into DMF and precipitated into water to remove any remaining salts.

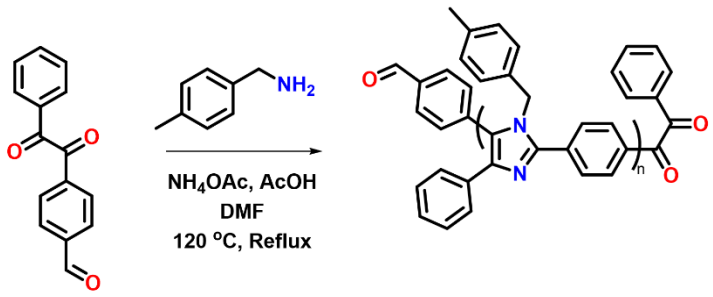

Figure 3-5: Synthesis of PDPI-Bz.

Reaction Bz-1 followed a procedure adapted from Chauveau et al.,[129] however the equivalence of NH_4OAc and 4-MBA were kept equal as the repeat unit of the poly(imidazole) contains 1 nitrogen from each of the compounds (Figure 3.13). However, NH_4OAc is likely more reactive than the bulky primary amine, therefore from Bz-3 onwards the equivalence was kept at 4:6 NH_4OAc 4-MBA, respectively. Toluene was used due to the azeotropic effect toluene has with water. This allowed for a Dean-Stark Trap to be used to continually remove water from the reaction and drive the reaction equilibrium towards imine formation. Bz-2 was set up to determine the impact of the AcOH. Reactions Bz-2 and Bz-3 show the impact of increasing the amount of AcOH on polymer formation. The addition of a strong acid catalyst (TFOAc) has been reported to improve the polymerisation reaction by decreasing the pH of the reaction.[103] In this case, TFOAc was added in catalytic amounts with respect to total amine equivalence. The reaction temperature had to kept above 118 °C for dissociation of NH_4OAc.

Synthesis of DMP-PPI-Bu

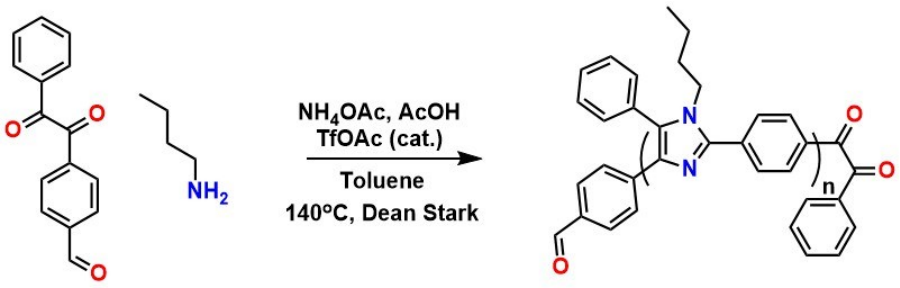

Figure 3-6: Synthesis of PDPI-Bu.

A 50 mL 2-neck pear-shaped flask and dean stark trap was dried in the oven. OPAB and NH_4OAc were dried under high vacuum for at least 5 hours before use. Solvent was dried before use.

Acetic acid (7.56 g, 125.90 mmol, 30 eq.) and trifluoroacetic acid (0.622 g, 5.81 mmol, 1.3 eq.) were mixed in the pear-shaped flask. The flask was submerged in a water bath at 20 ^{0}C and fitted with a condenser the hexylamine (3.33 mL, 25.19 mmol, 6 eq.) was added dropwise. OPBA (1.00 g, 4.197 mmol, 1 eq.), NH_4OAC (1.294 g, 16.79 mmol, 4 eq.) and toluene (7.74 g, 83.95 mmol, 20 eq.) were added to the reaction flask. The reaction was fitted with a dean stark trap and heated to 140 ^{o}C for 7 days. The reaction was precipitated into cold EtOAc, centrifuged, and left to dry. The polymer did not dissolve in DCM like the hexyl-derivative so was dissolved in DMF and precipitated again into cold EtOAc.

Synthesis of DMP-PPI-H

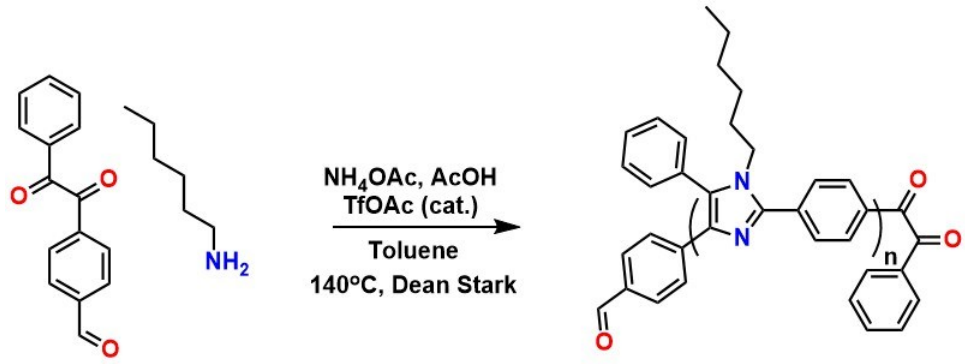

Figure 3-7: Synthesis of PDPI-H.

A 50 mL 2-neck pear-shaped flask and dean stark trap was dried in the oven. OPAB and NH_4OAc were dried under high vacuum for at least 5 hours before use. Solvent was dried before use.

Acetic acid (7.56 g, 125.90 mmol, 30 eq.) and trifluoroacetic acid (0.622 g, 5.81 mmol, 1.3 eq.) were mixed in the pear-shaped flask. The flask was submerged in a water bath at 20 ^{0}C and fitted with a condenser the hexylamine (3.33 mL, 25.19 mmol, 6 eq.) was added dropwise. OPBA (1.00 g, 4.197 mmol, 1 eq.), NH_4OAC (1.294 g, 16.79 mmol, 4 eq.) and toluene (7.74 g, 83.95 mmol, 20 eq.) were added to the reaction flask. The reaction was fitted with a dean stark trap and heated to 140 ^{o}C for 7 days. The toluene in the dean-stark was cloudy until day 5, then it appeared no more water was generated from the condensation reaction.

Once completed, the water (3.619 g, 200.89 mmol, 2.39 eq.) was collected from the dean stark. The reaction was precipitated into cold ethyl acetate, leaving a yellow sticky solid which was left to air dry overnight. Once dried the polymer formed a yellow translucent membrane which was dissolved into DMF (40 wt%, 45 mL) at 160 ^{o}C overnight. The translucent yellow solution was precipitated for a second time into cold ethyl acetate and centrifuged. The polymer was left to air dry overnight, leaving a gel-like ball.

Synthesis of PDPI-H-M

Figure 3-8: Synthesis of PDPI-H-M.

The single-alkylated poly(imidazole) (0.300 g, 1.04 mmol, 1eq.) was dissolved in DCM (10.40 mL, 162.86 mmol) at 35^{o}C overnight, giving a translucent yellow solution. The iodomethane (1.295 mL, 20.80 mmol, 20 eq.) was added dropwise to the stirring solution. The solution was stirred at 45 ^{o}C for 48hrs. At 24hrs, some precipitate was observed and DMSO (10.40 mL, 146.42 mmol) was added for solubility. Over 48hrs, the

reaction turned from yellow to orange. Once cooled, the solution was precipitated into ethyl acetate and centrifuged. The remaining polymer was air dried overnight, then dried at 80 °C for 24 hrs.

Synthesis of PDPI-φ-Bz Statistical Copolymers

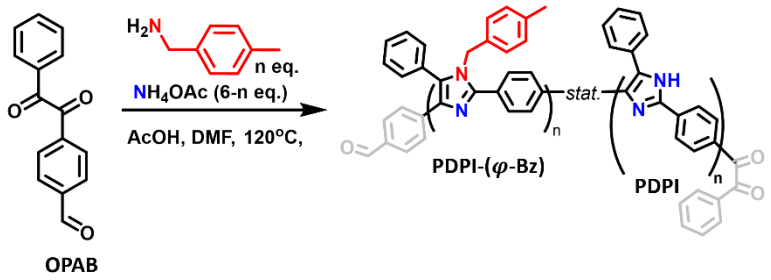

Figure 3-9: General synthesis of PDPI-φ-Bz.

A dry 100 mL round bottomed flask was charged with the 4-(2-oxo-2-phenylacetyl) benzaldehyde monomer (1.00 g, 4.20 mmol, 1 eq, 0.1 mol/L). The monomer was dissolved in DMF (39.79 mL). Acetic acid was added to the mixture dropwise (1.76 g, 29.38 mmol, 7 eq). Ammonium acetate and 4-methylbenzylamine were added at varying ratios (detailed in the table below) so the total amount of amine added to the reaction is always 6 eq.

Table 3.1: Synthesis of PDPI-φ-Bz, using different equivalence of 4-MBA and NH_4OAc.

REACTION	NH_4OAC			4-METHYLBENZYLAMINE		
	Eq	Moles (mmol)	Mass (g)	Eq	Moles (mmol)	Mass (g)
A	5	21.00	1.62	1	4.20	0.51
B	5.8	24.35	1.88	0.2	0.84	0.10
C	5.6	23.51	1.81	0.4	1.68	0.20
D (0.6G OF MONOMER)	5.4	13.56	1.05	0.6	1.51	0.18

E	5.2	21.83	1.68	0.8	3.36	0.41
F	4	16.79	1.29	2	8.39	1.02

The reaction was heated at 140°C under a blanket of argon and refluxed for 7 days (168 h).

The reaction mixture was precipitated dropwise into 1 M HCl (400 mL) and filtered under vacuum, using two filter papers. $NaHCO_3$ (200 ml) was poured over the polymer cake, along with water (3 x 200 mL) and left to air dry. All samples were dissolved in 50 wt% basic ethanol at 50 °C, precipitated into ethyl acetate and centrifuged. The resulting polymers were again dissolved in basic ethanol (10 mL) and heated until there was ~50 wt% basic ethanol. This step assumes excess ethyl acetate co-evaporated with the ethanol. The polymers were precipitated into 1M HCl to form the imidazole, then washed with water, sat. $NaHCO_3$ and water again. Yield: 585 – 83 mg, 58-8 %.

3.2.3. Polymer Characterisation

SEC Measurements

The analyses were obtained by using HPLC grade DMF (containing 0.05 M LiBr) eluent with a polystyrene standard for calibration. Mn = 20,052 g/mol, Mw = 22,312 g/mol, Mz = 29,348 g/mol, Mw/Mn = 1.113.

3.3. Results

3.3.1. Monomer Synthesis

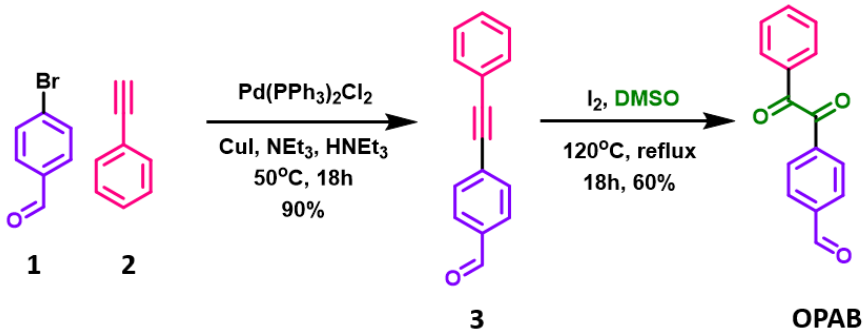

Figure 3-10: Synthesis of monomer 4-(2-oxo-2-phenylacetyl)benaldehyde.

The AB monomer, 4-(2-**o**xo-2-**p**heny**l**actyl) **b**enzaldehyde (**OPAB**), was synthesized *via* Sonogashira coupling, followed by oxidation (Figure 3.3).[114] A Sonogashira[130] cross-coupling between 4-bromobenzaldehyde and phenylacetylene formed the intermediate alkyne (**3**, Fig 4). The optimised reaction was conducted in an oxygen free environment with catalytic amounts of $Pd(PPh_3)_2Cl_2$ and CuI, using triethylamine as both the required base and reaction solvent. Small volumes of diethylamine were required to ensure dissolution of the CuI. Compound **3** was isolated by a simple extraction, purified by recrystallisation, and obtained at a high yield (90%). The potential for oxidation of the aldehyde functionality on compound 3, to a carboxylic acid makes the transformation from the alkyne to a diketone challenging. Only oxidation routes that are weak enough to target only the alkyne group can be considered. Subsequently, the alkyne (3) was reacted with DMSO and an iodine catalyst,[131] yielding OPAB (60%).

Synthesis of OPAB was confirmed using of Attenuated Total Reflectance Fourier Transform Infrared (ATR-FTIR) and $^{1}H/^{13}C$ NMR Spectroscopy (Figure 3.11). ATR-FTIR shows characteristic absorbance of functional groups and further confirms a successful monomer synthesis (Figure 3.11(a)). The aldehyde is maintained throughout the synthesis, shown by the absorbances at 1686, 1697 and 1702 cm^{-1} in spectra of 1, 2 and OPAB, respectively. The coupling of 1 and 2 is confirmed by the disappearance of the *sp* CH stretch (3291 cm^{-1}). The conjugated ketone peak at 1664 cm^{-1} in the spectra of OPAB is evidence for oxidation of alkyne to diketone.

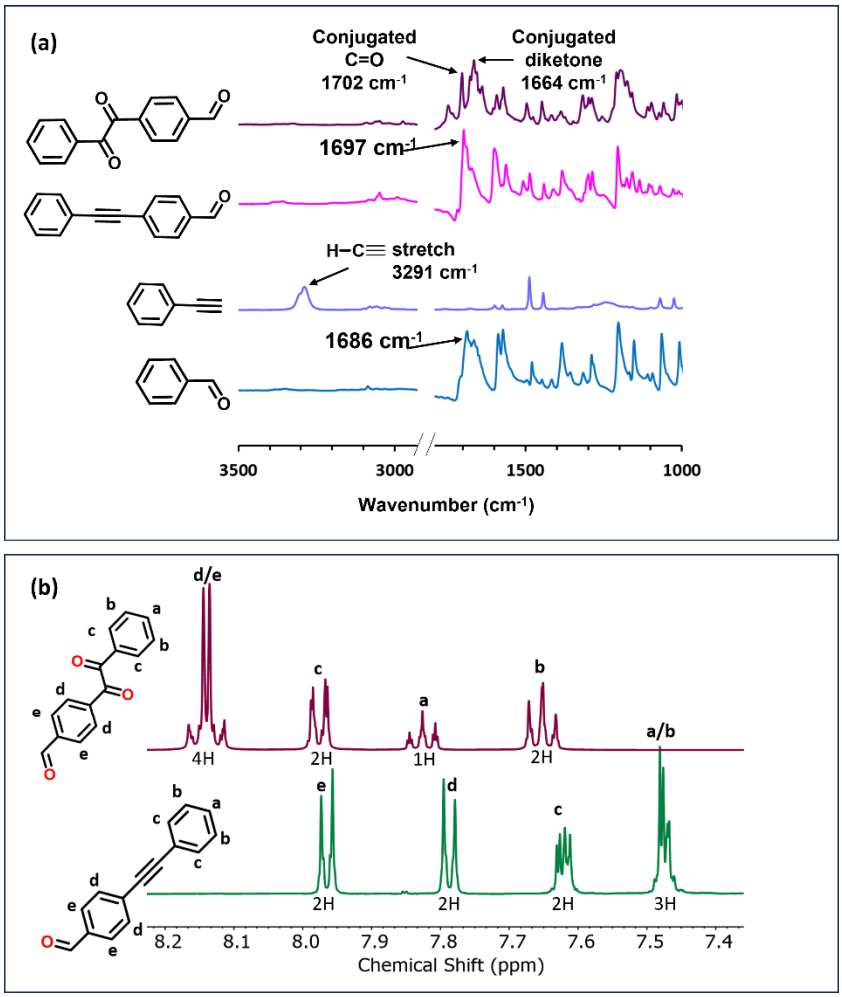

Figure 3-11: Analysis of monomer. ***(a) ATR-FTIR of compounds 1, 2, 3 and OPAB shows the change in absorption peaks as the functional groups change. (b) ^{1}H NMR shows the aromatic regions of 3 and OPAB, showing the change chemical shift before and after alkyne oxidation.***

The fully assigned aromatic regions ^{1}H NMRs of compound 3 and OPAB are shown in Figure 3.11(b). The downfield shift of all the aromatic protons in OPAB is caused by the addition of the diketone functionality. H^d/H^e are observed as an overlapping doublet of doublets (dd) in OPAB. The diketone has a greater shielding effect on H^a than H^b in OPAB, resulting an upfield shift. Crucially for the polycondensation, ^{1}H NMR confirms the high organic purity of OPAB.

Containing both the diketone and aldehyde functionalities required for the DR reaction, the AB-type monomer, OPAB, was able to be synthesised in just two steps. The reasonable efficiency of the monomer synthetic route is defined by the limited number of

reactions required, despite the lower yielding oxidation reaction. Building from OPAB, the polymerisation conditions must be discussed to ensure high yielding, efficient polymer synthesis.

3.3.2. Polymer Synthesis

Within the literature, similar reaction conditions for DR step growth polymerisation substituted poly(imidazole) synthesis have been used. The aldehyde and diketone are present in a 1:1 stoichiometry.[46,129,132,133] The total amine, both the ammonium and primary amine, is present in ~10 – 20 eq. with respect to the diketone.[46,129] The AcOH is in excess to the amine (~30-35 eq. with respect to the diketone)[46,129] and the solvent is usually non-polar[46,129] (~40 eq. with respect to diketone).[129] Additionally, a strong acid catalyst, such as trifluoroacetic acid can be used to drive the reaction further to completion.[129]

Considering these general conditions, the AB-type DR step growth polymerisation method used in this work was optimised using 4-MBA as the primary amine for synthesis of tetrasubstituted poly(imidazole)s (Appendix A, Table A.2). 4-MBA was selected for the model synthetic procedure as the Ar-CH_3 and N-CH_2 protons can act as internal probes in the ^{1}H NMR spectra to quantify the mole fraction of benzyl substituted repeating units (φ_{Bn}). The optimised reaction conditions required the OPAB monomer (1 eq.) to be reacted with acetic acid (30 eq.) and equal equivalence of ammonium acetate and 4-MBA (5:5 eq. with respect to OPAB), in dimethylformamide (DMF) at 120 °C (Figure 3.12(a)). The total equivalence of both amines was constant at 10 eq., as the amines are required for imidazole ring closing, as shown by the mechanism in (Figure 3.12(b)).[127,129]

The ^{1}H spectrum of PDPI-Bz confirms the success of the tetrasubstituted poly(imidazole) with a single 4-methylbenzyl N-functionalization (Appendix A, Figure A.3). The aryl-C$\boldsymbol{H}_3$ is observed as an upfield singlet at 2.21 ppm, which integrates to 3.00. The benzyl C$\boldsymbol{H}_2$ shoulder is seen at 5.17 ppm, integrating to 2.00. The aromatic region integrates to a total of 14.54, which is slightly higher than expected when comparing to the 13 x Ar-H protons present in the repeat unit of PDPI-Bz. This could be due several reasons: (i) the polymer may have a low molecular weight and therefore the Ar-*H* from the end groups may influence the integration, (ii) the φ_{Bn} may be < 1, but the N-H of the unsubstituted repeat units may be exchanging with the deuterated solvent and therefore

cannot be observed or (iii) the error associated with ^{1}H NMR integrations (~10%) could be impacting the final value.

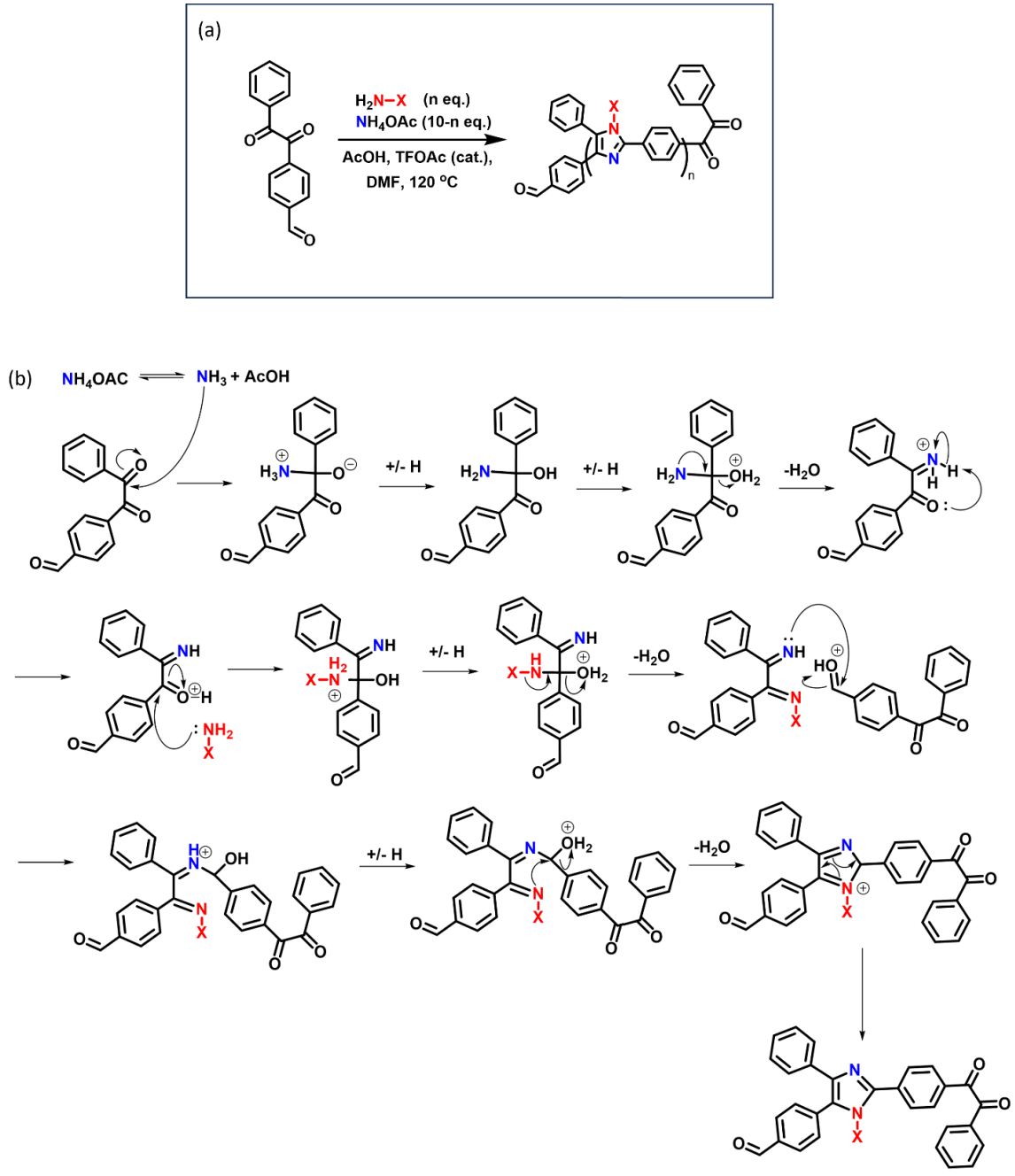

Figure 3-12: The DR reaction for tetra-substituted poly(imidazoles)s. ***(a) the synthetic procedure used in this work and (b) the reaction mechanism.***

To investigate the versatility of the one-pot DR synthetic route, butylamine and hexylamine were used as the primary amines. As observed in the ^{1}H NMRs of PDPI-Bu and PDPI-H (Appendix A, Figures A.6 and A.4, respectively), replacing 4-MBA with alkyl-amines was an effective method for varying the N-functionalities of tetra-substituted poly(imidazole)s. Unlike PDPI-Bz and PDPI-Bu, PDPI-H formed a free-standing membrane. Therefore, PDPI-H was selected for post-functionalization to form the cationic poly(imidazolium) PDPI-H-M polymer (Figure 3.6).

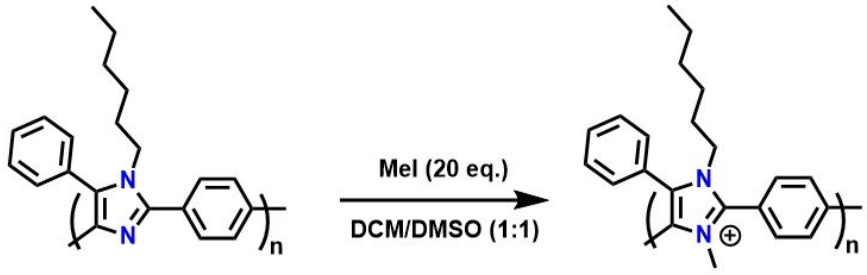

Figure 3-13: Post-functionalisation of PDPI-H with methyl iodide to form poly(imidazolium) PDPI-H-M.

Using the N-functionalization method described by Wright et al.,[105] PDPI-H was alkylated using methyl iodide. Methyl iodide was selected due to its high reactivity, in comparison to other alkyl-iodides,[48] and was therefore more likely to achieve a high number of charged repeat units. PDPI-H was dissolved in a 1:1 mixture of DCM and DMSO to ensure complete dissolution of both the starting material and product. An excess of methyl iodide (20 eq.) was added dropwise to the reaction mixture and left to stir for 48 h. The ^{1}H NMR spectra of PDPI-H-M (Appendix A, Figure A.5) shows an additional peak at 3.34 ppm which corresponds to the N-methyl functionalization. In DMSO-d_6, the water signal overlaps with the H_e signals. To obtain an unobstructed signal for H_e, a few drops of trifluoroacetic acid was added to the NMR sample. This acidified the sample and shifted the water peak from 3.33 ppm to a H_3O^+ peak at ~9 ppm. Using this method, the H_e protons were integrated to a value of 2.61. The close integration to the theoretically expected 3.00 of the N-C**H**$_3$ H_e protons suggests a high degree of methylation (dm < 0.87), giving an $IEC_{theoretical}$ = 2.87 mmol/g. Once purified, PDPI-H-M was cast into an AEM from hot DMSO, yielding a membrane with an average thickness of 33.5 µm. PDPI-H-M was characterised using TGA (Appendix A, Figure A.8) and SEC (Section 3.2.3).

3.3.3. Statistical Copolymer Investigation

This AB-type DR step growth polymerisation could also be utilised for the synthesis of poly(imidazole) copolymers. The controlled synthesis of copolymers, where the mole fraction (φ) of specific repeat units can be quantified, has the potential for the development of materials with tuneable macromolecular properties. This could be significant in the study of ICPs that require different properties dependent on the application within AEMFCs or AEMWE, where the ionomer at the cathode and anode, and the AEM must maintain high performance under very different conditions.

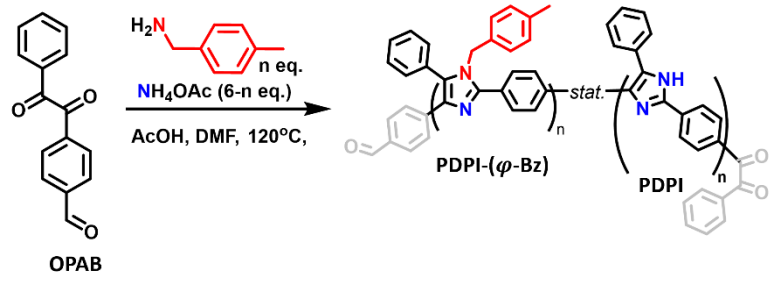

Figure 3-14: Polymer synthetic scheme for the formation of PDPI-(φ-Bz).

The φ of repeat units within a poly(imidazole) copolymer can be controlled using the DR reaction by varying the ratio of the nitrogen sources. For the one-pot tetrasubstituted poly(imidazole) synthesis described in this work, the ratio of ammonium acetate and primary amine was varied. PDPI-Bz was selected to be investigated as a copolymer as the 4-methlybenzyl unit provided ^{1}H NMR markers from the Ar-C***H***$_3$ group and the C***H***$_2$ benzyl group for quantification of the mole fraction of benzyl substituted repeat units (φ_{Bz}). The total amount of amine (NH_4OAc and 4-MBA) was maintained at 6 eq.,[129] with respect to monomer OPAB, while the equivalence of 4-MBA ranged from 0.2 – 2 eq (Figure 3.7).

Five samples of PDPI-(φ-Bz) were synthesised with the equivalence of 4-MBA being 0.2, 0.4, 0.8, 1.0, or 2.0, with respect to OPAB. Aside from the ammonium acetate and amine, the reaction conditions were the same as the homopolymer synthesis. As a representative sample, the ^{1}H NMR of PDPI-(φ-Bz) synthesised with 1.0 eq. of 4-MBA (PDPI-*0.45*-Bz) is shown in Figure 3.8. The Ar-C***H***$_3$ group is shown as two peaks between 2.42 to 1.89 ppm (Figure 3.8, pink). The C***H***$_2$ benzyl group is shown as a small broad peak

at 5.20 ppm (Figure 3.8, orange). The aromatic region is observed between 9.60 and 6.50 ppm, while the N***H*** from the unsubstituted imidazole repeat units (1-φ_{Bz}) is the broad peak at 12.90 ppm.

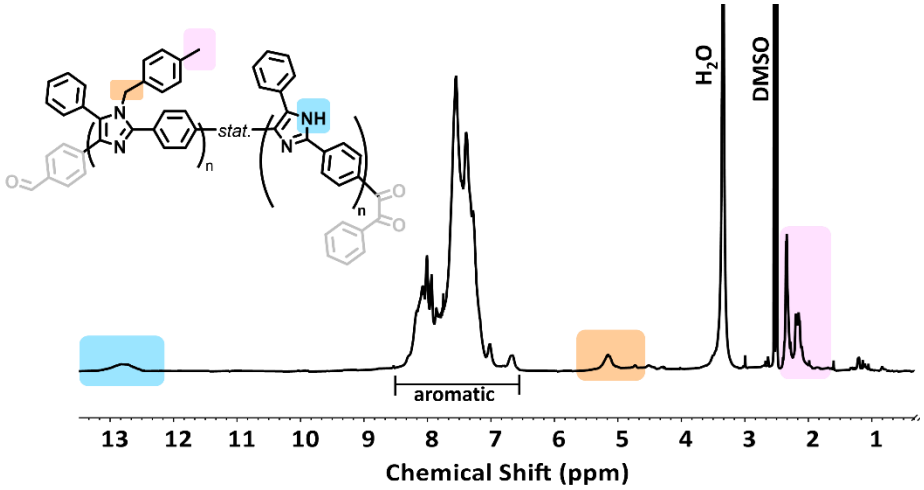

Figure 3-15: ^{1}H NMR of PDPI-(0.45-Bn), representative of PDPI-(φ-Bz) series.

The ratio of PDPI-(φ-Bz) : PDPI repeat units was calculated to obtain the $\varphi_{Bz.}$ The Ar-CH_3 region was normalised to 3H and the aromatic region (9.60 – 6.50 ppm) integrated. The ratio of PDPI repeat units with respect to one PDPI-(φ-Bz) repeat unit can be calculated using equation 11:

$$\frac{\int aromatic - 13}{9} \qquad (11)$$

The PDPI-(φ-Bz) repeat unit contribution is removed from the aromatic integration by subtracting the 13 aromatic protons, leaving the contribution from the PDPI unit. Dividing the remaining PDPI aromatic proton contribution gives the ratio of PDPI units to one PDPI-(φ-Bz) unit. Using this ratio, the φ_{Bz} can be calculated.

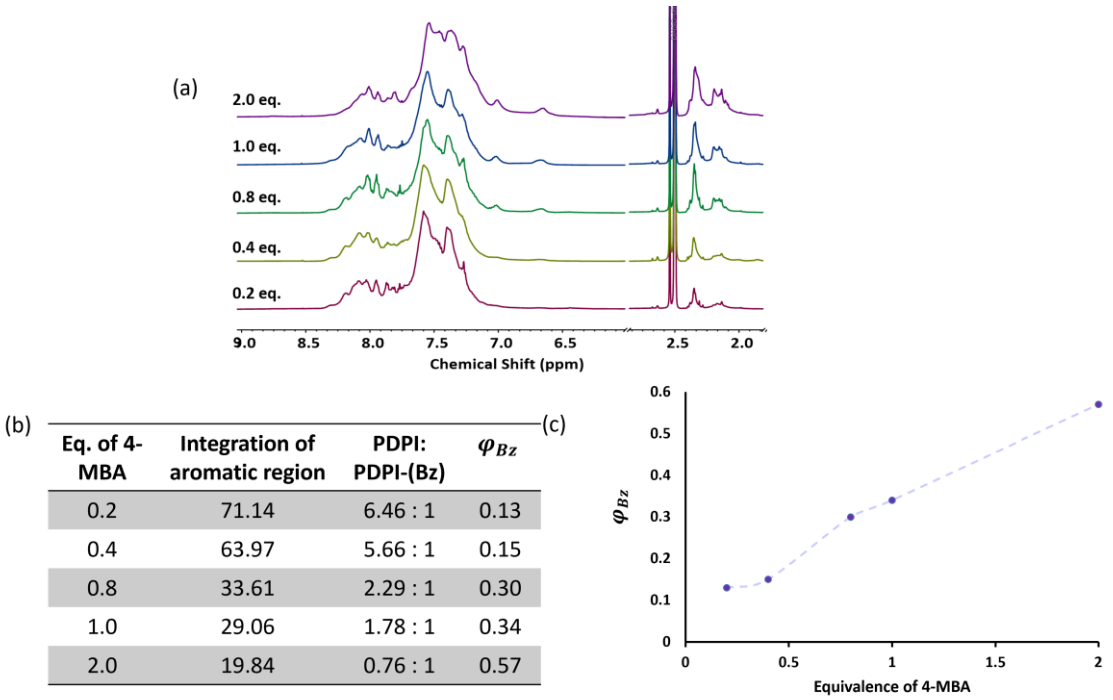

Eq. of 4-MBA	Integration of aromatic region	PDPI: PDPI-(Bz)	φ_{Bz}
0.2	71.14	6.46 : 1	0.13
0.4	63.97	5.66 : 1	0.15
0.8	33.61	2.29 : 1	0.30
1.0	29.06	1.78 : 1	0.34
2.0	19.84	0.76 : 1	0.57

Figure 3-16: Quantification of φ_{Bz} for the PDPI-φ-Bz series. ***(a) Stacked ^{1}H NMR showing aromatic and Ar-CH$_3$ regions of PDPI-(x-Bz) series organised by equivalence of 4-MBA added in the syntheses. Intensities were normalised to aromatic peaks, showing the increase in Ar-CH$_3$ with increasing eq. of amine. (b) A table showing the relationship between equivalence of 4-MBA used in the synthesis, the integration of the aromatic region, normalised by Ar-CH$_3$, and the φ_{Bz} calculated using equation 11. (c) The increase of φBz with increasing eq. of 4-methylbenzylamine.***

The increase of φ_{Bz} with increasing equivalence of 4-MBA was quantified using ^{1}H NMR (Figure 3.16). Figure 3.16(a) shows the Ar-C***H***$_3$ peak of the 4-methylbenzyl substituent and the aromatic region of the five PDPI-φ-Bz samples. The intensity of the aromatic region was normalised across all five samples to demonstrate increase of Ar-C***H***$_3$ with increasing equivalence of 4-MBA, indicating the increased φ_{Bz} of the copolymers. Figure 3.9(b) gives numerical values relating φ_{Bz} to the aromatic integration and equivalence of 4-MBA used in the relation. Figure 3.16(c) demonstrates the positive trend between increasing 4-MBA equivalence and φ_{Bz}.

The controlled variation of 4-MBA in an AB-type DR step growth polymerisation reaction can be used to create poly(imidazole) statistical copolymers with quantifiable φ

of repeat units. The quantification of φ_{Bz} for the PDPI-φ-Bz series using ^{1}H NMR suggests this synthetic route could be control and vary the repeat unit structure of poly(imidazole)s. The controlled variation of φ_{Bz} resulted in control of repeat unit molecular weight, which could have interesting impacts on IEC for poly(imidazolium)s and the related macromolecular properties.

3.4. Conclusions

In this chapter, a new polymerisation method using an AB-type monomer in a multicomponent Debus Radziszewski reaction for synthesis of tetrasubstituted poly(imidazole)s. The versatility of this synthetic route was demonstrated using 4-MBA, butylamine and hexylamine to synthesise polymers with varying N-functionalities: PDPI-Bz, PDPI-Bu and PDPI-H. Using this synthetic route, the final cationic poly(imidazolium) can be synthesised from commercial starting materials in just four steps and is a simplified method in comparison to AA-BB type polymerisations.

The same method could be used to synthesize statistical copolymers where the φ of repeat units could be quantified using ^{1}H NMR. The equivalence of 4-MBA was increased over five polymer syntheses, creating copolymers with an increasing φ_{Bz}. The φ_{Bz} was quantified using the change in integration of the aromatic region with respect to the Ar-C$\boldsymbol{H}_3$ group of the 4-methylbenzyl. The control of repeat unit structure could be of particular importance for the high-performance cationic poly(imidazolium)s. As discussed in Chapter 1, the IEC of ion conducting polymers plays an importance role in governing the macromolecular properties of these charged materials. The IEC is intrinsically tied to several ICP macromolecular properties such as, water uptake, swelling and conductivity. Therefore, if the average molecular weight of repeat units could be systematically changed without large changes in chemical structure, the corresponding IEC could be controlled. The range of theoretical IEC that could be given using this synthetic route and varying the φ_{Bz} is given in Figure 3.10, where the upper and lower bounds are the unsubstituted (φ_{Bz} = 0) and benzyl substituted (φ_{Bz} = 1) homopolymers. Using control of IEC, the water uptake, swelling and conductivity of the ICPs could be manipulated. This facile method to alter the polymer architecture and fundamental ICP properties using a single synthetic method could be instrumental in the tuning of next-generation poly(imidazolium)s for specific device requirements.

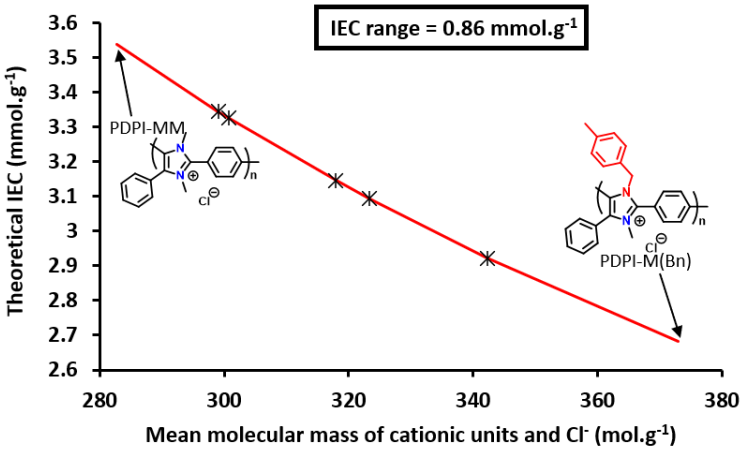

Figure 3-17: Plot showing the change in theoretical IEC with average mass of repeating units. ***The PDPI-MM series are shown as crosses on the red line, assuming 100% methylation. The upper and lower bounds have been described using PDPI-M-M and a hypothetical PDPI-Bz-M homopolymer.***

Chapter 4. Assessing Electrocatalyst-Ionomer Interactions: HOR/HER Activity of Pt/C Catalyst Layers incorporating Poly(imidazolium)

The work in this chapter is described in: Fraser, K; Doseav, K,; Savinova, E,; Holdcroft, S,; Asset, T. (submitted).

Kate Fraser, Prof. Elena Savinova and Prof. Steven Holdcroft envisioned the project. Kate Fraser performed the synthesis and material characterisations and aided in the preliminary electrochemical investigations. Dr. Kirill Doseav and Dr. Tristan Asset performed the electrochemical measurements and analysis. Prof. Steven Holdcroft, Prof. Elena Savinova and Dr. Tristan Asset advised and supervised the work conducted.

4.1. Introduction

In AEMWE and AEMFCs the hydroxide conducting polycations exist in two forms: (i) a solid electrolyte membrane for ion transport between the electrodes and (ii) an ionomer dispersed within the catalyst layers to bind the catalyst nanoparticles and facilitate hydroxide transport between catalyst and AEM.

Within the AEMFCs and AEMWEs, the membrane and ionomer must exhibit many of the same properties, with the high hydroxide conductivity and high alkaline stability being a major focus in material development. Less regularly discussed are the specific properties that an ICP must exhibit to be employed as a high-performance ionomer. Unlike the AEM, the ionomer is in direct contact with the catalyst nanoparticles, playing a crucial role in the transport of ionic reactant/product species within the catalyst layers. Therefore, it is imperative that the chemical structure of the ionomer has minimal binding interactions with the electrocatalytic active sites in order to avoid any adverse effects on its activity.[24,134] The impact of ionomer structure on the electrocatalytic active sites has rapidly become a growing area of research. Despite several viable catalyst alternatives identified for the oxygen evolution and reduction reactions (OER and ORR, respectively), platinum-based nanostructures remain the most studied catalysts for the hydrogen oxidation and evolution reactions (HER and HOR). This is withstanding the fact that Pt's activity is decreased by two orders of magnitude in alkaline *vs.* acidic environments and alternatives based on non-precious metals (*e.g.,* Ni and Ni-alloys) exhibit 100 times lower activities.[24,135–137]

Compatibility between the ionomer and Pt-based nanostructures is critical and can be discussed as (i) whether there is a specific adsorption of the ionomer component onto Pt and (ii) what is the nature of this adsorption. Li *et al*., identified two types of ionomer adsorption: cation-hydroxide-water coadsorption and phenyl adsorption (Figure 4.1). Cation-hydroxide-water coadsorption occurs when the OH^-, H_2O and the cationic ionomer interact with the Pt surface negatively impacting reactant/product permeation through the co-adsorbed layer.[138,139] Phenyl adsorption describes the planar adsorption of aromatic rings onto the Pt surface and is reported to lead to a larger reduction in electrocatalytic activity in comparison to the cation-hydroxide-water co-adsorption.[140]

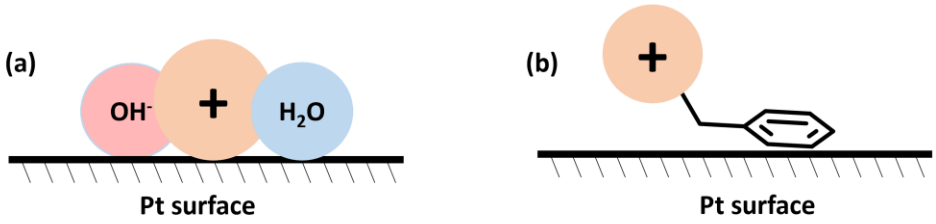

Figure 4-1: Diagram of the potential ionomer - catalyst interactions.
(a) Cation-hydroxide-water and (b) phenyl adsorption.

The Kim group has conducted several investigations to elucidate the ionomer-catalyst interactions by varying the phenylene moieties within the ionomers[83] and using different electrocatalytic surfaces (*e.g.,* Pt and Pt-alloys).[141] From their work, it is reported that reduced binding strength of the aromatic rings onto active sites can be achieved by: (i) decreasing the number of aromatic rings per repeat unit of ionomer, (ii) using Pt-alloys as opposed to Pt, and (iii) replacing the 'conventional' aromatic rings (*e.g.,* phenylenes) with other main chain groups with a rigid structures that limits the planar adsorption of aromatics rings on the surface (*e.g.,* 9,9-dimethyl fluorene; norbornene)[142] enhancing the performance of the electrocatalyst. Taking advantage of the aforementioned points, Maurya *et al.* reported AEMFCs exhibiting > 1 W cm^{-2} power density using PtRu/C as the anode catalyst and incorporating fluorene-based ionomers.[142]

The negative effect of phenyl groups is of particular concern in the development of novel high performance polycations, especially poly(imidazolium)s. The poly(imidazolium)-based ionomers require phenyl groups not only for accessible synthetic routes, but for the high alkaline stability. Therefore, it is critical to explore poly(imidazolium)

ionomers with a low density of phenyl groups per repeat unit, or with phenyl groups that cannot easily adsorb onto the electrocatalytic surface.

Based on the AB type DR step growth polymerization method established in Chapter 3, in this chapter a novel C2-protected poly(imidazolium) ionomer was synthesized that possessed only two aromatic rings per repeat unit. The monomer synthesis was adapted from Chapter 3 to synthesize an AB-type monomer with additional methyl units that, once polymerized, form the C2-steric protection required for high alkaline stability. The ionomer was soluble in low boiling point solvents for ease of processibility, but insoluble in basic solutions, required for device operation.

Using this ionomer, electrocatalyst-ionomer interactions were investigated in alkaline environment through the assessment of the HOR/HER exchange current density on Pt/C catalyst layers possessing increasing ionomer-to-carbon (I:C) ratio.

4.2. Experimental

4.2.1. Synthesis

Synthesis of 5-bromo-2-iodo-m-xylene: 5-bromo-2-iodo-1,3-dimethylbenzene (1 eq., 3.216 mmol, 4.00 g) and dry THF (32 mL) was bubbled with argon for 1 hour. The mixture was cooled to -15 °C and *i*-PrMgCl (2M in THF, 2 eq., 25.727 mmol, 12.863 mL) was added dropwise. The reaction was kept at -15 °C for 2 hours whilst stirring, then DMF (3 eq., 38.590 mmol, 2.988 mL) was added dropwise. The reaction was brought to room temperature and stirred overnight, forming a white precipitate. The mixture was quenched with 1M and left to stir for 30 min. The product was extracted in ethyl acetate, washed with 1M HCl, water, brine, and dried with $MgSO_4$. The crude product was dried onto silica and separated from remaining starting material by filtration over a pad of silica gel and hexanes as the eluent. The yield was 96 %. ^{1}H NMR (500 MHz, DCM-d_2, ppm) δ: 10.57 (s, 1H), 7.29 (s, 2H), 2.58 (s, 6H). ^{13}C NMR (125 MHz, DMSO-d_6, ppm) δ 193.48, 142.83, 131.92, 131.34, 126.48, 19.49.

Synthesis of 2,6-dimethyl-4-(phenylethynyl)-benzaldehyde: 4-bromo-2,6-dimethylbenzaldehyde (1 eq.) was dried overnight under vacuum then mixed with $Pd(PPh_3)_2Cl_2$ (1 mol%), and PPh_3 (1.5 mol%) in an oven dried Schlenk flask. The atmosphere was replaced with argon by placing under vacuum then filling the flask with

argon 3 times. The phenylacetylene (1.1 eq.) was mixed with triethylamine (16 eq.) and bubbled with argon. The phenylacetylene/TEA mixture was added to the Schlenk flask via cannula, and the reaction mixture was degassed via a freeze-pump-thaw cycle. The CuI (1 mol%) was dissolved in degassed diethylamine and added to the reaction via cannula. The reaction was run at 50 °C for 16 hrs. The crude product was taken up in diethyl ether, washed with NH_4Cl (1 M), HCl (1 M), water, brine and dried with $MgSO_4$. The product was dried under reduced pressure and excess phenylacetylene was removed via sublimation. The yield was 98 %. ^{1}H NMR (500 MHz, DCM-d_2, ppm) δ: 10.62 (s, 1H), 7.59 (m, 2H), 7.46 (m, 3H), 7.34 (s, 2H), 2.63 (s, 6H). ^{13}C NMR (125 MHz, DMSO) δ 193.64, 141.01, 132.04, 131.55, 129.31, 128.89, 126.45, 121.76, 91.93, 88.63, 19.71.

Synthesis of 2,6-dimethyl-4-(2-oxo-2-phenylacetyl)benzaldehyde: 2,6-dimethyl-4-(phenylethynyl)-benzaldehyde (1 eq.) was mixed with pyridine-N-oxide (5 eq.) and iodine (0.02 eq.) or PdI_2 (0.02 eq.) and heated to 140 °C for 20 hrs. The reaction was cooled to room temperature and extracted in ethyl acetate. The organic layer was washed with saturated NH_4Cl, saturated $Na_2S_2O_3$, 1 M HCl, water, brine and $MgSO_4$. The crude product was purified in a silica column with 1:4 ethyl acetate: hexanes. The yield was 90 %. ^{1}H NMR (500 MHz, DCM-d_2, ppm) δ: 10.68 (s, 1H), 7.98 (d, 2H), 7.80 (t, 1H), 7.73 (s, 2H), 7.64 (t, 2H), 2.65 (s, 6H). ^{13}C NMR (126 MHz, DMSO) δ 194.71, 194.42, 194.07, 141.07, 137.34, 135.65, 134.31, 132.09, 130.03, 129.77, 129.50, 19.64. S $[M+NH_4]^+$: Calculated for $C_{17}H_{14}O_3[NH_4+]$ 284.128, found 284.139, $[M+CH_3OH+H]^+$: calculated for $C_{17}H_{14}O_3[CH_3OH][H]^+$ 299.1278, found 284.139

Synthesis of DMP-PHPI: 2,6-dm(OPAB) and NH_4OAc was dried under vacuum for 16 hours. Acetic acid (30 eq. 112.66 mmol, 6.44 mL) and trifluoroacetic acid (1.3 eq. 4.882 mmol, 0.37 mL) were added to a 2 neck round bottomed flask, fitted with a condenser, and sealed. Hexylamine (6 eq. 22.531 mmol, 2.976 mL) was added dropwise over 30 mins. Toluene (20 eq., 75.103 mmol, 8.00 mL) was added to the reaction vessel. NH_4OAc (4 eq. 15.021 mmol, 1.158 g) and 2,6-dm(OPAB) were added to the reaction mixture. The reaction was heated to 140°C and refluxed with a dean-stark apparatus for 168 hrs. Once finished the reaction was precipitated into cold ethyl acetate and centrifuged. The resulting solid (1.24 g) was dried in the oven 80°C until a hard, yellow solid was formed. ^{1}H NMR (500 MHz, THF-d_8, ppm) δ: 7.72-7.11 (9H), 3.87 (2H), 2.38-2.08 (8H), 1.40-1.30 (2H), 1.29-0.92 (6H), 0.78-0.74 (3H). ^{1}H NMR (500 MHz, THF-

d_8+TFA, ppm) δ: 7.72-7.11 (9H), 3.87 (2H), 2.38-2.08 (8H), 1.40-1.30 (2H), 1.29-0.92 (6H), 0.78-0.74 (3H).

Synthesis of DMP-PHPI-M: DMP-PHPI (1 eq., 3.32 mmol, 1 g) was dissolved in DMF (10 mL) and iodomethane (20 eq. 66.47 mmol, 4.14 mL) was added. The reaction was heated in a pressure vessel to 100 °C for 16 hrs. Once cooled the reaction was precipitated into ethyl acetate and centrifuged. ^{1}H NMR (500 MHz, DMSO, ppm) δ: 7.74-7.58 (9H), 3.82 (3H), 3.63-3.52 (6H), 2.28 (6H), 1.24 (2H), 1.05-0.87 (6H), 0.70 (3H). ^{1}H NMR (500 MHz, DMSO+TFA, ppm) δ: 7.74-7.58 (9H), 3.82 (3H), 3.63-3.52 (6H), 2.28 (6H), 1.24 (2H), 1.05-0.87 (6H), 0.70 (3H)

4.2.2. Electrocatalyst-ionomer interactions

Electrochemical studies were carried out on an Gamry Reference 600 potentiostat/galvanostat. An Autolab Rotator disc electrode was used to perform electrochemical experiments on a rotating disc electrode (RDE). Electrochemical measurements were performed in a three-electrode electrochemical cell. To remove impurities that could poison the surface of the catalyst, the cell was thoroughly cleaned before measurements were taken. For this purpose, Caro's solution (mixture of H_2O_2 (30 %) and H_2SO_4 (96-98 %) in the ratio 1:1 by volume) was poured inside the cell overnight. Afterwards, the solution was removed, and the cell was washed thoroughly with ultrapure water (18.2 MΩ×cm, < 2 ppb TOC) was used for the preparation of all solutions as well as for washing, as traces of H_2O_2 and acid could lead to erroneous results. The obtained Caro's solution was stored a maximum of three months. Prior to measurements, the glassy carbon (GC) tips (0.196 cm^2) were polished with an aqueous suspension of aluminum oxide (with particle sizes of 1.0, 0.3 and 0.05 μm) to obtain a mirror surface. The GC tips were then washed with water, placed in Caro's acid for 5 minutes and then cleaned in an ultrasonic bath with acetone, ethyl alcohol and water, alternating for 5 minutes in each solution. Poly(imidazolium) as ionomer was stored in iodide form. To convert it from iodide form to hydroxide form it was exchanged in 1M KOH for 72h. The solution was renewed every 24h. The resulting ionomer was filtered from the solution on a paper filter and washed with a small amount of water. To prevent degradation, the ionomer was dissolved in water to obtain a concentration of 0.5 g/l without preparing a dry residue beforehand. Since without drying the mass of ionomer is not known exactly, to determine its exact concentration 5 mL of ionomer solution were dried overnight at 60^{0}C to determine the dry

residue. Afterwards the concentration of the solution was recalculated. Afterwards the concentration of the solution was recalculated. Experiments were also carried out with the initial ionomer, which was dissolved in acetonitrile (MeCN) with a concentration of 0.5 g/l. A suspension of commercial Pt/C (20 wt.% Pt on Vulcan XC-72, E-TEK) was prepared for electrochemical studies. For this purpose, 3.25 mL ultrapure water and 1.75 mL (isopropanol) IPA were added to 5 mg Pt/C. The mixture was then placed in an ultrasonic bath for 30 min, the temperature of the bath being kept constant by the continuous addition of ice. To investigate the effect of the ionomer, the required amount of the prepared ionomer solution was added to the suspension sample and the mixture was again placed in the ultrasonic bath for 15 min. The ionomer solution was added to obtain the following carbon to ionomer ratios: 0, 0.05, 0.1, 0.15, 0.2, 0.25. For electrochemical measurements, the Pt/C suspension was immobilized on the GC disc electrode. The Pt loading per electrode was 10 $\mu g_{Pt}\ cm^{-2}_{geo}$. The ink was applied to the electrode surface in two portions, with a volume of ca. 5 µL per portion, recalculated based on the dilution of the ink after addition of the ionomer solution. The electrode was dried in an N_2 flow with constant rotation (200 rpm). The working electrode was the aforementioned disc electrode. The counter electrode was a platinum grid, and the reference electrode was the Hg/HgO electrode. The reference electrode was calibrated with respect to the reversible hydrogen electrode and the potential of the electrode was - 0.938 V *vs.* RHE. 0.1M NaOH (from a 50 wt. % NaOH in H_2O, Sigma) was used as the electrolyte. The solution was pre-cleaned using the following technique: a platinized platinum electrode was cleaned by cycling between 0.06 V *vs.* RHE and 1.27 V *vs.* RHE, 5 mV s^{-1} in N_2-saturated 0.1 M NaOH. The electrode was then placed in a fresh N_2-saturated 0.1 M NaOH solution and a 0.1 V *vs* RHE potential was applied for 1 hour – to allow all the organic species to adsorb onto Pt. When investigating the effect of the iodide anion the necessary amount of NaI was added in the electrolyte (0.1M NaOH), leading to concentrations of 1 µM, 3 µM, 5 µM, 7 µM, 9 µM, 1mM, 0.1mM 0.01 mM of NaI. The Pt/C samples were characterized as following, in 0.1M NaOH (i) in N_2-saturated electrolyte, an electrochemical impedance spectroscopy (EIS) measurement was first performed at 0 V *vs.* RHE (Δ = 3 mV, 7 points per decade, 100 kHz – 0.1 Hz, identical for all EIS unless specified otherwise) to assess the electrolyte resistance, which was always found between 25 – 35 Ω. Then, (ii) a 50 cycles activation was performed at 500 mV s^{-1} between 0.06 V *vs.* RHE and 1.27 V *vs.* RHE, followed by 2 cycles in the same potential range at 20 mV s^{-1}. The 20 mV s^{-1} CVs were used to calculate the H_{upd}, using a 156 µF charge per centimeter square of Pt, *i.e.,* 210 µF cm^{-2} corrected

by the surface difference between 0.5 M H_2SO_4 and 0.1 M KOH (see **Fig. S1**); (ii) The electrode was moved in a cell with the same electrolyte but saturated with H_2. Cyclic voltammetry at 20 mV s^{-1}, 1600 rpm from – 0.05 to 1.1 V *vs.* RHE were recorded for 6 cycles, followed by (iii) 2 EIS at – 0.01 and 0.01 V *vs.* RHE. When investigating the degradation effects of the catalyst, the cycling range was extended to from – 0.05 to 1.27 V *vs.* RHE (see **Fig. S2**). To compare the catalytic activity, the microkinetic current (i^0_{micro}) was calculated using the following procedure: The last cycle was taken for cyclic voltammetry recorded in H_2 saturated solution. The following window of potential was considered [-10: 10] mV *vs*. RHE. Between the cathode and anode curves the average was taken. For the resulting curve, the positive currents in this potential window have been corrected for diffusion currents using the following equation:

$$\mathrm{I_k} = \frac{\mathrm{I_d} \cdot \mathrm{I}}{\mathrm{I_d} - \mathrm{I}} \tag{12}$$

I_d current was taken as the current at 0.4V *vs.* RHE. After adjusting for diffusion current, the date was fitted with linear regression (y = *a*x + b). The microkinetic current was calculated using the following equation:

$$i_0^{micro} = a\frac{RT}{F} \tag{13}$$

Where *a* is the slope of the curve

4.3. Results

4.3.1. Monomer Synthesis

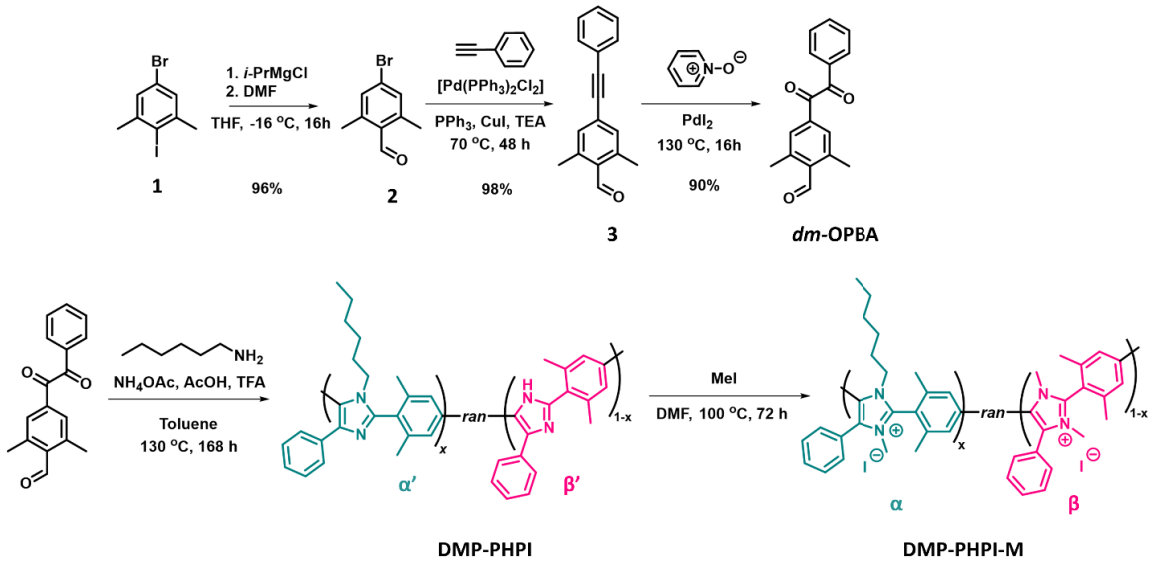

Figure 4-2: Synthesis of monomer and polymer. ***x denotes the mole fraction of hexyl-substituted repeat unit (α) and 1-x is the mole fraction of unsubstituted repeat unit (β).***

The difunctional monomer was synthesized *via* formylation,[143] Sonogashira,[130] and oxidation reactions,[114,144,145] which were high yielding (> 90%), had simple purification procedures, and could be scaled to over 20 g. The formylation reaction using the commercial starting material, 5-bromo-2-iodo-1,3-dimethylbenzene (**1,** Figure 4.2), and DMF was selective to the 2-iodo position due to the higher reactivity of iodo- groups *vs*. bromo groups. The 1,3-dimethyl groups are required for the C2 steric protection of the imidazole. The aldehyde was formed at the 2-position of compound 2 is required for the DR reaction.

A Sonogashira cross coupling between compound **2** and phenylacetylene formed the intermediate alkyne (**3**, Figure 4.2). Like Chapter 2, the reaction was conducted in an oxygen free environment using triethylamine, and small volumes of diethylamine, as both the required base and reaction solvent. However, the addition of the 1,3-dimethly groups on compound **2,** in comparison to the bromo-benzaldehyde used in Chapter 2, reduced

the reactivity of the Br group. To maintain high reaction yields, the catalyst loading was increased (from 0.01 eq. to 0.05 eq., with respect to compound **2**), the temperature was increased (from 50 °C to 70 °C) and reaction time was increased (from 16h to 48h).

The oxidation of the alkyne was previously conducted using DMSO as the oxygen source and solvent, and iodine as the catalyst.[131] However, the reaction yields were limited to ~60% and the sulfurous side products were challenging to remove. In this work, the PdI_2[145] catalyst was utilized in place of the I_2 and pyridine *N*-oxide was the oxidant.[144] This reaction produced *dm*-OPAB in high yields with a simple purification procedure without any oxidation of the aldehyde group. *Dm*-OPBA has the diketone and aldehyde functionalities required for the AB type DR step growth polymerization.

4.3.2. Polymer Synthesis

Using *dm*-OPAB, ionomer DMP-PHPI-M could be synthesised with just two aromatic rings per repeat unit to limit the potential phenyl adsorption onto the catalyst surface. DMP-PHPI-M possesses repeat units with hexyl chains for solubility in low boiling point solvents and insolubility in basic aqueous solutions, enabling simple processing and incorporation into electrochemical devices. *Dm*-OPBA was polymerized using an excess of hexylamine and ammonium acetate, in an acidic environment. The additional 1,3-dimethyl units incorporated into *dm*-OPAB, reduced the reactivity in comparison to OPAB (Chapter 3). In this work, the polymerisation was conducted in toluene using a dean-stark trap. The water produced in the polycondensation reaction could be removed through the low boiling point water-toluene azeotrope, driving the equilibrium towards reaction completion to improve the molecular weight of DMP-PHPI. The polymerisation reaction yielded a copolymer of hexyl substituted α' units and unsubstituted β' units. The lower molecular weight of the β' repeat units lowered the average molecular weight of DMP-PHPI and therefore made higher IECs more accessible, whilst maintaining the high solubility of α' units.

DMP-PHPI was characterized using ^{1}H NMR spectroscopy in THF-d_8 for polymer **1** (Appendix B, Figure B.7). A drop of TFA was added to the ^{1}H NMR sample to acidify the water and shift the water peak downfield to prevent any peaks being obscured (Appendix B, Figure B.8. The hexyl unit of the polymer is shown by the three broad peaks between 0.8 – 1.5 ppm with the CH_2-N appearing at 3.8 ppm. The methyl C2 protecting

groups are observed as a collection of peaks 2.0 – 2.3 ppm and the remaining aromatic protons overlapping between 7.0 – 8.0 ppm. The exchangeable N*H* from the β' repeat unit is observable as a broad peak at 11.0 ppm, confirming the existence of a copolymer. DMP-PHPI was dissolved in DMF for the quaternization step. High conversion to quaternized repeat units were achieved using a large excess of iodomethane (20 eq.). Iodomethane's high reactivity allowed complete quaternization of repeat units for high IEC.[110] The methylation was confirmed using ^{1}H NMR in d_6 – DMSO (Appendix B, Figure B.9, and with TFA Figure B.10) where the methyl was shown as two overlapping peaks between 3.73 and 3.44 ppm. After conversion of the ionomer into chloride form, DMP-PHPI-M was shown to have reasonable macromolecular properties giving an IEC = 3.01 ± 0.17 mmol/g; water uptake of 26.6 % at 80% RH and 60 ºC, and conductivity of 5.31 ± 0.02 mS/cm. The low water uptake and low number of phenylene groups per repeat unit make DMP-PHPI-M an interesting candidate for an ionomer-catalyst interaction investigation.

4.3.3. DMP-PHPI-M as an Ionomer

DMP-PHPI-M was investigated as an ionomer by exchanging the iodide counterion into a hydroxide. Catalyst inks were created using 3.25:1.75 (v/v) H_2O:isopropyl alcohol ratios, a 20 wt.% Pt/C electrocatalyst and an increasing ionomer:cabon (I:C) ratio. The catalyst inks were deposited onto a rotating disk electrode and used as the working electrode, with a 0.1 M NaOH electrolyte. An Hg/HgCl electrode was used as the reference and Pt wire was the counter electrode, to complete the three-electrode system. The following parameters were assessed: (i) pseudocapacitive current; (ii) electrochemical surface area (ECSA); (iii) exchange current density normalized by the geometrical surface and (iv) exchange current density normalized by the ECSA.

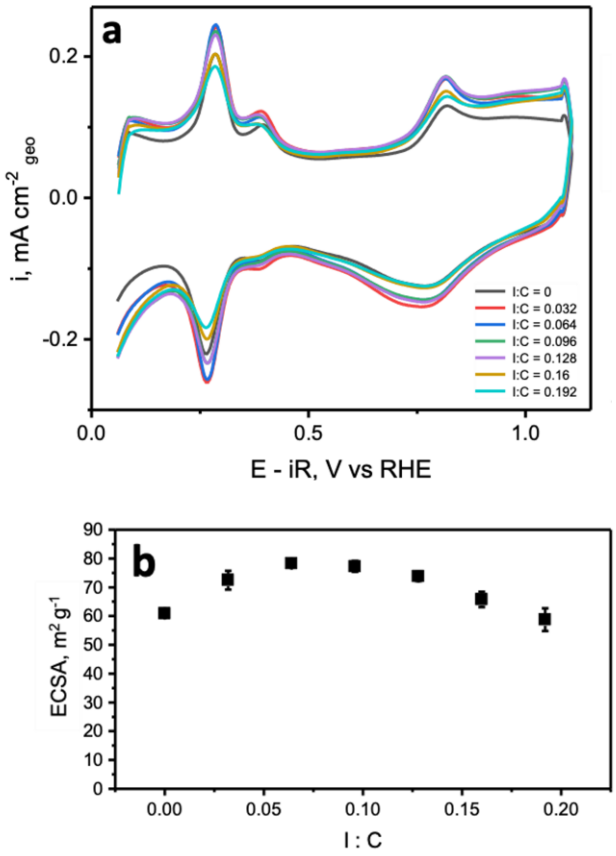

Figure 4-3: Effect of the presence of ionomer, DMP-PHPI-M, on Pt/C electrochemical performances in a N_2, alkaline environment. ***a) cyclic voltammetry of Pt/C in N_2-saturated 0.1 M NaOH, at 20 mV s^{-1}, b) surface area (ECSA) of Pt as a function of the I:C ratio.***

The current density at 0.5 V *vs.* RHE is due to the pseudo-capacitive charging, mainly from the carbon contribution. At this potential, all CVs exhibit the same current density, aside from I:C = 0, indicating the ionomer has little to no effect on the catalyst layer capacitance and the surface of the Pt/C is similarly exposed to the electrolyte when in the presence of ionomer. Significant differences in the current densities of the hydrogen adsorption/desorption (H_{upd}) region (~0.1 – 0.4 V) in hydrogen-free 0.1 M NaOH are observed with increasing I:C content (Figure 4.2), reflecting the differences in accessible electrochemical surface area of Pt (ECSA). The accessible surface area was estimated by integrating the anodic hydrogen desorption peaks and subtracting the capacitive charge, using a 156 μF cm^{-2}_{Pt} conversion coefficient obtained by comparing CVs in 0.1 M NaOH and 0.5 M H_2SO_4 (Appendix, Figure B.11). The 24 % increase in ECSA from I:C

ratios of 0.00 to 0.064 suggests the ionomer increases the stability of the catalyst layer, contrary to other reported ionomer interactions.[138]

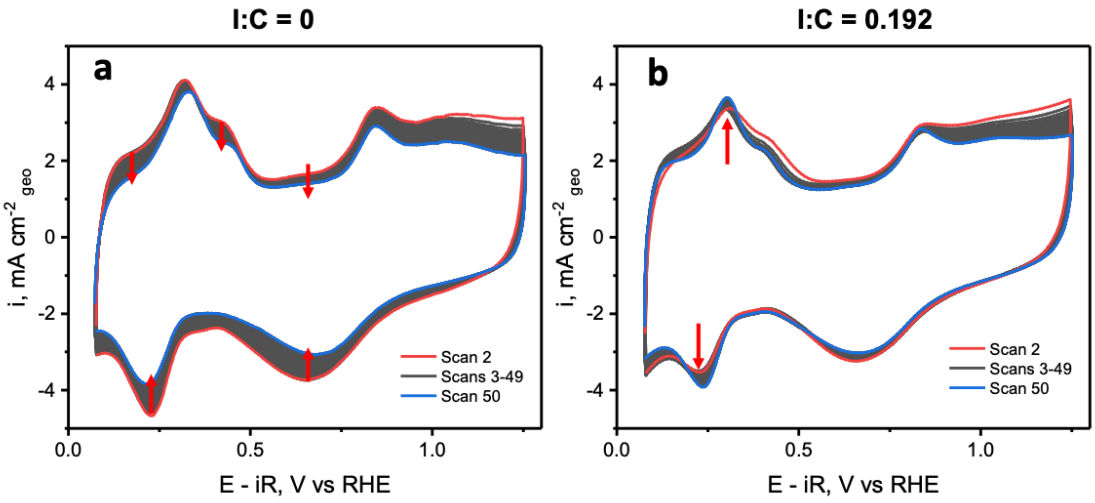

Figure 4-4: Evolution of CVs for Pt/C in N_2-saturated 0.1M NaOH, at 500 mV s^{-1}. ***a) sample without addition of ionomer b) sample with addition of ionomer (prepared in H2O). Red indicates the second scan, blue the 50th.***

In Figure 4.4, the electrocatalyst behaviour during the activation cycles was assessed for further explanation of reduced Pt/C degradation with increased ionomer loading. The CVs aim to clean the platinum surface from organic components, as the electrochemical purification of platinum is critical and highly dependent on the history and preparation of the sample.[146] The organic species are always present on the Pt-surface when in contact with air and cleaning of the surface is a balance between the efficient cleaning and minimal degradation of the Pt surface. For Pt/C without ionomer (Figure 4.3(a)), a mild H_{upd} and capacitive current decrease is observed, potentially related to the catalytic layer degradation.[147] However, when using an I:C ratio of 0.196, a stable H_{upd} is observed, with variation of the relative intensity between the H_{upd} peaks being induced by the surface activation. Hence, the ionomer-free or low-ionomer (I:C = 0.032) Pt/C electrodes are losing a small portion of their catalytic layer during the activation cycles, leading to the lower ECSA observed in Figure 4.3, whereas higher content of ionomer leads to a stable catalytic layer during the activation phase.

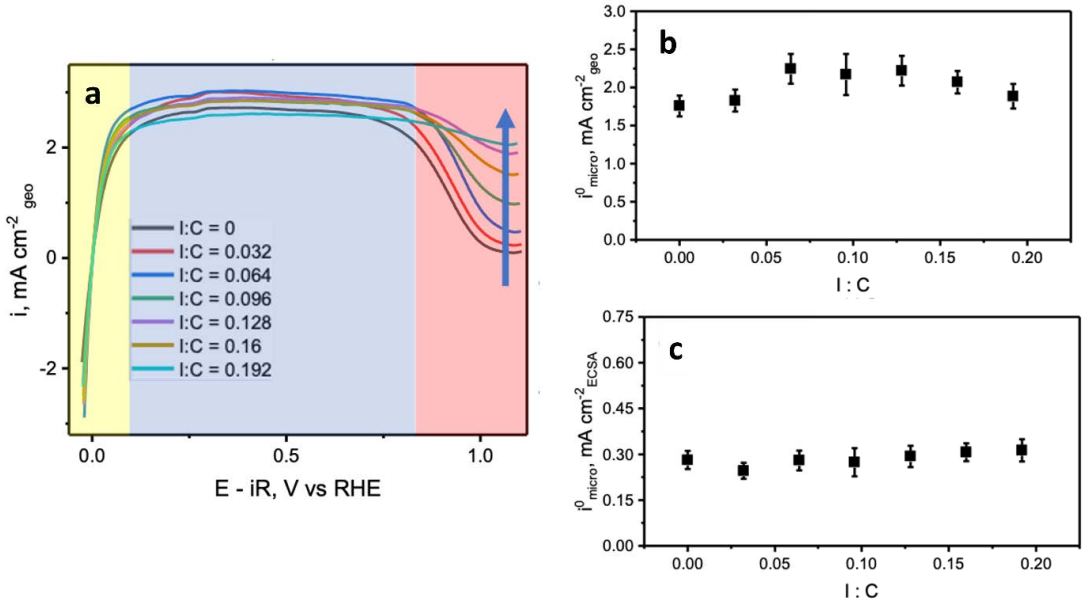

Figure 4-5: Effect of the presence of ionomer, DMP-PHPI-M, on Pt/C electrochemical performances in a H_2, alkaline environment
(a) cyclic voltammetry in H_2-saturated 0.1 M NaOH, at 20 mV s^{-1} and 1600 rpm, (b) exchange current density normalized to the geometric area (geo), (c) exchange current density normalized to ECSA of Pt, both (d) and (e) are calculated from the micropolarization region (-10 mV to 10 mV vs. RHE).

In a H_2-saturated electrolyte, the HER and HOR can be observed (Figure 4.5(a)). At potentials lower than 0.1 V *vs.* RHE (yellow region, Figure 4.5(a)), the hydrogen evolution reaction (HER, < 0 V *vs.* RHE) and hydrogen oxidation reaction (HOR, > 0 V *vs.* RHE) take place under kinetic in the 'micropolarization potential interval (from – 10 to + 10 mV) and then under mixed kinetic-mass transport control. At 0.1 < E < 0.8 V *vs.* RHE (blue region, Figure 4.5(a)), a H_2 diffusion-controlled state is reached and at E > 0.8 V *vs.* RHE (red region, Figure 4.5(a)), a current drop is observed, due to oxide formation on the Pt surface. The current drop at E > 0.8 V vs. RHE decreases with increasing ionomer content (Figure 4.5(a), red region) and was attributed to the decrease of interfacial pH during the HOR. The decrease in pH is likely amplified by the ionomer which exhibits a lower hydroxide transport rate than the liquid electrolyte or forms confined regions near the reactive interface with a decreased hydroxide concentration. The Pt oxide formation ($Pt + 2OH^- \rightarrow PtO + H_2O$) is dependent on the pH, therefore a local pH decrease would

result in a shift of the oxide formation towards higher potentials and, thus, higher activity at E > 0.8 V vs. RHE, as shown in Figure 4.5(a).

Within the low overpotential region, the exchange current density (i^0_{micro}) can be used to quantify the catalytic activity of the HER/HOR. In Figure 4.5(b) and (c), the i^0_{micro} is plotted as a function of ionomer loading and the same trend as was found for the ECSA is observed. A slight increase in i^0_{micro} is seen, up to ~0.1 I:C and subsequent reduction of i^0_{micro} above this I:C ratio until returning to the i^0_{micro} observed for I:C = 0. After normalization of i^0_{micro} to ECSA, the values of the specific exchange current density are independent of the ionomer fraction over the range of I:C (Figure 4.5(c)) evidencing for the absence of adverse effects of the poly(imidazolium) on the intrinsic HOR/HER activity of Pt. Although changes in ECSA and exchange current density with the ionomer fraction are relatively marginal, it is desirable to understand the origin of their slight decay at I:C > 0.1.

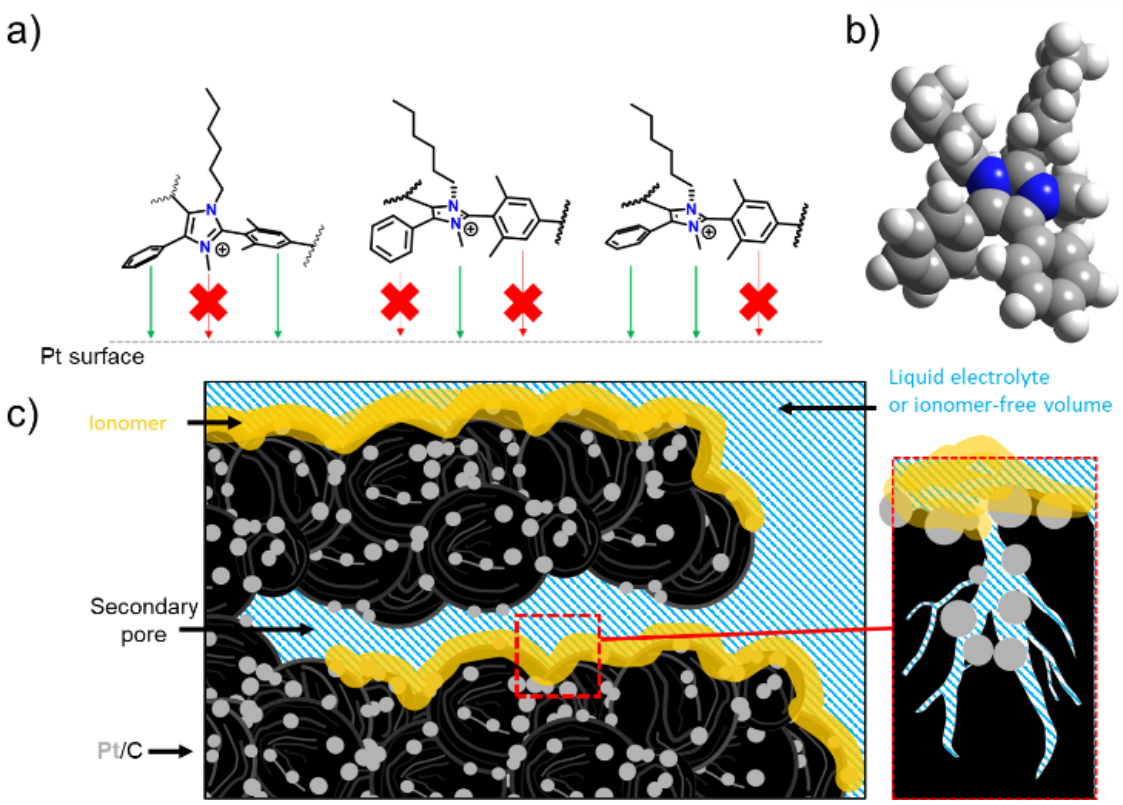

Figure 4-6: Illustrations of the ionomer and the catalytic layer: ***a) possible orientations of the phenyl and imidazolium groups allowing (green) or preventing (red) parallel adsorption to the Pt surface, indicating that complete blocking of the surface through phenyl adsorption cannot be achieved; b) space-filling model of the monomeric unit of the molecule (grey, carbon; white, hydrogen; and blue, nitrogen) illustrating steric encumberment around the imidazolium heterocycle; c) catalytic layer morphology, with the nanoparticles in contact with the ionomer being in the secondary pores, and with diffusion within the agglomerate inner porous network being assured by the liquid electrolyte or through surface diffusion onto the carbon/platinum surface.***

The presence of ionomer had only a mild impact on the ECSA between the I:C 0 -> 0.196 range (Figure 4.3(b) and Figure 4.5(c)) and could be attributed to the aforementioned 'cation-hydroxide-water co-adsorption' or 'phenyl adsorption' phenomena. The probability of the ionomer-related adsorption can be further addressed based on the understanding of its structure (Figure 4.6). In the ionomer, the mesityl groups are 90° to the imidazolium ring (Figure 4.6(a)), due to the steric hinderance from the methyl groups.[104] Furthermore, the mesityl groups are incorporated in both para positions from the aromatic ring (Figure 4.6(a-c)), which would lead to a substantial steric hinderance for

both the mesityl and the imidazolium ring adsorption. However, it is worth noting that the C4 phenyl group has more freedom to rotate and can be responsible for the slight decrease in ECSA observed on Figure 4.3(b) at high I:C ratios. Although it is worth underlining that the C4 phenyl group is the only group per repeating unit that might affect the Pt reactivity, thus explaining why only a negligible decrease of the ECSA is observed. Alternatively, a slight decrease of the HOR limiting current is observed at I:C = 0.196, indicative of a decreased accessibility of H_2 to the reactive interface, which is symptomatic of a 'cation-hydroxide-water' adsorption. However, this interaction is believed to remain minimal because of the important steric encumberment around the charged nitrogen functionalities (Figure 4.6(b)).

In addition to the ionomer structure, the marginal effect of the ionomer of the ECSA is also explained by the catalytic layer morphology (Figure 4.6(c)), which is consistent with the catalytic layer morphology in AEMFCs and AEMWEs. Specifically, the ionomer encapsulates the carbon agglomerates and accesses the secondary pores but does not access the agglomerates inner porous network or the porosities within the carbon primary particles, which explains why the pseudo-capacitive charging of the catalyst layer is independent of the I:C ratio.[148] Hence, an eventual poisoning effect of the ionomer would only affect the Pt NPs situated on the outside of the agglomerates, whereas the Pt NPs situated in the agglomerates/primary particles inner porous network shall not be affected. They remain nevertheless active for the HOR/HER as the ionic species shall diffuse to them through surface diffusion (AEMFCs) or in the liquid electrolyte (AEMWEs, this work). Thus, not only the structure of the ionomer is critical, but the morphology of the catalytic layer as well, with a poorly constructed catalytic layer or the use of molecular compounds (*e.g.,* monomers, I^-) leading to an exacerbated poisoning, owing to the fact that said compounds can diffuse into the carbon agglomerate/primary particles inner porosities.

4.4. Conclusion

In this Chapter a simple, scalable synthetic route was used to develop a novel C2-protected poly(imidazolium) with a limited number of freely rotating phenyl groups per repeat unit. Alongside the low density of phenyl groups, the insolubility of the DMP-PHPI-M in basic solutions enabled a detailed study on the impact of the interactions between this ionomer and the Pt/C catalyst, on the HER and HOR. The ionomer:carbon interactions and, especially, the specific adsorption of the ionomer through its aromatic rings or its

cation (*e.g.,* ‘cation-hydroxide-water co-adsorption’ or ‘phenyl adsorption’) were investigated on Pt surface. In terms of intrinsic activity, no negative effect was observed (*i.e.*, no variation of the microkinetic current calculated for the HER/HOR) for I:C ratios up to 0.196. A mild decrease of the Pt specific surface, and resulting overall activity, was observed at high I:C ratios, possibly induced an extremely small contribution of the specific adsorption of the ionomer through its cations or aromatic cycles. Opposingly, small I:C ratios led to an increased specific surface and activity *vs.* ionomer-free Pt/C, induced by an increased catalytic layer stability in presence of ionomer.

This family of ionomers presents not only a simple, scalable synthetic route with good solubility but also mitigates performance losses related to its interactions with the electrocatalyst. To elucidate the impact of poly(imidazolium) cation-water-hydroxide *vs* phenyl adsorption on Pt/C catalysts systematic structural variations of this material should be synthesised. The described synthetic method enables said systematic polymer modifications, which is discussed in more detail in Chapter 7.

Chapter 5. The First Investigation of Poly(imidazolium) End Group Alkaline Stability

Kate Fraser and Prof. Steven Holdcroft envisioned the project. Kate Fraser performed all synthesis and characterisations. Dr. Alessandra Stacchini Menandro performed the alkaline degradation test.

Prof. Steven Holdcroft advised and supervised the project.

5.1. Introduction

The most common synthetic method used for development of poly(imidazolium) ionenes is a step growth polymerization which can be classified as either AA-BB or AB, dependent on the monomers used.[53,102,103,114] AA-BB step growth polymerization has been used successfully to synthesize high molecular weight poly(imidazolium) ionenes.[103] Fan *et al*., used a terphenyl dialdehyde and reacted it with a *bis*-1,2-diketone *via* the Debus Radziszewski (DR) reaction to yield a high IEC poly(imidazolium) (Figure 5.1(a)). However, the use of two monomers results in a polymer sample with end groups that cannot be defined. The end groups could consist of two aldehydes, two diketones or a mixture of both functionalities (Figure 5.1(b)) and the high molecular weight of the polymers makes end group analysis impossible. Whilst the importance of model compounds to assist in the determination of alkaline stable polymer repeat units has not been understated in the literature,[21,38,39,41,76,90–94] the limited characterization of electrophilic carbonyl end groups are a concern for the continued development of highly alkaline stable ICPs.

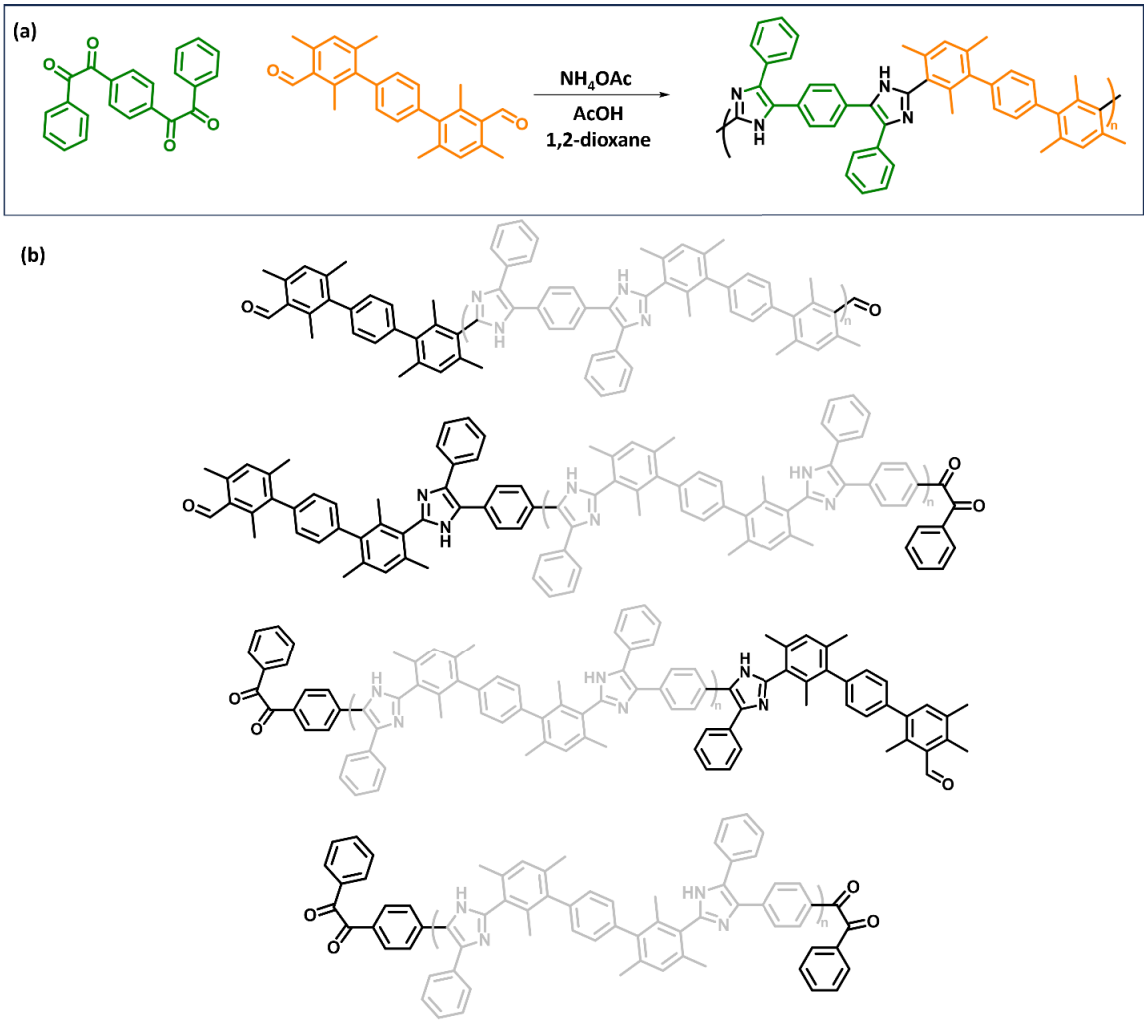

Figure 5-1: Poly(imidazole) AA-BB step growth polymerisation synthesis. ***(a) The AA-BB step growth polymerization demonstrated by Fan et al., The AA monomer (green) has two diketones and the BB monomer (orange) is a terphenyl dialdehyde that react together to from the uncharged poly (imidazole). (b) The four possible end group structures that exist in the AA-BB polymerization sample of the poly(imidazole).***

Polymer degradation beginning at reactive end groups is not a new concept. The commercially available Nafion polymer and its derivatives have carboxyl end groups that can be degraded through a radical mechanism resulting in an 'un-zipping' of the polymer chain. The end-capping of the reactive carboxyl groups increased the stability of Nafion and its derivatives with the sulfonic acid or trifluoromethyl terminated molecules degrading 400 times slower than the standard carboxyl terminated polymers.[149–151]

Until recently, the polymerisation methods prevented specific end group chemistries of poly(imidazolium)s to be known, making an end group alkaline stability investigation impossible. Using an AB-type step growth polymerization, Overton *et al.,*[114] were able to create a poly(imidazolium) with end groups defined by the difunctional monomer (Figure 5.2(a)). By using a single monomer containing diketone and aldehyde functionalities, the poly(imidazole) was formed with known diketone and aryl-aldehyde end groups (Figure 5.2(a)). The knowledge of end group chemistry enabled the authors to react the diketone end group with trimethyl benzaldehyde for molecular weight control (Figure 5.2(b)).

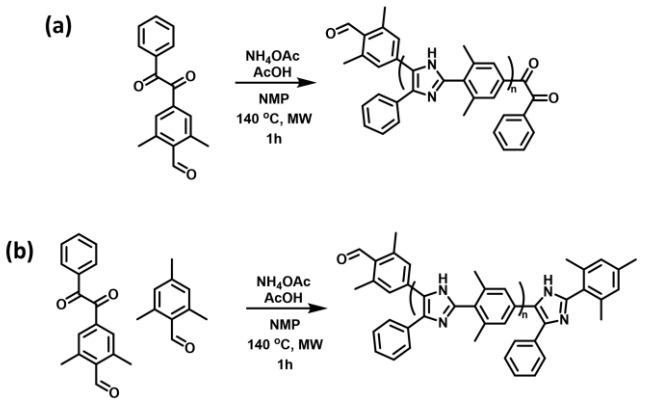

Figure 5-2: Poly(imidazole) AB step-growth polymerisation.
(a) the first synthesis of an AB step growth poly(imidazole) (b) the end capping with trimethylbenzaldehyde of the diketone end group in situ during the polymerization step.

Despite the low concentration of end groups with respect to main chain repeat units, the significant improvement in stability observed for the Nafion-type polymers when end capped with a degradation-resistant functionality, stresses the importance of investigating polymer end group stability. Whilst many studies have focused on the stability of the imidazolium functionality,[43,91,102] there has yet to be an investigation into the impact of end group alkaline stability.

In this work, a new approach to study the end group stability/degradation of promising poly(imidazolium)s was developed. Initial results are presented in this chapter. In this approach, model compounds are used that are analogous to the end groups of an AB-type poly(imidazolium) (Figure 5.3(a)), however synthetic challenges prevented

complete synthesis of the desired molecules. Therefore, oligomers identical to the poly(imidazolium)s, but lower molecular weight, were used to increase the concentration of end groups *vs* main chain units. The oligomers were synthesized using similar reaction conditions to the AB step growth polymerization described in Figure 5.2(a), but reaction time and polymer solubility were controlled to limit molecular weights. Three oligomers were synthesized: DMP-PPI-AD with aldehyde and diketone end groups that were end capped to form DMP-PPI-A with an exposed aldehyde and DMP-PPI-D with an exposed diketone end group (Figure 5.3(b)). The end groups were characterized by ^{1}H NMR and ^{13}C NMR and used to demonstrate that poly(imidazolium) polymers can be end capped to create end groups that are the same or similar functionalities to the main chain chemistry.

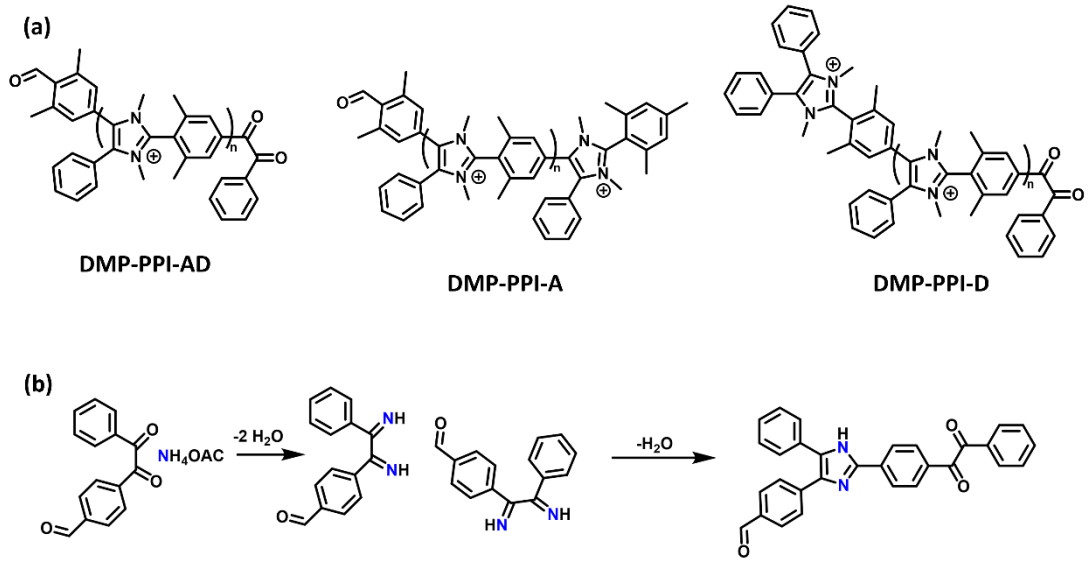

Figure 5-3: The oligomers synthesized in this study.
(a) DMP-PPI-AD with exposed aldehyde and diketone end groups, DMP-PPI-A with only exposed aldehyde end groups and DMP-PPI-D with only exposed diketone end groups (b) the first step of the AB step growth polymerization mechanism demonstrating how using this method leads to accurate knowledge of the polymer carbonyl end groups.

5.2. Experimental

Synthesis of 5-bromo-2-iodo-m-xylene: 5-bromo-2-iodo-1,3-dimethylbenzene (1 eq., 3.216 mmol, 4.00 g) and dry THF (32 mL) was bubbled with argon for 1 hour. The mixture was cooled to -15 °C and *i*-PrMgCl (2M in THF, 2 eq., 25.727 mmol, 12.863 mL) was added dropwise. The reaction was kept at -15 °C for 2 hours whilst stirring, then DMF (3 eq., 38.590 mmol, 2.988 mL) was added dropwise. The reaction was brought to room temperature and stirred overnight, forming a white precipitate. The mixture was quenched with 1M and left to stir for 30 min. The product was extracted in ethyl acetate, washed with 1M HCl, water, brine, and dried with $MgSO_4$. The crude product was dried onto silica and separated from remaining starting material by filtration over a pad of silica gel and hexanes as the eluent. The yield was 96 %. ^{1}H NMR (500 MHz, DCM-d_2, ppm) δ: 10.57 (s, 1H), 7.29 (s, 2H), 2.58 (s, 6H). ^{13}C NMR (125 MHz, DMSO-d_6, ppm) δ 193.48, 142.83, 131.92, 131.34, 126.48, 19.49.

Synthesis of 2,6-dimethyl-4-(phenylethynyl)-benzaldehyde: 4-bromo-2,6-dimethylbenzaldehyde (1 eq.) was dried overnight under vacuum then mixed with $Pd(PPh_3)_2Cl_2$ (1 mol%), and PPh_3 (1.5 mol%) in an oven dried Schlenk flask. The atmosphere was replaced with argon by placing under vacuum then filling the flask with argon 3 times. The phenylacetylene (1.1 eq.) was mixed with triethylamine (16 eq.) and bubbled with argon. The phenylacetylene/TEA mixture was added to the Schlenk flask via cannula, and the reaction mixture was degassed via a freeze-pump-thaw cycle. The CuI (1 mol%) was dissolved in degassed diethylamine and added to the reaction via cannula. The reaction was run at 50 °C for 16 hrs. The crude product was taken up in diethyl ether, washed with NH_4Cl (1 M), HCl (1 M), water, brine and dried with $MgSO_4$. The product was dried under reduced pressure and excess phenylacetylene was removed via sublimation. The yield was 98 %. ^{1}H NMR (500 MHz, DCM-d_2, ppm) δ: 10.62 (s, 1H), 7.59 (m, 2H), 7.46 (m, 3H), 7.34 (s, 2H), 2.63 (s, 6H). ^{13}C NMR (125 MHz, DMSO) δ 193.64, 141.01, 132.04, 131.55, 129.31, 128.89, 126.45, 121.76, 91.93, 88.63, 19.71.

Synthesis of 2,6-dimethyl-4-(2-oxo-2-phenylacetyl)benzaldehyde: 2,6-dimethyl-4-(phenylethynyl)-benzaldehyde (1 eq.) was mixed with pyridine-N-oxide (5 eq.) and iodine (0.02 eq.) or PdI_2 (0.02 eq.) and heated to 140 °C for 20 hrs. The reaction was cooled to room temperature and extracted in ethyl acetate. The organic layer was washed with saturated NH_4Cl, saturated $Na_2S_2O_3$, 1 M HCl, water, brine and $MgSO_4$. The crude

product was purified in a silica column with 1:4 ethyl acetate: hexanes. The yield was 90 %. ^{1}H NMR (500 MHz, DCM-d_2, ppm) δ: 10.68 (s, 1H), 7.98 (d, 2H), 7.80 (t, 1H), 7.73 (s, 2H), 7.64 (t, 2H), 2.65 (s, 6H). ^{13}C NMR (126 MHz, DMSO) δ 194.71, 194.42, 194.07, 141.07, 137.34, 135.65, 134.31, 132.09, 130.03, 129.77, 129.50, 19.64. S $[M+NH_4]^+$: Calculated for $C_{17}H_{14}O_3[NH_4+]$ 284.128, found 284.139, $[M+CH_3OH+H]^+$: calculated for $C_{17}H_{14}O_3[CH_3OH][H]^+$ 299.1278, found 284.139

Synthesis of 1-(4-(4,5-diphenyl-1H-imidazol-2-yl)-3,5-dimethylphenyl)-2-phenylethane-1,2-dione: Benzil (0.118 g, 0.563 mmol, 1.5 eq.) was stirred with ammonium acetate (0.290 g, 3.76 mmol, 10 eq.) in acetic acid (10 mL) until dissolved. Compound 4 (0.100 g, 0.376 mmol, 1 eq.) was then added to the reaction. The pressure vessel was heated at 130 ºC for 16 hrs. Once cooled, the reaction was precipitated into an ammonium hydroxide/water mixture and the solid was filtered and washed with water. The reaction was purified on a silica column and 9.5:0.5 DCM/Ethyl acetate eluent giving a yellow gel. Yield = 17 %. ^{1}H NMR (500 MHz, Acetone) δ 11.56 (s, 1H), 8.03 – 7.97 (m, 2H), 7.84 – 7.77 (m, 1H), 7.75 (s, 2H), 7.71 – 7.62 (m, 4H), 7.57 (d, *J* = 7.6 Hz, 2H), 7.51 – 7.08 (m, 7H), 2.38 (s, 6H).

Synthesis of 1-(3,5-dimethyl-4-(1-methyl-4,5-diphenyl-1H-imidazol-2-yl)phenyl)-2-phenylethane-1,2-dione: 1-(4-(4,5-diphenyl-1H-imidazol-2-yl)-3,5-dimethylphenyl)-2-phenylethane-1,2-dione (0.460 g, 1.01 mmol, 1 eq.) was dissolved in DMSO (20 mL). KOH (6 M, 0.252 mmol, 1.51 mmol, 1.5 eq.) was added dropwise and stirred for 30 mins. Iodomethane (0.126 mL, 2.02 mmol, 2 eq.) was added and the reaction was stirred at room temperature for 2 hours. Diethyl ether (100 mL) was added, and the organic layer was washed with water (150 mL). The organics were then evaporated under reduced pressure leaving a yellow solid. Yield = 99% ^{1}H NMR (500 MHz, DMSO) δ 8.00-7.95 (m, 2H) 7.87 – 7.78 (m, 2H), 7.77 (s, 2H), 7.59 – 7.42 (m, 11H), 7.22 (td, *J* = 7.6, 5.5 Hz, 2H), 7.18 – 7.10 (m, 1H), 3.13 (s, 3H), 2.20 (s, 6H).

Synthesis of DMP-PPI-AD: In a 150 mL pressure vessel, acetic acid (40 mL) and ammonium acetate (8.68 g, 10 eq., 112.67 mmol) were stirred at room temperature until dissolution. 2,6-dimethyl-4-(2-oxo-2-phenylacetyl)benzaldehyde (3.00 g, 1 eq., 11.27 mmol) was added and the reaction was heated at 130 ºC, for 5 h. Once cooled, the reaction was precipitated into 0.01 M NH_4OH. The yellow solid was filtered under vacuum and washed with water until the filtrate was neutral. The sample was dried in an 80 ºC

oven, overnight to yield a yellow solid. Yield = 82 %. ^{1}H NMR (500 MHz, DMSO) δ 7.72 – 7.46 (m, 7H), 2.25 (s, 6H).

Synthesis of DMP-PPI-AD[+]: In a 100 mL round bottomed flask, DMP-PPI-AD (1 g, 1 eq., 4.03 mmol) was suspended in DMSO (40 mL) and stirred with Na_2CO_3 (3 g, 7eq., 28.30 mmol) at room temperature. The reaction turned from yellow to orange. Methyl iodide (0.26 mL, 1.1 eq., 4.43 mmol) was added dropwise and the reaction was stirred at room temperature, for 16 h. The reaction was then precipitated into water and filtered. The yellow solid was dried in an 80 °C oven, overnight and used without further purification. The single methylated DMP-PPI-AD was dissolved in DMF (20 mL) in a 60 mL pressure vessel and methyl iodide (0.52 mL, 2 eq., 8.04 mmol) was added dropwise. The reaction was heated to 60 °C for 16 h. Once cooled the reaction was precipitated in ethyl acetate and the yellow solid collected with gravity filtration. The solid was dried in an 80 °C oven overnight. Yield 95%. ^{1}H NMR (500 MHz, DMSO) δ 7.72 – 7.46 (m, 7H), 2.25 (s, 6H). %. ^{1}H NMR (500 MHz, DMSO + TFA) δ 7.72 – 7.46 (m, 7H), 3.58 – 3.49 (m, 4H), 2.25 (s, 6H).

Synthesis of DMP-PPI-D: In a 48 mL pressure vessel benzil (0.026 g, 0.3 eq., 0.123 mmol) was stirred with ammonium acetate (0.019 g, 0.6 eq., 0.246 mmol) in acetic acid (6 mL). Once dissolved, DMP-PPI-AB (0.1 g, 1 eq., 0.41 mmol) was added, along with 3 drops of trifluoroacetic acid. The reaction was heated to 130 °C for 3 days. Once cooled, the reaction was precipitated into 0.01 M NH_4OH. The yellow solid was collected using gravity filtration, washed with water, and dried in the oven overnight at 80 °C. ^{1}H NMR (500 MHz, DMSO) δ 7.72 – 7.46 (m, 7H), 2.25 (s, 6H).

Synthesis of DMP-PPI-D[+]: In a 100 mL round bottomed flask, DMP-PPI-D (0.1 g, 1 eq., 0.403 mmol) was suspended in DMSO (40 mL) and stirred with Na_2CO_3 (0.3 g, 7eq., 2.830 mmol) at room temperature. The reaction turned from yellow to orange. Methyl iodide (0.026 mL, 1.1 eq., 0.443 mmol) was added dropwise and the reaction was stirred at room temperature, for 16 h. The reaction was then precipitated into water and filtered. The yellow solid was dried in an 80 °C oven, overnight and used without further purification. The single methylated DMP-PPI-D was dissolved in DMF (20 mL) in a 60 mL pressure vessel and methyl iodide (0.052 mL, 2 eq., 0.804 mmol) was added dropwise. The reaction was heated to 60 °C for 16 h. Once cooled the reaction was precipitated in ethyl acetate and the yellow solid collected with gravity filtration. The solid was dried in an

80 ºC oven overnight. Yield 87%. ^{1}H NMR (500 MHz, DMSO) δ 7.72 – 7.46 (m, 7H), 2.25 (s, 6H). %. ^{1}H NMR (500 MHz, DMSO + TFA) δ 7.72 – 7.46 (m, 7H), 3.58 – 3.49 (m, 4H), 2.25 (s, 6H).

5.3. Results

5.3.1. Model Compound Synthesis

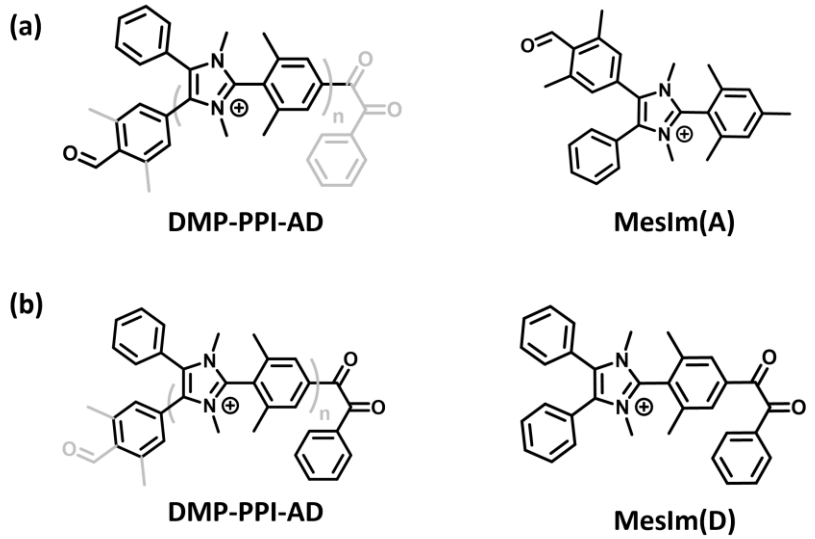

Figure 5-4: The model compounds designed analogous to poly(imidazolium) end groups. ***(a) The model polymer, DMP-PPI-AD with exposed aldehyde (A) and diketone (D) end groups. The areas in black represent the areas that were selected as important for a model compound representing the aldehyde end group. MesIm(A) is the model compound designed to represent the aldehyde end group. (b) the model polymer, DMP-PPI-AD with exposed aldehyde (A) and diketone (D) end groups. The areas in black represent the areas that were selected as important for a model compound representing the diketone end group. MesIm(D) is the model compound designed to represent the diketone end group.***

The end group model compounds designed for this work are shown in Figure 5.4. MesIm(A) and MesIm(D) were designed to be exact small molecule analogues of the final unit of the polymer chains and therefore contain an imidazolium and either an aryl aldehyde (A) or diketone (D). The model compound synthesis was done using the same DR reaction as the original AB-type step growth polymerisation; however, the reactions were terminated when a single repeat unit was created.

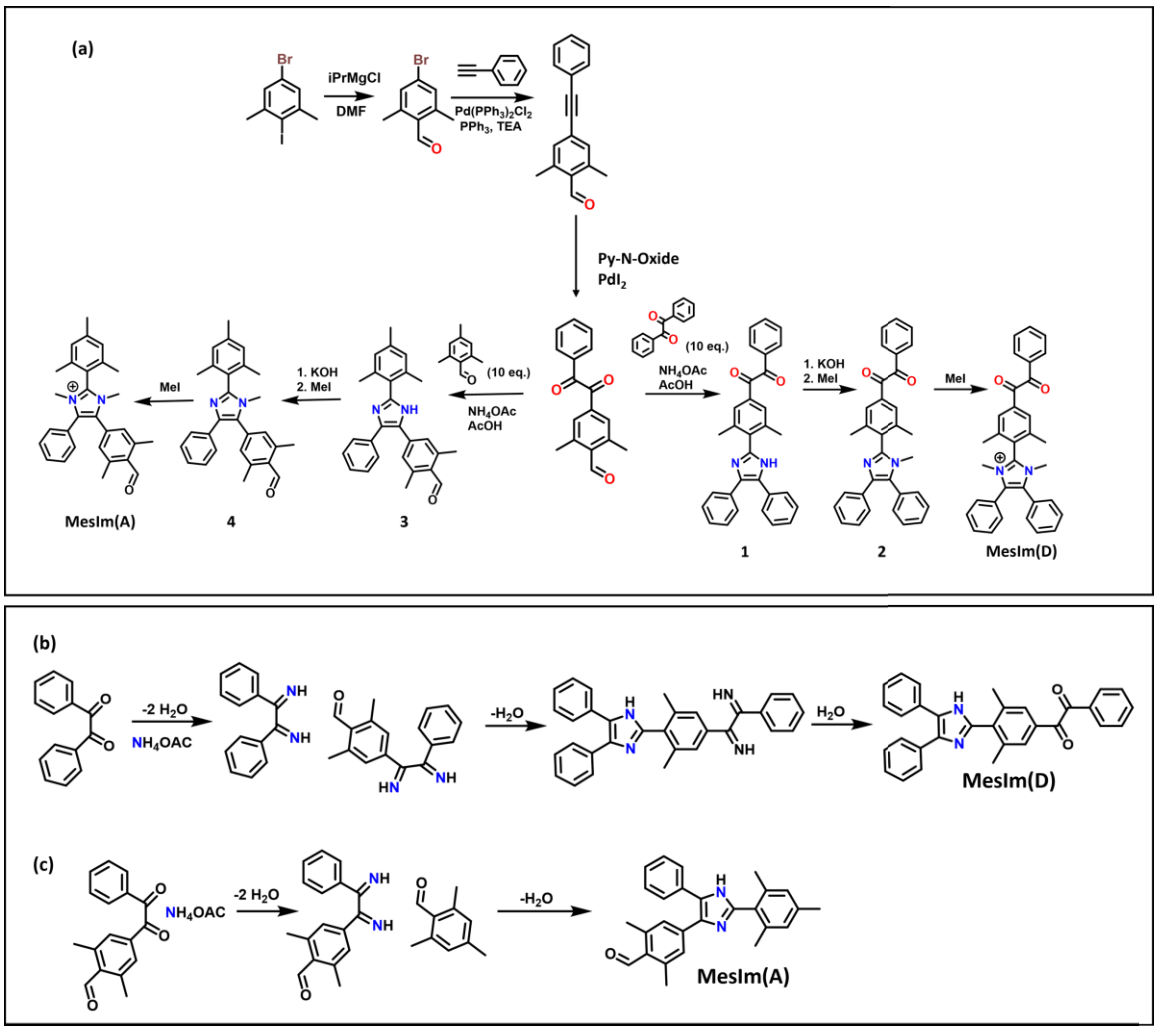

Figure 5-5:The designed synthetic route for end group model compounds MesIm(A) and MesIm(D). ***The DR reaction that will be terminated by using an excess of (b) benzil and (c) trimethylbenzaldehyde*.**

The model compound syntheses began with the same monomer synthesis procedure conducted in Chapter 3 (Figure 5.5(a)). The AB-type difunctional monomer can be used in the DR reaction, however if conducted in the same conditions as Chapter 3, a polymerisation reaction would occur rather than the desired model compound. By adding a large excess of benzil (Figure 5.5(b), MesIm(D)) or trimethyl benzaldehyde (Figure 5.5(c), MesIm(A)), the polymerisation would be terminated at the aldehyde and diketone end groups, respectively, leaving model compounds with just one end group functionality exposed. In the case of MesIm(D), adding a large excess of benzil with respect to *dm*-OPAB would mean that the aldehyde groups were more likely to react with a benzil

molecule than the diketone functionality of *dm*-OPAB (Figure 5.5(b)). This would effectively terminate the polymerisation reaction at just one repeat unit, MesIm(D). The same prediction was used for the synthesis of MesIm(A) (Figure 5.5(c)).

Compound 1 was synthesised from *dm*-OPAB using the synthetic method described in Figure 5.4(a). The sharp peaks shown in the ^{1}H NMR (Figure 5.6(a)) suggested the polymerisation reaction did not occur and the respective integrations are as expected for compound 1. The imidazole N***H*** peak was observed at 11.55 ppm. The aromatic region could be assigned using a combination of splitting patterns and integrations. Notably, singlet H_f is at 7.75 ppm, H_d as a doublet of doublets, integrating to 2H at 8.15 ppm, H_c as a triplet at 7.80 ppm and H_g/H_e are overlapping between 7.63 and 7.71 ppm. The two methyl units (H_b) are observed as a singlet at 2.38 ppm, integrating to 6H. The first alkylation step was conducted to give compound 2 (Figure 5.6(b)) to give a ^{1}H NMR with similar peaks but the absence of the N***H*** peak at 11.55 ppm and the addition of a singlet alkyl peak at 3.12 ppm, integrating to 3H confirms the success of the reaction. However, upon attempting the final alkylation step, a large impurity was observed or side reaction. Upon further investigation of the synthesis of compound 1, there was an impurity that coeluted from the column with compound 1. This impurity could be the result of an unexpected side reaction that was either not NMR active until after the final methylation or in small quantities, unobservable under peaks from compound 1. Despite attempts to purify compound 1, there was no solvent system that would enable separation of compound 1 and the impurity. The impurity could also not be separated from compound 2 or 3 and therefore, MesIm(D) could not be synthesised as a model compound.

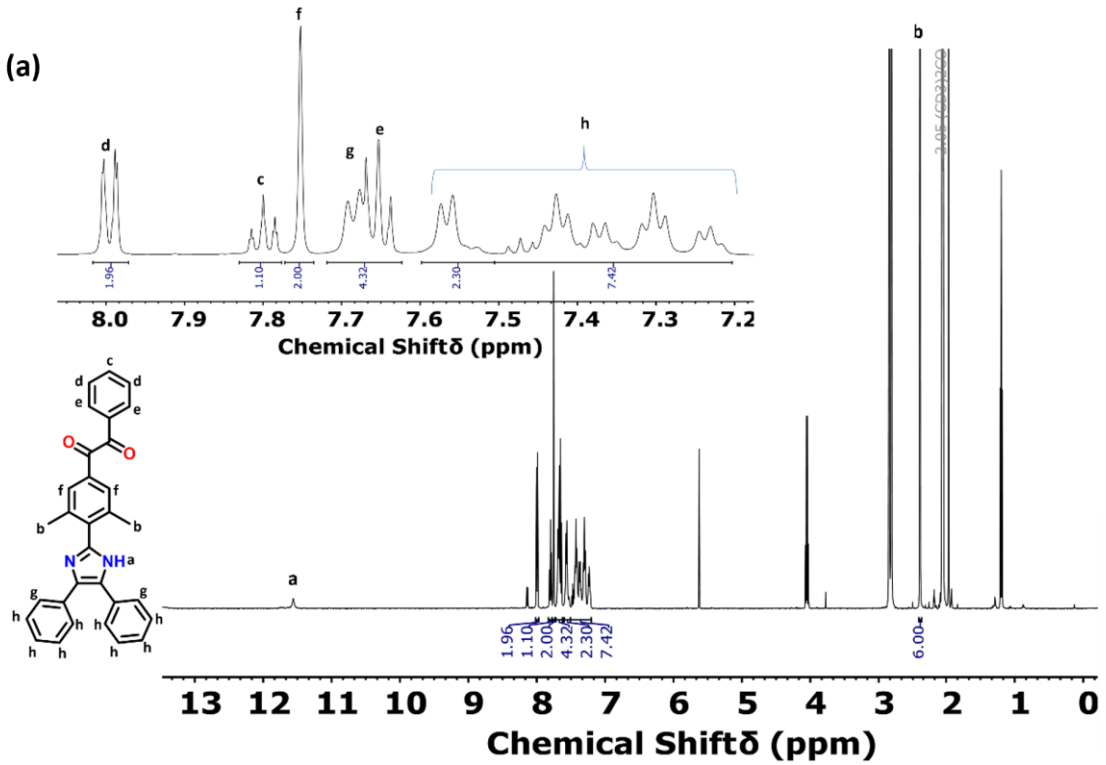

Figure 5-6: (a) ^{1}H NMR of precursor imidazole to MesIm(D).

Several different synthetic routes were attempted to synthesise compound MesIm(A) (Appendix C, Figures C.2 and C.3). Using the DR synthetic route, it was not possible to attain compound MesIm(A) due to the specific order the reagents must be added. The first step of the DR reaction is the formation of the diimine, from the diketone and ammonium acetate (Figure 3.5(b)). To ensure this step occurs, the molecule containing the diketone group must be mixed with NH_4OAc and AcOH. If the aldehyde functionality is present at this stage, the polymerisation reaction will begin to occur, which is an issue when synthesising compound 4. The addition of excess trimethyl benzaldehyde prior to the formation of the diimine was found to prevent the imidazole ring closing from occurring.

Despite the consensus within the literature that alkaline stability should be tested first on model compounds, it was not possible to obtain compounds for the end groups of the polymers. Therefore, the focus shifted towards synthesising oligomers that are

chemically identical to polymers of DMP-PPI-AD but have a lower molecular weight allowing for observation of the end groups.

5.3.2. Oligomer Synthesis

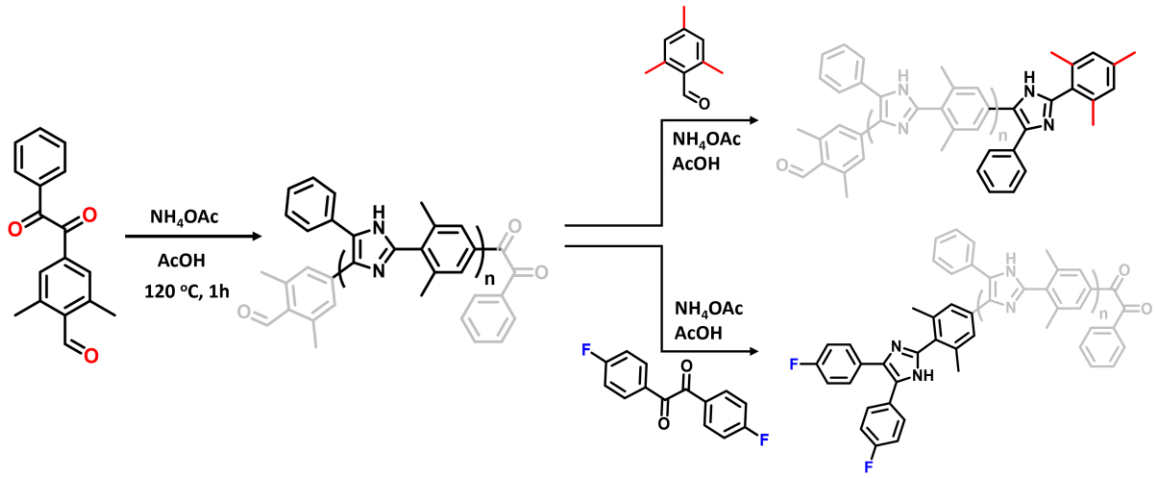

Figure 5-7: The oligomers synthesised in this work.

The monomer was prepared according to Figure 5.5(a), and the synthesis of the oligomers was optimized by varying reaction time and solvation of the reaction (Table 5.1). If the reaction time was too short the imidazole ring closing would not complete, yielding a molecule with an undefined mixture of imidazole and imine units (Table 5.1, reaction 1). If the reaction was too long, the end groups would be in low concentrations with respect to the main chain repeat units and impossible to observe using NMR methods (Table 5.1, reaction 3). The best conditions were found to be when the reagents were in a high enough concentration within the AcOH solvent that the monomer dissolved but the low molecular weight polymer was insoluble in AcOH (Table 1, reaction 4). The insolubility of the polymer chain in AcOH hindered the reaction from proceeding to high molecular weights.

Table 5.1: Optimisation of DMP-PPI-XX oligomer synthesis.

Reaction	Eq. of monomer	Mass of monomer (g)	Eq. AcOH	Volume of AcOH (mL)	Reaction time (h)

1	1	0.1	232	5.0	1
2	1	0.1	232	5.0	5
3	1	0.1	232	5.0	24
4	1	3.0	64	40.0	5

The polymerization reactions yielded a poly(imidazole)-based oligomer with aldehyde and diketone end groups (DMP-PPI-AD). The oligomer was insoluble in most organic solvents due to the hydrogen bonding between the imidazole N*Hs*. However, when protonated to form a poly(imidazolium) (Figure 5.8), the oligomer was soluble in DMSO. Figure 5.8 shows the ^{1}H NMR of the oligomer. The high intensity, broad peaks at 7.71 – 7.63 ppm (2H) and 7.58 – 7.47 ppm (3H) correspond to the aromatic protons H_a and H_c. The large upfield signal between 2.38 – 2.26 ppm (6H) is the methyl H_b protons that become the C2 steric protection. The low intensity signal at 10.51 ppm is the aldehyde end group (H_f) and the low intensity signals at 7.98 ppm and 7.83 ppm correspond to H_e and H_d, respectively.

The ^{1}H NMR of DMP-PPI-AD can be used to quantify the number average molecular weight of the oligomer sample. The single aldehyde peak (10.51 ppm) corresponds to one end group and the integration of the aromatic region, when divided by the 7Hs per repeat unit, gives the average number of repeat units. Using this method, it is estimated there are 40 repeat units per end group giving a number average molecular weight ~ 9800 g/mol.

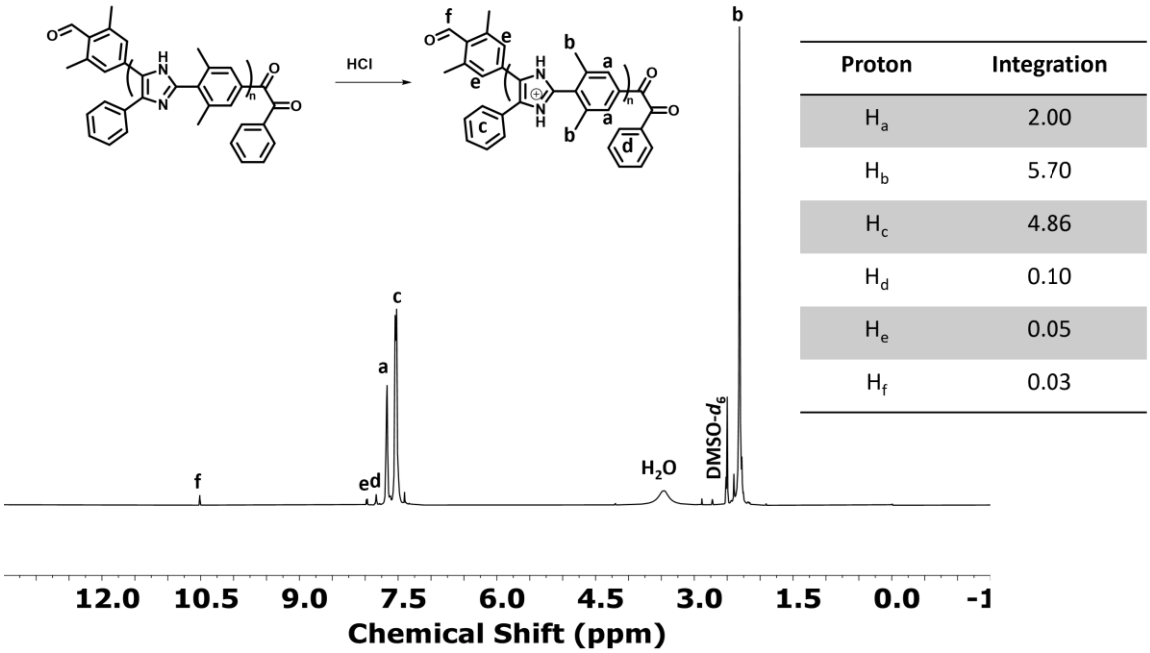

Proton	Integration
H_a	2.00
H_b	5.70
H_c	4.86
H_d	0.10
H_e	0.05
H_f	0.03

Figure 5-8: The ^{1}H NMR of oligomer DMP-PPI-AD.
The sample was protonated to improve the solubility of the oligomer. The integrations are given in the table and relative to protons Ha.

Observing the diketone end group was significantly more challenging as there were no unique ^{1}H NMR signals, aside from the small aromatic peak at 7.83 ppm. ^{13}C NMR was used to try and observe the C=O of the diketone, as the ketone carbonyl ^{13}C should be observable at ~200 ppm. However, ^{13}C NMR has a lower sensitivity in comparison to ^{1}H NMR, making observation of the low concentration end groups difficult. Several unsuccessful attempts were made to observe the diketone C=O shifts using ^{13}C NMR, even at the highest possible sample concentration, no carbonyl carbon peaks were observed. Using the 600 MHz NMR, the number of scans were increased to 5120 and the relaxation time to 6 s, again there were no observable C=O peaks. The AB polymerisation method defines that both end groups must be present in the same concentration, however the limitation of ^{13}C NMR resolution meant it was not possible further analyse the diketone end group.

DMP-PPI-AD was methylated in two steps. The first was a heterogeneous reaction using a DMSO solvent, Na_2CO_3 base to deprotonate the imidazole, and methyl iodide.

The second methylation was conducted as a homogeneous reaction using a DMF solvent and excess of iodomethane, yielding the charged poly(imidazolium) oligomer DMP-PPI-AD[+] (Appendix C, Figure C.4 and C.5.

5.3.3. Alkaline Stability and End Capping of DMP-PPI-AD[+]

The alkaline stability of DMP-PPI-AD[+] was investigated using ^{1}H NMR. DMP-PPI-AD[+] was dissolved in a 2.7 M solution of NaOD/CD_3CN/D_2O, heated to 80 ^{o}C and the change in ^{1}H NMR chemical shifts was observed (Figure 5.9). Within 24 h, the end group peaks were no longer visible on the spectrum and major changes to the peaks associated with the oligomer repeat unit structures were observed. Due to the extreme changes in ^{1}H NMR spectra, it was not possible to deconvolute main chain and end group degradation. However, previous reports suggest the C2-protected imidazolium repeat unit is highly stable in alkaline conditions, therefore it can be assumed the changes in the chemical structure of DMP-PPI-AD[+] were the result of the carbonyl end group.

The reaction of benzil in basic conditions at elevated temperature is known (Figure 5.10 (b)).[152] The hydroxide anions attack at a carbonyl C=O group which results in the reorganisation of the diketone to a carboxylic acid through a favourable carbanion migration.[152] Although not reported, it can be assumed the aldehyde end group reacts with hydroxide through a similar route (Figure 5.10(c)). The change in peaks associated with the repeat unit structure of DMP-PPI-AD[+] (Figure 5.10(a)) suggests the reorganisation of the end groups has a negative effect on the alkaline stability of the imidazoliums. This is the first evidence of the adverse effect of reactive end groups on poly(imidazolium)s with highly stable main chain repeating units.

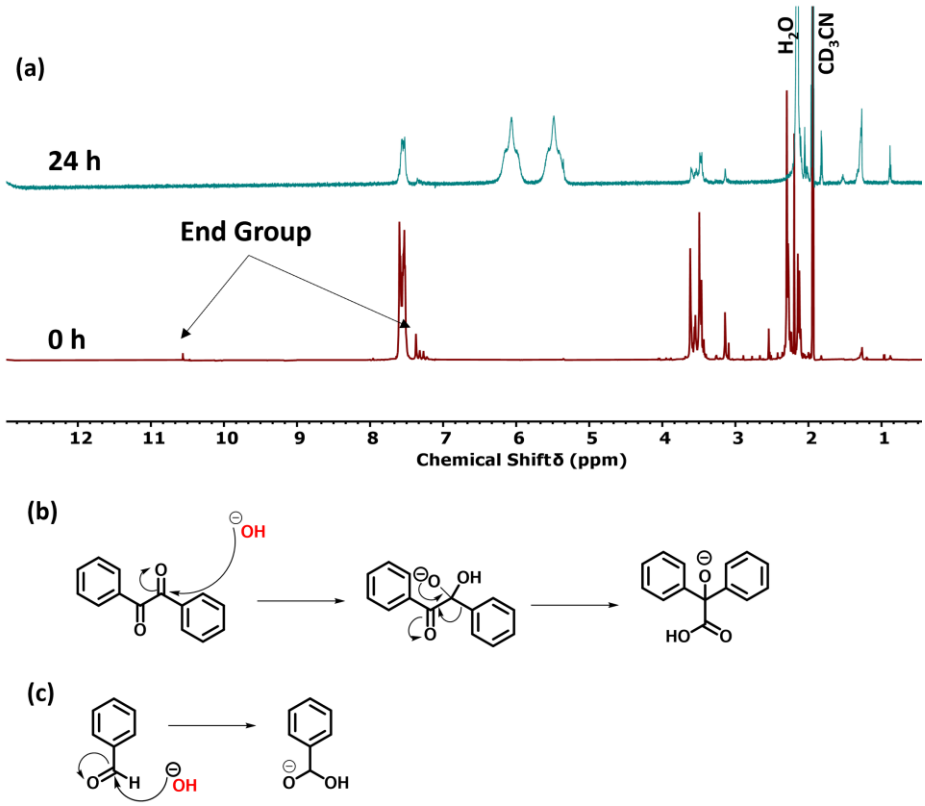

Figure 5-9: Poly(imidazolium) end group degradation analysis.
(a) ^{1}H NMR of DMP-PPI-AD reacted with NaOD/D_2O (40 wt%) in CD_3CN (1:3). The inital spectra (red) can be compared to the spectra after 24 h (green). (b) Benzil rearrangement in basic conditions (c) benzaldehyde rearrangemnt in basic conditions.

A method to potentially prevent the negative impact of the reactive carbonyl end groups on the overall alkaline stability of the poly(imidazolium)s is end capping. The diketone and aldehyde end groups can be reacted using trimethyl benzaldehyde and benzil, respectively, to yield end groups that have the same chemistry as the main chain repeat units. The aldehyde end group was capped using an excess of benzil (10 eq.), under the same conditions as the initial polymerization to form an imidazole end group. Trifluoroacetic acid was added to the reaction as an acid catalyst, with DMF to improve solubility of the oligomer. End capping the aldehyde group removed one of the two main polarizable groups, reducing the polarizability and therefore solubility of the oligomer. Even protonated, the end capped oligomer would not dissolve in available NMR solvents. The methylation steps were conducted in a heterogeneous reaction with DMSO. The second methylation was conducted in DMF to give oligomer DMP-PPI-D and could be purified through precipitation into ethyl acetate. The completion of the aldehyde end

capping could be confirmed through the disappearance of the aldehyde peak at 10.51 ppm in the ^{1}H NMR (Figure 5.10).

The diketone end group was capped using trimethyl benzaldehyde, to create the C2-protected imidazole end group. However, using ^{1}H NMR the 3 x CH_3 groups of the imidazole end group are at exactly the same chemical shift as the 2 x CH_3 groups of the main chain C2-protection.[114] Furthermore the inability to observe the diketone carbon shifts on the ^{13}C NMR prevented confirmation of end capping using this method. The insolubility of DMP-PPI-A after reaction with trimethyl benzaldehyde, similar to DMP-PPI-D, suggested a successful end-capping reaction, however no chemical analysis could be conducted to confirm this. Future work could focus on the capping of DMP-PPI-AD with 2,6-dimethyl-4-fluorobenzaldehyde and subsequent ^{19}F NMR analysis for confirmation of a successful reaction.

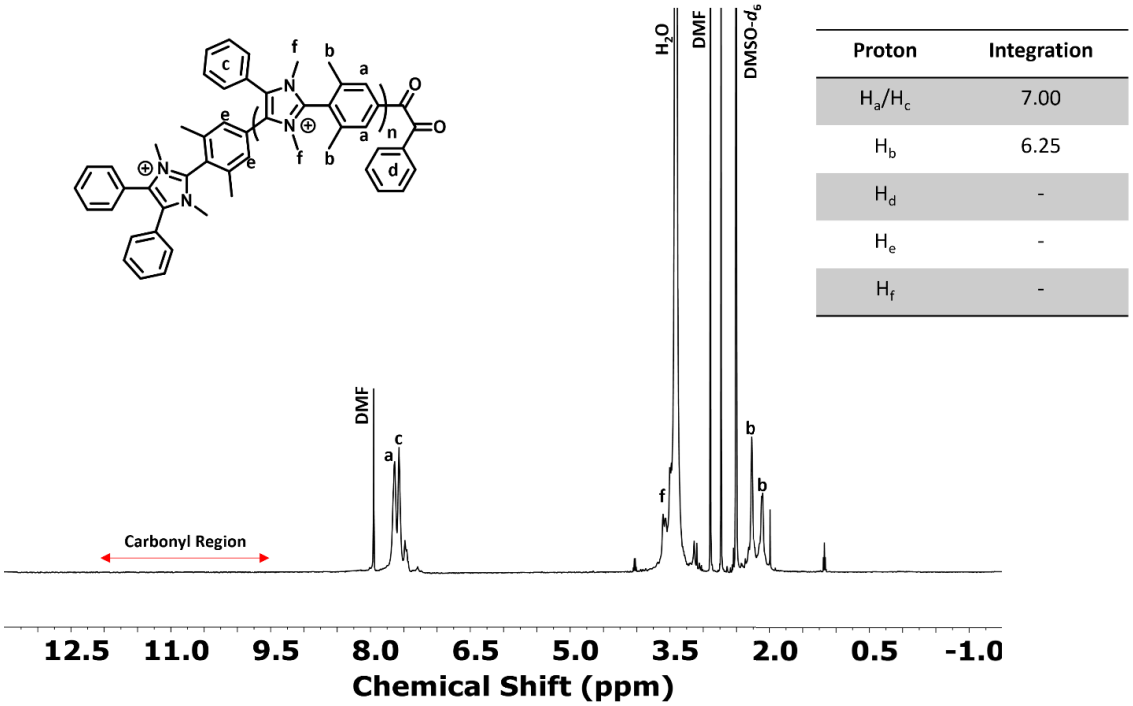

Proton	Integration
H_a/H_c	7.00
H_b	6.25
H_d	-
H_e	-
H_f	-

Figure 5-10: ^{1}H NMR of DMP-PPI-D[+].
Absence of peaks in the carbonyl region (red) suggest the aldehyde end group was end capped using benzil. Integrations for the relevant peaks are given in the table.

5.4. Conclusions

In this chapter, the importance of poly(imidazolium) end groups was discussed with respect to alkaline stability. Using the AB-type DR step growth polymerisation mechanism discussed in Chapters 3 and 4, the end groups of the poly(imidazolium) were defined and analysed using a low molecular weight oligomer. Using this new synthetic methodology end group degradation analysis for a promising poly(imidazolium) material could be conducted. Initial steps were taken towards the quantification of end group degradation and its effect on poly(imidazolium) main chain chemical stability. The developed synthetic route enables further investigation into end group control and possible improvement in chemical stability *via* end capping, as shown by these preliminary experiments.

The unexplored end group degradation of cationic ICPs could have wide-reaching impacts on the stability of next-generation materials. Further investigation into methods that enable end group degradation analysis are required for a more fruitful understanding of the connection between end group and main chain alkaline degradation. Once an exact degradation mechanism is established, potential candidates to improve the end group stabilitiy must be explored for improved alkaline stability of poly(imidazolium)s.

Chapter 6. Investigation into the Alkaline Stability of Novel Pedant Group Poly(Imidazolium)s and Analogous Model Compounds.

Dr. Thomas Skalski and Prof. Steven Holdcroft envisioned the project. Kate Fraser conducted all theoretical investigations. Dr. Thomas Skalski conducted all the synthesis and chemical analysis of small molecules. Kate Fraser and Dr. Anastasiia Konovalova conducted the polymer analysis. Dr. Anastasiia Konovalova conducted the small molecule and polymer degradation tests. Dr. Simon Cassegrain assisted in analysis and project direction.

Prof. Steven Holdcroft advised and supervised the project.

6.1. Introduction

ICPs with cationic pendant groups have gained increasing attention in alkaline electrochemical conversion devices due to the high tuneability and selectivity of the desired material.[153] These comb-like polymers have exhibited high ionic conductivity, along with high thermal and alkaline stability.[37,154] However, unlike ionenes, the stability of both the neutral polymer backbone and the cationic pendant group must be considered for development of a highly alkaline stable material.

The hydroxide stability of various model cationic groups has been investigated using both theoretical and experimental methods. The most common presentation of cation stability is through experimental solution-based degradation tests, with theoretical results to assist in the deconvolution of potential degradation mechanisms or investigation of unobservable molecular characteristics, (*i.e.,* electron density and orbital structure). However, a wide variety of methods and conditions have been employed to study cation alkaline stability, resulting in many inconsistencies within the literature. Experimentally, changing the hydroxide concentration,[91] water content,[94] solvent, temperature,[38] reaction vessel[39] and reaction time all influence the cation degradation. And although the theoretical studies are often used as explanation or supporting data to the experimentally studied degradation, the variety in theoretical method, basis set, solvent, and temperature, mean the theoretical results cannot be compared throughout the literature.

The wide variety of conditions and experiments has made it challenging to extrapolate cationic alkaline stability into polycation alkaline stability. Often when incorporated into a polymer, the alkaline stability of the polycation is much reduced when compared to the model compound prediction. For example, the Coates group measured the change in conductivity of various ammonium cations tethered to a poly(ethylene) backbone in 1 M KOH solutions,[155] which show significantly less stability than the analogous model compounds reported by Marino *et al.* in elevated temperatures at 6 M KOH.[38] Similarly, spirocyclic quaternary ammonium model compounds were found to degrade only 10% over 2000 h in 1 M at 80 °C, however when incorporated as a pendant group onto a polymer backbone, a 10 % loss in conductivity was observed at the same conditions in just 250 h.[156] However, the high alkaline stability of imidazolium model compounds was maintained when incorporated into a polymer as an ionene.[102]

The inconsistency in the alkaline stability of model compounds, and pendant group and ionene ICPs could be attributed to: (i) the different hydration environments and (ii) dihedral bond angles exhibited in model compounds and polymers. The impact of hydration environment on model compound alkaline stability has been documented in the literature,[94,102] and the variation of imidazolium stability with high and low hydration environments is demonstrated in Figure 6.1. The imidazolium compounds with no observable degradation in the high hydrated environment exhibited drastically reduced half-lives in the low hydration alkaline environment. This phenomenon has been explained by the decreased solvation shell of hydroxide in low hydration environments increasing the reactivity of the nucleophile.[157] The alkaline stability of model compounds is usually assessed in reasonably hydrated environments, whereas when the same cations are implemented as pendant groups, the polymer backbone and linker units are often hydrophobic potentially exposing the cation to low hydration environments. The dihedral bond angle is crucial for the alkaline stability of cations that use steric protection to hinder hydroxide attack, such as benzimidazolium and imidazoliums.[44,45] The bond angles exhibited in highly solvated model compounds compared to a less flexible and less solvated polymer environment could be significantly different, negatively impacting the alkaline stability. Building from this, the similarity between model compound and ionene stability could be due to the structural similarities, where no additional backbones or linkages are required resulting in a limited change in cation hydration environment or dihedral angle.

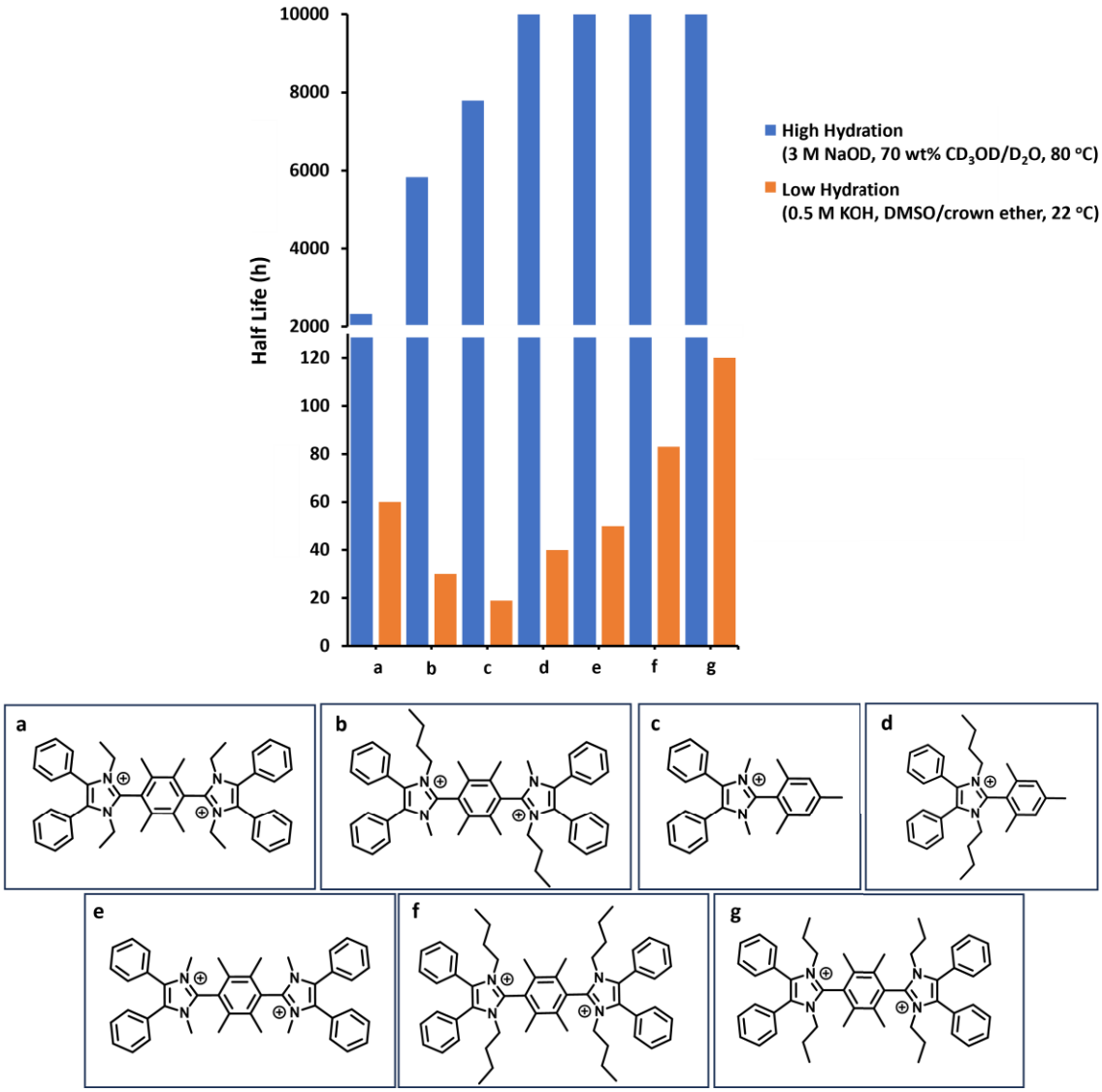

Figure 6-1: The half-lives of various imidazolium model compounds in hydrated conditions (blue, 70 wt%, CD3OD/D2O, 3 M NaOD at 80 °C) and dry conditions (orange, DMSO/crown ether, 0.5 M KOH, 22 °C). [Ref. 43].

Despite several investigations of C2-protected imidazoliums as model compounds[91] and ionenes[102,103] that have exhibited high alkaline stability, these groups are yet to be used an cationic pendant groups. In this work, poly(olefin)-based ICPs were synthesised with C2-protected imidazolium pendant groups, alongside the analogous

model compounds. Using these materials, various experimental and theoretical methods were used and compared to evaluate the different contributions impacting imidazolium alkaline stability.

6.2. Experimental

6.2.1. Synthesis

***Synthesis of 2-mesityl-4,5-triphenyl-1H-imidazole*:** In a 1 L, 2-necked round bottom flask, equipped with a magnetic stirrer, reflux condenser, and thermometer, benzil (19.99g, 1.000 eq, 93.2 ,mol) was added, along with 2,4,6-trimethylbenzaldehyde (14.38g, 14.30 mL, 1.020 eq, 95.1mmol), ammonium acetate (59.22 g, 8 eq, 745.8 mmol), aniline (53.14g, 51.99 mL, 6 eq., 559mmol) and glacial acetic acid (0.7 L). The reaction was refluxed for 24 h and then cooled to room temperature. The reaction was precipitated into water (4 L) and left to stir for 2 h. The white solid was recovered using vacuum filtration and washed with water (2 x 200 mL). The solid was then stirred in hexanes for 2h and filtered. The product was a white solid (35.30g, 91.3%, 85.2 mmol).^{1}H NMR (500 MHz, CD_2Cl_2) δ (ppm): 7.58 (d, J_d = 7.59 Hz, 2H), 7.12-7.27 (m, 11H), 6.91 (d, J_d 7.64 = Hz, 2H), 6.83 (s, 2H), 2.25 (s, 3H), 2.11 (s, 6H).^{13}C NMR (125MHz, CD_2Cl_2) δ (ppm): δ 147.05, 139.37, 138.84, 138.13, 137.11, 135.57, 131.65, 131.60, 131.57, 129.55, 128.97, 128.93, 128.68, 128.57, 128.34, 128.15, 127.76, 127.61, 126.85, 21.44, 20.52. HRMS (m/z): $[M+H]^+$ calculated for $C_{30}H_{26}N_2$: 414.2096 found : 415.2284.

Synthesis of 2-mesityl-4,5-diphenyl-1H-imidazole: In a 3L, three-neck round bottom flask equipped with a mechanical stirrer, a reflux condenser, and a thermometer, benzil (245.57 g, 1.000 eq, 1.137 mol) was added, 2,4,6-trimethylbenzaldehyde (172.86g, 172 mL, 1.005 eq, 1.143 mol), ammonium acetate (471.72 g, 9 eq, 10.24 mol) followed glacial acetic acid (1.3 L). The reaction was heated to reflux for 24h then cooled to room temperature and poured into DI water (16 L) creating a white precipitate. The beakers were left to stir for 2 h, and the solid was recovered by vacuum filtration and washed with water (2 x 500 mL). The solid was then stirred in hexanes for 2h. The solid was recovered by vacuum filtration, air dried and used without further purification. The product was a white solid (311.24g, 80.9%, 0.920 mol).^{1}H NMR (500 MHz, DMSO-d_6) δ (ppm): 12.33 (s, 1H), 7.56 (d, Jd = 7.40 Hz, 2H), 7.47 (d, Jd = 7.82 Hz, 2H), 7.39 (t, J_t = 7.32 Hz, 2H), 7.29 (m, 3H), 7.20 (t, Jt = 7.20 Hz, 1H), 6.98 (s, 2H), 2.30 (s, 3H), 2.18 (s, 6H).^{13}C NMR

(125MHz, DMSO-d_6) δ (ppm): 145.00, 137.81, 137.59, 136.08, 135.63, 131.33, 128.94, 128.62, 128.10, 127.89, 127.75, 127.26, 127.12, 126.47, 126.26, 20.75, 19.99.HRMS (m/z): $[M+H]^+$ calculated for $C_{24}H_{22}N_2$: 338.4449, found : 339.1851.

General synthesis of compounds 2b-d: In a 500 mL round bottomed flask, equipped with a magnetic stirrer, compound 1b (15.0802g, 1.0 eq, 43.7 mmol) was dissolved in DMSO (5mL per 1.0 mmol of 1b). The solution was stirred for 20 min, then KOH (60 mL, 5.0 mol/L) was added dropwise. The reaction vessel was closed and left to stir for 20 min. Compound R-X (1.2 eq.) was added dropwise over 5 min. The reaction was left to stir at room temperature for 16 h. The reaction was precipitated into water (1 L) and left to stir for 1 h. The white precipitate was recovered using vacuum filtration and washed twice with water (2 x 200 mL). The product was collected, stirred in methanol over 16 h and collected using vacuum filtration.

General synthesis of compounds 3a-d: In a 100 mL round bottom flask compound 2a-d (1 eq) was dissolved in 25 mL of acetonitrile. Benzyl bromide (1.1 eq.) was added to the reaction and the vessel was heated to 80 °C for 24 h. After cooling, the reaction was precipitated in 150 mL of ethyl acetate, filtered under vacuum, and rinsed with 10 mL of ethyl acetate. The compound was dried in the oven at 80 °C for 16 h. The compounds were a pale grey powder.

General synthesis of compounds 4a and b: In a 100 mL round bottomed flask, compounds 2a-d (1.0 eq.) were dissolved in acetonitrile (100 mL). Chloromethyl styrene (1.15 eq.) was added dropwise, and the reaction was heated to 80 °C for 24 h. After cooling, the reaction was precipitated in 150 mL of ethyl acetate, filtered under vacuum, and rinsed with 10 mL of ethyl acetate. The compound was dried in the oven at 80 °C for 16 h. The compounds were a white powder.

General synthesis of PSIM-Bz and PSIM-Ph: In a 16 mL Schlenk tube, compound 4 (1.0 eq.) was dissolved in NMP (2.5 mL), and AIBN (0.01 eq.) was added. The Schlenk reaction was freeze-pump-thawed four times, to replace the atmosphere with argon. The reaction was heated at 80 °C for 5 days. After cooling, the polymers were precipitated into ice cold water and stirred for 1h. The polymers were recovered as fine powders and dried in the oven overnight.

6.2.2. Model Compound Degradation

DFT Calculations

Electronic structure calculations were performed using Gaussian G09, B3LYP density functional theory (DFT). Pre-optimisation was performed using the 6-31G(d) basis set and final calculations were performed using the 6-311++G(2d,2p) basis set.[44,46] Vibrational frequency calculations at the same level of theory were performed at 298.15 K.

Dihedral angle measurements

The Polarisable Continuum Model (PCM) was used for implicit solvent using the G09 integrated integral equation formalism (IEFPCM) with water as solvent (ε = 78.36).

Transition State Theory

The calculations were conducted in accordance with previous literature reports of similar compounds.[43,44,103,158]Reagents (A^+) and products (P) were optimised to an energy minimum. Transition states (TS) were optimised using either the Berny algorithm or Transit Guided Quasi-Newton Method (QST3). The TS were optimised to one imaginary frequency. Frequency analysis at 298.15 K was performed to obtain reaction free energy (ΔG) and reaction free energy of activation ($\Delta G^{\neq}$). The values are given as a change in free energy with respect to the reagent and are calculated by:

$$\Delta G_{TS}^{\neq} = G([A \cdots OH]^{\neq}) - G(A^+) - G(OH^-)$$

$$\Delta G_P = G(P) - G(A^+) - G(OH^-)$$

Whilst complete degradation pathways have been previously calculated for imidazoliums,[44] the rate determining step corresponds to hydroxide attack at either the electrophilic C2 position or the α-C on the N-functionality.

Frequency Calculations

The optimised geometries for the reagents and products should have no imaginary frequencies and the TS structures should have a single imaginary frequency. The vibration associated with the imaginary frequency should correspond to the reaction coordinates of the degradation pathway (Figure 6.2).

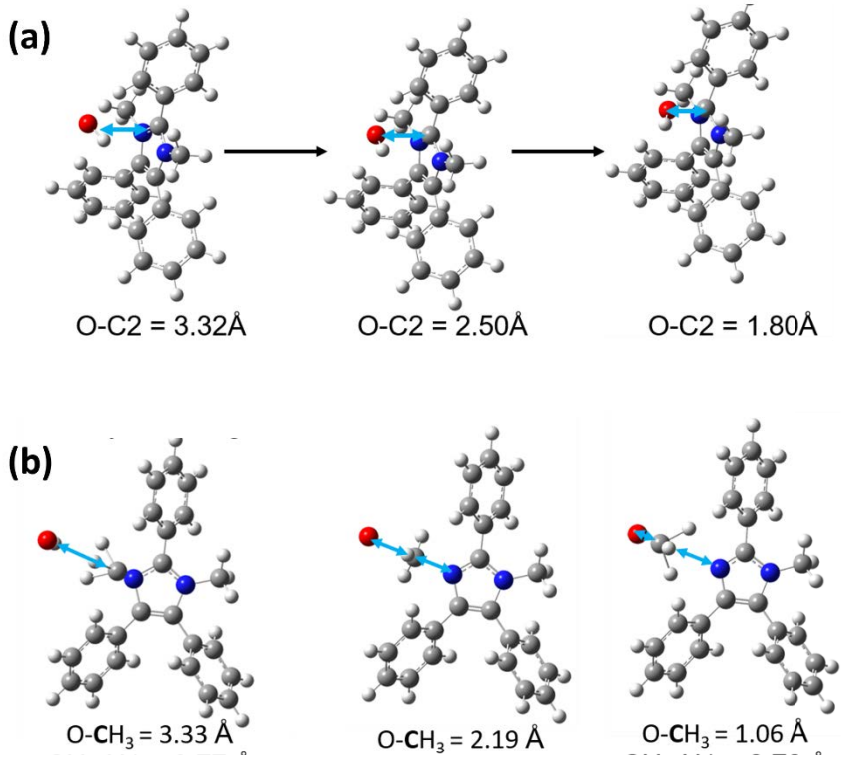

Figure 6-2: The vibrations associated with transition states. ***(a) Ring opening degradation pathway and (b) dealkylation degradation pathway. The distances between the oxygen of the hydroxide and atoms on the imidazolium are there as an indicator to show the movement of the system due the vibration associated with the imaginary frequency.***

6.3. Results and Discussion

Four imidazolium cations were designed for suppression of both C2-hydroxide attack and defunctionalisation degradation mechanisms (Figure 6.3). The mesityl group on the imidazoliums was selected for C2 steric protection with additional encumberment provided by different bulky N-functionalities (methyl, butyl, phenyl, and benzyl). The methyl N-functionality has been shown to exhibit good steric protection regarding the C2 hydroxide attack,[103] while the butyl group has improved resistance against dealkylation.[48] The phenyl group was selected due to the absence of an α-carbon, inhibiting the dealkylation reaction and the benzyl group was used to investigate the stability of the linker unit between the backbone and cation.

The model compound imidazolium alkaline stability was studied using various theoretical (dihedral angle, transition state theory (TST) and lowest unoccupied molecular orbital (LUMO) energies) and experimental methods (dihedral angle and a solution-based NMR study). As a polymer, the poly(imidazolium) stability was investigated using a thermogravimetric method that varies the hydration environment. The results were compared to give an overview of the methodologies available to probe alkaline stability.

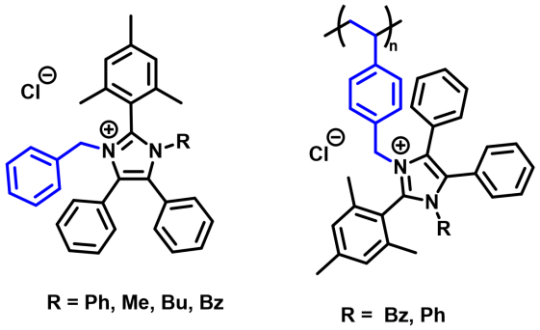

Figure 6-3: Imidazolium model compounds and polymers investigated in this study.

6.3.1. Model Compound Investigation

The four selected imidazolium model compounds containing a C2-protecting mesityl group, a N-benzyl functionality and either methyl, butyl, phenyl, or benzyl as the other N-functionality, were synthesised as described in Figure 6.4. Compound 1a was synthesised in a 4-component condensation, using benzil, trimethyl benzaldehyde, ammonium acetate, and an excess of aniline (Figure 6.4(a)). Compound 1b was synthesised through a 3-component (benzil, trimethyl benzaldehyde, and ammonium acetate) condensation reaction as per previously reported in the literature (Figure 6.4(a)).[46] 1b was dissolved in DMSO, deprotonated with excess KOH and reacted with iodomethane, butyl-bromide or benzil-bromide to yield the single N-alkylated imidazole (Figure 6.4(b)). The second alkylation of compounds 1a, and 2b-d proceeded through nucleophilic substitution of the unsubstituted nitrogen with benzyl chloride to create model imidazolium compounds (compounds 3a-d, Figure 6.4(c)). The model compounds and

monomers were characterized using ^{1}H NMR, ^{13}C NMR, single crystal XRD and mass spectrometry.

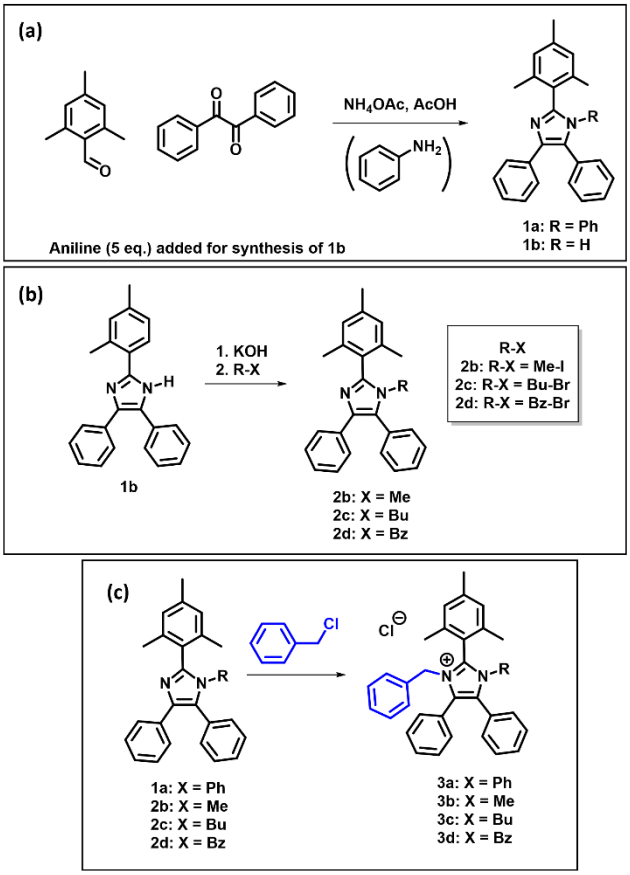

Figure 6-4: Synthesis conducted in this work.
(a) Synthesis of imidazole monomer precursors (b) first N-functionalisation step (c) second N-functionalisation for synthesis of imidazolium model compounds.

Experimental and theoretical dihedral angle investigations were conducted to probe the impact of the various N-functionalities on steric encumberment around the C2 position. Changing the C2-aromatic group and N-functionalities to maintain a 90 ° angle between the imidazolium ring and the C2-aromatic group offers the best steric protection against hydroxide C2 attack.[103] In this work, compounds 3a,b and d were recrystallised and analysed by XRD to obtain experimental dihedral angles (Table 1). It was not possible to recrystalise 3c, as the butyl chain resulted in the sample being an oil. The experimental dihedral angles of compounds 3a, b and d were very similar: 80.3, 80.5 and 81.7°,

respectively, suggesting similar protection against C2 hydroxide attack. Dihedral angle was also investigated *via* density functional theory (DFT) calculations and compared to experimental results, enabling the steric hindrance of compound 3c to be considered. The DFT dihedral angles consist of two values dependent on which side of the mesityl-imidazolium compound was measured (Appendix D, Figure D.3). Quantitatively, the DFT calculated values were slightly different from the XRD crystal values. The discrepancy between the experimental and theoretical values could be due to different conditions, where the theoretical molecules are in an 'ideal' environment, in comparison to the 'real' environment experienced for the XRD experiments. However, qualitatively the same trend is observed between the theoretical and experimental dihedral angles. Compound 3a has the closest theoretical dihedral angle to 90°, followed by 3d, then 3b and 3c. This predicts a stability trend of: 3a > 3d > 3b > 3c.

Table 6.1: Experimental and theoretically calculated dihedral angles for imidazolium model compounds 3a-d.

COMPOUND	DIHEDRAL ANGLE – XRD (°)	DIHEDRAL ANGLE – DFT (°)
3A	81.7	76.5/78.6
3B	80.3	75.8/77.2
3C	-	78.5/78.7
3D	80.7	82.3/86.8

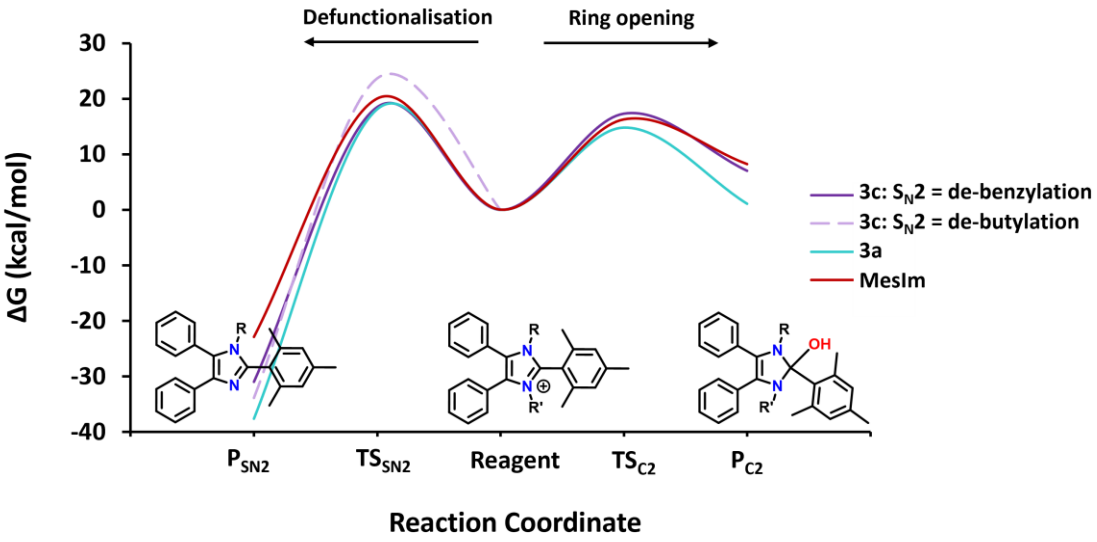

Figure 6-5: Comparison of activation energy barriers for defunctionalisation and ring opening steps of compound 3c (purple), 3a (blue) and MesIm (red).

Transition state theory has also been considered as a valuable theoretical method to investigate the alkaline stability of imidazoliums and provides information on the energy barriers associated with degradation mechanisms.[43,103] This method calculates the free energy (G) of transition states and reaction intermediates along the degradation pathway. The ΔG between starting geometries and transition state geometries provides information on the energy barriers associated with each reaction pathway. However, the optimisation of unstable transition state structures can be highly challenging, particularly in systems with many rotational degrees of freedom and in asymmetric molecules (Appendix D, Figure D.2). When the energy barrier associated with the C2 ring opening degradation is higher than the N defunctionalisation, the defunctionalisation becomes the observed degradation route.[43,44,103] Due to the asymmetry of compounds 3a-d, defunctionalisation could occur at the benzyl position or the Me/Bu/Ph positions. The energy barriers associated with the defunctionalisation of compound 3c (Figure 6.5) were calculated and compared to the demethylation of MesIm. It was not possible to calculate the defunctionalisation pathways for the remaining molecules. As expected,[91,102,103] the de-butylation of compound 3c has a higher activation energy barrier than the demethylation of a comparative well-studied imidazolium, MesIm (Figure 6.1, compound c). The butyl

group exhibits stronger electron donating effects onto the imidazolium ring, reducing the electrophilicity of the ***C***H_2 group.[48] The energy barrier of the de-benzylation step is only slightly lower than the demethylation of MesIm, but significantly lower than the de-butylation. In previous reports of quaternary ammoniums,[38] the benzyl linkage has been shown to be highly unstable at high pH due to the electron withdrawing nature increasing the electrophilicity of the ***C***H_2 group. However in benzimidazoliums, the benzyl group was shown to be alkaline stable,[73] and in imidazoliums, the N-benzyl stability was shown to be bettered only by the butyl group.[91] The electron donating nature of the nitrogen in the (benz)imidazolium rings likely decreased the electrophilicity of the benzyl ***C***H_2 group in comparison to that of the quaternary ammoniums.

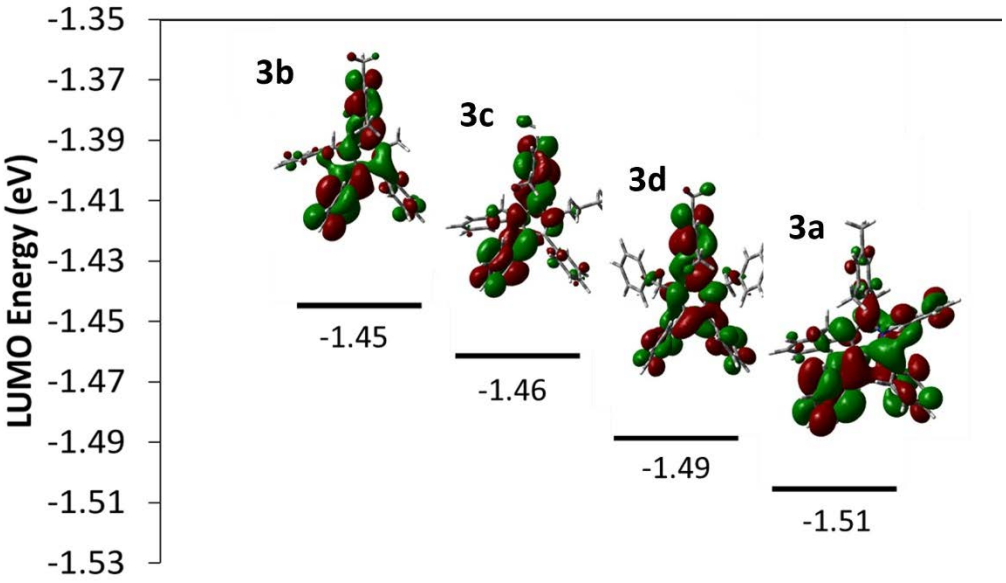

Figure 6-6: LUMO energies and isosurfaces for imidazolium model compounds (3a-d).

The TST calculations provide an understanding of the energy barriers associated with the degradation pathways with both steric and electronic effects considered, whereas dihedral angles only provide information of the steric effects. The electronic effect of structural variation on the alkaline stability of imidazoliums can be decoupled from the TST calculations by modelling the imidazolium LUMOs. The degradation reactions require the correct energy difference between the LUMO and the highest occupied molecular orbital (HOMO) of the hydroxide anion. The lower the energy of the LUMO, the more susceptible

the compound is to hydroxide attack. The electronic impact on alkaline stability for compounds 3a-d was investigated by calculating the LUMO energies and isosurfaces (Figure 6.6). Interestingly, the energies of the LUMOs were in the order 3b > 3c > 3d > 3a, which disagrees with the result obtained from the theoretical and experimental dihedral angles. However, there was very little difference in the values of the LUMOs, possibly suggesting there is a contribution from both the steric and electronic effects that impact the stability of the imidazoliums. Some reports have suggested that electronic effects associated with alkaline stability of imidazoliums are not dependent on LUMO energy alone, with the LUMO isosurface being another important factor. The isosurface provides an insight into the structure of the LUMO to understand the overlap between the LUMO of the cation and HOMO of the hydroxide. Hydroxide anions have been reported to have π-type HOMOs,[159] likely resulting in a strong overlap with the π-type LUMOs on the imidazoliums. However, LUMO localisation on the imidazolium can be interpreted as the region of major overlap between the hydroxide HOMO and imidazolium LUMO and therefore the position where the reaction would be likely to occur. The LUMO isosurfaces were generated for compounds 3a-d (Figure 6.6). In all compounds, there is a LUMO contribution at the α-carbons of the N-benzyl functionality, suggesting the hydroxide attack would be focussed on these positions. This observation is particularly prevalent on compound 3b. The isosurface for compounds 3a and 3d are spread over the C2, C4 and C5 aromatic groups, along with the imidazolium ring, whereas compounds 3b and 3c have limited LUMO contribution on the C5 rings. The isosurface for compound 3a has significant contributions from the N-phenyl functionality, in addition to the C2, C4, C5 and imidazolium rings. The more the LUMO is dispersed over the imidazolium compounds, the more challenging it is for the hydroxide to have a direct attack site.

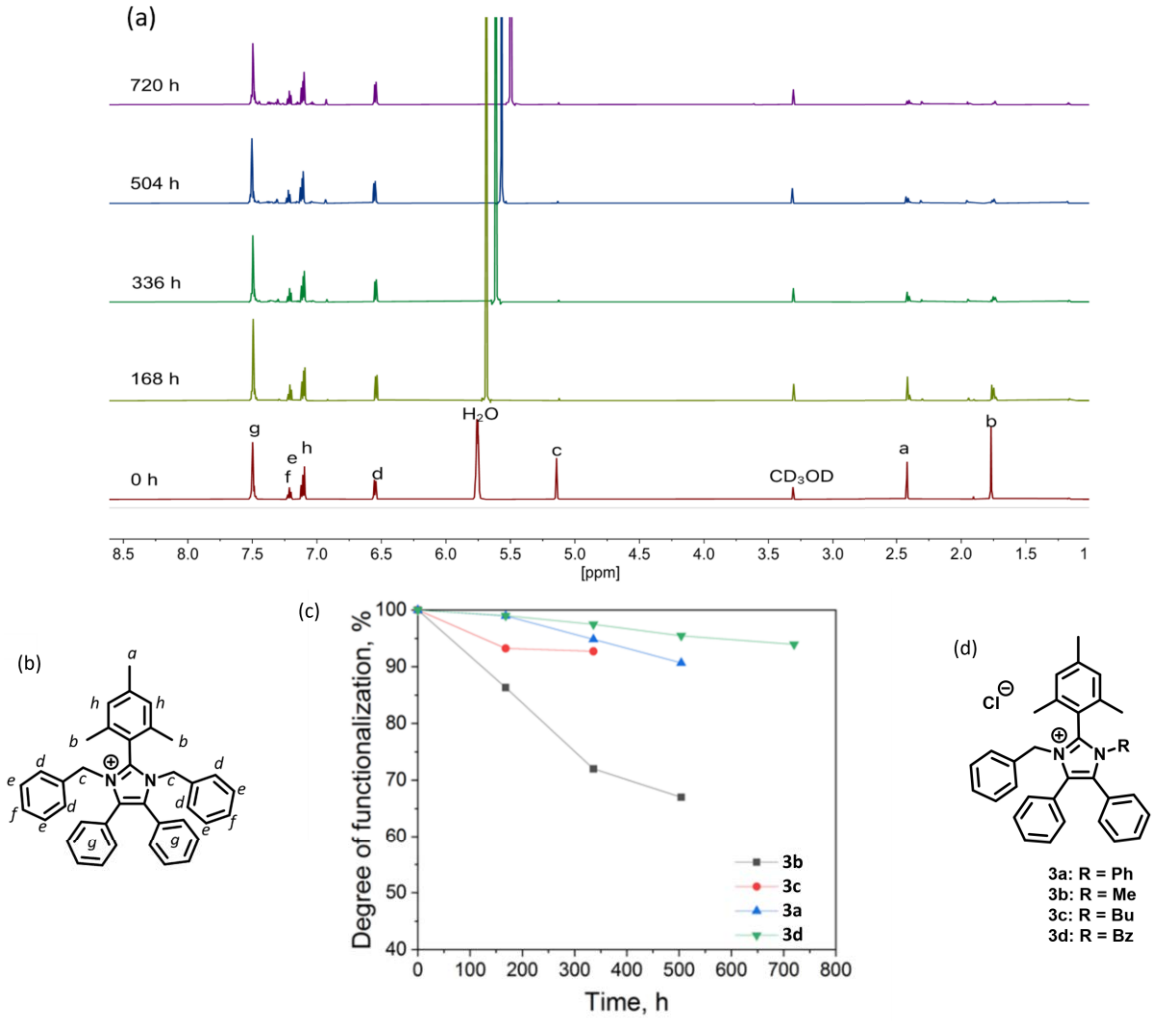

Figure 6-7: The alkaline stability anlaysis of compounds 3a-d.

(a) ^{1}H NMR of compound 3d in 3 M NaOD/CD_3OD/D_2O at 80 °C at various intervals over 720 h. (b) Proton labelling of compound 3d. (c) the degree of functionalisation remaining of compounds 3a-d. (d) The compounds investigated

The hydroxide stability of compounds 3a-d was measured experimentally using the methods described by the Coates Group.[76] The compounds (0.02 M) were dissolved in a mixture of 3M NaOD in CD_3OD/D_2O, stored at 80 °C and the change in chemical

structure was monitored using ^{1}H NMR. Figure 6.7(a) shows the ^{1}H NMR evolution of compound 3d, which was observed to be the most stable compound, over a period of 720 h. Significant deuterium exchange was observed for the -C***H***$_2$ benzyl protons and the -C***H***$_3$ protons on the mesityl group.[73] The extent of degradation was quantified by comparing the change in integration of the benzyl -C***H*** protons (Figure 6.7(b)), protons *d, e,* and *f*, 6.50, 7.12, and 7.21 ppm, respectively). After 720 h, only 6% of compound 3d was degraded, with the observable degradation pathway occurring through de-benzylation. The ^{1}H NMR observed degradation of compounds 3a-d was exponentially fitted to calculate the half-life ($t_{1/2}$). As predicted by the dihedral angles, and TST calculations of 3c, the steric protection provided by the mesityl, and N-substituted groups was sufficient to raise the energy barrier of C2-hydroxide attack to prevent any observable ring opening degradation in all compounds 3a-d. Despite the similarity in energy barrier associated with the de-methylation of MesIm and the de-benzylation of 3c (Figure 6.4), compound 3b had a half-life of only 852 h due to the labile demethylation reaction. This result correlates with the LUMO localization of 3b on the α-carbon of the methyl group, increasing the orbital crossover of this position with the hydroxide anion and increasing the possibility of attack. The addition of butyl (3c), phenyl (3a) and benzyl (3d) groups to replace the unstable methyl group, created a five-fold increase in stability for the compounds with half-lives of 3410, 3520 and 7730 h, respectively.

The alkaline stability of cationic groups occurs through various steric and electronic contributions, highlighting the importance of using various theoretical methods to explain the observable experimental degradation pathways. In this model compound analysis, alkaline stability could be explained using a combination of both steric effects (dihedral angles) and LUMO isosurfaces (electronic effects), however caution must be taken when extrapolating these results to encompass polymer stability. Whilst model compound studies are useful in the selection of possible alkaline stable cations, once integrated into an ICP, the different steric congestion and hydration environments experienced in a polymer structure will impact the alkaline stability. Based on the solution-based alkaline stability test, cations 3a and 3d were deemed to be most likely to exhibit high alkaline stability when incorporated in a polymer and were therefore incorporated as pendant groups on a poly(olefin) backbone for further investigation.

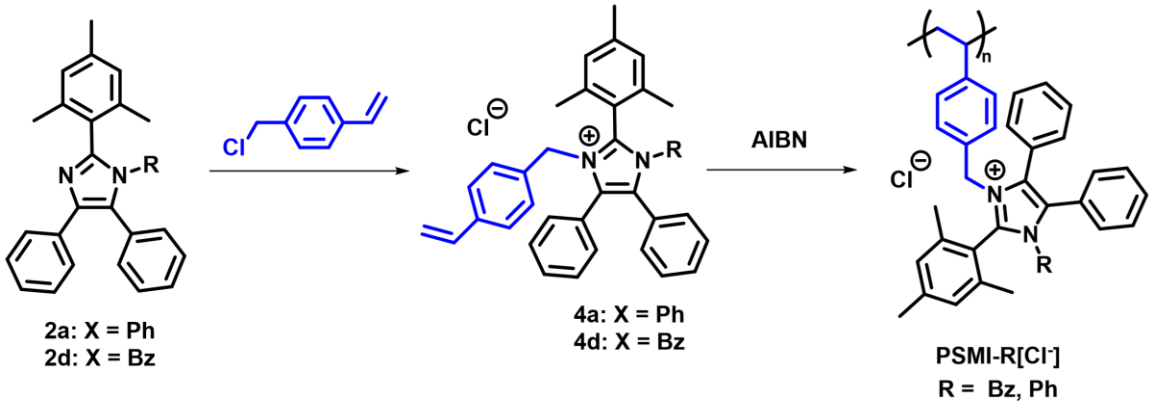

Figure 6-8: The second N-functionalisation of compounds 2a and d, followed by the polymerisation of compounds 4a and d.

Polymers, PSMI-R (R = Bz, Ph), were synthesised according to Figure 6.8. The second N-functionalization used vinylbenzylchloride to yield a positively charged imidazolium monomers with vinyl groups for free-radical initiated polymerisation. The novel free-radical initiated chain growth polymerisation yielded poly(vinyl imidazolium)s without any required post functionalization steps. The synthesis of the PSMI-R[Cl^-] polymers was conducted using 1 eq. of compound 8a-d, and 0.05 eq. of radical initiator (AIBN), in NMP for 168 h. The chemical structure of the monomer, coupled with the free-radical polymerisation method, defined the position of the C2-protected imidazolium pendant groups at every repeat unit, alleviating issues regarding the degree or location of pendant cationic functionalities. The highly insoluble poly(olefin) backbone rendered both polymer samples insoluble in any organic solvent, preventing ^{1}H NMR analysis, therefore the chemical structure of the polymers was investigated using elemental analysis (Appendix D, Table D.2).

Due to the insolubility of PSMI-Bz and PSMI-Ph, the alkaline stability could not be investigated using the solution-based ^{1}H NMR method as used for the model compounds. A thermogravimetric analysis method was utilised as described by Kreuer *et al.*[160] The polymer samples were exchanged to hydroxide form and the change in mass with changing the relative humidity (RH) of the environment was measured (Figure 6.9). Reducing the RH increases the reactivity of the hydroxide anion by reducing the hydration

shell.[94,161] At high hydration levels (90% RH) the water uptake of the samples is measured. At low RH levels (PSMI-Bz: 10% RH and PSMI-Ph: 30% RH) hydroxide degradation is expected to occur. As degradation occurs, the IEC of the polymers is reduced, either through C2-hydroxide attack or defunctionalisation. Reducing the IEC also reduces the water uptake, correlating hydroxide degradation of the samples with the fully hydrated mass (measured at 90% RH). Some reduction of mass at 90 % RH can also be attributed to the loss of volatile degradation products from the polymer samples.

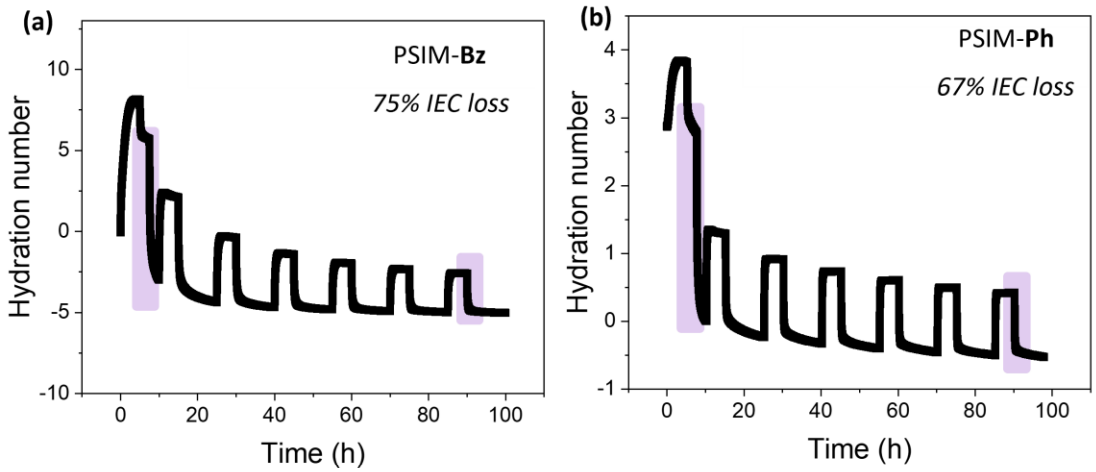

Figure 6-9:Degradation of PSIM-Bz and PSIM-Ph.
(a) The TGA traces pf PSIM-Bz showing the change in hydration number as the RH is cycled from 90 % to 70 % RH for removal of excess water. Then the RH is cycled between 70 % and 10 % to probe hydroxide degradation under dry conditions. The purple boxes represent the first and last degradation point (highest IEC and lowest IEC points). (b) The TGA traces pf PSIM-Ph showing the change in hydration number as the RH is cycled from 90 % to 70 % RH for removal of excess water. Then the RH is cycled between 70 % and 30 % to probe hydroxide degradation under dry conditions. The purple boxes represent the first and last degradation point.

The alkaline degradation mechanism for PSMI-Bz and PSMI-Ph can be correlated with model compound degradation. When exposed to hydroxide the main degradation pathway for compounds 3a and 3d was the de-benzylation mechanism. In the case of PSMI-Bz and PSMI-Ph, it is possible the de-benzylation was also the main degradation mechanism. However, when integrated into the polymer, the benzyl units were acting both as the sterically encumbering N-functionality and the linker unit between the imidazolium cation and the poly(olefin) backbone. Tethering the benzyl onto the poly(olefin) backbone

likely changed the orientation in comparison the model compounds. Therefore, it is possible the benzyl unit did not provide the same C2 steric protection as described by the model compound dihedral angle investigation, opening the possibility of C2 hydroxide attack being the more favourable degradation pathway. The TST calculations of compound 3a (Figure 6.6) showed the C2 ring opening degradation pathway to have a lower energy barrier than the corresponding de-benzylation, suggesting that this could be experienced by PSMI-Ph, especially if the dihedral angle is forced further from 90^{o} when in a polymer structure. The same could be said for PSMI-Bz, if linking to the polymer backbone shifted the orientation out of the favourable close to 90^{o} angle, C2 hydroxide attack could be observed. Or if this was not the case, the degradation was likely initiated by the de-benzylation as observed in compound 3d (Figure 6.7(a)). Regardless of the degradation mechanism occurring first in the polymer samples, the change in cationic structure would have an impact on the orientation of the polymer, changing the position of cationic groups and possibly the degradation pathway.

Comparison of degradation between the model compounds and polymers was also challenging due to the different experimental conditions. The solution-based degradation had a higher hydration than the low RH (10% and 30 % RH) points of the thermogravimetric degradation method, resulting in the latter being significantly less hydrated conditions. The solution degradation had a higher ratio of hydroxide anions to imidazolium cations (150:1), in comparison to the thermogravimetric method where the hydroxide was the counterion to the imidazolium and therefore the ratio of hydroxide to imidazolium was 1:1. The rapid degradation of PSMI-Bz and PSIM-Ph using the thermogravimetric method, in comparison to the relatively slow degradation of compounds 3a and 3d, suggests that the hydration environment is much more important than the concentration of hydroxide anions in the sample.

6.4. Conclusion

In this chapter, various methodologies were used to study the hydroxide-mediated degradation of pendant group poly(imidazolium)s at different stages of development. Model compounds were synthesised and used to probe cation alkaline stability. DFT results enabled the discussion of the various steric and electronic effects that contribute to stability, whilst a solution-based experimental study provided information on the observable degradation pathways. The de-methylation of compound 3a was the most

labile degradation pathway, explained using the localisation of the LUMO isosurface. The increase in steric hinderance through bulky N-functionalities improved the stability of the remaining compounds with 3a and 3d exhibiting the highest stability using this method.

The thermogravimetric degradation analysis of PSIM-Ph and PSIM-Bz was used to demonstrate the change in alkaline stability between polycations and the analogous model compounds. The degradation of the polymer was much more rapid than the small molecule, showing the lack of correlation between polymer and model compound stability, under these conditions. The solution-based hydroxide degradation and DFT investigations are appropriate for the design and screening of potential alkaline stabile cations, the low stability of the analogous polymers suggest more relevant conditions should be used. For real application of ICPs, the discussed thermogravimetric method should be used to probe potential model compounds to more accurately assess whether the alkaline stability would translate to conditions experienced in application.

Chapter 7. Conclusions and Future Work

7.1. Conclusions

Chapter 3 of this thesis described the implementation of the DR reaction as the step growth polymerisation mechanism for synthesis of tetrasubstituted poly(imidazole)s. An AB step growth polymerisation was used, enabled by the development of a difunctional monomer with aldehyde and diketone functionalities (OPAB). Reacting OBAB with ammonium acetate and a secondary amine, in an acidic environment, a tetrasubstituted poly(imidazole) could be synthesised. The synthetic route is simplified, in comparison to an AA-BB type polymerisation and highly versatile, as demonstrated by using various secondary amines. The most promising candidate (PDPI-H) was quaternized, requiring only a single post-polymerisation functionalization step.

The same polymerisation method was used for the controlled synthesis of statistical copolymers, where the φ of repeat units would be quantified using ^{1}H NMR. The control of repeat unit structure could be of particular importance for high-performance cationic poly(imidazolium)s, where the IEC is integral in governing many crucial macromolecular properties. This Chapter demonstrated a facile synthetic route for manipulation of polymer architecture and subsequent control of fundamental ICP properties that could be crucial in the tuning of next-generation poly(imidazolium)s for specific device applications.

Chapter 4 built upon the synthetic method developed in Chapter 3 by integrating C2 steric protection and developing a novel poly(imidazolium) that could be integrated, as an ionomer, into the catalyst layer. The copolymer structure of DMP-PHPI enabled the high IEC material to be designed specifically for investigation of its interactions with the Pt/C catalyst and the subsequent impact on the HER/HOR. DMP-PHPI-M was designed with a limited number of freely rotating phenyl groups for reduced unfavourable adsorption onto the catalyst layers, insolubility in basic solutions for electrochemical testing, and solubility in organic solvents for simple integration into the catalyst layers. The ionomer:carbon interactions and, especially, the specific adsorption of the ionomer through its aromatic rings or its cation (*e.g.,* ‘cation-hydroxide-water co-adsorption’ or ‘phenyl adsorption’) were investigated on Pt surface. No negative effect on the activity of the HER/HOR was observed for I:C ratios up to 0.196, then a mild decrease of Pt specific

surface occurred at high I:C ratios, reducing the overall activity. This was either induced by the presence of I^- traces in the ionomer mixture or an extremely small contribution of the specific adsorption of the ionomer through its cations or aromatic cycles. Opposingly, small I:C ratios led to an increased specific surface and activity *vs.* ionomer-free Pt/C, induced by an increased catalytic layer stability in presence of ionomer, which makes those ionomer extremely promising candidates for AEMFC and AEMWE applications.

In Chapter 5, the importance of poly(imidazolium) end groups was discussed with respect to alkaline stability. Here the under-investigated significance of reactive carbonyl end groups on poly(imidazolium)s with highly stable main chain repeat units was investigated. The challenging synthesis of model compounds analogous to the carbonyl-imidazolium end groups was discussed, with the best method for end group investigations being the synthesis of a low molecular weight oligomer, DMP-PPI-AD. The AB-type DR step growth polymerisation method, as described in Chapters 3 and 4, enabled the definition of DMP-PPI-AD end groups consisting of an aryl-aldehyde and diketone. The aryl-aldehyde could be analysed using ^{1}H NMR, enabling the investigation of end group alkaline stability. The first evidence of the adverse effect reactive end groups have on poly(imidazolium)s was demonstrated through the major structural changes observed using a standard alkaline degradation test. A synthetic route was demonstrated to end cap the poly(imidazolium)s and yield a material with identical structural units, including the commonly disregarded end groups. The work developed in this Chapter provided a baseline for further investigations on the alkaline stability of end groups and a potential method for the mitigation of end group degradation through polymer end capping.

In Chapter 6, various theoretical and experimental methods were discussed and used for investigation of the stability of imidazolium compounds and polymers. Model compounds were used as the basis for investigation on the impact of various bulky N-substituents on alkaline stability. The experimental solution-based model compound degradation tests provided information on the observable hydroxide-mediated degradation mechanisms that governed the alkaline stability of these imidazoliums. The DFT data provided information on the unobservable properties (LUMOs, transition states *etc*.) of these model compounds that impact the overall alkaline stability to further develop the understanding of these contributions. Novel pendant groups poly(imidazolium)s were synthesised, and the alkaline stability was investigated using a thermogravimetric degradation analysis. The polymer was demonstrated to be less stable than the model

compounds, in the low hydration conditions used. However, the information on experimental and theoretical model compound alkaline stability, coupled with the corresponding polymer stability was used to hypothesise the degradation mechanism that occurred in the insoluble polymers. The discussions posed in this Chapter have provided an oversight into some of the complementary experimental and theoretical methods available for analysis of cation and polymer alkaline stability.

7.2. Future Work

The high hydroxide conductivity and stability of poly(imidazolium)s has resulted in the rapid development of novel high-performance materials. However, the conditions at the cathode, anode, and polyelectrolyte of AEMWEs and AEMFCs are vastly different requiring different ICP chemistries for optimal device performance. The focus on poly(imidazolium)s has been centered on the development of AEMs with little attention on the creation of specific poly(imidazolium) chemistries specifically for ionomer purposes, despite the different operating environments. Three synthetic routes are discussed in this chapter, that could enable the development of poly(imidazolium)s with tunable macromolecular properties.

7.2.1. Varying the Poly(imidazolium) Backbone

The broad commercial availability of benzaldehydes and acetylenes enables the variation of the AB-type monomer (Figure 7.1). The monomer must include a diketone, an aldehyde, and the 2,6-disubstituted units for the imidazolium C2 steric protection. For synthetic ease, the steric protection and aldehyde groups would be best integrated into the monomer as a 2,6-disubstituted-benzaldehyde group.

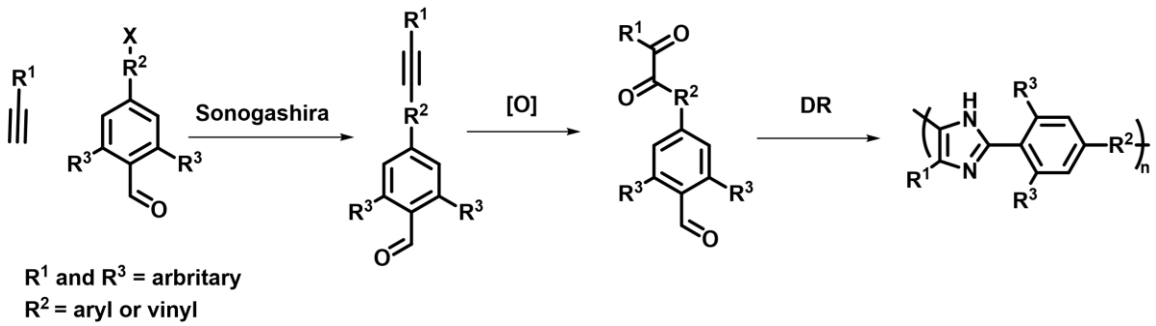

Figure 7-1: Structural Variation of monomer dm-OPAB.

The variation of R group when synthesizing the monomer will change the structure of the resulting poly(imidazole). Changing the structure of the poly(imidazolium) backbone will have an impact on resulting IEC. As discussed in Chapter 1, changing the IEC has an impact on the water uptake, hydration number, swelling, and conductivity of the material. Therefore, systematic changes in the monomer structure could be a method for detailed analysis of poly(imidazolium) structure-property correlations whilst using the same AB-type DR step growth polymerization step.

7.2.2. Varying the linearity of Poly(imidazolium)s

The water channels play a crucial role in the ion transport and conductivity of ICP materials. Changing the linearity of the polymer chain has been shown to have interesting implications on the macromolecular properties of hydrocarbon-based PEMs.[162] However, despite the importance of water channels in hydroxide conducting ICPs, there has not been a study on changing poly(imidazolium) linearity and the impact this has on the ion transport-related macromolecular properties such as conductivity, water uptake and swelling. Using the monomer synthetic route described in Chapter 4, the linearity of the poly(imidazolium) can be varied, as shown in Figure 7.2(a). Copolymers could also be synthesized by using the two different monomers in one polymerization reaction, to create a poly(imidazolium) material with non-uniform linearity (Figure 7.2(b)).

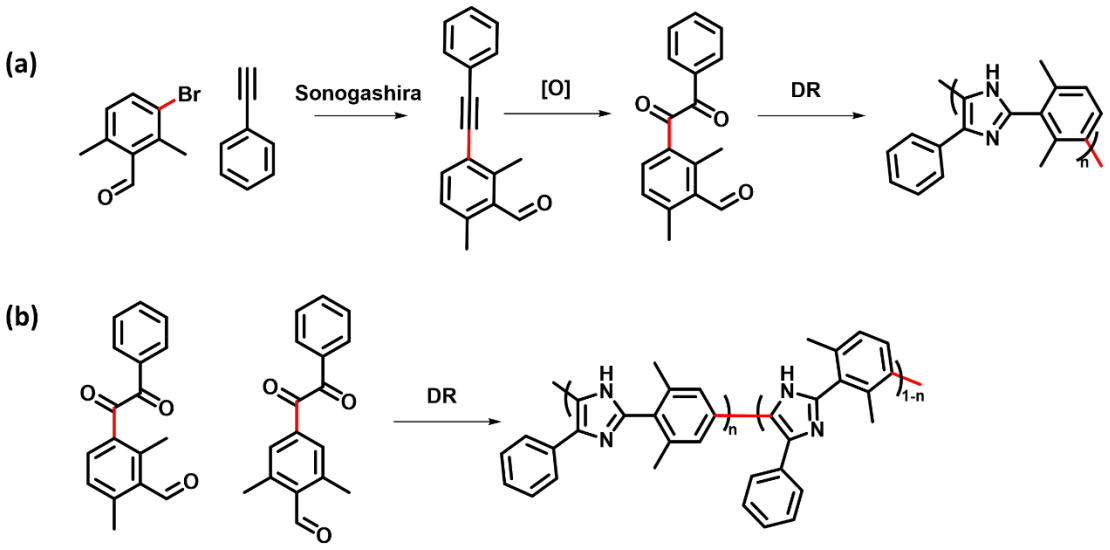

Figure 7-2: Varying the linearity of poly(imidazolium)s. (a) Using 3-bromo-2,6-dimethylbenzaldehyde and (b) synthesis of a copolymer using structural variations of the monomer.

7.2.3. Poly(imidazolium) Copolymers

Poly(imidazolium) copolymers can be created using two methods: during polymerization and post polymerization. The prior method was described in Chapters 3 and 4, where varying the proportion of secondary amine with respect to ammonium acetate enabled the formation of statistical and random copolymers. However, this method is limited to repeat units with imidazole/imidazolium functionalities whereas, the post-polymerization copolymer synthesis route can be used for any kind of repeat unit functionality. As described in Chapter 5, the AB-type polymerization defines the end groups of the poly(imidazolium) material to be an aryl-aldehyde and a 1,2-disubstituted diketone. Copolymerization reactions could take place using a polymer material with end groups that will react with either the diketone or aldehyde of the poly(imidazolium) (Figure 7.3). This method could be used to combine the favorable macromolecular properties of the poly(imidazolium), such as the high hydroxide conductivity, with other polymer materials that could balance the water uptake or other issues that have plagued the development of cationic ICPs for alkaline electrochemical conversion devices.

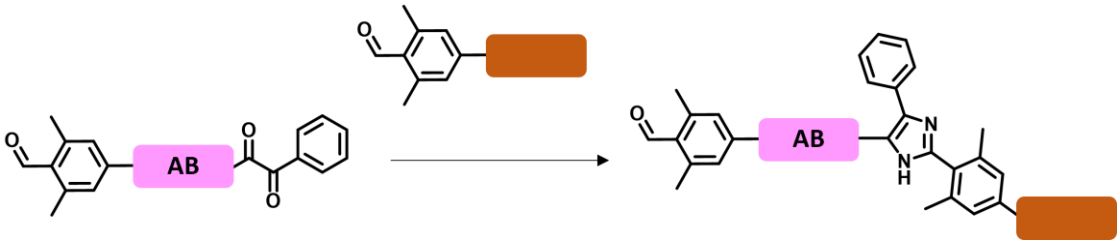

Figure 7-3: Copolymers synthesised via end group reactions. ***Pink block represents the polymer synthesized using AB type polymerisaiton and the brown block represents a different polymer with a known, corresponding end group.***

The three methodologies described in this Chapter, can be implemented to gain a further understanding into the impact of poly(imidazolium) structure on resulting physicochemical and electrochemical properties. From this structure-property correlations can be established for the informed and targeted design of future high-performance poly(imidazolium) materials for alkaline energy conversion devices.

References

1. International Energy Agency. *IEA: Key World Energy Statistics 2021*. (2021).

2. Ansari, D., Holz, F. & Al-Kuhlani, H. *Energy, climate, and policy towards 2055: An interdisciplinary energy outlook (DIW-REM outlook)*. (2019).

3. The Future of Hydrogen. *Futur. Hydrog.* (2019) doi:10.1787/1e0514c4-en.

4. Denholm, P., O'Connell, M., Brinkman, G. & Jorgenson, J. Overgeneration from Solar Energy in California: A Field Guide to the Duck Chart. *Tech. Rep.* 46 (2015).

5. Ball, M. & Weeda, M. The Hydrogen Economy - Vision or Reality? *Int. J. Hydrogen Energy* **40**, 7903–7919 (2015).

6. Abe, J. O., Popoola, A. P. I., Ajenifuja, E. & Popoola, O. M. Hydrogen energy, economy and storage: Review and recommendation. *Int. J. Hydrogen Energy* **44**, 15072–15086 (2019).

7. Kruse, B., Grinna, S. & Buch, C. *Hydrogen: Status og Muligheter*. (2002).

8. Marshall, A., Børresen, B., Hagen, G., Tsypkin, M. & Tunold, R. Hydrogen production by advanced proton exchange membrane (PEM) water electrolysers-Reduced energy consumption by improved electrocatalysis. *Energy* **32**, 431–436 (2007).

9. Santarelli, M., Medina, P. & Calì, M. Fitting regression model and experimental validation for a high-pressure PEM electrolyzer. *Int. J. Hydrogen Energy* **34**, 2519–2530 (2009).

10. Guerrero Moreno, N., Cisneros Molina, M., Gervasio, D. & Pérez Robles, J. F. Approaches to polymer electrolyte membrane fuel cells (PEMFCs) and their cost. *Renew. Sustain. Energy Rev.* **52**, 897–906 (2015).

11. Peighambardoust, S. J., Rowshanzamir, S. & Amjadi, M. Review of the proton exchange membranes for fuel cell applications. *Int. J. Hydrogen Energy* **35**, 9349–9384 (2010).

12. Phillips, R. & Dunnill, C. W. Zero gap alkaline electrolysis cell design for renewable energy storage as hydrogen gas. *RSC Adv.* **6**, 100643–100651 (2016).

13. Bernhart, W., Riederle, S. & Yoon, M. *Fuel cells: A realisitc alternative for zero emission?* (2014).

14. Borup, R. & Weber, A. Z. *DOE 2022: Annual Merit Review and Peer Evaluation Meeting*. (2022).

15. Kusoglu, A. & Weber, A. Z. New Insights into Perfluorinated Sulfonic-Acid Ionomers. *Chem. Rev.* **117**, 987–1104 (2017).

16. Kerres, J. A. Design Concepts for Aromatic Ionomers and Ionomer Membranes to be Applied to Fuel Cells and Electrolysis Design Concepts for Aromatic Ionomers and Ionomer Membranes to be Applied to Fuel Cells. *Polym. Rev.* **55**, 273–306 (2015).

17. Ghassemzadeh, L. *et al.* Chemical degradation of proton conducting perflurosulfonic acid ionomer membranes studied by solid-state nuclear magnetic resonance spectroscopy. *J. Power Sources* **186**, 334–338 (2009).

18. Qiao, J. *et al.* Degradation of Perfluorinated Ionomer Membranes for PEM Fuel Cells during Processing Degradation of Perfluorinated Ionomer Membranes for PEM Fuel Cells during Processing with H 2 O 2. *J. ele* **153**, 967–974 (2006).

19. Borup, R. *et al.* Scientific aspects of polymer electrolyte fuel cell durability and degradation. *Chem. Rev.* **107**, 3904–3951 (2007).

20. Kreuer, K. D. Ion conducting membranes for fuel cells and other electrochemical devices. *Chemistry of Materials* vol. 26 361–380 (2014).

21. Yang, Y. *et al.* Electrocatalysis in Alkaline Media and Alkaline Membrane-Based Energy Technologies. *Chem. Rev.* **122**, 6117–6321 (2022).

22. Gottesfeld, S. *et al.* Anion exchange membrane fuel cells: Current status and remaining challenges. *J. Power Sources* **375**, 170–184 (2018).

23. Gottesfeld, S. *et al.* Anion exchange membrane fuel cells: Current status and

remaining challenges. *J. Power Sources* **375**, 170–184 (2018).

24. Ferriday, T. B. & Middleton, P. H. Alkaline fuel cell technology - A review. *Int. J. Hydrogen Energy* **46**, 18489–18510 (2021).

25. You, W., Noonan, K. J. T. & Coates, G. W. Alkaline-stable anion exchange membranes: A review of synthetic approaches. *Prog. Polym. Sci.* **100**, 101177 (2020).

26. Varcoe, J. R. *et al.* Anion-exchange membranes in electrochemical energy systems. *Energy Environ. Sci.* **7**, 3135–3191 (2014).

27. Wierzbicki, S., Douglin, J. C., Kostuch, A., Dekel, D. R. & Kruczała, K. Are Radicals Formed During Anion-Exchange Membrane Fuel Cell Operation? *J. Phys. Chem. Lett.* **11**, 7630–7636 (2020).

28. Wierzbicki, S., Douglin, J. C., Singh, R. K., Dekel, D. R. & Kruczała, K. Operando EPR Study of Radical Formation in Anion-Exchange Membrane Fuel Cells. *ACS Catal.* **13**, 2744–2750 (2023).

29. Marx, D., Chandra, A. & Tuckerman, M. E. Aqueous basic solutions: Hydroxide solvation, structural diffusion, and comparison to the hydrated proton. *Chem. Rev.* **110**, 2174–2216 (2010).

30. Long, H., Kim, K. & Pivovar, B. S. Hydroxide Degradation Pathways for Substituted Trimethylammonium Cations: A DFT Study. *J. Phys. Chem. C* **116**, 9419–9426 (2012).

31. Odian, G. *Principals of Polymerisation*. (John Wiley & Sons, Inc., 2004).

32. Odian, G. *Principles of Polymerization*. (John Wiley & Sons, Inc., 2004).

33. Carothers, H. Polymers and polyfunctionality. (1935).

34. Flory, P. J. Distribution in Linear. *J. Am. Chem. Soc.* **58**, 1877–1885 (1936).

35. Flory, P. J. Fundemental Principals of Condensation Polymerisation. *Chem. Rev.* (1946).

36. Holdcroft, S. & Fan, J. Sterically-encumbered ionenes as hydroxide ion-conducting polymer membranes. *Current Opinion in Electrochemistry* vol. 18 99–105 (2019).

37. Jannasch, P. & Weiber, E. A. Configuring Anion-Exchange Membranes for High Conductivity and Alkaline Stability by Using Cationic Polymers with Tailored Side Chains. *Macromol. Chem. Phys.* **217**, 1108–1118 (2016).

38. Marino, M. G. & Kreuer, K. D. Alkaline stability of quaternary ammonium cations for alkaline fuel cell membranes and ionic liquids. *ChemSusChem* **8**, 513–523 (2015).

39. Sturgeon, M. R., Macomber, C. S., Engtrakul, C., Long, H. & Pivovar, B. S. Hydroxide based Benzyltrimethylammonium Degradation: Quantification of Rates and Degradation Technique Development. *J. Electrochem. Soc.* **162**, F366–F372 (2015).

40. Zhang, B. *et al.* Relating alkaline stability to the structure of quaternary phosphonium cations. *RSC Adv.* **8**, 26640–26645 (2018).

41. Womble, C. T. *et al.* Rapid Analysis of Tetrakis(dialkylamino)phosphonium Stability in Alkaline Media. *Organometallics* **36**, 4038–4046 (2017).

42. Xue, B. *et al.* Synthesis of novel guanidinium-based anion-exchange membranes with controlled microblock structures. *J. Memb. Sci.* **537**, 151–159 (2017).

43. Long, H. & Pivovar, B. Hydroxide Degradation Pathways for Imidazolium Cations: A DFT Study. *J. Phys. Chem. C* **118**, 9880–9888 (2014).

44. Wright, A. G., Weissbach, T. & Holdcroft, S. Poly(phenylene) and m-Terphenyl as Powerful Protecting Groups for the Preparation of Stable Organic Hydroxides. *Angew. Chemie - Int. Ed.* **55**, 4818–4821 (2016).

45. Thomas, O. D., Soo, K. J. W. Y., Peckham, T. J., Kulkarni, M. P. & Holdcroft, S. A Stable Hydroxide-Conducting Polymer. *J. Am. Chem. Soc* **134**, 34 (2012).

46. Fan, J. *et al.* Cationic Polyelectrolytes, Stable in 10 M KOH_{aq} at 100 °C. *ACS Macro Lett.* **6**, 1089–1093 (2017).

47. Hugar, K. M., Kostalik, H. A. & Coates, G. W. Imidazolium Cations with Exceptional Alkaline Stability: A Systematic Study of Structure-Stability Relationships. *J. Am. Chem. Soc.* **137**, 8730–8737 (2015).

48. Fan, J. *et al.* Poly(bis-arylimidazoliums) possessing high hydroxide ion exchange capacity and high alkaline stability. *Nat. Commun.* **10**, 2306–2316 (2019).

49. Tuckerman, M. E., Marx, D. & Parrinello, M. The nature and transport mechanism of hydrated hydroxide ions in aqueous solution. *Nature* **417**, 923–925 (2002).

50. Dekel, D. R. Review of cell performance in anion exchange membrane fuel cells. *J. Power Sources* **2018**, 158–169 (2017).

51. Marino, M. G., Melchior, J. P., Wohlfarth, A. & Kreuer, K. D. Hydroxide, halide and water transport in a model anion exchange membrane. *J. Memb. Sci.* **464**, 61–71 (2014).

52. Ostroverkhova, O. *Handbook of Organic Materials for Electronic and Photonic Devices*. (Woodhead Publishing, 2018).

53. Overton, P., Li, W., Cao, X. & Holdcroft, S. Tuning Ion Exchange Capacity in Hydroxide-Stable Poly(arylimidazolium) Ionenes: Increasing the Ionic Content Decreases the Dependence of Conductivity and Hydration on Temperature and Humidity. *Macromolecules* **53**, 10548–10560 (2020).

54. Diederichsen, K. M., Buss, H. G. & McCloskey, B. D. The Compensation Effect in the Vogel-Tammann-Fulcher (VTF) Equation for Polymer-Based Electrolytes. *Macromolecules* **50**, 3831–3840 (2017).

55. Porcarelli, L. *et al.* Single-Ion Block Copoly(ionic liquid)s as Electrolytes for All-Solid State Lithium Batteries. *ACS Appl. Mater. Interfaces* **8**, 10350–10359 (2016).

56. Ryu, S.-W. *et al.* Effect of Counter Ion Placement on Conductivity in Single-Ion Conducting Block Copolymer Electrolytes. *J. Electrochem. Soc.* **152**, A158 (2005).

57. Zelovich, T. *et al.* Hydroxide Ion Diffusion in Anion-Exchange Membranes at Low Hydration: Insights from Ab Initio Molecular Dynamics. *Chem. Mater.* **31**, 5778–

5787 (2019).

58. Mittal, V. *Polymers for Energy Storage and Conversion*. (John Wiley & Sons, Inc., 2013).

59. Gu, G. Y. *et al.* 2-Methoxyethyl (methyl) carbonate-based electrolytes for Li-ion batteries. *Electrochim. Acta* **45**, 3127–3139 (2000).

60. Zhang, S., Dou, S., Colby, R. H. & Runt, J. Glass transition and ionic conduction in plasticized and doped ionomers. *J. Non. Cryst. Solids* **351**, 2825–2830 (2005).

61. Fragiadakis, D., Dou, S., Colby, R. H. & Runt, J. Molecular mobility and Li+ conduction in polyester copolymer ionomers based on poly(ethylene oxide). *J. Chem. Phys.* **130**, 1–11 (2009).

62. Kreuer, K. D. & Portale, G. A critical revision of the nano-morphology of proton conducting ionomers and polyelectrolytes for fuel cell applications. *Adv. Funct. Mater.* **23**, 5390–5397 (2013).

63. Chen, C., Tse, Y. L. S., Lindberg, G. E., Knight, C. & Voth, G. A. Hydroxide Solvation and Transport in Anion Exchange Membranes. *J. Am. Chem. Soc.* **138**, 991–1000 (2016).

64. Dong, D., Zhang, W., Van Duin, A. C. T. & Bedrov, D. Grotthuss versus Vehicular Transport of Hydroxide in Anion-Exchange Membranes: Insight from Combined Reactive and Nonreactive Molecular Simulations. *J. Phys. Chem. Lett* **9**, 829 (2018).

65. Zelovich, T. *et al.* Ab Initio Molecular Dynamics Study of Hydroxide Diffusion Mechanisms in Nanoconfined Structural Mimics of Anion Exchange Membranes. *J. Phys. Chem. C* **123**, 4638–4653 (2019).

66. Dang, H. & Jannasch, P. Exploring Different Cationic Alkyl Side Chain Designs for Enhanced Alkaline Stability and Hydroxide Ion Conductivity of Anion-Exchange Membranes. *Macromolecules* **48**, 5742–5751 (2015).

67. Lee, W., Mohanty, A. D. & Bae, C. Fluorene-Based Hydroxide Ion Conducting Polymers for Chemically Stable Anion Exchange Membrane Fuel Cells. *ACS*

Macro Lett **4**, 453–457 (2015).

68. Lee, W., Kim, Y. S. & Bae, C. Robust Hydroxide Ion Conducting Poly(biphenyl alkylene)s for Alkaline Fuel Cell Membranes. *ACS Macro Lett.* **4**, 814–818 (2015).

69. Lee, W.-H. *et al.* Poly(terphenylene) Anion Exchange Membranes: The Effect of Backbone Structure on Morphology and Membrane Property. *ACS Macro Lett.* **6**, 566–570 (2017).

70. Luo, X., Wright, A., Weissbach, T. & Holdcroft, S. Water permeation through anion exchange membranes. *J. Power Sources* **375**, 442–451 (2018).

71. Hagesteijn, K. F. L., Jiang, S. & Ladewig, B. P. A review of the synthesis and characterization of anion exchange membranes. *J. Mater. Sci.* **53**, 11131–11150 (2018).

72. Duan, Q., Ge, S. & Wang, C. Y. Water uptake, ionic conductivity and swelling properties of anion-exchange membrane. *J. Power Sources* **243**, 773–778 (2013).

73. Weissbach, T. *et al.* Simultaneous, Synergistic Control of Ion Exchange Capacity and Cross-Linking of Sterically-Protected Poly(benzimidazolium)s. *Chem. Mater.* **28**, 8060–8070 (2016).

74. Wei, Q. *et al.* On the stability of anion exchange membrane fuel cells incorporating polyimidazolium ionene (Aemion+®) membranes and ionomers. *Sustain. Energy Fuels* **6**, 3551–3564 (2022).

75. You, W. *et al.* Degradation of Organic Cations under Alkaline Conditions. *J. Org. Chem.* **86**, 254–263 (2021).

76. Hugar, K. M., You, W. & Coates, G. W. Protocol for the Quantitative Assessment of Organic Cation Stability for Polymer Electrolytes. *ACS Energy Lett.* **4**, 1681–1686 (2019).

77. Li, N., Zhang, Q., Wang, C., Lee, Y. M. & Guiver, M. D. Phenyltrimethylammonium functionalized polysulfone anion exchange membranes. *Macromolecules* **45**, 2411–2419 (2012).

78. Hibbs, M. R., Fujimoto, C. H. & Cornelius, C. J. Synthesis and characterization of poly(phenylene)-based anion exchange membranes for alkaline fuel cells. *Macromolecules* **42**, 8316–8321 (2009).

79. Zarrin, H., Wu, J., Fowler, M. & Chen, Z. High durable PEK-based anion exchange membrane for elevated temperature alkaline fuel cells. *J. Memb. Sci.* **394**–**395**, 193–201 (2012).

80. Dang, H. S., Weiber, E. A. & Jannasch, P. Poly(phenylene oxide) functionalized with quaternary ammonium groups via flexible alkyl spacers for high-performance anion exchange membranes. *J. Mater. Chem. A* **3**, 5280–5284 (2015).

81. Sudre, G., Inceoglu, S., Cotanda, P. & Balsara, N. P. Influence of bound ion on the morphology and conductivity of anion-conducting block copolymers. *Macromolecules* **46**, 1519–1527 (2013).

82. Noh, S., Jeon, J. Y., Adhikari, S., Kim, Y. S. & Bae, C. Molecular Engineering of Hydroxide Conducting Polymers for Anion Exchange Membranes in Electrochemical Energy Conversion Technology. (2019) doi:10.1021/acs.accounts.9b00355.

83. Park, E. J. & Kim, Y. S. Quaternized aryl ether-free polyaromatics for alkaline membrane fuel cells: Synthesis, properties, and performance-a topical review. *J. Mater. Chem. A* **6**, 15456–15477 (2018).

84. Mohanty, A. D., Tignor, S. E., Krause, J. A., Choe, Y. & Bae, C. Systematic Alkaline Stability Study of Polymer Backbones for Anion Exchange Membrane Applications. *Macromolecules* **49**, 3361–3372 (2016).

85. Arges, C. G., Wang, L., Parrondo, J. & Ramani, V. Best Practices for Investigating Anion Exchange Membrane Suitability for Alkaline Electrochemical Devices: Case Study Using Quaternary Ammonium Poly(2,6-dimethyl 1,4-phenylene)oxide Anion Exchange Membranes. *J. Electrochem. Soc.* **160**, F1258–F1274 (2013).

86. Miyanishi, S. & Yamaguchi, T. Ether cleavage-triggered degradation of benzyl alkylammonium cations for polyethersulfone anion exchange membranes. *Phys. Chem. Chem. Phys.* **18**, 12009–12023 (2016).

87. Parrondo, J., Jung, M. J., Wang, Z., Arges, C. G. & Ramani, V. Synthesis and Alkaline Stability of Solubilized Anion Exchange Membrane Binders Based on Poly(phenylene oxide) Functionalized with Quaternary Ammonium Groups via a Hexyl Spacer. *J. Electrochem. Soc.* **162**, F1236–F1242 (2015).

88. Hibbs, M. R. Alkaline Stability of Poly (phenylene) -Based Anion Exchange Membranes with Various Cations. *J. Polym. Sci. Part B Polym. Phys.* **51**, 1736–1742 (2013).

89. Olsson, J. S., Pham, T. H. & Jannasch, P. Poly(N,N-diallylazacycloalkane)s for Anion-Exchange Membranes Functionalized with N-Spirocyclic Quaternary Ammonium Cations. *Macromolecules* **50**, 2784–2793 (2017).

90. Mohanty, A. D. & Bae, C. Mechanistic analysis of ammonium cation stability for alkaline exchange membrane fuel cells. *J. Mater. Chem. A* **2**, 17314–17320 (2014).

91. Hugar, K. M., Kostalik, H. A. & Coates, G. W. Imidazolium Cations with Exceptional Alkaline Stability: A Systematic Study of Structure-Stability Relationships. *J. Am. Chem. Soc.* **137**, 8730–8737 (2015).

92. Gu, L., Dong, H., Sun, Z., Li, Y. & Yan, F. Spirocyclic quaternary ammonium cations for alkaline anion exchange membrane applications: An experimental and theoretical study. *RSC Adv.* **6**, 94387–94398 (2016).

93. You, W., Hugar, K. M. & Coates, W. Synthesis of Alkaline Anion Exchange Membranes with Chemically Stable Imidazolium Cations: Unexpected Cross-Linked Macrocycles from Ring-Fused ROMP Monomers. (2018) doi:10.1021/acs.macromol.8b00209.

94. Dekel, D. R. *et al.* Effect of Water on the Stability of Quaternary Ammonium Groups for Anion Exchange Membrane Fuel Cell Applications. *Chem. Mater.* **29**, 4425–4431 (2017).

95. Varcoe, J. R. *et al.* Anion-exchange membranes in electrochemical energy systems †. *Energy Environ. Sci.* **7**, 3135–3191 (2014).

96. You, W. *et al.* Degradation of Organic Cations under Alkaline Conditions. *J. Org. Chem.* **86**, 254–263 (2021).

97. Noonan, K. J. T., Hugar, K. M., Kostalik, H. A. & Lobkovsky, E. B. Phosphonium-Functionalized Polyethylene: A New Class of Base- Stable Alkaline Anion Exchange Membranes. *J. Am. Chem. Soc* **134**, 18161–18164 (2012).

98. Sun, Z., Lin, B. & Yan, F. Anion-Exchange Membranes for Alkaline Fuel-Cell Applications : The Effects of Cations. *Chem. Sus. Chem* **11**, 58–70 (2018).

99. Li, W. *et al.* Degradation of guanidinium-functionalized anion exchange membrane during alkaline environment. *Int. J. Hydrogen Energy* **39**, 13710–13717 (2014).

100. Huang, A., Xia, C., Xiao, C. & Zhuang, L. Composite anion exchange membrane for alkaline direct methanol fuel cell: Structural and electrochemical characterization. *J. Appl. Polym. Sci.* **100**, 2248–2251 (2006).

101. Wright, A. G. & Holdcroft, S. Hydroxide-stable ionenes. *ACS Macro Lett.* **3**, 444–447 (2014).

102. Fan, J. *et al.* Poly(bis-arylimidazoliums) possessing high hydroxide ion exchange capacity and high alkaline stability. *Nat. Commun.* **10**, 2306 (2019).

103. Fan, J. *et al.* Cationic Polyelectrolytes, Stable in 10 M KOH aq at 100 °C. *ACS Macro Lett.* **6**, 1089,1093 (2017).

104. Thomas, O. D., Soo, K. J. W. Y., Peckham, T. J., Kulkarni, M. P. & Holdcroft, S. A Stable Hydroxide-Conducting Polymer. *J. Am. Chem. Soc.* **134**, 10753–10756 (2012).

105. Wright, A. G. *et al.* Hexamethyl-p-terphenyl poly(benzimidazolium): a universal hydroxide-conducting polymer for energy conversion devices. *Energy Environ. Sci.* **9**, 2130–2142 (2016).

106. Aili, D., Yang, J., Jankova, K., Henkensmeier, D. & Li, Q. From polybenzimidazoles to polybenzimidazoliums and polybenzimidazolides. (2020) doi:10.1039/d0ta01788d.

107. Thomas, O. D., Soo, K. J. W. Y., Peckham, T. J., Kulkarni, M. P. & Holdcroft, S. Polymer Chemistry Anion conducting poly (dialkyl benzimidazolium) salts †. *Polym. Chem.* **2**, 1641–1643 (2011).

108. Henkensmeier, D. *et al.* Polybenzimidazolium hydroxides - Structure, stability and degradation. *Polym. Degrad. Stab.* **97**, 264–272 (2012).

109. Henkensmeier, D. *et al.* Anion conducting polymers based on ether linked polybenzimidazole (PBI-OO). *Int. J. Hydrogen Energy* **39**, 2842–2853 (2013).

110. Wright, A. G. *et al.* Hexamethyl-: P -terphenyl poly(benzimidazolium): A universal hydroxide-conducting polymer for energy conversion devices. *Energy Environ. Sci.* **9**, 2130–2142 (2016).

111. Saxer, S., Marestin, C., Mercier, R. & Dupuy, J. The multicomponent Debus-Radziszewski reaction in macromolecular chemistry. *Polym. Chem.* **9**, 1927–1933 (2018).

112. Chauveau, E., Marestin, C., Schiets, F. & Mercier, R. Synthesis of 2,4,5-triarylimidazoles in aqueous solution, under microwave irradiation. *Green Chem.* **12**, 1018–1022 (2010).

113. Vogel, H. & Marvel, C. S. Polybenzimidazoles, New Thermally Stable Polymers. *J. Polym. Sci. Part A Polym. Chem.* 511–539 (1961).

114. Overton, P., Konovalova, A., Fraser, K. & Holdcroft, S. The First Example of a Poly(arylimidazole) by Polycondensation of AB-type Monomers: Control of Molecular Mass by End-Capping, and Functionalization to Poly(arylimidazolium)s. *Macromolecules* **56**, 2801–2808 (2023).

115. Akutsu, F., Kataoka, T., Naruchi, K., Miura, M. & Nagakubo, K. Preparation of Polyamides having 2-phenyl-4,5-imidazolediyl Units in the Main Chain. *Int. J. Sci. Technol. Polym.* **28**, 1787–1790 (1987).

116. Olah, G., Ohannesian, L. & Arvanaghi, M. Formylating Agents. *Chem. Rev.* **87**, (1987).

117. Muzart, J. Pd-catalyzed oxidation of alkynes. *J. Mol. Catal. A Chem.* **338**, 7–17

(2011).

118. Mousset, C. *et al.* DMSO-PdI2 as a powerful oxidizing couple of alkynes into benzils: one-pot synthesis of nitrogen-containing five- or six-membered heterocycles. *Tetrahedron* **64**, 4287–4294 (2008).

119. Dömling, A., Wang, W. & Wang, K. Chemistry and biology of multicomponent reactions. *Chem. Rev.* **112**, 3083–3135 (2012).

120. Kakuchi, R. Multicomponent reactions in polymer synthesis. *Angew. Chemie - Int. Ed.* **53**, 46–48 (2014).

121. Saxer, S., Marestin, C., Mercier, R. & Dupuy, J. The multicomponent Debus-Radziszewski reaction in macromolecular chemistry. *Polym. Chem.* **9**, 1927–1933 (2018).

122. Stuparu, M. C. & Khan, A. *Multi-Component and Sequential Reactions in Polymer Synthesis*. *Advances in Polymer Science* (2015).

123. Brunel, R., Marestin, C., Martin, V., Mercier, R. & Schiets, F. Assisted microwave synthesis of high molecular weight poly(aryletherketone) s. *High Perform. Polym.* **20**, 185–207 (2008).

124. Krannig, K. S., Esposito, D. & Antonietti, M. Highly efficient transfer of amino groups to imidazolium entities for polymer coupling and cross-linking. *Macromolecules* **47**, 2350–2353 (2014).

125. Das, B., Kashanna, J., Kumar, R. A. & Jangili, P. Synthesis of 2,4,5-trisubstituted and 1,2,4,5-tetrasubstituted imidazoles in water using p-dodecylbenzenesulfonic acid as catalyst. *Monatshefte fur Chemie* **144**, 223–226 (2013).

126. Nagarapu, L., Apuri, S. & Kantevari, S. Potassium dodecatugstocobaltate trihydrate (K5CoW12O40·3H2O): A mild and efficient reusable catalyst for the one-pot synthesis of 1,2,4,5-tetrasubstituted imidazoles under conventional heating and microwave irradiation. *J. Mol. Catal. A Chem.* **266**, 104–108 (2007).

127. Chauveau, E., Marestin, C. & Martin, V. Microwave-assisted polymerization process: A way to design new, high molecular weight poly(arylimidazole) s.

Polymer (Guildf). **49**, 5209–5214 (2008).

128. Chauveau, E. & Marestin, C. Microwave-assisted synthesis of tetrasubstituted aryl imidazole based polymers via cascade polycondensation process. **55**, 4–7 (2014).

129. Chauveau, E., Marestin, C. & Mercier, R. Microwave-assisted synthesis of tetrasubstituted aryl imidazole based polymers via cascade polycondensation process. *Polymer (Guildf).* **55**, 6435–6438 (2014).

130. Sonogashira, K., Tohda, Y. & Hagihara, N. A convenient synthesis of acetylenes: catalytic substitutions of acetylenic hydrogen with bromoalkenes, iodoarenes and bromopyridines. *Tetrahedron Lett.* **16**, 4467–4470 (1975).

131. Yusubov, M. & Filimonov, V. Iodine in Dimethyl Sulfoxide as a New General Reagent for the Preparative Oxidation of 1,2-Diarylethenes and 1,2-Diarylethynes to Aromatic 1,2-Diketones. *Synthesis (Stuttg).* **11**, 132 (1991).

132. Lindner, J. P. Imidazolium-Based Polymers via the Poly-Radziszewski Reaction. *Macromolecules* **49**, 2046–2053 (2016).

133. Chauveau, E., Marestin, C., Schiets, F. & Mercier, R. Synthesis of 2,4,5-triarylimidazoles in aqueous solution, under microwave irradiation. *Green Chem.* **12**, 1018–1022 (2010).

134. Pan, J., Chen, C., Zhuang, L. & Lu, J. Designing advanced alkaline polymer electrolytes for fuel cell applications. *Acc. Chem. Res.* **45**, 473–481 (2012).

135. Durst, J. *et al.* New insights into the electrochemical hydrogen oxidation and evolution reaction mechanism. *Energy Environ. Sci.* **7**, 2255–2260 (2014).

136. Rheinländer, P. J., Herranz, J., Durst, J. & Gasteiger, H. A. Kinetics of the Hydrogen Oxidation/Evolution Reaction on Polycrystalline Platinum in Alkaline Electrolyte Reaction Order with Respect to Hydrogen Pressure. *J. Electrochem. Soc.* **161**, F1448–F1457 (2014).

137. Davydova, E. S., Mukerjee, S., Jaouen, F. & Dekel, D. R. Electrocatalysts for Hydrogen Oxidation Reaction in Alkaline Electrolytes. *ACS Catal.* **8**, 6665–6690 (2018).

138. Li, D., Chung, H. T., Maurya, S., Matanovic, I. & Kim, Y. S. Impact of ionomer adsorption on alkaline hydrogen oxidation activity and fuel cell performance. *Curr. Opin. Electrochem.* **12**, 189–195 (2018).

139. Chung, H. T., Martinez, U., Matanovic, I. & Kim, Y. S. Cation-Hydroxide-Water Coadsorption Inhibits the Alkaline Hydrogen Oxidation Reaction. *J. Phys. Chem. Lett.* **7**, 4464–4469 (2016).

140. Maurya, S., Fujimoto, C. H., Hibbs, M. R., Narvaez Villarrubia, C. & Kim, Y. S. Toward Improved Alkaline Membrane Fuel Cell Performance Using Quaternized Aryl-Ether Free Polyaromatics. *Chem. Mater.* **30**, 2188–2192 (2018).

141. Leonard, D. P. *et al.* Phenyl-Free Polynorbornenes for Potential Anion Exchange Ionomers for Fuel Cells and Electrolyzers. **2203488**, (2023).

142. Maurya, S. *et al.* Rational design of polyaromatic ionomers for alkaline membrane fuel cells with 41 W cm À2 power density †. *Energy Environ. Sci* **11**, 3283 (2018).

143. Niño, P. *et al.* Efficient three-component synthesis of diversely substituted tetrahydro-1H-cyclopenta[c]quinolines. *Indian J. Chem.* **55**, 854–881 (2016).

144. Sawama, Y., Takubo, M., Mori, S., Monguchi, Y. & Sajiki, H. Pyridine N-oxide mediated oxidation of diarylalkynes with palladium on carbon. *European J. Org. Chem.* 3361–3367 (2011) doi:10.1002/ejoc.201001641.

145. Mousset, C. *et al.* DMSO-PdI2 as a powerful oxidizing couple of alkynes into benzils: one-pot synthesis of nitrogen-containing five- or six-membered heterocycles. *Tetrahedron* **64**, 4287–4294 (2008).

146. Fernández, P. S. *et al.* Platinum nanoparticles produced by EG/PVP method : The effect of cleaning on the electro-oxidation of glycerol. *Electrochim. Acta* **98**, 25–31 (2013).

147. Meier, J. C. *et al.* Design criteria for stable Pt/ fuel cell catalysts. *Beilstein J. Nanotechnol.* **5**, 44–67 (2014).

148. Holdcroft, S. Fuel cell catalyst layers: A polymer science perspective. *Chem. Mater.* **26**, 381–393 (2014).

149. Schiraldi, D. A. Perfluorinated polymer electrolyte membrane durability. *Polym. Rev.* **46**, 315–327 (2006).

150. Zhou, C., Zawodzinski, T. & Schiraldi, D. A. Chemical changes in Nafion membranes under simulated fuel cell conditions. in *228th American Chemical Society National Meeting* (2004).

151. Schiraldi, D. A., Zhou, C. & Zawodzinski, T. Chemical durability studies of PFSA polymers and model compounds under mimic fuel cell conditions. in *230th American Chemical Society National Meeting* (2005).

152. Yamabe, S., Tsuchida, N. & Yamazaki, S. A FMO-controlled reaction path in the benzil-benzilic acid rearrangement. *J. Org. Chem.* **71**, 1777–1783 (2006).

153. Qian, W., Texter, J. & Yan, F. Frontiers in poly(ionic liquid)s: syntheses and applications. *Chem. Soc. Rev* **46**, 1124–1159 (2017).

154. Ban, T., Guo, M., Wang, Y., Zhang, Y. & Zhu, X. High-performance aromatic proton exchange membranes bearing multiple flexible pendant sulfonate groups : Exploring side chain length and main chain polarity. *J. Memb. Sci.* **668**, 121255 (2023).

155. Peltier, C. R. *et al.* Quaternary Ammonium-Functionalized Polyethylene-Based Anion Exchange Membranes: Balancing Performance and Stability. *ACS Energy Lett.* **8**, 2365–2372 (2023).

156. Chu, X., Liu, L., Huang, Y., Guiver, M. D. & Li, N. Practical implementation of bis-six-membered N-cyclic quaternary ammonium cations in advanced anion exchange membranes for fuel cells: Synthesis and durability. *J. Memb. Sci.* **578**, (2019).

157. Dekel, D. R. *et al.* The critical relation between chemical stability of cations and water in anion exchange membrane fuel cells environment. *J. Power Sources* **375**, 351–360 (2018).

158. Long, H., Kim, K. & Pivovar, B. S. Hydroxide degradation pathways for substituted trimethylammonium cations: A DFT study. *J. Phys. Chem. C* **116**, 9419–9426

(2012).

159. Matsuyama, K., Ohashi, H., Miyanishi, S., Ushiyama, H. & Yamaguchi, T. Quantum chemical approach for highly durable anion exchange groups in solid-state alkaline fuel cells. *RSC Adv.* **6**, 36269–36272 (2016).

160. Kreuer, K. & Jannasch, P. A practical method for measuring the ion exchange capacity decrease of hydroxide exchange membranes during intrinsic degradation. *J. Power Sources* **375**, 361–366 (2018).

161. Diesendruck, C. E. & Dekel, D. R. Water – A key parameter in the stability of anion exchange membrane fuel cells. *Curr. Opin. Electrochem.* **9**, 173–178 (2018).

162. Peressin, N. *et al.* Structure-Property Relationships in Sterically Congested Proton-Conducting Poly(phenylene)s: The Impact of Biphenyl Linearity. *Macromolecules* (2020) doi:10.1021/acs.macromol.0c00310.

Appendix A. Supporting Information for Chapter 3

Table A.1: The sonogashira coupling reaction optimisation.

Reaction	Base	Eq. of Base	Eq. [$Pd(PPh_3)Cl_2$]	Eq. CuI	Yield (%)
1	TEA	8	0.01	0.01	34
2	TEA	8	0.01 (+0.02PPh_3)	0.01	59
3	TEA	8	0.01	0.02	53
4	TEA	6	0.01	0.01	36
5	DIPA	8	0.01	0.01	66
6	DIPA	8	0.05	0.05	65
7	TEA	8	0.05	0.05	72
8	TEA	16	0.05	0.05	67
9	TEA	8	0.025 (+0.025 PPh_3)	0.05	70
10	TEA/DEA	8	0.05	0.05	90

Table A.2: Optimisation of DMP-PDPI-Bn. 4-methylbenzylamine (MBA).

REACTION	EQ. OPAB	EQ. NH_4OAC	EQ. 4-MBA	EQ. ACOH	EQ. TFOAC	SOLVENT	YIELD (%)
BZ-1	1	5	5	30	1.3	DMF	95
]BZ-2	1	5	5	30	1.3	Toluene	95
BZ-3	1	5	5	1	-	Toluene	7
BZ-4	1	4	6	6.5	-	Toluene	24

BZ-5	1	4	6	30	1.3	Dioxane	-
BZ-6	1	4	6	30	1.3	Toluene	95

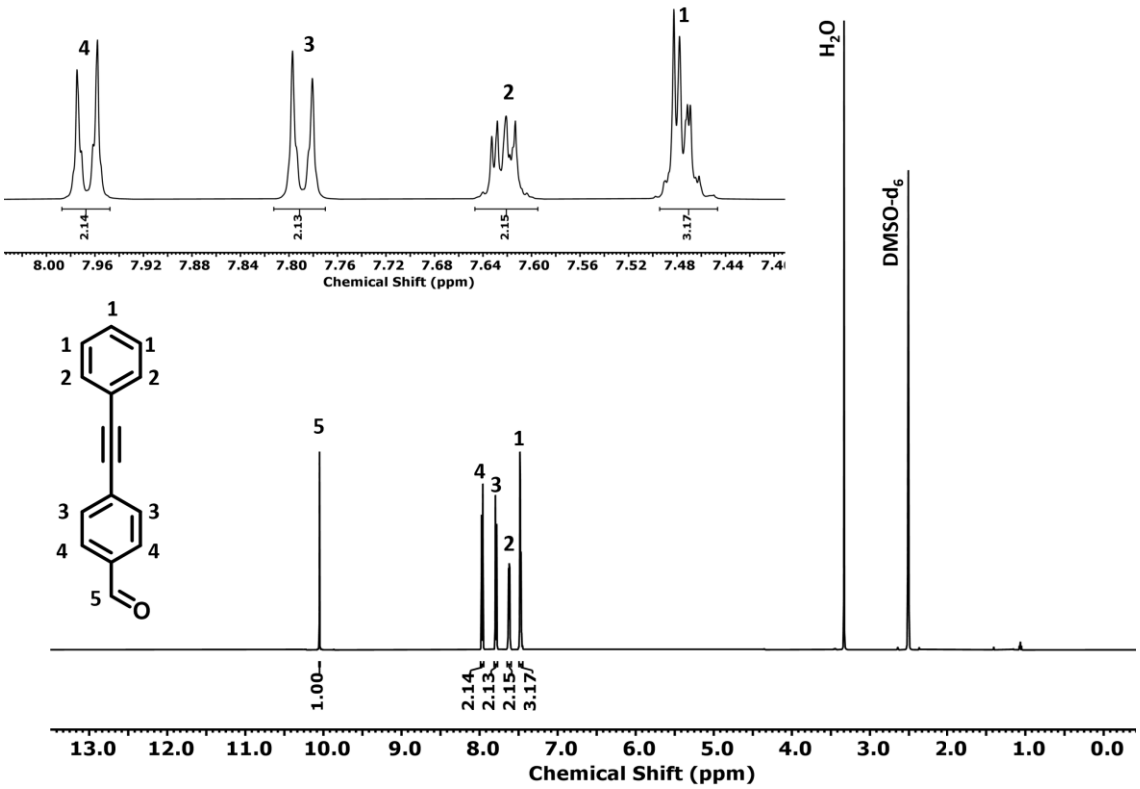

Figure A. 1: ^{1}H NMR of PEB.

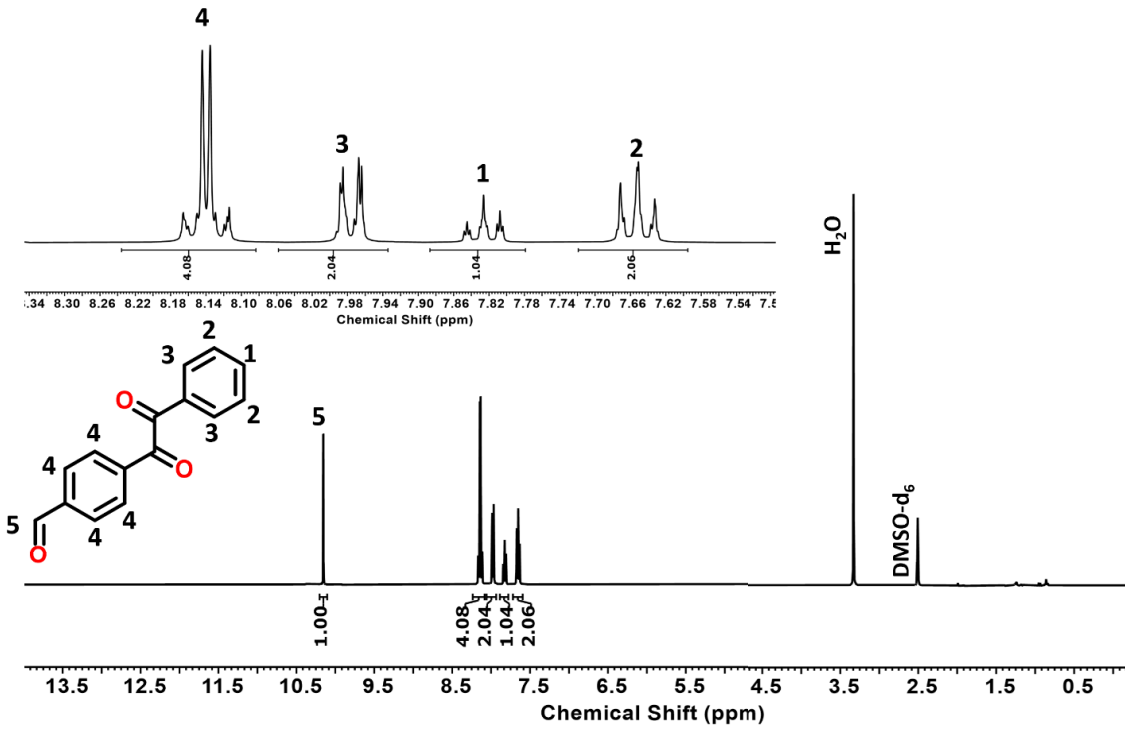

Figure A. 2: ^{1}H NMR of OPAB.

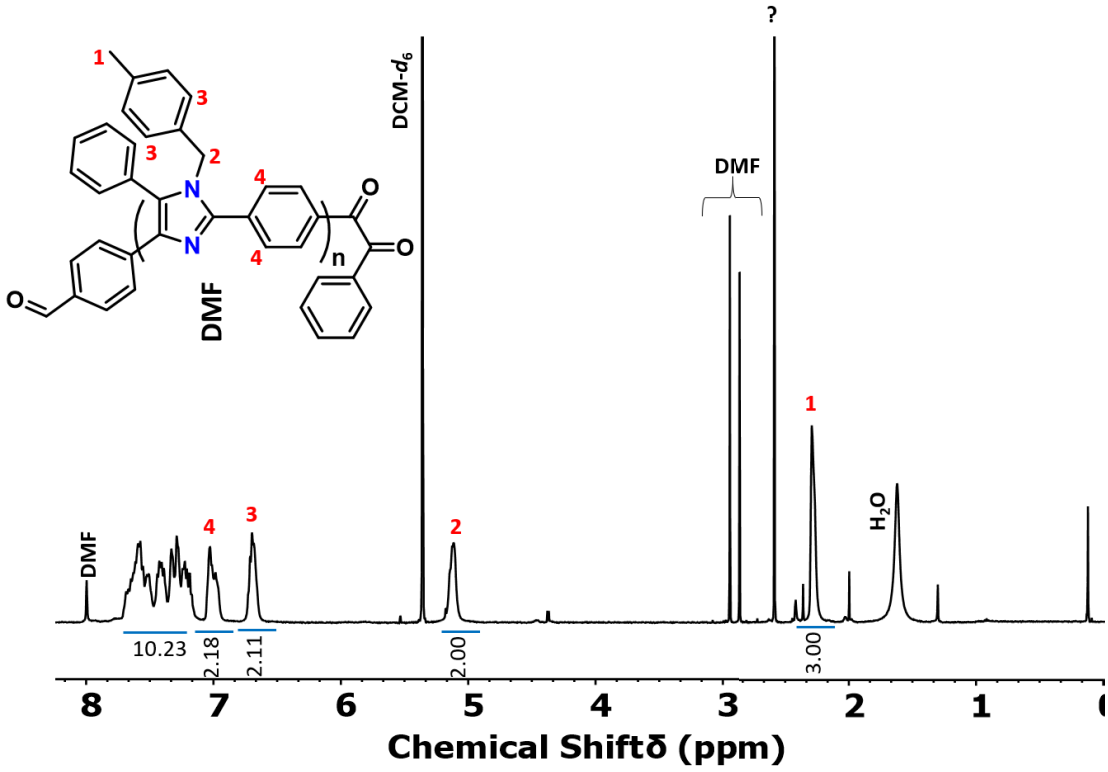

Figure A. 3: ^{1}H NMR of PDPI-Bz.

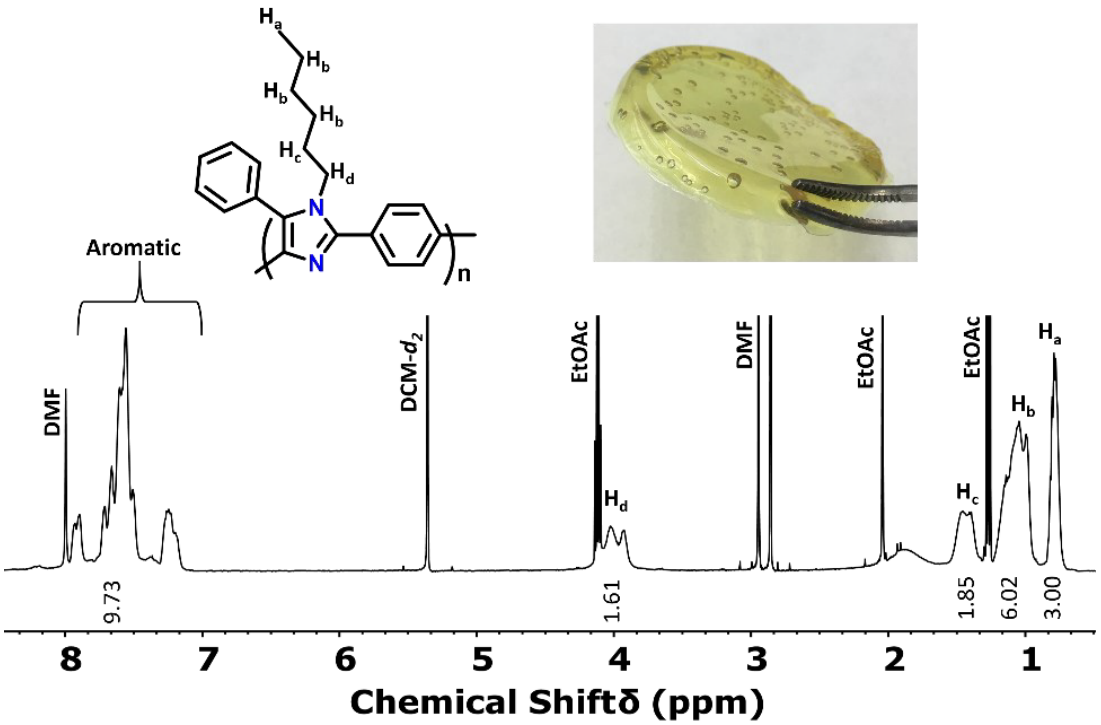

Figure A. 4: ^{1}H NMR of PDPI-H.

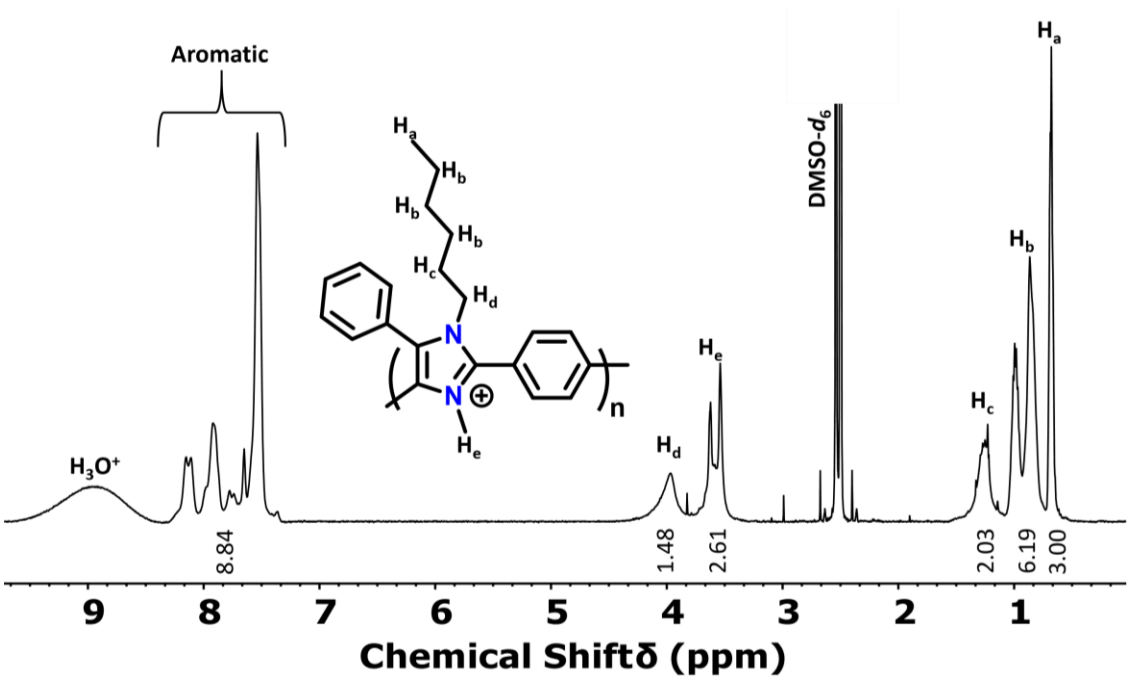

Figure A. 5: ^{1}H NMR of PDPI-H-M.

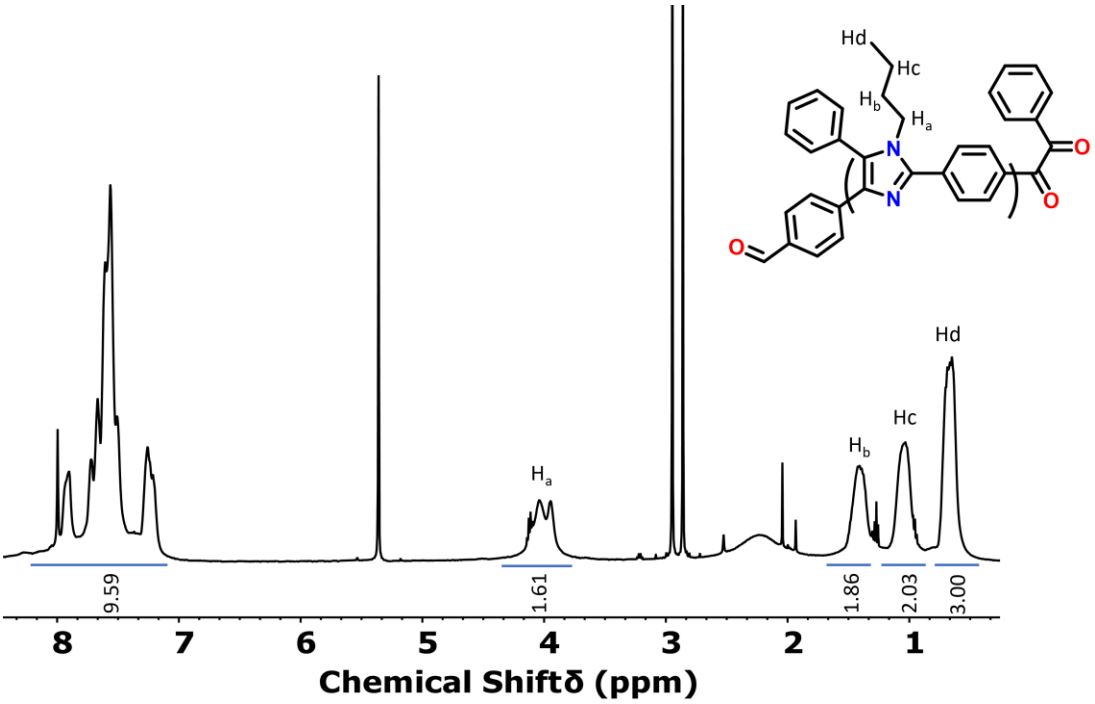

Figure A. 6: ^{1}H NMR of PDPI-Bu.

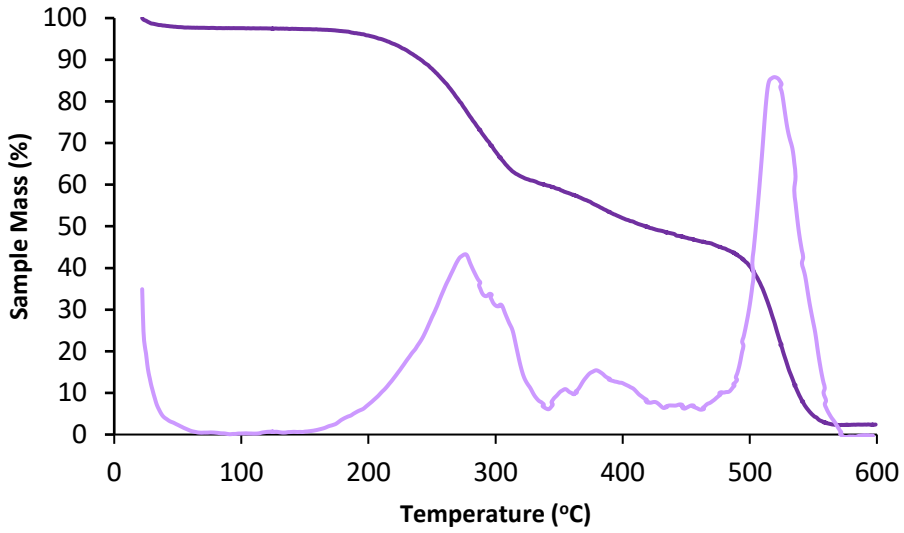

Figure A.7: Thermogram (dark purple) and thermogram derivative of PDPI-H-M.

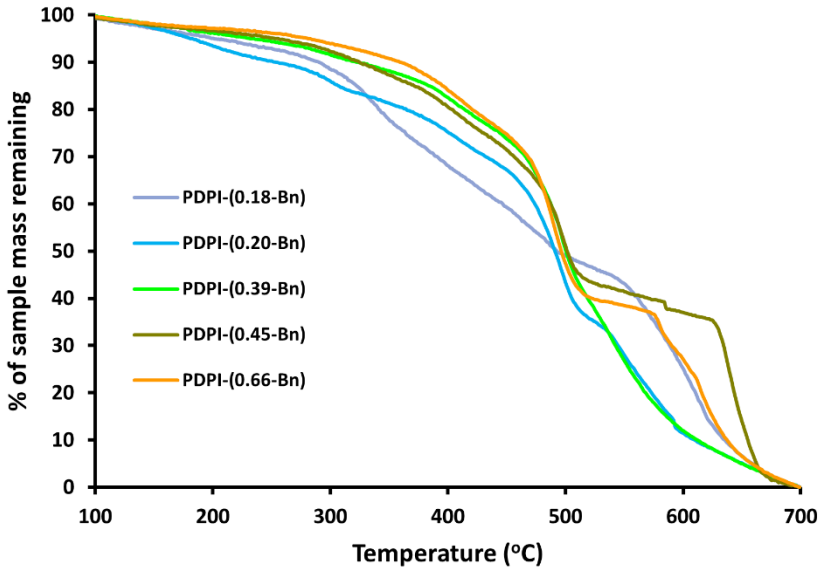

Figure A.8: Thermograms of the PDPI-φ-Bz series.

Appendix B. Supporting Information of Chapter 4

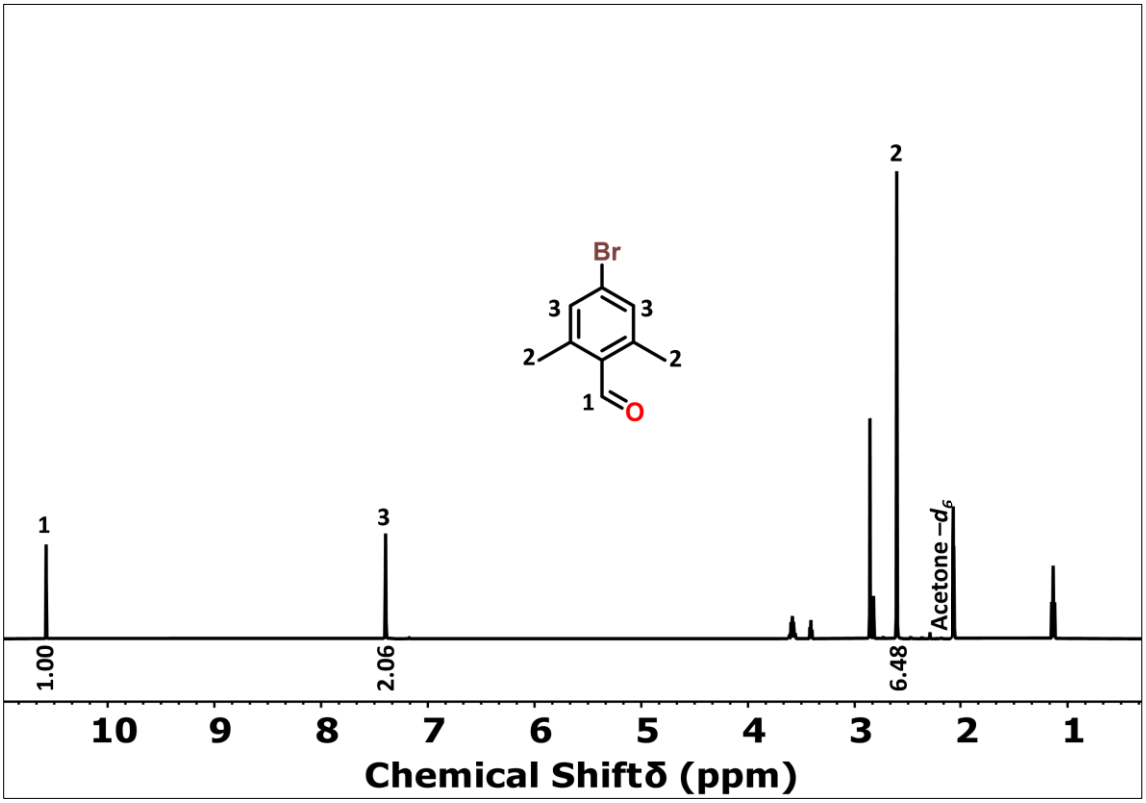

Figure B.1: ^{1}H NMR of 2,6-dimethyl-4-bromobenzaldehyde.

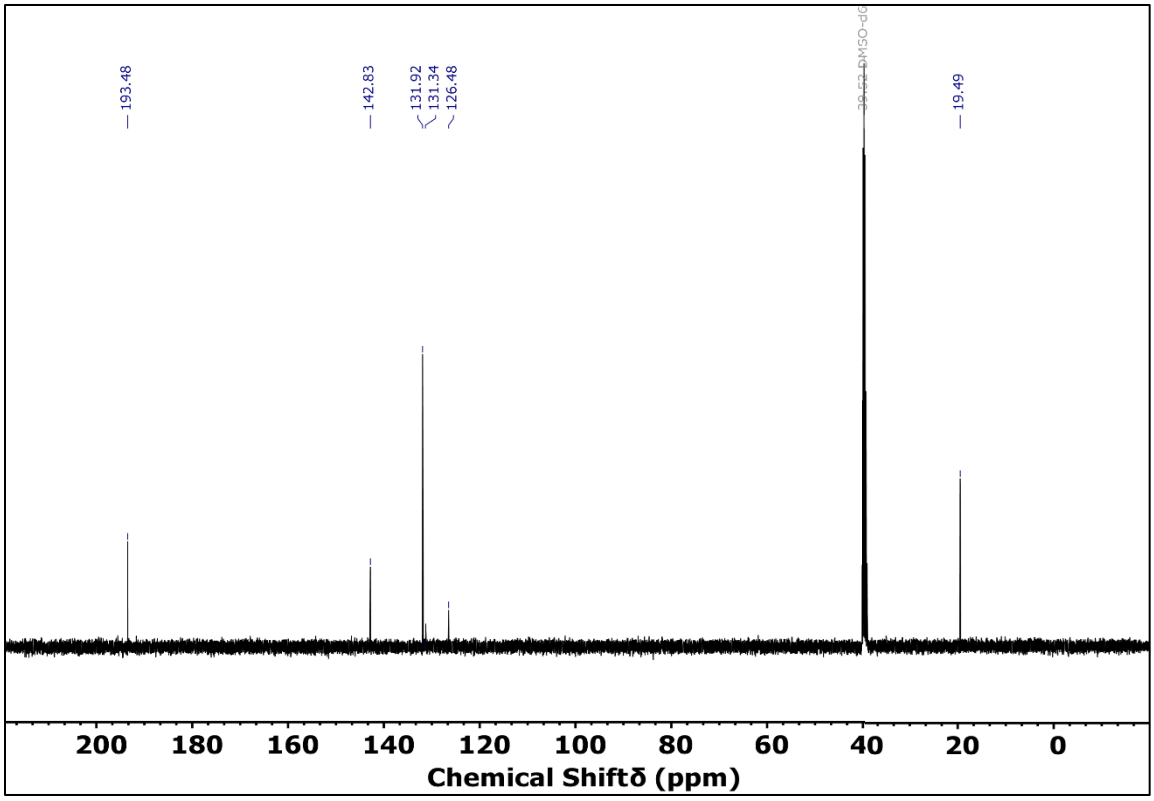

Figure B.2: ^{13}C NMR of 2,6-dimethyl-4-bromobenzaldehyde.

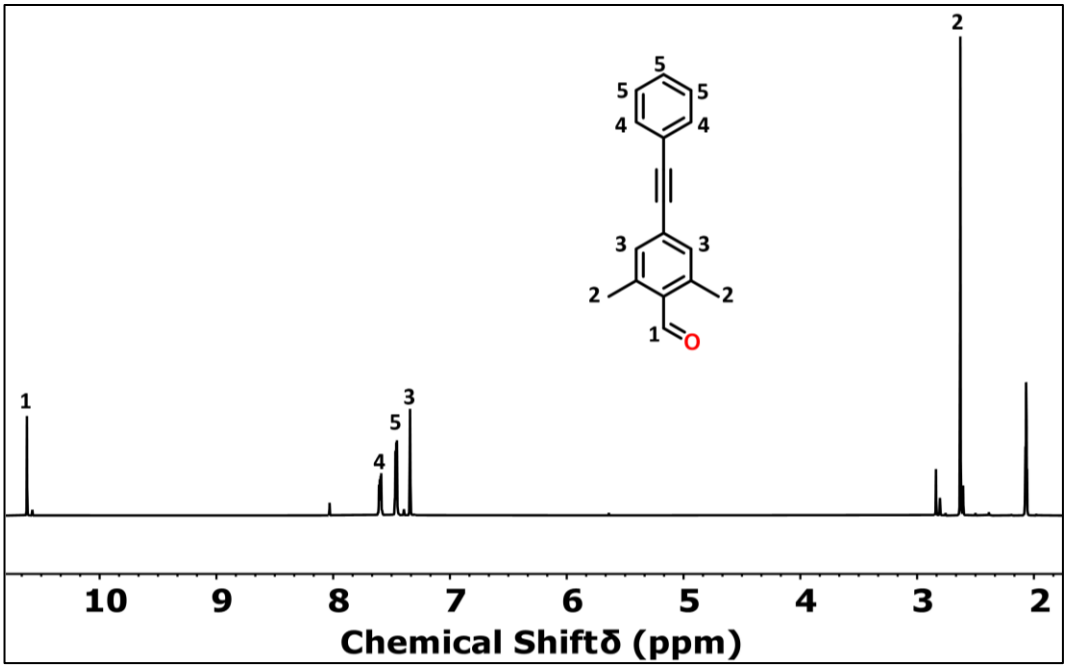

Figure B.3: ^{1}H NMR of 2,6-dimethyl-4-(phenylethynyl)-benzaldehyde.

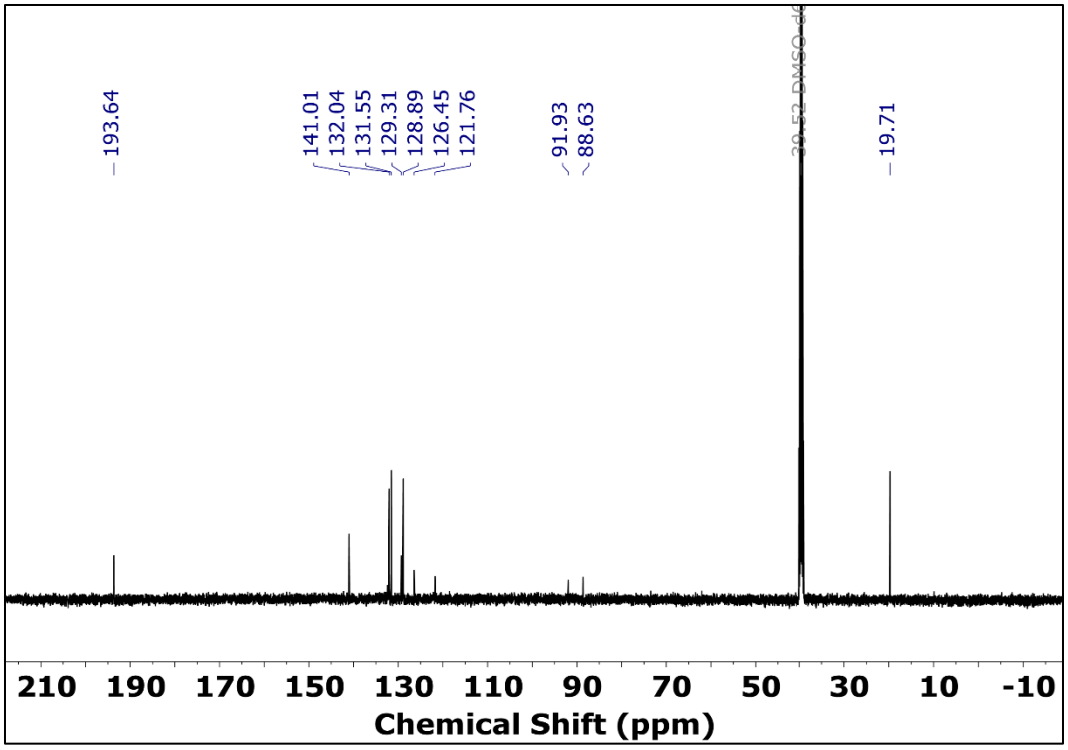

Figure B.4: ^{13}C NMR of 2,6-dimethyl-4-(phenylethynyl)-benzaldehyde.

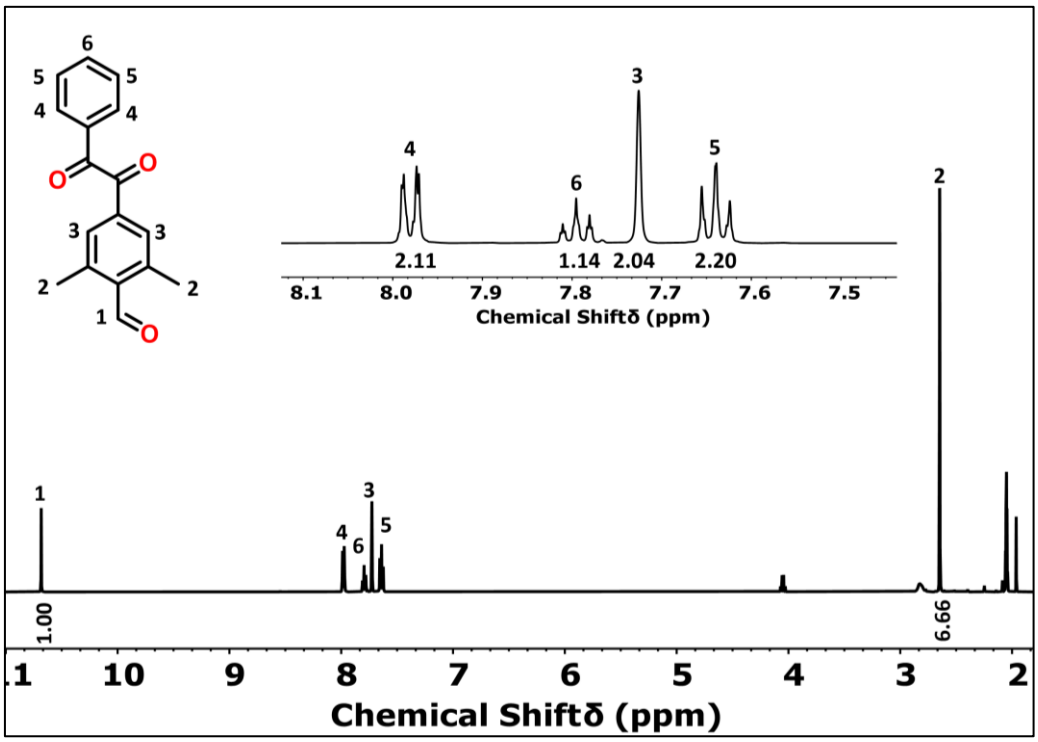

Figure B.5 ^{1}H NMR of 2,6-dimethyl-4-(2-oxo-2-phenylacetyl)benzaldehyde.

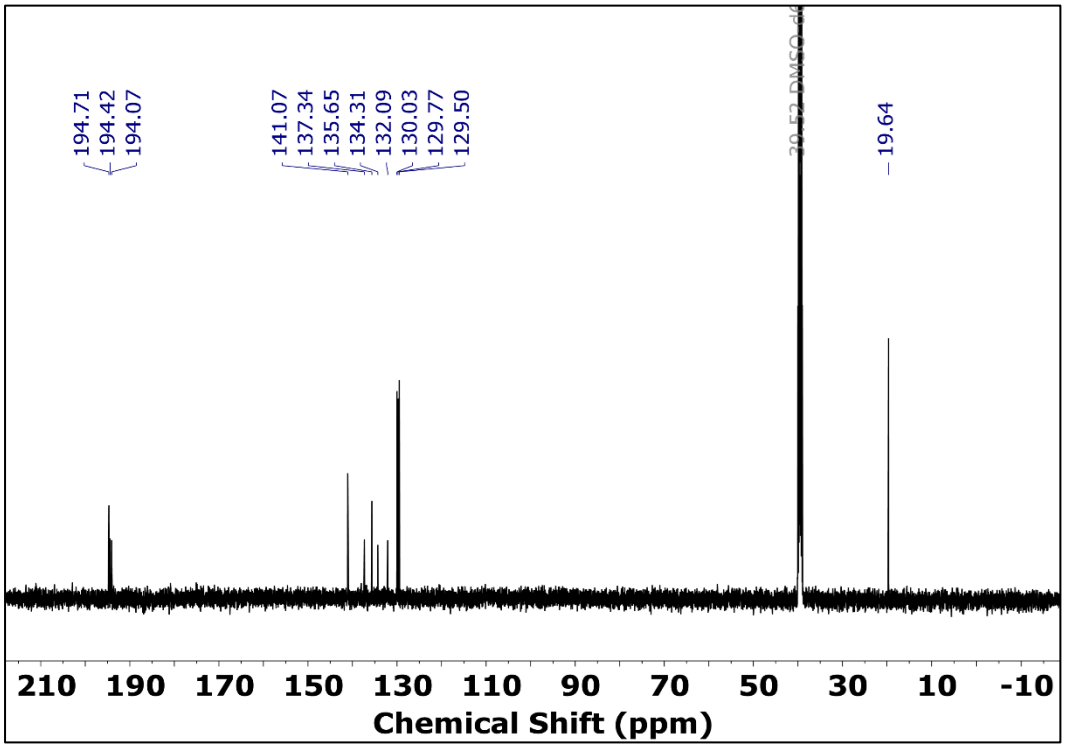

Figure B.6: ^{13}C NMR of 2,6-dimethyl-4-(2-oxo-2-phenylacetyl) - benzaldehyde.

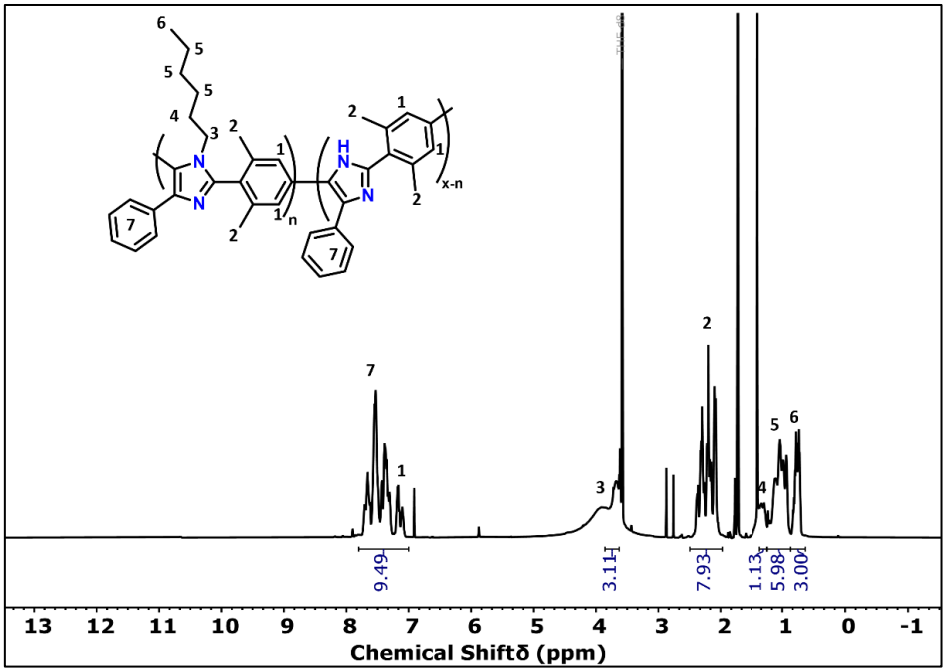

Figure B.7: ^{1}H NMR of DMP-PHPI.

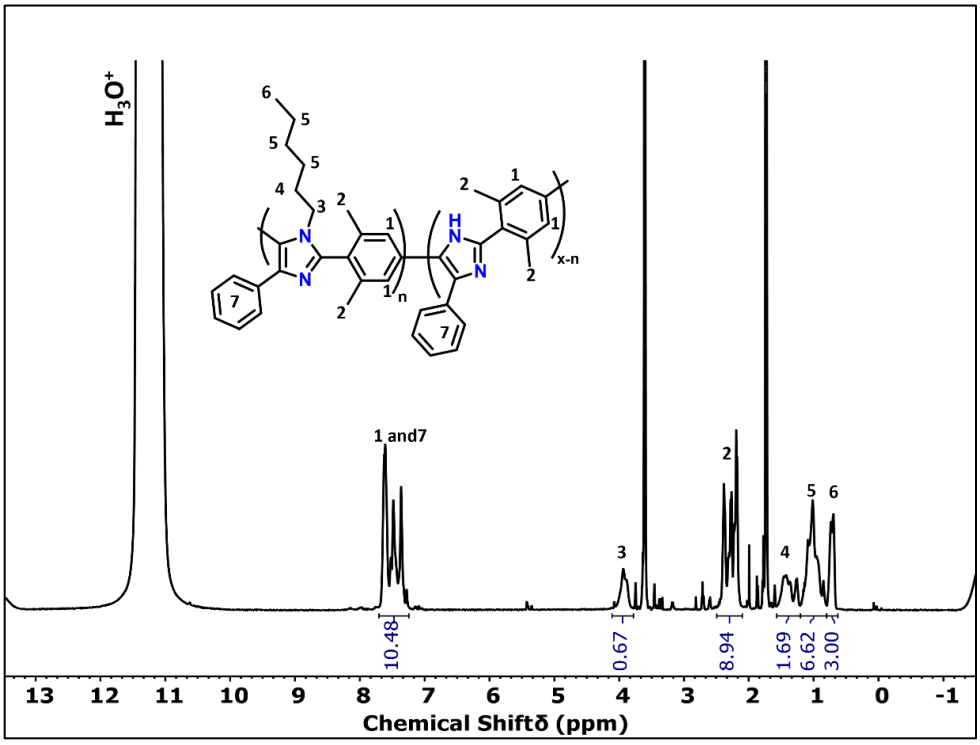

Figure B.8: ^{1}H NMR of DMP-PHPI with drops of TFA.

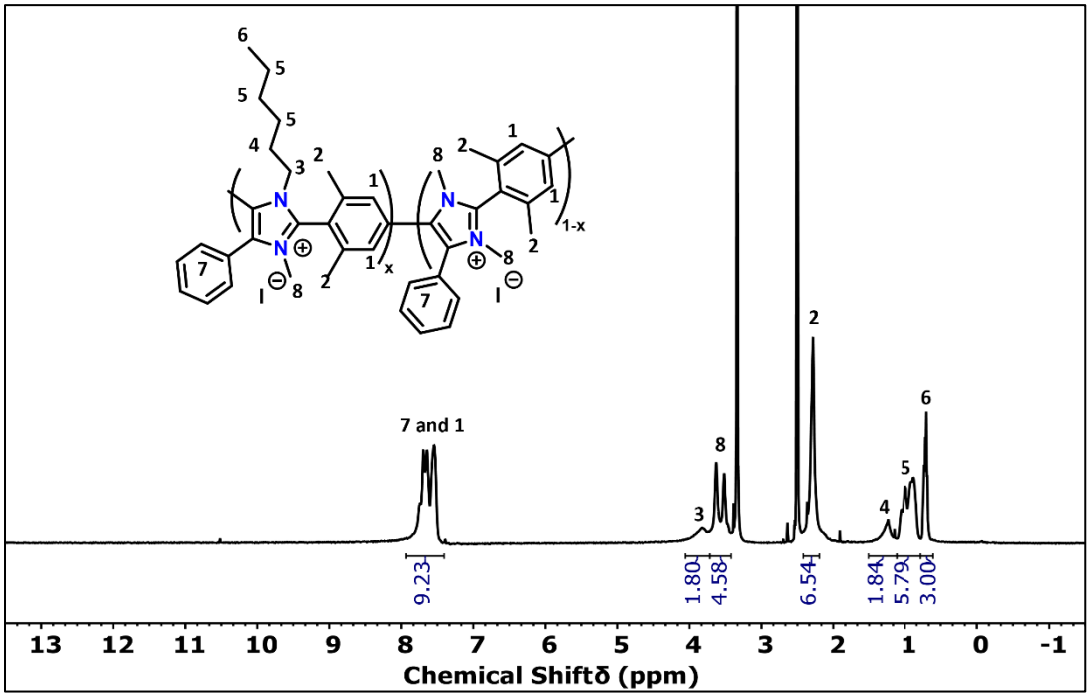

Figure B.9: ^{1}H NMR of DMP-PHPI-M.

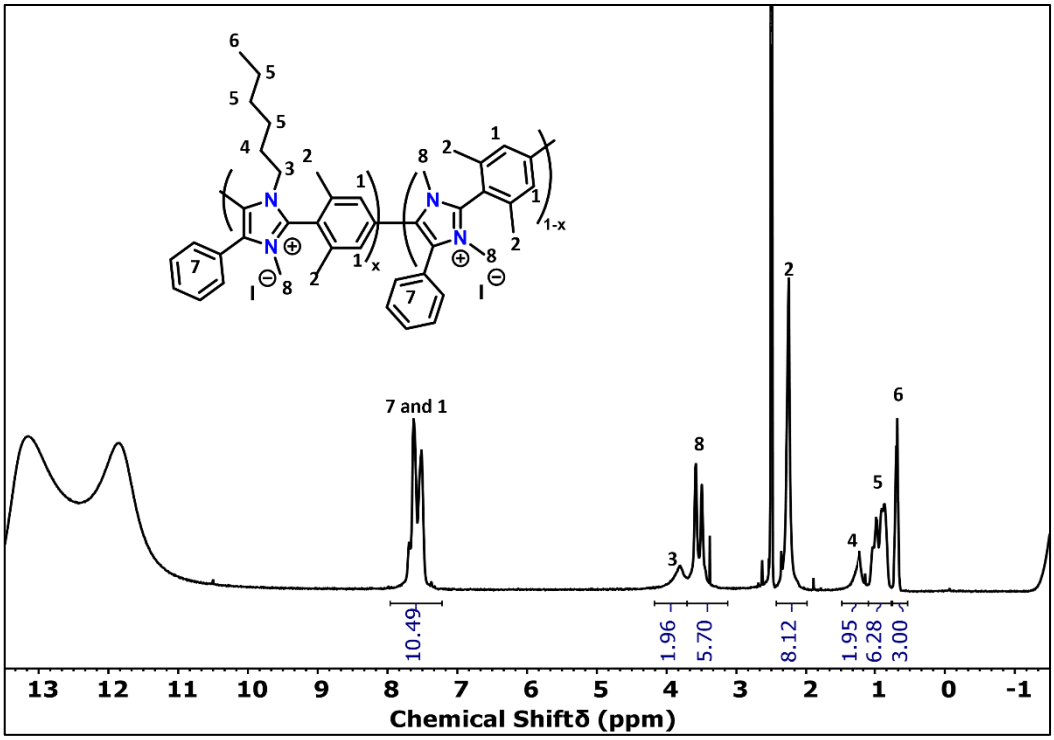

Figure B.10: ^{1}H NMR of DMP-PHPI-M with drops of TFA.

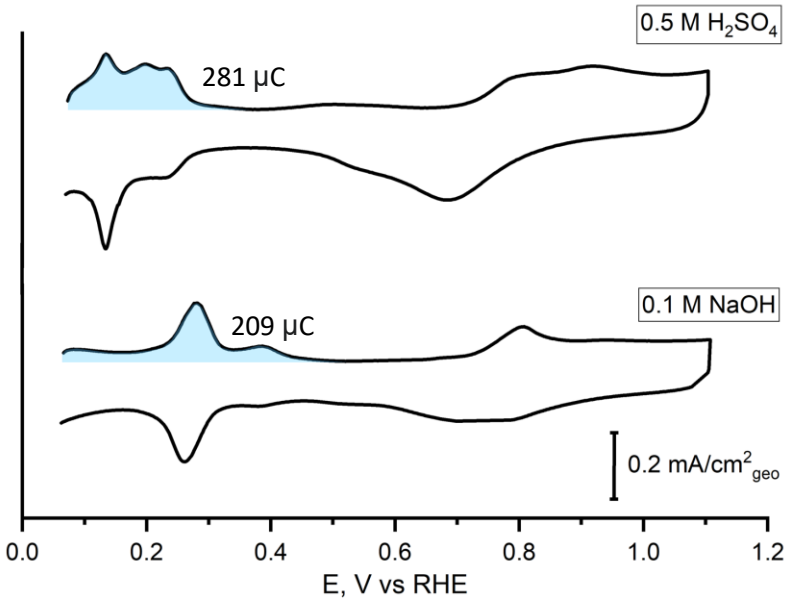

Figure B.11: CVs for Pt/C in N_2-saturated 0.5M H2SO4 (top) and 0.1M NaOH (bottom) and at 20 mV s^{-1}. ***The area used for charge integration and further calculation of the platinum surface area is highlighted. CVs are obtained for the same electrode in different electrolytes.***

Appendix C. Supporting Information of Chapter 5

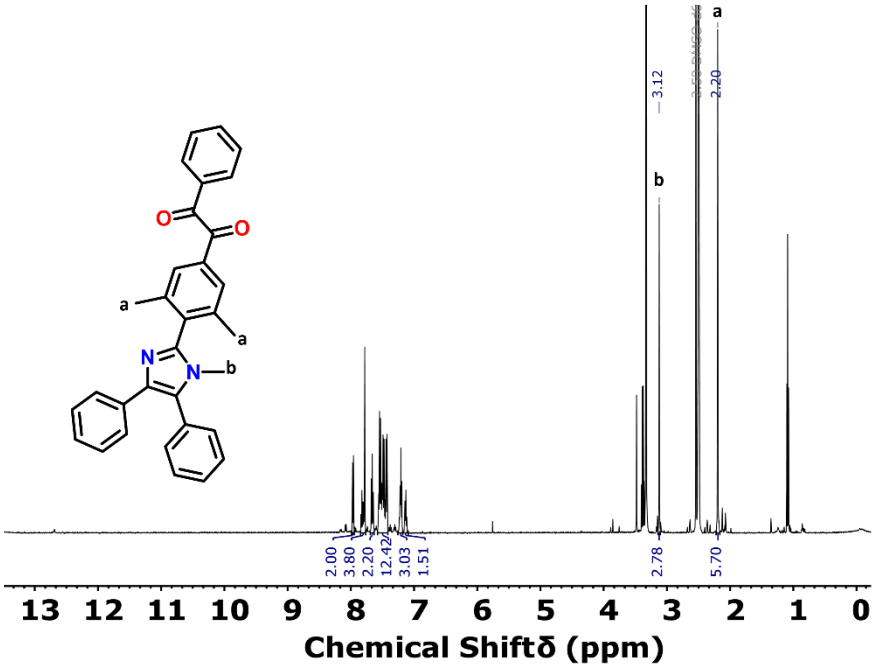

Figure C.1: ^{1}H NMR of 1-(3,5-dimethyl-4-(1-methyl-4,5-diphenyl-1H-imidazol-2-yl)phenyl)-2-phenylethane-1,2-dione

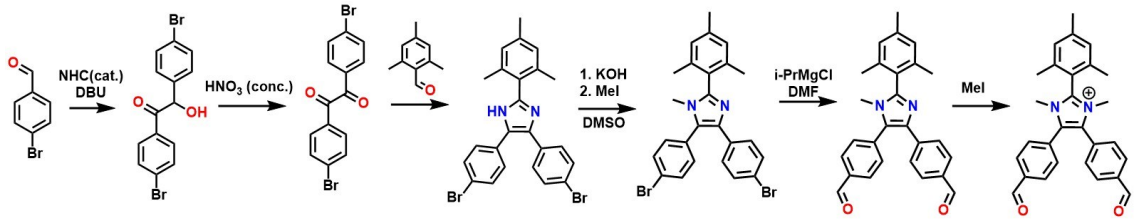

Figure C.2: Synthetic route initally attempted for synthesis of compound MesIm(A).

Synthesis of 4,5-bis(4-bromophenyl)-2-mesityl-1-methyl-imidazole

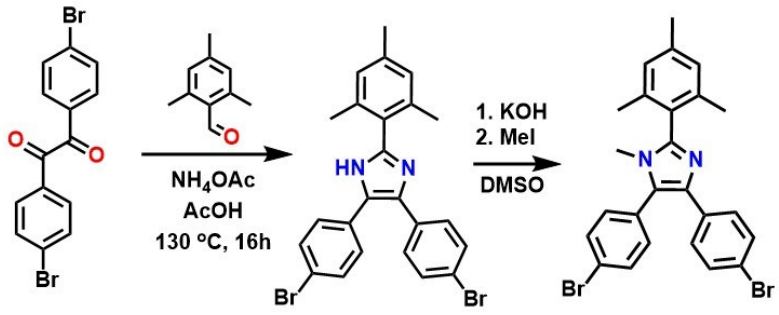

4,4' – dibromobenzil (5.00 g, 21.20 mmol, 1 eq). was added to a dried 150 mL pressure vessel. Acetic acid (40 mL) and ammonium acetate (16.34 g, 212.00, 10 eq.) were added to the reaction, and it was stirred for 10 mins. The mesityl benzaldehyde (3.75 mL, 25.44 mmol, 1.2 eq.) was added and the reaction was stirred at 130 °C for 16 h. Once cooled the reaction was precipitated into ammonium hydroxide (80 mL in 700 mL) water. The solid was filtered and triturated in acetonitrile until when filtered the solution was clear colourless. The solid was dried under vacuum and used for the next reaction. Dibromoimidazole (5.00 g, 10.08 mmol, 1 eq.) was dissolved in DMSO (50 mL). Potassium hydroxide (6 M, 3.36 mL, 20.16 mmol, 2 eq.) was added to the reaction and stirred for 1h. Iodomethane (0.628 mL, 10.08 mmol, 1 eq.) was added to the reaction dropwise and the reaction was stirred for 3 h at room temperature. The product precipitated out of the reaction and was filtered, dissolved in ethyl acetate, and washed with water, brine and $MgSO_4$. The reaction yielded an off-white solid. (5.83 g, 55 %).^{1}H NMR (400 MHz, Acetone) δ 7.73 (d, *J* = 8.5 Hz, 0H), 7.54 – 7.43 (m, 0H), 7.39 (d, *J* = 8.7 Hz, 0H), 7.03 – 6.98 (m, 0H), 3.22 (s, 0H), 2.33 (s, 0H), 2.10 (s, 1H).

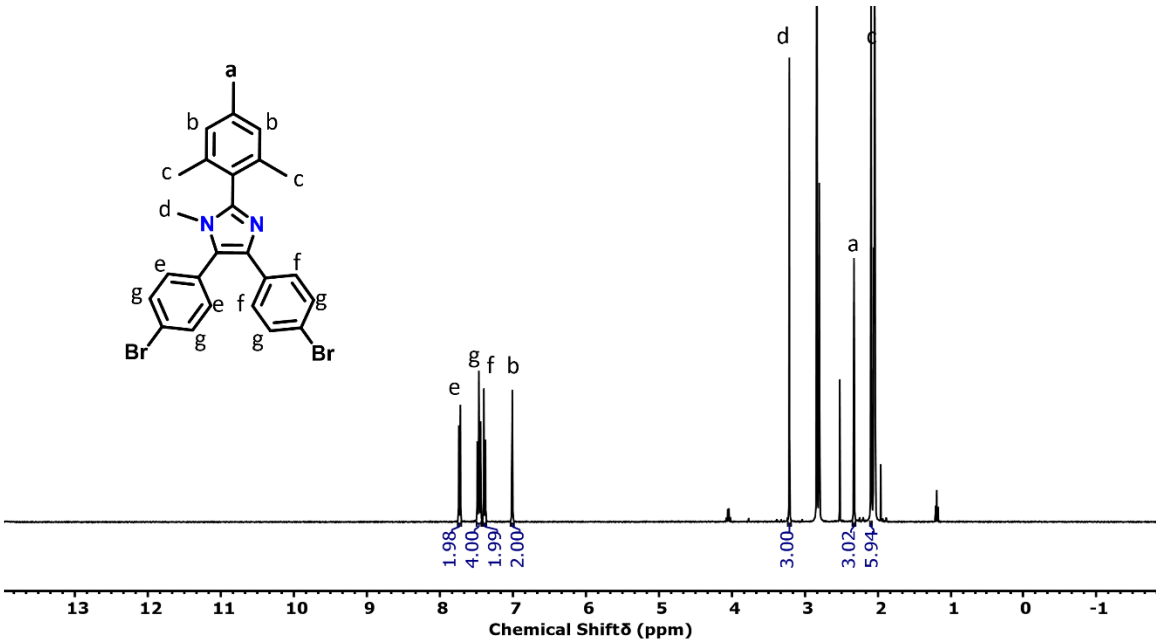

Figure C.3: ^{1}H NMR of 4,5-bis(4-bromophenyl)-2-mesityl-1-methyl-1l4,3l2-imidazole.

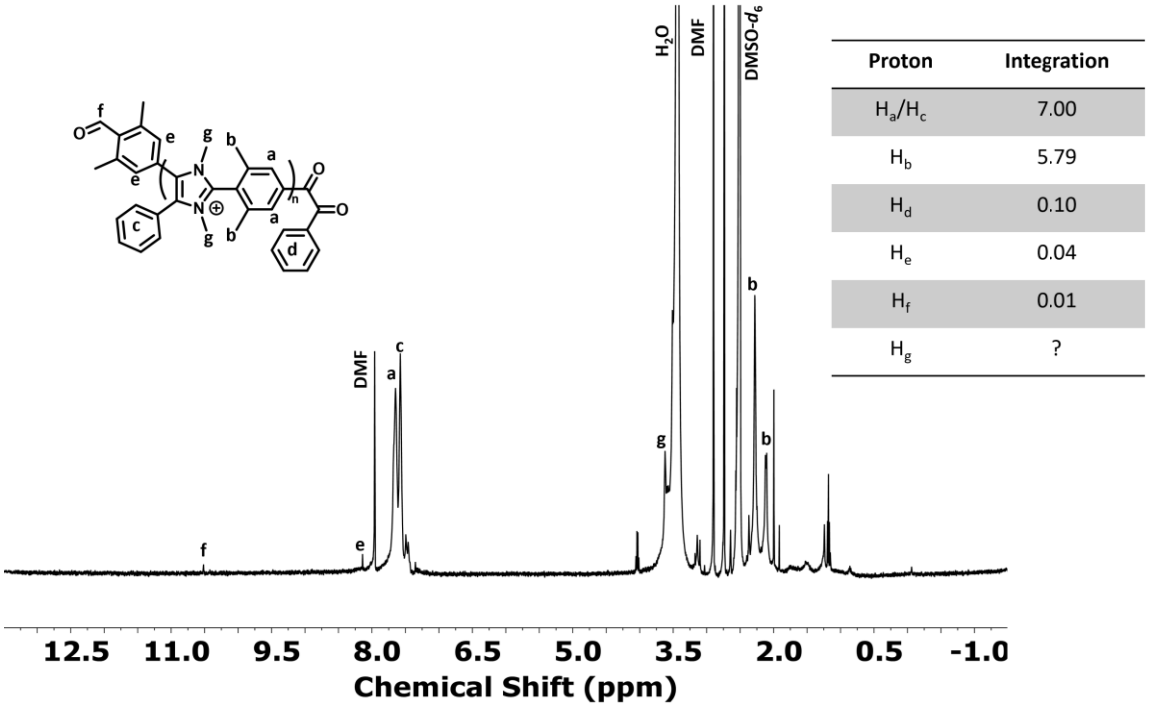

Proton	Integration
H_a/H_c	7.00
H_b	5.79
H_d	0.10
H_e	0.04
H_f	0.01
H_g	?

Figure C.4: ^{1}H NMR of DMP-PPI[+]-AD.

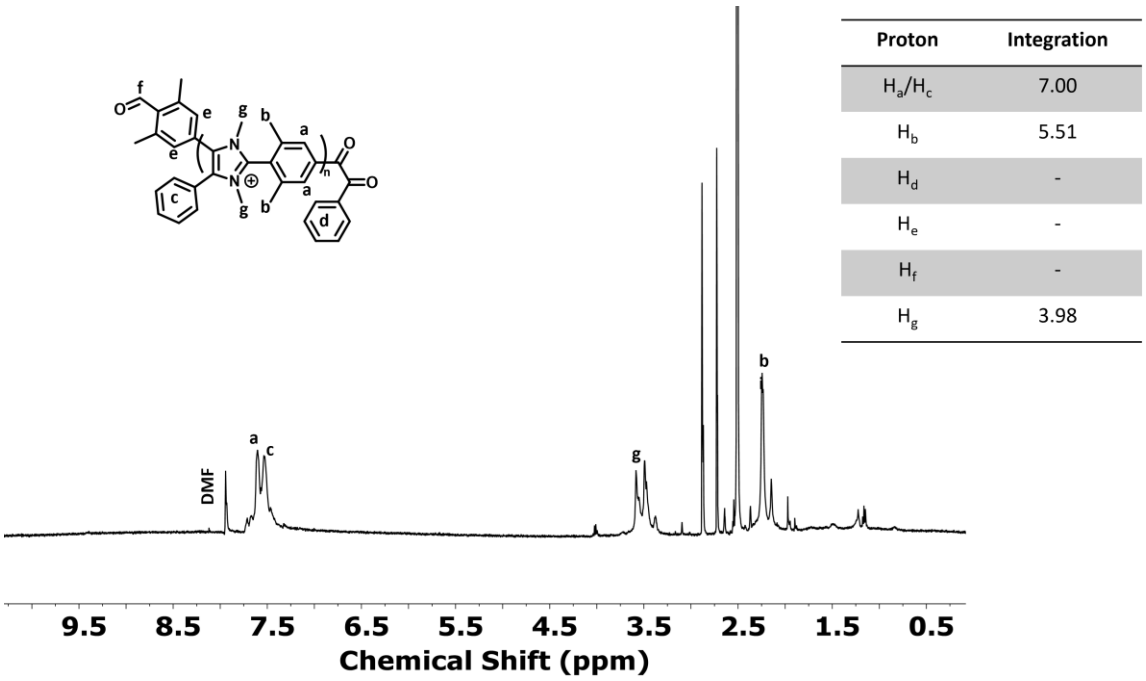

Proton	Integration
H_a/H_c	7.00
H_b	5.51
H_d	-
H_e	-
H_f	-
H_g	3.98

Figure C.5: 1H NMR of DMP-PPI[+]-AD with TFA.

Appendix D. Supporting Information of Chapter 6

Table D.1: The optimised geometries of intermediary compounds along the degradation pathways (B3LYP/6-311++(2d,p). Grey boxes show a reaction that does not occur for this molecule and '–' shows the geometry could not be optimised for this compound.

Compound	Reaction Pathway						
	Reagent (kcal/mol)	$P_{SN2\text{-}Bz}$ (kcal/mol)	$TS_{SN2\text{-}Bz}$ (kcal/mol)	P_{SN2} (kcal/mol)	TS_{SN2} (kcal/mol)	P_{C2} (kcal/mol)	TS_{C2} (kcal/mol
3a	0.00	-37.61	18.10			1.08	14.79
3b	0.00	-30.98	-	-32.20	19.58	8.07	16.86
3c	0.00	-30.98	18.51	-33.87	23.65	7.03	17.32
3d	0.00	-66.63	-			-	-
MesIm	0.00			-22.92	20.01	8.20	16.25

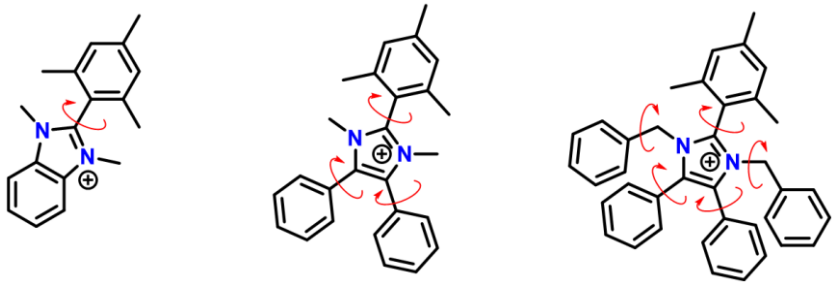

Figure D.0-1: Rotational degrees of freedom for a C2 protected benzimidazolium, imidazolium and benzyl-substituted imidazolium.

Table D.2: Elemental analysis of PSIM-Bz and PSIM-Ph.

Sample	H (%)	N (%)	C (%)
PSMI-Ph (theoretical)	6.17	4.94	82.51
PSMI-Ph (experimental)	**6.59**	**5.15**	**79.95**
PSMI-Bz (theoretical)	6.37	4.82	82.59
PSMI-Bz (experimental)	**6.34**	**4.91**	**79.57**

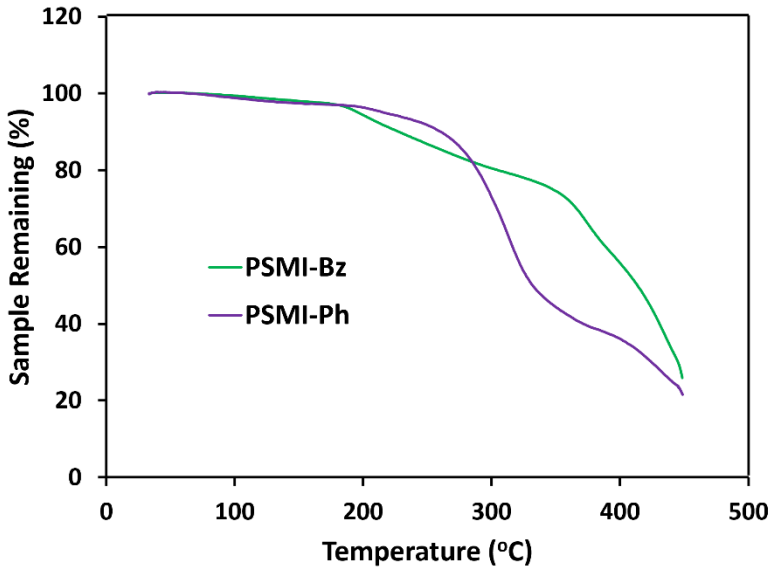

Figure D.0-2: TGA data of PSMI-Bz and PSMI-Ph.

Analysis of PSIM-Bz: The water uptake was 6.8 % at 70 % RH and 80 °C, with a hydration number of 2.06. The conductivity was 1.18 mS/cm at 80 °C and 90 % RH.

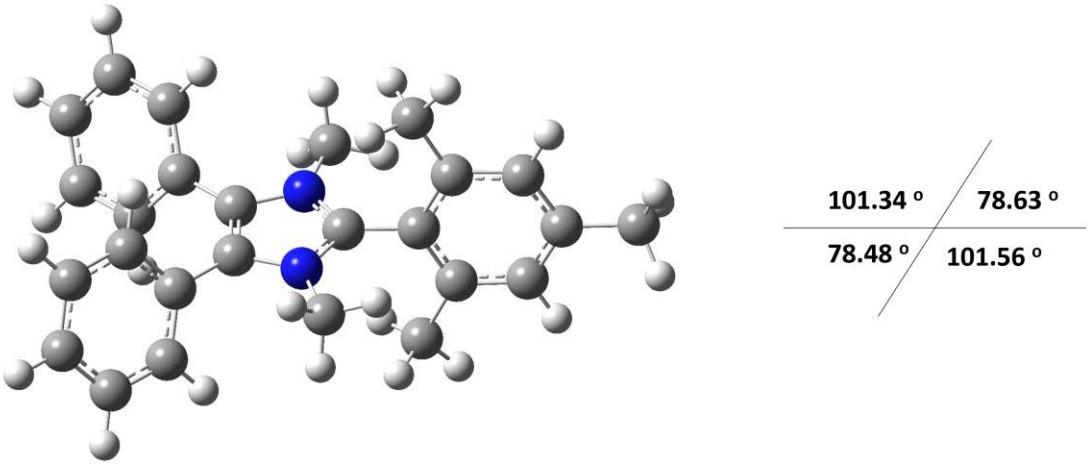

Figure D.3: The dihedral angles associated with MesIm.

Computational Data

Table D.3: Cartesian coordinates in Å for Reagent 3a

Atom	X	Y	Z
C	-0.46192	1.38889	-0.0494
C	-1.24652	0.31095	-0.37995
N	-0.39976	-0.7972	-0.45321
C	0.8695	-0.419	-0.19617
C	2.07841	-1.27132	-0.27501
C	2.70628	-1.42833	-1.53733
C	2.59627	-1.90223	0.87374
C	3.85178	-2.21736	-1.61424
C	3.75386	-2.67944	0.74008
C	-2.70314	0.25658	-0.6248
C	-3.59992	0.56332	0.40991
C	-3.20151	-0.06643	-1.8971
C	-4.97452	0.53721	0.17686
H	-3.21717	0.81355	1.39454
C	-4.5777	-0.09638	-2.12368
H	-2.51495	-0.27686	-2.71237
C	-5.46561	0.20401	-1.08798
H	-5.66136	0.77342	0.98431
H	-4.95439	-0.34598	-3.11124
H	-6.53674	0.18214	-1.26699
C	-0.84263	2.79779	0.16166
C	-1.59123	3.47049	-0.81752
C	-0.48892	3.47275	1.34162
C	-1.97681	4.79587	-0.61914
C	-0.87404	4.79897	1.53282
C	-1.61778	5.46321	0.55419
H	-2.55265	5.3077	-1.38463
H	-0.59747	5.31088	2.44986
C	4.39463	-2.85063	-0.48688
C	-0.80854	-2.18097	-0.78003
H	-1.1933	-2.18327	-1.80184
H	0.11352	-2.76712	-0.77782
H	4.33845	-2.3398	-2.57891
H	4.15937	-3.16349	1.62533
H	-1.91694	6.49629	0.70619

H	0.07633	2.95825	2.11218
H	-1.86259	2.95613	-1.73391
C	2.171	-0.75388	-2.78003
H	1.11729	-0.99446	-2.96195
H	2.24613	0.33772	-2.70961
H	2.7385	-1.06663	-3.66019
C	1.94498	-1.80644	2.23498
H	1.22374	-0.98852	2.30934
H	1.41215	-2.73516	2.47296
H	2.69916	-1.66053	3.01497
C	5.6379	-3.69758	-0.61009
H	5.96717	-4.07011	0.36403
H	5.4607	-4.56222	-1.26133
H	6.46171	-3.12648	-1.054
C	-1.83049	-2.77948	0.16871
C	-1.74873	-2.61078	1.55621
C	-2.8493	-3.58057	-0.36075
C	-2.67212	-3.23133	2.39887
H	-0.97175	-1.98672	1.98615
C	-3.76694	-4.21013	0.48228
H	-2.92771	-3.71203	-1.43695
C	-3.68206	-4.03533	1.86483
H	-2.59996	-3.0868	3.47312
H	-4.55232	-4.82813	0.05641
H	-4.39959	-4.51874	2.52174
C	2.02819	1.73239	0.23532
C	2.75736	1.66192	1.42194
C	2.40387	2.59399	-0.79761
C	3.89308	2.46018	1.56802
H	2.43872	1.00534	2.22323
C	3.53807	3.39025	-0.63792
H	1.81549	2.64413	-1.70797
C	4.28413	3.32184	0.54119
H	4.46628	2.40922	2.48844
H	3.83671	4.06137	-1.43712
H	5.16713	3.94229	0.6608
N	0.84932	0.91101	0.05716

Table D.4: Cartesian coordinates in Å for TS_{C2} 3a

Atom	X	Y	Z
C	0.468238	1.464873	-0.00298
C	1.279421	0.405919	0.252494
N	0.458954	-0.69364	0.543139
C	-0.84152	-0.27206	0.637277
C	-1.9769	-1.22568	0.330241
C	-2.74474	-1.94976	1.270904
C	-2.2215	-1.42746	-1.05532
C	-3.75728	-2.79276	0.799603
C	-3.24491	-2.28259	-1.45893
C	2.756944	0.36508	0.337708
C	3.542514	0.193556	-0.80526
C	3.387612	0.519971	1.576388
C	4.930326	0.181745	-0.71299
H	3.064814	0.064028	-1.76609
C	4.77559	0.505104	1.668841
H	2.790124	0.661033	2.466652
C	5.549492	0.336668	0.52408
H	5.5261	0.050938	-1.60576
H	5.250462	0.630845	2.632108
H	6.628433	0.328101	0.595421
C	0.837776	2.869529	-0.25777
C	0.42273	3.882328	0.616604
C	1.637859	3.212155	-1.35225
C	0.802719	5.201356	0.401727
C	2.021793	4.532974	-1.5632
C	1.604967	5.531248	-0.68848
H	0.4778	5.970438	1.088905
H	2.640525	4.780522	-2.41478
C	-4.04148	-2.96572	-0.54836
C	0.916022	-1.96399	1.115341
H	1.452208	-1.75556	2.039401
H	0.016606	-2.50863	1.389878
H	-4.33752	-3.34316	1.529118
H	-3.40951	-2.42439	-2.51978
H	1.90105	6.557911	-0.85402
H	1.95065	2.445088	-2.04532
H	-0.19159	3.635469	1.471272
C	-2.57386	-1.91704	2.770024
H	-1.53451	-1.99191	3.071664
H	-2.92871	-0.97756	3.188297
H	-3.1396	-2.73537	3.212671
C	-1.42856	-0.7669	-2.16375

H	-0.37703	-0.63554	-1.92523
H	-1.49378	-1.37061	-3.06711
H	-1.83371	0.216071	-2.40448
C	-5.16599	-3.8581	-1.0059
H	-6.08038	-3.27997	-1.15851
H	-4.9277	-4.34293	-1.95217
H	-5.38587	-4.62903	-0.2687
C	1.77038	-2.82449	0.206832
C	1.340503	-3.19185	-1.06986
C	2.983332	-3.32826	0.676538
C	2.112882	-4.03348	-1.86316
H	0.397911	-2.82252	-1.44703
C	3.756157	-4.17682	-0.11184
H	3.329547	-3.05202	1.663877
C	3.324423	-4.5293	-1.38641
H	1.766527	-4.30651	-2.85072
H	4.695185	-4.55567	0.268048
H	3.924344	-5.18439	-2.0031
C	-2.04296	1.793105	-0.02489
C	-2.20745	2.572174	-1.17072
C	-3.03289	1.770963	0.956979
C	-3.36445	3.326164	-1.33108
H	-1.44132	2.589116	-1.93099
C	-4.19246	2.518283	0.77937
H	-2.85657	1.187035	1.848477
C	-4.36283	3.298227	-0.36109
H	-3.48652	3.928931	-2.22025
H	-4.9591	2.498613	1.541827
H	-5.26346	3.881807	-0.49229
N	-0.85951	1.012323	0.144898
O	-0.90658	0.189469	2.696311
H	-0.31455	0.945558	2.617258

Table D.5: Cartesian coordinates in Å for P_{C2} 3a.

Atom	X	Y	Z
C	-0.14061	1.56671	0.02952
C	0.96835	0.84752	0.34855
N	0.6022	-0.49751	0.58732
C	-0.8577	-0.55587	0.74978
C	-1.4652	-1.83219	0.12967
C	-2.12698	-2.83814	0.88376
C	-1.32458	-2.0132	-1.27733

C	-2.61556	-3.97403	0.21508
C	-1.83131	-3.16877	-1.88017
C	2.39066	1.26808	0.29143
C	3.04608	1.40257	-0.94289
C	3.10359	1.55027	1.4681
C	4.38081	1.80678	-0.99942
H	2.50255	1.1908	-1.85919
C	4.43958	1.95151	1.41204
H	2.60354	1.46808	2.42943
C	5.08159	2.07995	0.17797
H	4.87314	1.90752	-1.96292
H	4.97586	2.16989	2.3315
H	6.12064	2.39468	0.13405
C	-0.21787	2.92261	-0.536
C	0.60624	3.95997	-0.05925
C	-1.11415	3.21692	-1.58257
C	0.55514	5.23305	-0.6261
C	-1.16709	4.49254	-2.14269
C	-0.33111	5.50811	-1.67077
H	1.20234	6.01633	-0.23994
H	-1.8625	4.69214	-2.95395
C	-2.4819	-4.16879	-1.1561
C	1.40944	-1.42368	1.38786
H	1.77405	-0.94616	2.30676
H	0.72926	-2.21961	1.70655
H	-3.1214	-4.73628	0.80338
H	-1.71316	-3.28525	-2.95554
H	-0.37462	6.50235	-2.10682
H	-1.76518	2.43627	-1.96268
H	1.2834	3.76656	0.76596
C	-2.38319	-2.82461	2.38302
H	-1.46228	-2.7409	2.96477
H	-3.01725	-1.98657	2.68274
H	-2.88545	-3.75341	2.67073
C	-0.67311	-1.00984	-2.21081
H	-1.31053	-0.13247	-2.35946
H	0.28372	-0.64665	-1.83213
H	-0.5036	-1.47265	-3.18834
C	-2.99997	-5.41512	-1.83342
H	-3.52404	-5.1751	-2.76558
H	-2.1783	-6.0949	-2.09453
H	-3.68973	-5.96495	-1.18547
C	2.58056	-2.0503	0.64679
C	2.39661	-2.69708	-0.58356

C	3.8563	-2.05494	1.22248
C	3.46571	-3.32244	-1.22614
H	1.409	-2.71442	-1.03471
C	4.92905	-2.68349	0.5841
H	4.01394	-1.55567	2.17545
C	4.73734	-3.31735	-0.64468
H	3.30573	-3.81894	-2.17986
H	5.9131	-2.67226	1.04547
H	5.56989	-3.80411	-1.14564
C	-2.58184	1.19624	0.41634
C	-3.70961	0.57304	-0.13864
C	-2.76512	2.28577	1.28189
C	-4.99228	1.02249	0.17794
H	-3.57526	-0.25861	-0.82143
C	-4.04928	2.744	1.57883
H	-1.90084	2.77578	1.71895
C	-5.16963	2.11256	1.03371
H	-5.85479	0.5268	-0.25969
H	-4.17227	3.59167	2.24789
H	-6.16867	2.46845	1.26932
N	-1.28044	0.70482	0.08372
O	-1.2032	-0.50433	2.12859
H	-0.80066	0.31005	2.47892

Table D.6: Cartesian coordinates in Å for TS_{SN2} 3a.

Atom	X	Y	Z
C	-1.68509	-0.47986	0.00948
C	-1.29757	0.80303	0.33455
N	0.08268	0.815	0.47425
C	0.54321	-0.41651	0.255
C	1.95476	-0.86277	0.35535
C	2.45909	-1.25797	1.61884
C	2.77748	-0.88993	-0.78676
C	3.78658	-1.67378	1.7078
C	4.10339	-1.32255	-0.64558
C	-2.15692	1.99997	0.49079
C	-2.87073	2.50084	-0.60913
C	-2.29503	2.63252	1.73738
C	-3.69843	3.61542	-0.46703
H	-2.77145	2.01536	-1.57484
C	-3.11991	3.7491	1.87548
H	-1.76863	2.23901	2.60168

C	-3.82227	4.24357	0.77401
H	-4.24349	3.9935	-1.32652
H	-3.21857	4.22763	2.84498
H	-4.46481	5.11188	0.88332
C	-3.02964	-1.02707	-0.25047
C	-4.07273	-0.77555	0.65628
C	-3.29996	-1.7784	-1.40679
C	-5.35573	-1.26347	0.41106
C	-4.58276	-2.26989	-1.64464
C	-5.61414	-2.01373	-0.73805
H	-6.1512	-1.06303	1.12227
H	-4.77754	-2.84745	-2.54312
C	4.62617	-1.71788	0.58524
C	1.06673	2.21534	1.01839
H	0.26922	2.76195	1.48548
H	1.72391	1.68415	1.68527
H	4.17787	-1.97401	2.67669
H	4.74117	-1.34307	-1.52602
H	-6.61265	-2.3962	-0.92648
H	-2.50904	-1.96866	-2.12444
H	-3.87281	-0.20287	1.55575
C	1.5866	-1.25583	2.85329
H	1.06651	-0.30262	2.98978
H	0.81884	-2.03589	2.79696
H	2.18366	-1.44467	3.74817
C	2.29731	-0.46546	-2.15589
H	1.27294	-0.08902	-2.14659
H	2.93464	0.33058	-2.55172
H	2.34764	-1.30169	-2.86207
C	6.0543	-2.1892	0.71566
H	6.57805	-1.64957	1.51169
H	6.09407	-3.25424	0.9719
H	6.60915	-2.04758	-0.2151
C	1.66771	2.79136	-0.21462
C	0.88658	3.52007	-1.12462
C	3.02785	2.59424	-0.50805
C	1.45212	4.05271	-2.28626
H	-0.16878	3.67554	-0.92096
C	3.59114	3.12278	-1.6669
H	3.644	2.03775	0.19049
C	2.80544	3.85683	-2.56405
H	0.83113	4.61968	-2.97434
H	4.64688	2.96682	-1.87116
H	3.24595	4.26993	-3.46672

C	-0.4385	-2.67052	-0.1709
C	0.10276	-3.24177	-1.32288
C	-0.92404	-3.46899	0.86765
C	0.17286	-4.63196	-1.42677
H	0.45277	-2.60882	-2.12962
C	-0.85534	-4.85735	0.75137
H	-1.35335	-3.00608	1.74974
C	-0.30397	-5.43949	-0.39236
H	0.59513	-5.0805	-2.32011
H	-1.23085	-5.48126	1.55591
H	-0.24979	-6.52005	-0.47864
N	-0.51174	-1.23533	-0.03725
O	2.09015	3.84537	2.15784
H	2.20561	4.49592	1.45143

Table D.7: Cartesian coordinates in Å for P_{SN2} 3a

Atom	X	Y	Z
C	1.86357	0.72044	0.05387
C	0.68869	1.43336	-0.12987
N	-0.37623	0.55281	-0.21984
C	0.11368	-0.66639	-0.08362
C	-0.69441	-1.91414	-0.10502
C	-0.83785	-2.64233	-1.30575
C	-1.35539	-2.33368	1.0682
C	-1.60672	-3.80975	-1.29706
C	-2.11438	-3.50922	1.02999
C	0.46889	2.89144	-0.18578
C	1.28249	3.7888	0.52954
C	-0.59577	3.41454	-0.94229
C	1.05165	5.16305	0.47308
H	2.09036	3.40804	1.14533
C	-0.82623	4.78931	-0.99324
H	-1.24572	2.73949	-1.48946
C	-0.00184	5.67166	-0.29077
H	1.69133	5.83689	1.037
H	-1.65271	5.17175	-1.58667
H	-0.18198	6.74239	-0.33253
C	3.26833	1.15701	0.17897
C	3.84664	1.95995	-0.81906
C	4.04877	0.7931	1.28988
C	5.16786	2.3922	-0.7058
C	5.37217	1.2214	1.39779
C	5.93541	2.02315	0.40193

H	5.59984	3.01145	-1.4871
H	5.9612	0.93276	2.26394
C	-2.2485	-4.26441	-0.13918
C	-3.78629	0.05757	-1.5465
H	-4.48901	0.05558	-2.3892
H	-3.62011	-0.99191	-1.26274
H	-1.7113	-4.37581	-2.22037
H	-2.61257	-3.84191	1.9381
H	6.96552	2.35746	0.48815
H	3.61464	0.1797	2.07384
H	3.25496	2.24011	-1.68548
C	-0.219	-2.15329	-2.5956
H	-0.6321	-1.17466	-2.86766
H	0.86835	-2.04208	-2.5177
H	-0.42588	-2.84891	-3.41417
C	-1.28925	-1.52556	2.34524
H	-0.26447	-1.24218	2.60962
H	-1.85774	-0.59293	2.24593
H	-1.71096	-2.0874	3.18364
C	-3.0882	-5.52027	-0.16366
H	-3.2399	-5.9199	0.84389
H	-4.07976	-5.32374	-0.59224
H	-2.62275	-6.30028	-0.77599
C	-4.39188	0.80749	-0.374
C	-4.63466	2.18635	-0.46279
C	-4.7283	0.141	0.81011
C	-5.20353	2.87977	0.60525
H	-4.36973	2.7144	-1.37518
C	-5.30207	0.83149	1.88256
H	-4.53793	-0.92682	0.89465
C	-5.54071	2.20309	1.78251
H	-5.38708	3.94787	0.52077
H	-5.55682	0.2982	2.79478
H	-5.98443	2.74318	2.61466
C	2.36005	-1.75742	0.14583
C	2.2904	-2.64899	1.21903
C	3.2815	-1.96158	-0.88678
C	3.1403	-3.75593	1.25142
H	1.58453	-2.47461	2.02342
C	4.1345	-3.0647	-0.84117
H	3.32955	-1.2595	-1.71284
C	4.06341	-3.96511	0.22467
H	3.08363	-4.4491	2.08548
H	4.85028	-3.22121	-1.64274

H	4.7261	-4.82501	0.25566
N	1.47933	-0.62346	0.0921
O	-2.59034	0.64802	-2.0472
H	-1.91633	0.62883	-1.32658

Table D.8: Cartesian coordinates in Å for Reagent 3b

Atom	X	Y	Z
C	-0.97047	-1.45332	-0.03213
C	-1.03895	-0.14789	0.370278
N	0.379296	-1.76092	-0.16959
N	0.272556	0.314429	0.453891
C	1.12048	-0.68189	0.130849
C	2.595753	-0.63001	0.167682
C	3.243328	-0.71554	1.421484
C	3.336466	-0.52865	-1.02069
C	4.630894	-0.6811	1.451874
C	4.72991	-0.49848	-0.9326
C	-2.22834	0.668401	0.679993
C	-3.16615	0.944974	-0.31926
C	-2.45074	1.141862	1.977112
C	-4.30397	1.687915	-0.02635
H	-2.99943	0.583871	-1.32407
C	-3.58739	1.888666	2.26529
H	-1.74713	0.911919	2.765216
C	-4.51519	2.163609	1.264664
H	-5.02194	1.897834	-0.80682
H	-3.75113	2.247611	3.271716
H	-5.3994	2.74328	1.490556
C	-2.05467	-2.42658	-0.25606
C	-2.92334	-2.7531	0.790301
C	-2.24041	-3.0198	-1.5094
C	-3.95908	-3.65759	0.585321
C	-3.27483	-3.92654	-1.70925
C	-4.13569	-4.24706	-0.66309
H	-4.62382	-3.90399	1.401408
H	-3.41174	-4.37595	-2.68278
C	5.394233	-0.56816	0.286188
C	0.686909	1.685633	0.802695
H	0.331386	1.903251	1.805896
C	0.918422	-3.07982	-0.51354
H	0.339695	-3.84035	-7.7E-05
H	1.952089	-3.12679	-0.19129

H	0.86408	-3.24171	-1.58646
H	1.77374	1.668738	0.838503
H	5.132658	-0.75534	2.408252
H	5.305132	-0.42085	-1.84642
H	-4.94077	-4.95118	-0.82075
H	-1.58832	-2.76171	-2.33215
H	-2.78267	-2.30342	1.76284
C	2.467232	-0.85494	2.708421
H	1.952064	0.070326	2.972436
H	1.712586	-1.63952	2.647019
H	3.1369	-1.0992	3.529706
C	2.697123	-0.4313	-2.3843
H	1.639343	-0.68269	-2.38035
H	2.794756	0.58133	-2.77928
H	3.195696	-1.09884	-3.08619
C	6.898182	-0.53	0.360308
H	7.344413	-0.49871	-0.63163
H	7.236979	0.348239	0.91259
H	7.285933	-1.40587	0.882359
C	0.212332	2.754054	-0.16096
C	0.242666	2.573222	-1.54372
C	-0.20181	3.983474	0.351965
C	-0.13734	3.603214	-2.39796
H	0.555151	1.628046	-1.96397
C	-0.57413	5.017704	-0.50143
H	-0.23634	4.134023	1.422931
C	-0.54429	4.829663	-1.87973
H	-0.11338	3.447078	-3.46763
H	-0.8937	5.964511	-0.08849
H	-0.83891	5.629688	-2.54463

Table D.9: Cartesian coordinates in Å for TS_{C2} 3b.

Atom	X	Y	Z
C	-1.77283	-0.86747	0.09231
C	-1.39012	0.4264	0.26915
N	-0.62763	-1.66018	0.23284
N	-0.00193	0.42202	0.50662
C	0.41499	-0.8835	0.65431
C	1.83706	-1.29166	0.32679
C	2.9165	-1.40284	1.23328
C	2.07602	-1.53342	-1.05444

C	4.16364	-1.80709	0.74128
C	3.34204	-1.92887	-1.47939
C	-2.21692	1.64504	0.24518
C	-1.90843	2.73082	-0.58436
C	-3.35393	1.72791	1.05945
C	-2.71488	3.86337	-0.60049
H	-1.04493	2.68614	-1.23187
C	-4.16403	2.85737	1.03569
H	-3.59703	0.90528	1.71668
C	-3.84675	3.93016	0.20716
H	-2.46238	4.6895	-1.25087
H	-5.03782	2.90216	1.67119
H	-4.47454	4.81031	0.1918
C	-3.09722	-1.40867	-0.26576
C	-3.74591	-2.34305	0.55126
C	-3.73869	-0.97697	-1.43262
C	-5.00217	-2.83068	0.20923
C	-4.99798	-1.46098	-1.77035
C	-5.63294	-2.39053	-0.95156
H	-5.49098	-3.5484	0.85356
H	-5.47876	-1.11695	-2.67578
C	4.40269	-2.09086	-0.59606
C	0.73585	1.54059	1.09568
H	0.00198	2.31268	1.32051
C	-0.6015	-3.11361	0.24531
H	-1.27641	-3.49557	-0.51462
H	-0.89486	-3.49893	1.22073
H	0.40649	-3.45225	0.02863
H	1.1281	1.20046	2.05119
H	4.98162	-1.89105	1.44519
H	3.50079	-2.10176	-2.53651
O	0.17398	-1.14262	2.69522
H	-0.78822	-1.10707	2.66173
H	-6.61068	-2.76937	-1.21536
H	-3.2443	-0.26393	-2.07703
H	-3.27542	-2.67718	1.46532
C	2.87472	-1.10067	2.71188
H	2.57002	-0.07422	2.90618
H	2.15614	-1.72527	3.23101
H	3.86712	-1.24346	3.13593
C	1.02628	-1.38097	-2.13686
H	0.37384	-0.52656	-1.98004
H	1.51559	-1.25686	-3.10098
H	0.39015	-2.26402	-2.21046

C	5.75409	-2.55558	-1.07369
H	6.54046	-2.27666	-0.37385
H	5.77532	-3.643	-1.17668
H	5.99543	-2.13418	-2.0494
C	1.84476	2.14578	0.25595
C	1.8196	2.16332	-1.13796
C	2.90608	2.77385	0.91268
C	2.8302	2.79278	-1.86
H	1.0168	1.67354	-1.66922
C	3.91501	3.40798	0.19497
H	2.94525	2.76485	1.99457
C	3.88069	3.41965	-1.19688
H	2.79517	2.79129	-2.94102
H	4.72944	3.88584	0.72234
H	4.66611	3.90721	-1.75779

Table D.10: Cartesian coordinates in Å for P_{C2} 3b.

Atom	X	Y	Z
C	-1.20902	-1.40771	0.24082
C	-1.13361	-0.06899	0.40781
N	0.096269	-1.96247	0.333877
N	0.230547	0.287784	0.585522
C	0.950373	-0.94267	0.918448
C	2.392079	-0.96274	0.345065
C	3.565178	-0.98335	1.138214
C	2.537048	-0.95573	-1.06908
C	4.817032	-0.99578	0.508504
C	3.81117	-0.96547	-1.63438
C	-2.21248	0.933394	0.262807
C	-2.76874	1.203661	-0.9928
C	-2.72196	1.61122	1.376715
C	-3.80829	2.118546	-1.13032
H	-2.38342	0.691074	-1.86322
C	-3.75741	2.529686	1.240282
H	-2.31844	1.403862	2.358383
C	-4.30545	2.785334	-0.01411
H	-4.22744	2.311189	-2.10868
H	-4.14178	3.038191	2.114046
H	-5.11384	3.495836	-0.11991
C	-2.37342	-2.21488	-0.1519
C	-3.59974	-2.08381	0.514905

C	-2.29344	-3.13173	-1.21185
C	-4.70862	-2.82758	0.126085
C	-3.40044	-3.88023	-1.59464
C	-4.61517	-3.73099	-0.92943
H	-5.64384	-2.70868	0.656551
H	-3.31585	-4.57565	-2.4189
C	4.97134	-0.98649	-0.86886
C	0.658129	1.525722	1.231381
H	0.110429	1.714881	2.158306
C	0.302301	-3.32883	0.800697
H	-0.07806	-3.50034	1.810615
H	1.369411	-3.54171	0.79219
H	-0.18299	-4.02539	0.122676
H	1.702866	1.380914	1.51307
H	5.70161	-1.01286	1.13215
H	3.893433	-0.9581	-2.71443
O	0.905238	-1.18077	2.346101
H	1.392076	-0.49612	2.811647
H	-5.47578	-4.31392	-1.22744
H	-1.36341	-3.243	-1.75131
H	-3.6779	-1.40112	1.348602
C	3.633305	-0.98978	2.65688
H	3.231565	-0.07543	3.101613
H	3.111409	-1.83504	3.097276
H	4.674508	-1.03896	2.967893
C	1.387813	-0.96448	-2.05679
H	0.97456	-1.96702	-2.16302
H	0.571006	-0.31492	-1.76129
H	1.748813	-0.646	-3.03414
C	6.333791	-0.98066	-1.51333
H	6.391617	-1.71011	-2.32192
H	6.556821	-0.00304	-1.94621
H	7.115456	-1.20967	-0.79073
C	0.599349	2.766732	0.357173
C	1.100486	2.759915	-0.94608
C	0.114606	3.965541	0.88009
C	1.111206	3.922833	-1.70937
H	1.482257	1.839546	-1.36359
C	0.126566	5.133376	0.120746
H	-0.28019	3.986909	1.887734
C	0.623947	5.115427	-1.17846
H	1.501995	3.89916	-2.71786
H	-0.25757	6.052352	0.542667
H	0.630934	6.019297	-1.77221

Table D.11: Cartesian coordinates in Å for TS_{SN2} (de-benzylation) 3b.

Atom	X	Y	Z
C	1.7527	-1.07229	0.14483
C	1.39708	0.21453	-0.20084
N	0.56653	-1.79631	0.20163
N	0.01963	0.25748	-0.34611
C	-0.46472	-0.96472	-0.10487
C	-1.88504	-1.38762	-0.15671
C	-2.43138	-1.84632	-1.37459
C	-2.66825	-1.34262	1.01645
C	-3.77322	-2.23741	-1.39849
C	-4.0023	-1.75393	0.94415
C	2.28948	1.37599	-0.44458
C	2.539	2.31765	0.5662
C	2.92207	1.52811	-1.6881
C	3.39706	3.39414	0.33457
H	2.0652	2.19895	1.53642
C	3.78	2.60513	-1.91839
H	2.7397	0.79946	-2.47286
C	4.01785	3.54016	-0.90837
H	3.58376	4.11431	1.12614
H	4.26283	2.71179	-2.88566
H	4.68641	4.37747	-1.08775
C	3.08379	-1.65207	0.40925
C	3.53675	-2.7797	-0.29729
C	3.93307	-1.06164	1.35996
C	4.80451	-3.30668	-0.05217
C	5.20382	-1.58609	1.59674
C	5.64174	-2.71128	0.89448
H	5.14064	-4.17734	-0.60799
H	5.84844	-1.11892	2.33587
C	-4.57397	-2.20272	-0.25131
C	-0.86967	1.62368	-1.09904
H	0.00458	2.16079	-1.42337
C	0.43384	-3.20703	0.5713
H	0.66205	-3.85347	-0.27932
H	-0.59076	-3.38884	0.89314
H	1.11963	-3.42939	1.38946
H	-1.39316	1.06362	-1.85461
H	-4.20197	-2.58314	-2.33639
H	-4.61167	-1.71673	1.84423
O	-1.73038	3.19831	-2.43909

H	-1.22036	2.87649	-3.20469
H	6.63007	-3.12116	1.08241
H	3.59138	-0.19525	1.91712
H	2.90401	-3.23375	-1.05405
C	-1.59536	-1.93492	-2.63204
H	-1.12262	-0.97816	-2.88088
H	-0.78879	-2.67112	-2.52734
H	-2.20984	-2.23649	-3.48464
C	-2.09263	-0.85507	2.32654
H	-1.25113	-1.47544	2.6587
H	-1.72397	0.17286	2.23943
H	-2.8509	-0.87698	3.11413
C	-6.01126	-2.66442	-0.29833
H	-6.08078	-3.74693	-0.12795
H	-6.6146	-2.17419	0.47222
H	-6.46466	-2.46035	-1.27377
C	-1.68834	2.235	-0.01967
C	-1.10685	3.08157	0.93556
C	-3.06096	1.95992	0.07884
C	-1.87692	3.64796	1.95426
H	-0.04662	3.31019	0.87289
C	-3.8314	2.52322	1.09487
H	-3.52607	1.31192	-0.65792
C	-3.24303	3.37056	2.03991
H	-1.40747	4.30718	2.68023
H	-4.89445	2.30203	1.14972
H	-3.84365	3.8094	2.83225

Table D.12: Cartesian coordinates in Å for P_{SN2} (de-benzylation) 3b.

Atom	X	Y	Z
C	-2.31086	0.6744	-0.01458
C	-1.58007	-0.44915	0.35359
N	-1.3783	1.70038	-0.11517
N	-0.24528	-0.11553	0.48348
C	-0.15036	1.17175	0.19656
C	1.10965	1.96073	0.20866
C	1.81688	2.17892	-0.9924
C	1.60887	2.45937	1.4313
C	3.01254	2.9047	-0.94822
C	2.81032	3.17511	1.42877
C	-2.02717	-1.83609	0.5754
C	-1.29872	-2.67156	1.44275
C	-3.15094	-2.37534	-0.07716

C	-1.68795	-3.99301	1.65996
H	-0.42569	-2.27018	1.94734
C	-3.54135	-3.6959	0.14528
H	-3.71363	-1.76197	-0.77308
C	-2.81419	-4.51204	1.01571
H	-1.11177	-4.61775	2.33775
H	-4.41137	-4.09115	-0.37278
H	-3.11863	-5.54112	1.18606
C	-3.75821	0.89596	-0.20883
C	-4.26655	1.3879	-1.42383
C	-4.65972	0.61511	0.83303
C	-5.6366	1.59582	-1.59002
C	-6.02928	0.81585	0.66267
C	-6.52204	1.30945	-0.54837
H	-6.01182	1.97494	-2.53661
H	-6.71125	0.59416	1.47901
C	3.52829	3.40802	0.2503
C	1.91304	-2.86865	-1.50425
H	1.02434	-2.68674	-0.88633
C	-1.6604	3.10126	-0.41258
H	-1.81533	3.25645	-1.48416
H	-0.81124	3.70259	-0.08722
H	-2.55536	3.41994	0.12533
H	1.89201	-3.91839	-1.8308
H	3.55617	3.0774	-1.87484
H	3.19253	3.56411	2.37039
O	1.91417	-1.99526	-2.64769
H	1.06938	-2.12882	-3.10798
H	-7.58868	1.46925	-0.67925
H	-4.27753	0.24177	1.77856
H	-3.58729	1.59375	-2.24634
C	1.32506	1.61642	-2.30776
H	1.41035	0.52225	-2.32637
H	0.27356	1.86191	-2.4945
H	1.91374	2.01158	-3.14132
C	0.86213	2.2386	2.72813
H	-0.12542	2.71655	2.7115
H	0.69474	1.1726	2.91598
H	1.41858	2.65269	3.57396
C	4.83764	4.16178	0.27719
H	4.84269	4.92741	1.06018
H	5.67828	3.48514	0.48081
H	5.03834	4.6498	-0.68207
C	3.16256	-2.60168	-0.70216

C	3.1662	-1.61364	0.29223
C	4.34607	-3.30238	-0.96775
C	4.33232	-1.33458	1.00841
H	2.24757	-1.07029	0.50367
C	5.5133	-3.02633	-0.25237
H	4.35128	-4.07182	-1.73673
C	5.50815	-2.03999	0.73752
H	4.32309	-0.56731	1.77836
H	6.42358	-3.58076	-0.46514
H	6.41482	-1.8248	1.29695

Table D.13: Cartesian coordinates in Å for Reagent 3c.

Atom	X	Y	Z
C	0.532664	1.35322	-0.16199
C	1.176249	0.25768	0.342105
N	0.223283	-0.75318	0.447195
C	-0.973	-0.28523	0.039539
C	-2.25486	-1.02081	0.056121
C	-2.92278	-1.19594	1.286315
C	-2.80848	-1.51251	-1.14137
C	-4.14341	-1.86407	1.288813
C	-4.03464	-2.17197	-1.0816
C	2.591112	0.107839	0.732887
C	3.602406	0.256501	-0.22069
C	2.938231	-0.14391	2.064312
C	4.937641	0.149159	0.150922
H	3.341926	0.448642	-1.25167
C	4.274487	-0.25591	2.431485
H	2.167325	-0.23239	2.817389
C	5.276317	-0.11037	1.475939
H	5.711632	0.264168	-0.595
H	4.531568	-0.44764	3.463815
H	6.31518	-0.19541	1.762983
C	1.076096	2.690886	-0.47058
C	1.574666	3.495746	0.558237
C	1.126251	3.156451	-1.78878
C	2.109837	4.747043	0.273094
C	1.657691	4.410117	-2.06944
C	2.149382	5.207553	-1.03972
H	2.491568	5.361642	1.076292
H	1.694437	4.758932	-3.09194
C	-4.71551	-2.36229	0.118567
C	0.478584	-2.13761	0.878552

H	0.868279	-2.1113	1.892277
H	-0.49289	-2.62495	0.915243
H	-4.66586	-1.98829	2.228724
H	-4.46861	-2.54291	-2.00122
H	2.563683	6.181522	-1.26008
H	0.766499	2.533369	-2.59592
H	1.538181	3.142714	1.5791
C	-2.34947	-0.69256	2.588769
H	-1.58601	-1.37191	2.973484
H	-1.88764	0.288715	2.48948
H	-3.1285	-0.62173	3.344445
C	-2.11215	-1.38521	-2.47451
H	-1.52739	-0.47231	-2.56652
H	-1.43252	-2.22473	-2.63219
H	-2.83817	-1.40028	-3.28489
C	-6.0282	-3.09995	0.156365
H	-6.53733	-3.05323	-0.8048
H	-5.86891	-4.15424	0.393783
H	-6.68938	-2.69183	0.919817
C	1.417018	-2.91978	-0.01882
C	1.455171	-2.74262	-1.4009
C	2.222326	-3.90119	0.560596
C	2.28363	-3.53411	-2.19085
H	0.848354	-1.98198	-1.87062
C	3.044794	-4.69873	-0.22852
H	2.208698	-4.04233	1.633432
C	3.078187	-4.51685	-1.60807
H	2.306222	-3.38155	-3.26106
H	3.663524	-5.45435	0.23548
H	3.721341	-5.13136	-2.22257
C	-1.88479	1.903401	-0.76104
H	-1.50367	2.495853	-1.5878
H	-2.68958	1.282389	-1.14199
N	-0.80117	0.99385	-0.3374
C	-2.38741	2.803676	0.366866
H	-2.75896	2.185089	1.185873
H	-1.55828	3.393021	0.761741
C	-3.49986	3.736204	-0.12025
H	-3.12479	4.344909	-0.94679
H	-4.32079	3.138785	-0.52472
C	-4.02799	4.647979	0.988027
H	-3.23455	5.282429	1.386514
H	-4.82006	5.298365	0.616495
H	-4.4355	4.065001	1.815722

Table D.14: Cartesian coordinates in Å for TS_{C2} 3c.

Atom	X	Y	Z
C	0.79112	1.196	-0.19828
C	1.19154	-0.00579	0.32177
N	0.0291	-0.7424	0.57802
C	-1.0618	0.04673	0.35784
C	-2.44221	-0.49359	0.1283
C	-3.28791	-0.99329	1.153
C	-2.88022	-0.56644	-1.22874
C	-4.56786	-1.4492	0.80373
C	-4.16261	-1.04179	-1.51022
C	2.55773	-0.50019	0.58712
C	3.48324	-0.63745	-0.45922
C	2.96134	-0.80354	1.89834
C	4.78225	-1.07522	-0.20022
H	3.17746	-0.40741	-1.47534
C	4.25879	-1.24801	2.15365
H	2.26286	-0.67099	2.72003
C	5.17191	-1.38571	1.10504
H	5.48827	-1.17914	-1.01938
H	4.55856	-1.47684	3.17246
H	6.18285	-1.72976	1.30475
C	1.62726	2.31076	-0.68693
C	2.5943	2.88876	0.15204
C	1.49445	2.791	-2.00104
C	3.40643	3.92388	-0.31134
C	2.30282	3.83185	-2.45883
C	3.26059	4.40132	-1.61617
H	4.14853	4.36176	0.35034
H	2.18981	4.19079	-3.47795
C	-5.03782	-1.46693	-0.50711
C	-0.01467	-2.1255	1.07059
H	0.42215	-2.15795	2.07207
H	-1.07044	-2.37435	1.17384
H	-5.21182	-1.81513	1.60078
H	-4.48102	-1.09201	-2.54922
H	3.89053	5.2104	-1.97494
H	0.77262	2.33483	-2.67232
H	2.70097	2.52769	1.17027
C	-2.89051	-1.12552	2.60664
H	-2.06677	-0.43564	2.84941
H	-3.75558	-0.91618	3.2478

H	-2.59402	-2.16292	2.82131
C	-2.02024	-0.18427	-2.42
H	-2.06318	0.89005	-2.63313
H	-0.96693	-0.44437	-2.28841
H	-2.38315	-0.70064	-3.31352
C	-6.43481	-1.93362	-0.83803
H	-7.10942	-1.07956	-0.98308
H	-6.45257	-2.51781	-1.76458
H	-6.85211	-2.54874	-0.03474
C	0.66165	-3.14058	0.1661
C	0.30923	-3.25357	-1.18543
C	1.59956	-4.03326	0.6971
C	0.89434	-4.22972	-1.99228
H	-0.43072	-2.58048	-1.60846
C	2.18107	-5.017	-0.10638
H	1.88203	-3.95547	1.74382
C	1.83272	-5.11536	-1.45456
H	0.61289	-4.30281	-3.03925
H	2.90927	-5.70077	0.32119
H	2.2873	-5.87658	-2.08258
C	-1.44339	2.38386	-0.45507
H	-1.23746	2.75907	-1.46153
H	-2.47716	2.03392	-0.44194
N	-0.60548	1.19216	-0.2312
C	-1.25732	3.48624	0.59628
H	-1.31803	2.98983	1.5749
H	-0.25632	3.92493	0.49761
C	-2.31225	4.58835	0.43704
H	-2.27858	4.99753	-0.58359
H	-3.3151	4.15386	0.55796
C	-2.12927	5.72854	1.4446
H	-1.15125	6.21035	1.32282
H	-2.89891	6.49913	1.3201
H	-2.18959	5.35769	2.47509
O	-1.15236	1.10071	2.49321
H	-0.18921	1.21915	2.43811

Table D.16: Cartesian coordinates in Å for P_{C2} 3c.

Atom	X	Y	Z
C	-1.51499	-0.12427	0.131018
C	-0.58226	-1.02009	-0.27165
N	0.625786	-0.32464	-0.53902

C	0.306018	1.101536	-0.64136
C	1.416316	2.009661	-0.06261
C	2.22474	2.87344	-0.8424
C	1.65039	1.946281	1.337548
C	3.204085	3.646886	-0.20302
C	2.64289	2.739136	1.910596
C	-0.67215	-2.49728	-0.28259
C	-0.70937	-3.21638	0.917746
C	-0.74541	-3.2084	-1.48627
C	-0.82197	-4.60338	0.915751
H	-0.65118	-2.68231	1.855965
C	-0.85199	-4.59526	-1.49049
H	-0.73821	-2.67119	-2.42481
C	-0.89102	-5.29769	-0.28878
H	-0.85275	-5.14056	1.854108
H	-0.91309	-5.12564	-2.43112
H	-0.97663	-6.37573	-0.29147
C	-2.84486	-0.40046	0.696246
C	-3.73311	-1.27357	0.051211
C	-3.25718	0.184611	1.903259
C	-4.97817	-1.56155	0.598419
C	-4.50662	-0.09679	2.444857
C	-5.37395	-0.97256	1.796878
H	-5.64507	-2.23806	0.080904
H	-4.79858	0.362776	3.379593
C	3.431941	3.606531	1.163604
C	1.686643	-0.84867	-1.39548
H	1.285842	-1.28728	-2.31238
H	2.279288	0.010543	-1.70772
H	3.812766	4.30227	-0.81285
H	2.802304	2.669476	2.979791
H	-6.34548	-1.19071	2.218487
H	-2.58696	0.845634	2.433456
H	-3.44641	-1.719	-0.89036
C	2.161647	3.063703	-2.3478
H	2.252713	2.126633	-2.89077
H	1.224336	3.516068	-2.66388
H	2.975835	3.717056	-2.65644
C	0.881632	1.067253	2.303713
H	-0.08494	1.505775	2.549845
H	0.690431	0.073704	1.911315
H	1.447266	0.969833	3.229776
C	4.496814	4.45131	1.815492
H	4.073776	5.083114	2.598254

H	5.26024	3.828281	2.285323
H	4.989864	5.096708	1.090289
C	2.617724	-1.84929	-0.73276
C	3.139581	-1.62773	0.543536
C	3.030913	-2.98251	-1.43398
C	4.048746	-2.51901	1.104709
H	2.831118	-0.75389	1.099155
C	3.943446	-3.87603	-0.8779
H	2.631698	-3.17242	-2.4221
C	4.455064	-3.64758	0.395607
H	4.442418	-2.33153	2.094823
H	4.24793	-4.75075	-1.43678
H	5.160663	-4.34106	0.832479
C	-1.7288	2.409624	0.038745
H	-2.23552	2.539875	0.996529
H	-1.00714	3.223366	-0.03491
N	-0.95019	1.173288	0.091252
C	-2.76902	2.546037	-1.08359
H	-2.27386	2.494604	-2.0541
H	-3.46853	1.708693	-1.03632
C	-3.54714	3.860536	-0.97843
H	-4.0307	3.917324	0.000991
H	-2.8469	4.699826	-1.02135
C	-4.6009	4.022157	-2.07531
H	-5.33521	3.215306	-2.03642
H	-5.13814	4.965947	-1.97369
H	-4.1431	4.005056	-3.06619
O	0.099173	1.471462	-2.02093
H	-0.60609	0.901096	-2.34918

Table D.17: Cartesian coordinates in Å for TS_{SN2} (de-butylation) 3c.

Atom	X	Y	Z
C	-0.38827	1.29046	0.14315
C	-1.23011	0.3269	-0.37424
N	-0.45704	-0.82287	-0.51643
C	0.81434	-0.54079	-0.10841
C	1.95524	-1.48894	-0.17678
C	2.56602	-1.73865	-1.42724
C	2.43658	-2.11472	0.99522
C	3.64962	-2.62027	-1.47993
C	3.52585	-2.9844	0.88921
C	-2.66163	0.40822	-0.73026
C	-3.60976	0.77804	0.23752

C	-3.09282	0.1541	-2.04326
C	-4.95881	0.88569	-0.09962
H	-3.2855	0.9746	1.25486
C	-4.4443	0.25385	-2.37512
H	-2.36784	-0.10026	-2.81143
C	-5.38022	0.61967	-1.40487
H	-5.68141	1.17141	0.65952
H	-4.76325	0.05567	-3.39443
H	-6.43182	0.69991	-1.66529
C	-0.70293	2.69235	0.49068
C	-1.25421	3.5553	-0.46983
C	-0.47566	3.17717	1.78939
C	-1.56298	4.8757	-0.14041
C	-0.78095	4.49896	2.11512
C	-1.32395	5.35198	1.15092
H	-1.98582	5.53328	-0.89481
H	-0.60149	4.85946	3.12412
C	4.14288	-3.2562	-0.33635
C	-0.93949	-2.14891	-0.92051
H	-1.40662	-2.06445	-1.90433
H	-0.04878	-2.77094	-1.0418
H	4.12625	-2.8065	-2.43963
H	3.90242	-3.46178	1.79094
H	-1.56257	6.38081	1.40555
H	-0.07583	2.51177	2.54927
H	-1.43267	3.1899	-1.4767
C	2.08111	-1.07437	-2.69721
H	1.12136	-1.48688	-3.03315
H	1.94031	0.00386	-2.56689
H	2.80006	-1.2245	-3.50732
C	1.79986	-1.88025	2.34674
H	1.6749	-0.81487	2.56594
H	0.80621	-2.34062	2.40264
H	2.41074	-2.3184	3.14078
C	5.29873	-4.2238	-0.42529
H	4.94009	-5.24597	-0.60473
H	5.97246	-3.96668	-1.24888
H	5.87851	-4.24112	0.50308
C	-1.90141	-2.80585	0.05762
C	-1.97712	-2.44835	1.4077
C	-2.70903	-3.84933	-0.41408
C	-2.84021	-3.12661	2.27278
H	-1.37496	-1.63022	1.79025
C	-3.56639	-4.53106	0.44992

H	-2.66587	-4.13054	-1.46379
C	-3.63462	-4.17145	1.79858
H	-2.8903	-2.83324	3.31771
H	-4.1859	-5.33758	0.06754
H	-4.30539	-4.69782	2.47175
C	2.42888	1.56079	0.71852
H	2.04476	2.10438	1.56581
H	2.96568	0.66143	0.95635
N	0.87019	0.7306	0.2903
C	2.78526	2.32837	-0.55094
H	3.74698	1.94882	-0.90992
H	2.04826	2.11716	-1.33807
C	2.88831	3.84578	-0.35461
H	1.93331	4.23417	0.02537
H	3.64461	3.99404	0.42208
C	3.26225	4.58442	-1.64286
H	2.51218	4.43151	-2.42993
H	3.34672	5.66446	-1.47249
H	4.22611	4.23536	-2.03573
O	4.36883	2.18268	1.66673
H	3.98095	2.78196	2.32745

Table D.18: Cartesian coordinates in Å for P_{SN2} (de-butylation) 3c

Atom	X	Y	Z
C	0.40602	-1.49095	-0.22461
C	1.49726	-0.66677	-0.45134
N	0.97338	0.62118	-0.55144
C	-0.38716	0.52835	-0.38845
C	-1.32705	1.67565	-0.50929
C	-1.80755	2.0319	-1.78977
C	-1.77638	2.36487	0.6367
C	-2.69916	3.10264	-1.90279
C	-2.67736	3.4236	0.47549
C	2.9421	-0.96286	-0.56211
C	3.63542	-1.5219	0.52472
C	3.64314	-0.71504	-1.75477
C	4.99373	-1.8214	0.42263
H	3.10333	-1.71695	1.45102
C	5.00478	-1.00674	-1.85219
H	3.11633	-0.3111	-2.61506
C	5.68342	-1.56073	-0.76449
H	5.515	-2.25293	1.27266
H	5.53165	-0.80952	-2.78163

H	6.74235	-1.79085	-0.84209
C	0.34311	-2.95416	-0.05856
C	1.25702	-3.81777	-0.68852
C	-0.67405	-3.52036	0.73099
C	1.16408	-5.19937	-0.52013
C	-0.76754	-4.90198	0.89452
C	0.15325	-5.74911	0.27252
H	1.87872	-5.84856	-1.01922
H	-1.55947	-5.31715	1.51243
C	-3.13973	3.81795	-0.78376
C	1.72849	1.85846	-0.74752
H	2.3655	1.74319	-1.62861
H	0.99231	2.62963	-0.99097
H	-3.06885	3.37595	-2.88886
H	-3.02776	3.95213	1.35961
H	0.08151	-6.82571	0.40054
H	-1.38718	-2.86556	1.22154
H	2.03371	-3.40761	-1.32535
C	-1.42373	1.23573	-3.01689
H	-0.33811	1.13244	-3.12542
H	-1.8434	0.22438	-2.95277
H	-1.80907	1.70885	-3.92477
C	-1.31066	1.98735	2.02503
H	-1.29386	0.90172	2.16415
H	-0.29601	2.35445	2.221
H	-1.96831	2.42009	2.78476
C	-4.08053	4.99038	-0.93387
H	-4.69515	5.12771	-0.03831
H	-3.52379	5.92353	-1.09272
H	-4.74727	4.86145	-1.79283
C	2.57176	2.30812	0.43756
C	2.44308	1.76517	1.71954
C	3.49908	3.33896	0.22938
C	3.22286	2.24691	2.7758
H	1.7413	0.95692	1.89878
C	4.27477	3.82299	1.28256
H	3.61418	3.76566	-0.76471
C	4.13889	3.27733	2.56245
H	3.11238	1.81078	3.76493
H	4.98848	4.62237	1.1026
H	4.7449	3.65027	3.38341
C	-4.34701	-1.0342	-0.70837
H	-4.20781	0.02674	-0.4447
H	-5.19769	-1.08193	-1.40073

N	-0.74871	-0.72912	-0.18923
C	-4.66558	-1.84197	0.55255
H	-4.77849	-2.89828	0.27111
H	-3.80463	-1.7901	1.23529
C	-5.92598	-1.35806	1.28124
H	-5.80926	-0.29767	1.5468
H	-6.78331	-1.40792	0.59481
C	-6.23799	-2.16749	2.54428
H	-5.41283	-2.10922	3.26483
H	-7.14263	-1.799	3.04163
H	-6.39519	-3.22664	2.30578
O	-3.21995	-1.53498	-1.41863
H	-2.4134	-1.30922	-0.89829

Table D.18: Cartesian coordinates in Å for TS_{SN2} (de-benzylation) 3c.

Atom	X	Y	Z
C	-1.36407	0.87551	0.18352
C	-1.22784	-0.38546	-0.35969
N	0.12568	-0.64171	-0.51181
C	0.80611	0.43021	-0.09193
C	2.28022	0.59432	-0.09217
C	2.95711	0.8202	-1.31164
C	2.99342	0.53651	1.12784
C	4.34665	0.97602	-1.28615
C	4.38151	0.6969	1.09809
C	-2.30038	-1.33016	-0.73684
C	-3.25251	-1.73345	0.21252
C	-2.40428	-1.815	-2.05127
C	-4.27873	-2.6098	-0.14138
H	-3.17932	-1.36509	1.2313
C	-3.42636	-2.69821	-2.401
H	-1.69412	-1.48627	-2.80458
C	-4.36526	-3.0992	-1.44695
H	-5.00619	-2.91558	0.60533
H	-3.49409	-3.06497	-3.42133
H	-5.16181	-3.78524	-1.7209
C	-2.58624	1.62884	0.53568
C	-3.5315	1.93785	-0.45618
C	-2.83457	2.02552	1.86073
C	-4.69643	2.63286	-0.13011
C	-3.9974	2.72641	2.18204
C	-4.93033	3.03175	1.18806
H	-5.41848	2.86647	-0.90734

H	-4.17757	3.02579	3.21055
C	5.07791	0.91374	-0.09613
C	0.89802	-2.16734	-1.0587
H	0.2568	-2.36759	-1.898
H	1.86311	-1.75419	-1.29261
H	4.86963	1.15525	-2.22263
H	4.93338	0.65055	2.03425
H	-5.83637	3.57545	1.44022
H	-2.12553	1.76859	2.64287
H	-3.34678	1.63462	-1.48235
C	2.22232	0.89536	-2.63211
H	1.88945	-0.09458	-2.96701
H	1.33016	1.52789	-2.57207
H	2.87324	1.30349	-3.41016
C	2.2945	0.31633	2.45186
H	1.54818	-0.48206	2.39206
H	3.01783	0.04432	3.22575
H	1.7775	1.22125	2.79526
C	6.58126	1.05572	-0.09869
H	6.93343	1.59108	0.78929
H	7.06751	0.07134	-0.09692
H	6.93094	1.5919	-0.98633
C	0.81445	-3.0893	0.10394
C	-0.26673	-3.97489	0.25541
C	1.79605	-3.059	1.10931
C	-0.35172	-4.81405	1.36549
H	-1.03465	-4.01344	-0.51111
C	1.71134	-3.90051	2.22009
H	2.64145	-2.38391	1.00756
C	0.63565	-4.78164	2.35604
H	-1.19283	-5.49663	1.4586
H	2.48781	-3.86636	2.98025
H	0.56705	-5.43553	3.22122
C	0.27331	2.75168	0.7313
H	-0.33608	3.01678	1.59742
H	1.31671	2.74055	1.04934
N	-0.07461	1.37294	0.34244
C	0.07242	3.76328	-0.40287
H	0.69507	3.47354	-1.25891
H	-0.97059	3.73218	-0.74072
C	0.43194	5.18728	0.0419
H	-0.18699	5.46421	0.90631
H	1.47417	5.20828	0.38877
C	0.24246	6.21872	-1.07485

H	-0.79858	6.24232	-1.41885
H	0.50418	7.22527	-0.73026
H	0.87453	5.98589	-1.94031
O	1.93931	-3.83458	-2.12035
H	2.22224	-4.38947	-1.37648

Table D.19: Cartesian coordinates in Å for P_{SN2} (de-benzylation) 3c.

Atom	X	Y	Z
C	2.22707	-0.26975	-0.32
C	1.27351	-1.27312	-0.20776
N	0.00741	-0.71657	-0.20159
C	0.17392	0.59125	-0.31367
C	-0.92052	1.59462	-0.40592
C	-1.59418	2.03444	0.75036
C	-1.30266	2.08064	-1.68009
C	-2.62973	2.97027	0.61336
C	-2.3422	3.00764	-1.76779
C	1.45513	-2.73417	-0.1318
C	2.55286	-3.38276	-0.72691
C	0.49728	-3.52431	0.5294
C	2.69497	-4.76813	-0.6461
H	3.2912	-2.80129	-1.26897
C	0.63824	-4.90946	0.60535
H	-0.35783	-3.03871	0.98823
C	1.74027	-5.53972	0.02119
H	3.5502	-5.24662	-1.11642
H	-0.1134	-5.49794	1.1254
H	1.85111	-6.61902	0.08099
C	3.70544	-0.31467	-0.32699
C	4.4035	-0.79282	0.79546
C	4.44124	0.10296	-1.44989
C	5.79743	-0.85142	0.79482
C	5.83615	0.05111	-1.44617
C	6.518	-0.42653	-0.32445
H	6.32082	-1.22379	1.67118
H	6.38882	0.37633	-2.32327
C	-3.01701	3.4709	-0.63001
C	-3.36554	-1.92087	1.89995
H	-3.43909	-2.94583	2.29348
H	-2.32796	-1.75718	1.57989
H	-3.14684	3.31185	1.50804
H	-2.63844	3.37491	-2.74841

H	7.6036	-0.46935	-0.32322
H	3.9163	0.45249	-2.33481
H	3.84521	-1.11687	1.66896
C	-1.26445	1.51348	2.13214
H	-1.99934	0.76014	2.4456
H	-0.27501	1.05195	2.17915
H	-1.29923	2.32395	2.86885
C	-0.6111	1.60428	-2.93887
H	0.41522	1.98611	-3.01125
H	-0.54668	0.5111	-2.97211
H	-1.14998	1.94214	-3.82889
C	-4.12217	4.49391	-0.75337
H	-3.71612	5.49169	-0.96524
H	-4.80543	4.24622	-1.57364
H	-4.70712	4.56439	0.16889
C	-4.29273	-1.75332	0.7201
C	-3.78571	-1.45757	-0.55072
C	-5.67826	-1.89932	0.88246
C	-4.64689	-1.31995	-1.64385
H	-2.7131	-1.33057	-0.67997
C	-6.53927	-1.75576	-0.20527
H	-6.07977	-2.12293	1.86758
C	-6.02447	-1.46787	-1.47385
H	-4.2406	-1.09097	-2.62566
H	-7.6111	-1.87142	-0.0664
H	-6.6949	-1.35859	-2.32225
C	2.06301	2.27564	-0.39088
H	2.92092	2.29637	-1.06731
H	1.29907	2.93587	-0.80812
N	1.50686	0.91714	-0.39672
C	2.47354	2.75657	1.00664
H	1.59892	2.72296	1.66903
H	3.21573	2.06457	1.4244
C	3.04895	4.1783	0.97824
H	3.91663	4.20565	0.30446
H	2.30472	4.8638	0.54959
C	3.4643	4.67679	2.36617
H	4.23241	4.02866	2.80535
H	3.87218	5.69262	2.31641
H	2.60951	4.69258	3.05328
O	-3.73548	-0.98208	2.92204
H	-3.21419	-1.2005	3.71157

Table D.20: Cartesian coordinates in Å for Reagent 3d.

Atom	X	Y	Z
C	0.519417	1.530799	0.348801
C	-0.66204	1.47603	-0.34095
N	-0.94891	0.124917	-0.53946
C	0.031004	-0.62565	-0.00231
C	0.101489	-2.10008	-0.00568
C	0.518238	-2.77248	-1.17155
C	-0.25389	-2.8138	1.154957
C	0.566192	-4.16307	-1.1497
C	-0.17848	-4.20382	1.124115
C	-1.51015	2.58749	-0.81324
C	-2.07151	3.480333	0.104614
C	-1.73424	2.786106	-2.18044
C	-2.85043	4.543574	-0.33632
H	-1.89618	3.342413	1.16236
C	-2.51767	3.847296	-2.61745
H	-1.27934	2.12367	-2.90496
C	-3.07873	4.726316	-1.69619
H	-3.27959	5.227263	0.382484
H	-2.68159	3.992582	-3.67587
H	-3.68646	5.552425	-2.03729
C	1.257063	2.715632	0.828103
C	1.729527	3.66409	-0.08401
C	1.461777	2.926194	2.196564
C	2.402915	4.794439	0.363749
C	2.139839	4.054962	2.640376
C	2.613348	4.989641	1.724766
H	2.763992	5.520762	-0.35065
H	2.289593	4.208624	3.699719
C	0.227623	-4.89854	-0.01404
C	-2.18929	-0.42214	-1.14511
H	-2.58546	0.365687	-1.77838
H	-1.89835	-1.24972	-1.78486
H	0.883381	-4.68599	-2.04275
H	-0.4566	-4.75872	2.010718
H	3.139064	5.868147	2.071158
H	1.072994	2.218545	2.916825
H	1.567653	3.51669	-1.14262
C	0.93519	-2.02906	-2.4173
H	0.142686	-1.3866	-2.80477
H	1.803278	-1.39601	-2.22891
H	1.201157	-2.7274	-3.20711
C	-0.74078	-2.11921	2.403512

H	-1.66168	-1.56554	2.216048
H	-0.94511	-2.84385	3.187962
H	-0.01026	-1.41083	2.797903
C	0.320523	-6.40147	-0.01275
H	-0.33629	-6.84116	0.735719
H	0.059626	-6.81662	-0.98528
H	1.339019	-6.72365	0.215112
C	-3.22838	-0.88081	-0.14477
C	-3.61872	-2.21908	-0.12132
C	-3.84613	0.022666	0.723473
C	-4.60542	-2.65251	0.759159
H	-3.15157	-2.92743	-0.79274
C	-4.82528	-0.41144	1.608895
H	-3.57577	1.069594	0.701438
C	-5.20679	-1.75039	1.628874
H	-4.90272	-3.6918	0.763324
H	-5.2999	0.296532	2.27393
H	-5.97398	-2.08489	2.312983
C	2.222033	-0.21693	1.141572
H	2.012246	-1.07228	1.776567
C	3.299228	-0.56802	0.137967
C	3.825184	0.395167	-0.72651
C	3.817441	-1.86201	0.107521
C	4.840425	0.062245	-1.61511
H	3.454721	1.410858	-0.69905
C	4.840172	-2.19357	-0.7761
C	5.349899	-1.2333	-1.64208
H	5.243138	0.81605	-2.27719
H	5.236933	-3.19907	-0.78567
H	6.144798	-1.48862	-2.32867
H	3.422277	-2.61533	0.77621
H	2.541548	0.601533	1.779287
N	0.934579	0.212281	0.53944

Table D.21: Cartesian coordinates in Å for Reagent MesIm.

Atom	X	Y	Z
C	-1.05063	-0.68406	0.0699
C	-1.04959	0.68441	-0.07085
N	0.28397	-1.08182	0.11361
N	0.28559	1.08019	-0.11402
C	1.08316	-0.00138	-0.00004
C	2.56076	-0.002	0.00083

C	3.25485	0.37984	1.17079
C	3.25671	-0.38825	-1.16793
C	4.6519	0.36411	1.14623
C	4.65263	-0.37957	-1.13976
C	-2.18311	1.61895	-0.20647
C	-3.13029	1.42166	-1.2247
C	-2.34114	2.69828	0.67869
C	-4.21323	2.29054	-1.35475
H	-3.01052	0.59209	-1.91463
C	-3.423	3.56738	0.54099
H	-1.62977	2.84803	1.48539
C	-4.36035	3.3657	-0.47493
H	-4.93843	2.1303	-2.14719
H	-3.53645	4.39713	1.23241
H	-5.20315	4.04289	-0.57946
C	-2.18563	-1.61682	0.2054
C	-3.13312	-1.41734	1.22294
C	-2.3448	-2.69652	-0.67908
C	-4.21746	-2.28447	1.35298
C	-3.42809	-3.56385	-0.5414
C	-4.36572	-3.36002	0.47384
H	-4.94287	-2.12255	2.14488
H	-3.54241	-4.39391	-1.23229
C	5.36865	-0.00632	0.00373
C	0.76127	2.4501	-0.3356
H	0.1359	2.92195	-1.0934
H	1.79236	2.40653	-0.68279
C	0.75752	-2.4523	0.33624
H	0.13111	-2.92275	1.09406
H	1.7885	-2.41004	0.68396
H	0.70573	-3.02777	-0.58972
H	0.70987	3.025	0.59075
H	5.1934	0.6465	2.04572
H	5.19524	-0.67171	-2.03568
H	-5.20962	-4.03585	0.57836
H	-1.63321	-2.84794	-1.48528
H	-3.01247	-0.58747	1.91235
C	2.52831	0.79791	2.42921
H	2.10657	1.80643	2.3345
H	1.70201	0.12202	2.67435
H	3.2139	0.8128	3.28057
C	2.53038	-0.80851	-2.42579
H	2.10176	-1.81375	-2.32752
H	1.70904	-0.12825	-2.6757

H	3.21762	-0.83154	-3.27562
C	6.87799	0.01646	-0.00602
H	7.28571	-0.8089	-0.59877
H	7.24986	0.94893	-0.45029
H	7.28558	-0.05026	1.00717

Table D.22: Cartesian coordinates in Å for TS_{C2} MesIm.

Atom	X	Y	Z
N	-0.71428	-0.96328	-0.56293
N	-0.75081	0.81763	0.70516
C	0.04018	-0.24644	0.32751
C	1.52166	-0.05073	0.09796
C	2.53652	-0.94238	0.51641
C	1.88593	1.08203	-0.67685
C	3.86968	-0.61347	0.25231
C	3.23375	1.3581	-0.90336
C	4.24905	0.53952	-0.42358
H	4.63676	-1.30392	0.58007
H	3.48964	2.22872	-1.49412
C	-0.21628	-2.0658	-1.36692
H	-0.76959	-2.10887	-2.3002
H	0.83242	-1.89571	-1.59032
H	-0.31914	-3.01874	-0.84849
C	-0.38259	1.72365	1.78308
H	-0.81703	1.40115	2.72802
H	0.69757	1.72591	1.88038
H	-0.71843	2.73225	1.55993
C	0.88905	2.01252	-1.33796
H	0.04406	1.47812	-1.7668
H	0.4894	2.75214	-0.64411
H	1.38331	2.55761	-2.14011
C	2.3166	-2.27087	1.20148
H	2.10919	-2.14096	2.26045
H	1.46666	-2.80986	0.79727
H	3.21019	-2.8833	1.08699
O	-0.05425	-1.32054	2.03507
H	-0.9582	-1.08141	2.26603
C	5.70068	0.87812	-0.64341
H	6.30773	-0.02092	-0.74511
H	5.83528	1.48796	-1.53597
H	6.09795	1.44451	0.20226
C	-2.06339	0.58907	0.27449

C	-3.20021	1.44328	0.66197
C	-3.20821	2.81433	0.37506
C	-4.30592	0.88893	1.31735
C	-4.29185	3.60741	0.73516
H	-2.37396	3.25826	-0.15018
C	-5.393	1.6819	1.6695
H	-4.30848	-0.16564	1.55448
C	-5.38861	3.0439	1.38233
H	-4.28305	4.66322	0.50165
H	-6.23895	1.23636	2.17474
H	-6.23195	3.66113	1.65967
C	-2.04378	-0.51701	-0.51909
C	-3.14104	-1.1558	-1.2625
C	-3.953	-0.3987	-2.11642
C	-3.41175	-2.52345	-1.11932
C	-5.01037	-0.98955	-2.79933
H	-3.7483	0.65421	-2.24794
C	-4.46436	-3.11397	-1.80873
H	-2.8083	-3.12358	-0.45283
C	-5.2687	-2.34938	-2.65011
H	-5.62622	-0.38894	-3.45468
H	-4.66094	-4.16979	-1.68227
H	-6.08793	-2.80966	-3.185

Table D.23: Cartesian coordinates in Å for P_{C2} MesIm.

Atom	X	Y	Z
C	1.06144	0.6445	0.34254
C	1.05887	-0.70607	0.17949
N	-0.28037	1.08712	0.52797
N	-0.2811	-1.16251	0.2474
C	-1.08796	-0.10614	0.82234
C	-2.51285	-0.02664	0.20895
C	-3.70049	-0.34884	0.9198
C	-2.62713	0.35319	-1.16021
C	-4.94165	-0.2194	0.2738
C	-3.89191	0.46041	-1.74674
C	2.17316	-1.59049	-0.22222
C	2.89859	-1.33009	-1.39904
C	2.54539	-2.70139	0.55736
C	3.96561	-2.14515	-1.77798
H	2.61684	-0.48328	-2.01751
C	3.60711	-3.52112	0.17333
H	2.01082	-2.9136	1.47882

C	4.32281	-3.24549	-0.99475
H	4.51258	-1.92523	-2.69105
H	3.88034	-4.37147	0.79241
H	5.15093	-3.88314	-1.29182
C	2.18628	1.58379	0.22603
C	3.41439	1.3176	0.86137
C	2.07034	2.77491	-0.51805
C	4.48804	2.19932	0.74438
H	3.51664	0.41594	1.45733
C	3.14208	3.66147	-0.62389
H	1.14009	2.99234	-1.03517
C	4.35715	3.37881	0.00555
H	5.4258	1.97134	1.24458
H	3.02909	4.57166	-1.20724
C	-5.07033	0.19875	-1.04685
C	-0.66929	-2.54336	0.47011
H	-0.12185	-3.19047	-0.21907
H	-1.73684	-2.64335	0.25548
C	-0.56376	2.25386	1.35649
H	-0.2463	2.13098	2.40231
H	-1.64097	2.44814	1.33415
H	-0.06007	3.13126	0.94822
H	-0.48808	-2.89076	1.49713
H	-5.84006	-0.46773	0.83467
H	-3.95233	0.75106	-2.79373
H	5.1914	4.07003	-0.07686
O	-1.10362	-0.34876	2.24495
H	-1.7126	0.27687	2.66645
C	-3.79034	-0.85703	2.35357
H	-3.06006	-1.63468	2.57825
H	-3.65633	-0.05606	3.09395
H	-4.79075	-1.26402	2.52771
C	-6.42302	0.35739	-1.69895
H	-6.413	-0.00249	-2.73382
H	-7.19742	-0.19073	-1.15291
H	-6.72615	1.41237	-1.72904
C	-1.45	0.64117	-2.07382
H	-1.02424	1.63096	-1.88385
H	-0.64225	-0.08147	-1.94496
H	-1.78126	0.60949	-3.11735

Table D.24: Cartesian coordinates in Å for TS_{SN2} MesIm.

Atom	X	Y	Z
C	-1.18545	-0.8393	0.03943
C	-1.07857	0.53582	-0.00147
N	0.1168	-1.32346	0.06687
N	0.26407	0.86539	0.00359
C	0.96763	-0.26229	0.04235
C	2.4462	-0.3683	0.0531
C	3.14997	-0.1704	1.25789
C	3.13362	-0.66595	-1.14079
C	4.54222	-0.28009	1.24438
C	4.52634	-0.76157	-1.10557
C	-2.15488	1.54381	-0.05937
C	-3.18673	1.42649	-1.00188
C	-2.17134	2.63089	0.82687
C	-4.21042	2.37011	-1.05419
H	-3.18007	0.59902	-1.70149
C	-3.19345	3.57597	0.77041
H	-1.38946	2.72864	1.57073
C	-4.21699	3.44827	-0.16905
H	-4.99879	2.26668	-1.79123
H	-3.19311	4.40891	1.46439
H	-5.01232	4.1837	-0.21141
C	-2.3756	-1.71014	0.10043
C	-3.29848	-1.56423	1.14616
C	-2.61281	-2.6832	-0.88149
C	-4.43204	-2.37199	1.20699
H	-3.12138	-0.82047	1.9142
C	-3.74411	-3.4935	-0.81564
H	-1.92135	-2.79617	-1.70854
C	-4.657	-3.33986	0.22795
H	-5.1357	-2.24909	2.02245
H	-3.91585	-4.23885	-1.58379
C	5.2489	-0.57168	0.0749
C	1.02729	2.57937	-0.30903
H	0.24976	2.88408	-0.98346
H	1.93914	2.17254	-0.70363
C	0.50918	-2.72819	0.19386
H	-0.11563	-3.21248	0.94265
H	1.54897	-2.77078	0.50929
H	0.40066	-3.24901	-0.75764
H	0.98414	2.88925	0.71683
H	5.08717	-0.13683	2.17218
H	5.05877	-0.98853	-2.024

H	-5.53797	-3.96957	0.27728
O	1.80172	4.45988	-0.73132
H	2.66681	4.4657	-0.30488
C	2.43215	0.14927	2.54842
H	1.95943	1.1348	2.50904
H	1.643	-0.57637	2.76394
H	3.13003	0.14721	3.38674
C	6.75583	-0.65198	0.0798
H	7.1182	-1.37304	-0.65618
H	7.1956	0.31942	-0.1711
H	7.13602	-0.93935	1.06224
C	2.39687	-0.88365	-2.44199
H	1.86644	-1.84117	-2.44705
H	1.65458	-0.1022	-2.62331
H	3.09316	-0.89075	-3.28162

Table D.25: Cartesian coordinates in Å for P_{SN2} MesIm.

Atom	X	Y	Z
C	1.21297	-0.85772	-0.00292
C	1.07885	0.51672	-0.05096
N	-0.08157	-1.35701	-0.00483
N	-0.26243	0.84346	-0.09043
C	-0.93494	-0.29382	-0.06026
C	-2.41342	-0.41651	-0.07844
C	-3.10267	-0.36713	-1.3038
C	-3.11729	-0.56493	1.12788
C	-4.49197	-0.47159	-1.29709
C	-4.50868	-0.6634	1.08774
C	2.11741	1.55934	-0.05301
C	3.30811	1.41483	0.67198
C	1.9219	2.74303	-0.77781
C	4.27506	2.41389	0.66046
H	3.47321	0.52091	1.25958
C	2.88787	3.74284	-0.78546
H	1.00703	2.8741	-1.34135
C	4.07138	3.58237	-0.06927
H	5.1865	2.28277	1.23202
H	2.71745	4.64801	-1.35671
H	4.82476	4.361	-0.07597
C	2.40419	-1.72712	-0.01638
C	3.31821	-1.64853	-1.07418

C	2.65228	-2.6382	1.01754
C	4.45043	-2.45513	-1.09496
H	3.13502	-0.95342	-1.88439
C	3.78172	-3.44946	0.99268
H	1.96758	-2.7015	1.85475
C	4.68509	-3.35961	-0.06271
H	5.14662	-2.38168	-1.92197
H	3.95951	-4.1464	1.80296
C	-5.21451	-0.61775	-0.11244
C	-1.414	3.96219	1.24034
H	-0.35305	4.19995	1.37966
H	-1.74578	3.34733	2.08507
C	-0.46262	-2.76519	-0.03355
H	0.15197	-3.29827	-0.75676
H	-1.50602	-2.83705	-0.32924
H	-0.33964	-3.22552	0.94668
H	-1.97882	4.8955	1.2546
H	-5.0241	-0.43986	-2.24243
H	-5.05281	-0.77788	2.01943
H	5.56606	-3.98993	-0.08048
O	-1.65541	3.32548	-0.00741
H	-1.14969	2.47972	-0.02979
C	-2.36482	-0.20885	-2.61101
H	-1.83402	0.74502	-2.65465
H	-1.61833	-0.99525	-2.75018
H	-3.05704	-0.25019	-3.45215
C	-6.71977	-0.70283	-0.13507
H	-7.16322	0.28234	-0.30884
H	-7.06755	-1.35815	-0.93657
H	-7.11129	-1.07976	0.81066
C	-2.39748	-0.61474	2.45377
H	-1.77392	-1.50876	2.54102
H	-1.73997	0.24788	2.5832
H	-3.10906	-0.62622	3.2795